Magnetic Vortices in Gauge/Gravity Duality

Dissertation by Migael Strydom

Magnetic Vortices in Gauge/Gravity Duality

Dissertation
an der Fakultät für Physik
der Ludwig–Maximilians–Universität
München

vorgelegt von
Migael Strydom
aus Pretoria

München, den 20. Mai 2014

Dissertation

submitted to the faculty of physics of the
Ludwig–Maximilians–Universität München

by Migael Strydom

supervised by Prof. Dr. Johanna Karen Erdmenger
Max-Planck-Institut für Physik, München

1st Referee: Prof. Dr. Johanna Karen Erdmenger
2nd Referee: Prof. Dr. Dieter Lüst

Date of submission: 20 May 2014
Date of oral examination: 18 July 2014

Zusammenfassung

Wir untersuchen stark gekoppelte Phänomene unter Verwendung der Dualität zwischen Eich- und Gravitationstheorien. Dabei liegt ein besonderer Fokus einerseits auf Vortex Lösungen, die von einem magnetischem Feld verursacht werden, und andererseits auf zeitabhängigen Problemen in holographischen Modellen. Das wichtigste Ergebnis ist die Entdeckung eines unerwarteten Effektes in einem einfachen holografischen Modell: ein starkes nicht abelsches magnetisches Feld verursacht die Entstehung eines Grundzustandes in der Form eines dreieckigen Gitters von Vortices.

Die Dualität zwischen Eich- und Gravitationstheorien ist ein mächtiges Werkzeug welches bereits verwendet wurde um stark gekoppelte Systeme vom Quark-Gluonen Plasma in Teilchenbeschleunigern bis hin zu Festkörpertheorien zu beschreiben. Die wichtigste Idee ist dabei die der Dualität: Eine stark gekoppelte Quantenfeldtheorie kann untersucht werden, indem man die Eigenschaften eines aus den Einsteinschen Feldgleichungen folgenden Gravitations-Hintergrundes bestimmt.

Eine der Gravitationstheorien, die in dieser Arbeit behandelt werden, ist eine Einstein–Yang–Mills Theorie in einem AdS–Schwarzschild Hintergrund mit $SU(2)$-Eichsymmetrie. Der Ansatz für das Eichfeld ist so gewählt, dass die zugehörige Quantenfeldtheorie einem externen Magnetfeld ausgesetzt ist. Oberhalb eines kritischen Magnetfeldes wird die Konfiguration instabil und zeigt einen Phasenübergang zu einem Supraleiter.

Die Instabilität wird mit zwei Ansätzen untersucht. Zum einen werden Fluktuationen des Hintergrunds betrachtet und die Quasinormalmoden analysiert. Zum anderen zeigt die numerische Analyse der Bewegungsgleichungen, dass das effektive Schrödinger-Potential mit stärker werdendem Magnetfeld sich so lange verändert, bis ein gebundener Zustand möglich wird. Der sich ergebende supraleitende Grundzustand ist durch ein dreieckiges Vortexgitter gegeben, wie eine störungstheoretische Entwicklung über einem kleinen Parameter proportional zur Größe des Kondensats zeigt. Zur Bestimmung des energetisch bevorzugten Zustands wird mithilfe der holographischen Übersetzungsvorschrift die Gesamtenergie verschiedener Lösungen berechnet. Hierfür wird die Lösung der Bewegungsgleichungen zur dritten Ordnung in oben genanntem Parameter berechnet. Zusätzlich wird gezeigt, dass dieses Ergebnis auch für den Fall einer AdS–hard wall Geometrie gilt, also einer Feldtheorie mit Confinement.

Als nächstes erweitern wir das einfache Gravitationsmodell um ein chemisches Potential und wiederholen die Untersuchung. Sind das chemische Potential, das magnetische Feld oder beide groß genug, so befindet sich das System in einer supraleitenden Phase. Wir berechnen das Phasendiagramm des Systems numerisch. Der Grundzustand der supraleitenden Phase nahe dem Phasenübergang ist ein dreieckiges Vortexgitter, wobei der Gitterabstand nur von der Stärke des magnetischen Feldes abhängt. Die Relevanz dieser Ergebnisse wird im Zusammenhang mit inhomogenen Grundzuständen in holographischen Supraleitern diskutiert, einem Themengebiet welches in letzter Zeit viel Interesse auf sich gezogen hat. Die erhaltenen Resultate sind nicht nur aufgrund der vorher unbekannten inhomogenen Lösung der Gravitationstheorie mit Schwarzem Loch neuartig. Es ist auch interessant, dass ein großes magnetisches Feld die Vortexstruktur im Grundzustand induziert anstatt sie zu unterdrücken.

Des Weiteren untersuchen wir zeitabhängige Phänomene in einer holographischen Erweiterung des Kondomodells. Letzteres beschreibt ein einfaches Modell in der Festkörperphysik, in welchem eine magnetische Verunreinigung stark an ein Elektronenreservoir koppelt. Die holographische Beschreibung erfordert Techniken der numerischen Relativitätstheorie und erlaubt uns die Entwicklung des Systems nach einem plötzlichen Sprung in der Kopplungskonstante zu simulieren.

Diese Doktorarbeit basiert auf Ergebnissen, die der Autor während des Studiums am Max-Planck-Institut-für-Physik in München, Deutschland unter der Betreuung von PD Dr. J. K. Erdmenger von August 2011 bis Mai 2014 erreicht hat. Die relevanten Veröffentlichungen sind:

[1] M. Ammon, J. Erdmenger, P. Kerner, and M. Strydom, "Black Hole Instability Induced by a Magnetic Field," *Phys.Lett.* **B706** (2011) 94–99, `arXiv:1106.4551 [hep-th]`,

[2] Y.-Y. Bu, J. Erdmenger, J. P. Shock, and M. Strydom, "Magnetic field induced lattice ground states from holography," *JHEP* **1303** (2013) 165, `arXiv:1210.6669 [hep-th]`.

Abstract

We study strongly-coupled phenomena using gauge/gravity duality, with a particular focus on vortex solutions produced by magnetic field and time-dependent problems in holographic models. The main result is the discovery of a counter-intuitive effect where a strong non-abelian magnetic field induces the formation of a triangular vortex lattice ground state in a simple holographic model.

Gauge/gravity duality is a powerful theoretical tool that has been used to study strongly-coupled systems ranging from the quark-gluon plasma produced at particle colliders to condensed matter theories. The most important idea is that of duality: a strongly coupled quantum field theory can be studied by investigating the properties of a particular gravity background described by Einstein's equations.

One gravity background we study in this dissertation is AdS–Schwarzschild with an $SU(2)$ gauge field. We switch on the gauge field component that gives the field theory an external magnetic field. When the magnetic field is above a critical value, we find that the system is unstable, indicating a superconducting phase transition.

We find the instability in two ways. Firstly, we do a quasinormal mode analysis, studying fluctuations about the background. Secondly, we rewrite the equations in Schrödinger form and numerically find that, as the magnetic field is increased, the potential deepens until it is capable of supporting a bound state. Next we show that the resulting superconducting ground state is a triangular vortex lattice. This is done by performing a perturbative expansion in a small parameter proportional to the condensate size. After solving the equations to third order, we use the holographic dictionary to calculate the total energy of different lattice solutions and identify the minimum energy state. In addition, we show that the result holds in an AdS–hard wall model as well, which is dual to a confining theory.

Next we extend the simple gravity model to include a chemical potential and repeat the analysis. When the chemical potential, magnetic field or both are large, the system is in a superconducting phase. We calculate the precise phase diagram numerically. The ground state in the superconducting phase near the phase transition line is shown to be a triangular vortex lattice with lattice spacing depending only on the magnetic field strength. We comment on the relevance of the results to the study of inhomogeneous ground states in holographic superconductors, a topic in which there has been much interest recently. Our results are novel not only because of the previously unknown inhomogeneous black hole solution, but also because of the effect of a large magnetic field inducing rather than inhibiting the vortex lattice ground state in a holographic model.

We also study time-dependent phenomena in a holographic generalisation of the Kondo model, a simple condensed matter model of a magnetic impurity coupled strongly to a sea of electrons. This requires techniques from numerical relativity and allows us to determine the response of the system to a quench in the coupling.

This dissertation is based on work the author did during a PhD fellowship under the supervision of PD Dr. J. K. Erdmenger at the Max-Planck-Institut für Physik in Munich, Germany from August 2011 to May 2014. The relevant publications are:

[1] M. Ammon, J. Erdmenger, P. Kerner, and M. Strydom, "Black Hole Instability Induced by a Magnetic Field," *Phys.Lett.* **B706** (2011) 94–99, arXiv:1106.4551 [hep-th],

[2] Y.-Y. Bu, J. Erdmenger, J. P. Shock, and M. Strydom, "Magnetic field induced lattice ground states from holography," *JHEP* **1303** (2013) 165, arXiv:1210.6669 [hep-th].

Samevatting

Ons bestudeer sterk gekoppelde fenomene deur die gebruik van dualiteit tussen ykteorieë en gravitasieteorieë. Ons fokus spesifiek op vorteks oplossings wat deur magnetiese velde voortgebring word, asook tyd-afhanklike probleme in holografiese modelle. Die belangrikste resultaat is die ontdekking van 'n onverwagte effek waar sterk nie-abelse magnetiese velde 'n driehoekige vorteksrooster grondtoestand uitlok in 'n holografiese model.

Die dualiteit tussen ykteorieë en gravitasie is 'n nuttige instrument wat al gebruik is om sterk-gekoppelde stelsels te bestudeer wat wissel van die kwark-gluon plasma, wat geproduseer is by deeltjieversnellers, tot gekondenseerde materie teorieë. Die belangrikste begrip is dualiteit: 'n sterk gekoppelde kwantumveldteorie kan bestudeer word deur die eienskappe van 'n spesifieke swaartekrag agtergrond, wat beskryf word deur Einstein se vergelykings, te ondersoek.

Een swaartekrag agtergrond wat ons bestudeer is AdS–Schwarzschild met 'n $SU(2)$ ykveld. Ons skakel die ykveld komponent aan wat in die veldteorie duaal is aan 'n eksterne magnetiese veld. Wanneer die magnetiese veld bo 'n spesifieke waarde val, vind ons dat die stelsel onstabiel is, wat dui op 'n supergeleidende fase oorgang.

Ons vind die onstabiliteit op twee maniere. Eerstens, doen ons 'n quasinormale modus analise, waarin ons versteurings van die agtergrond bestudeer. Tweedens, herskryf ons die vergelykings in Schrödinger vorm en vind numeries dat soos die magnetiese veld sterker word, verdiep die potensiaal totdat dit diep genoeg is vir 'n gebonde toestand om te vorm. Volgende wys ons dat die gevolglike supergeleidende grondtoestand 'n rooster van driehoekige vortekse is. Dit word gedoen deur die uitvoering van 'n versteuringsuitbreiding in 'n klein parameter wat proporsioneel is tot die grootte van die kondensaat. Na die oplossing van die vergelykings tot op die derde orde, gebruik ons die holografiese vertalingsvoorskrif om die totale energie van verskillende rooster oplossings te bereken en die minimum energie toestand te identifiseer. Daarna wys ons dat die gevolge in 'n AdS–hard wall model ook waar is. Die AdS–hard muur model is duaal tot 'n teorie met *confinement*.

Volgende brei ons die eenvoudige swaartekrag model uit sodat dit 'n chemiese potensiaal in sluit en dan herhaal ons die analise. Wanneer die chemiese potensiaal, magnetiese veld of albei groot is, is die stelsel in 'n supergeleidende fase. Ons bereken die fase diagram numeries. Die grondtoestand in die supergeleidende fase naby die fase-oorgangslyn vorm 'n driehoekige vorteksrooster met rooster spasiëring wat afhang van die sterkte van die magnetiese veld. Ons lewer kommentaar op die toepaslikheid van die resultate tot nie-homogene grondtoestande in holografiese supergeleiers, 'n onderwerp waarin daar onlangs baie belangstelling was. Die nuwigheid van ons resultate lê in beide die voorheen onbekende swartkolk oplossing en die effek van 'n groot magnetiese veld wat die vorteksrooster grondtoestand in 'n holografiese model eerder voortbring as verhinder.

Ons bestudeer ook tyd-afhanklike fenomene in 'n holografiese veralgemening van die Kondo model, 'n eenvoudige gekondenseerde materie model van 'n magnetiese onreinheid wat sterk koppel aan 'n see van elektrone. Dit vereis tegnieke van numeriese relatiwiteit en laat ons toe om die reaksie van die stelsel te bepaal na 'n vinnige sprong in die koppeling.

Hierdie verhandeling is gebaseer op die werk wat die skrywer tydens 'n PhD program onder die toesig van PD Dr JK Erdmenger by die Max Planck-Institut-

für Physik in München, Duitsland vanaf Augustus 2011 tot Mei 2014 gedoen het. Die toespaslike publikasies is:

[1] M. Ammon, J. Erdmenger, P. Kerner, and M. Strydom, "Black Hole Instability Induced by a Magnetic Field," *Phys.Lett.* **B706** (2011) 94–99, `arXiv:1106.4551 [hep-th]`,

[2] Y.-Y. Bu, J. Erdmenger, J. P. Shock, and M. Strydom, "Magnetic field induced lattice ground states from holography," *JHEP* **1303** (2013) 165, `arXiv:1210.6669 [hep-th]`.

To the lovely T. L. v. G.

Contents

"The quantum theory of black holes ... is a 'trackless swamp' with many false but seductive paths and no maps. ... The true path through the swamp at times becomes so narrow it seems to be a dead end, while all around false paths beckon. Beware the will-o'-the-wisp and don't lose your nerve."

— Leonard Susskind and James Lindesay

Chapter 1

Introduction

A black hole has entropy. This simple fact shook up fundamental physics when first discovered, but at the time no one could have predicted that it would end up bringing together such diverse areas of physics as gravity, quantum field theory, fluid dynamics, condensed matter theory and heavy ion interactions. And, as this thesis shows, it has revealed some remarkable properties in systems we thought we understood.

Classically, black holes should have no entropy at all. They are some of the simplest solutions to Einstein's equations, completely determined by just a few parameters like mass, charge and angular momentum. But quantum theory brings in extra degrees of freedom. Near the event horizon there is a quantum soup of particles, created from the vacuum in the gravitational background. It is there that we obtain the clearest glimpse of a theory of quantum gravity.

But the two theories, quantum mechanics and general relativity, work together in a surprising way. The entropy of a black hole is proportional to the area of its event horizon [5, 6]. In other words, all the information about the black hole can be written in the quantum particles living at its edge, approximately one bit per Planck area. Moreover, it is impossible to have an equivalent region of space that has a higher entropy. From here we are led naturally to the *holographic principle* [7,8]. It states that the description of a volume of space can in some way be encoded on the boundary of that volume. If we take this conjecture further, it implies that we can treat two theories, one on the d-dimensional boundary and one in the $(d+1)$-dimensional interior, as one and the same. The theories are *dual*: both contain exactly the same physical information. It is through a specific realisation of this holographic duality that we can relate diverse areas of physics, studying one area by solving equations in another. The two areas we study in this thesis, a gauge theory in d dimensions and a gravity theory in $(d+1)$ dimensions, are related by *gauge/gravity duality*, a field that not only provides profound insights into the interplay between gravity and quantum theory, but also yields fruitful applications.

The most successful gauge theory to date is the *standard model* of particle physics. It has withstood experimental scrutiny up to energies of order 100 GeV [9], culminating in the long-anticipated discovery of a Higgs boson in 2012 [10,11]. Its gauge group, $SU(3)_C \times SU(2)_L \times U(1)_Y$, signifies its theoretical success because of the simple way it encapsulates three of the four fundamental forces. The $SU(3)_C$ component describes quantum chromodynamics, the theory of the strong interaction between gluons and quarks. The $SU(2)_L \times U(1)_Y$ component describes the

electroweak force. At low energies it is broken by the Higgs mechanism [12–14] to the electromagnetic $U(1)_{em}$ group, leaving massive $W^{\pm}$ and Z^0 bosons, the mediators of the weak force. The gauge bosons as well as the associated matter particles, the quarks, leptons and the Higgs scalar itself, make up the entirety of the standard model and have all been observed by experiment.

Gravity, on the other hand, is conspicuously absent from the standard model. It is described by an entirely classical theory, Einstein's *general relativity* [15]. General relativity concerns spacetime itself, forming the backdrop for the physics of the standard model. It has also enjoyed much experimental success, from explaining the curvature of starlight around the sun to the possible confirmation of gravitational waves and the theory of inflation by the recent BICEP2 experiment [16, 17].

One of the goals of contemporary fundamental physics research is to unify the three forces of the standard model with gravity. Unification can lead to greater understanding of the underlying physics as well as to new predictions. Maxwell showed how to relate electricity and magnetism, which brought greater insight into the field of optics and the nature of light. Electroweak unification predicted the existence of the Higgs particle in addition to showing that the weak and electromagnetic forces join into a single force at energies of the order 100 GeV. At even higher energies it is expected that the electroweak force and strong force also unify and can be described by a single coupling constant. A framework describing this unification is known as a *grand unified theory* [18], or GUT. Unifying a GUT with gravity, which would involve incorporating the principles of quantum mechanics into general relativity, would provide a *theory of everything*.

The most promising candidate for a theory of everything is *string theory* [19–21]. It starts from the slightly absurd premise that, on a fundamental level, matter does not consist of point particles but rather of extended 1-dimensional objects called strings. The different vibration modes of the strings give rise to particles with different spin, charge and mass. What makes string theory promising is found in the oscillations of closed strings — a spin-2 particle, the graviton. So string theory has all the right ingredients: it is a quantum theory with a graviton in its spectrum, and it is believed to be consistent and UV finite.

But this humble starting point of quantum strings has an impressive array of further repercussions. For consistency of the quantum theory, more specifically for the cancellation of gauge anomalies, string theory requires 10-dimensional spacetime. These extra dimensions have not been observed, so it has to be assumed that they are compact with small volume. Another repercussion is the existence of higher-dimensional objects in addition to strings. In addition to having closed strings that form loops, there are also open strings with endpoints. These endpoints must end on higher-dimensional surfaces called *D-branes* [22, 23].

There has so far been no experimental test providing evidence for string theory, but its theoretical success is unquestioned. By studying D-branes, Juan Maldacena provided the first concrete example of the holographic principle [24]. Maldacena looked at the D-branes from two different perspectives: a low energy, near horizon perspective and a far away, long wavelength perspective. Although they appeared to give rise to different theories from these different points of view, he reasoned that they must still describe the same physical system. They are, after all, a single D-brane construction viewed in a low energy limit. So he had found two different theories describing the same physics — in other words, he had found a

duality. Moreover, the two theories are set in differing numbers of dimensions, so the duality is holographic. On the one hand is a theory of type IIB supergravity in five non-compact dimensions. On the other is a conformal supersymmetric gauge theory in four dimensions. Crucially, the latter theory does not contain gravity. But the two theories do contain the same information — and have the same entropy.

The duality is known as the *AdS/CFT correspondence*, and the conjecture is stated in three different forms. In its weak form, the higher-dimensional theory is a type IIB supergravity on $\mathrm{AdS}_5 \times S^5$. Meanwhile, the lower-dimensional theory is a conformal field theory, $\mathcal{N} = 4$ super Yang–Mills theory in $(3 + 1)$-dimensions with gauge group $SU(N)$. The field theory is strictly in the large N and strong coupling limits, $N, \lambda \to \infty$. Relaxing these restrictions gives different forms. In the strong form, the strong coupling restriction is relaxed in the field theory, which means that the gravity theory becomes a classical type IIB string theory. Relaxing the large N limit in the field theory gives the strongest form, where the gravity side is a full quantum type IIB superstring theory on asymptotically $\mathrm{AdS}_5 \times S^5$.

The stronger forms of the duality are not understood as well as the weak form, but the weak form can easily be generalised in other directions. The first thing to do is add a black hole to the gravity spacetime [25]. This brings us back to where the idea of holography started — by considering the implications of a black hole's entropy. The dual description of the black hole spacetime is, appropriately, a field theory at a specific temperature, with the temperature equal to the black hole's black body temperature. And it can be shown that the entropy of the field theory, calculated in the usual way from its free energy, is precisely equal to a quarter of the area of the black hole horizon in Planck units, just as Bekenstein and Hawking showed it ought to be.

$\mathcal{N} = 4$ super Yang–Mills theory is conformal, unlike the QCD of the standard model. To break the conformal symmetry in the gauge theory, we need to ensure that the physics is in general not the same on different energy scales. On the gravity side of the duality, the energy scale is identified with the radial position in AdS space, with positions closer to the AdS boundary corresponding to higher energies. So conformal symmetry can be broken by, for example, choosing a gravity solution with a dilaton field changing as a function of the radial coordinate. Different radial positions then have different values of the dilaton field. On the field theory side, this introduces a renormalisation group flow.

Further generalisations serve to make the AdS/CFT duality more applicable to real-world systems, breaking it away from the specific super Yang–Mills and supergravity theories to become the more general *gauge/gravity duality* [26, 27]. A chemical potential is added to the field theory by imposing a non-vanishing boundary condition on the time component of the gauge field vector potential. Matter fields behaving like quarks are added through the introduction of light D7-branes to the gravity background. Magnetic fields in the field theory are simply described by magnetic fields in the gravity theory. A well-defined dictionary exists, mapping field theory expectation values and properties to quantities on the gravity side. And because the two sides are dual, any physical quantity calculated on one side must agree with the corresponding quantity on the other side.

This latter point makes gauge/gravity duality an especially powerful tool, because, coming from the weak form of the AdS/CFT conjecture, it is also a strong/weak coupling duality. The gravity side is weakly coupled, while the field

theory side is considered in a limit where the coupling constant formally tends to infinity. By exploring solutions to Einstein's equations on an Anti-de Sitter background we can therefore provide answers to the question, *how does strongly coupled matter behave?*

To understand why this is an important question, let us focus on the example of quantum chromodynamics. QCD is asymptotically free [28, 29], meaning that the coupling is weak at high energies but strong at low energies. The standard method for calculating observables in field theories is to make a perturbative expansion in terms of the coupling constant, with each term of the expansion represented as a Feynman diagram for intuitive clarity. Since the expansion is asymptotic, this technique does not work when the coupling constant is large. So at low energies, QCD cannot be solved with the perturbative approach.

A possible method for solving QCD at low energies is *lattice QCD*, a particular lattice gauge theory formulated on a discrete grid of points in spacetime. The discretisation renders the otherwise infinite-dimensional path integrals finite. They can then be calculated using the Monte Carlo method. Lattice QCD has had some great successes, such as the calculation of the mass of various light hadrons with errors of only a few percent [30]. It does however have some downsides. Lattice gauge theories require a Euclidean time action so that the weighting factor in the path integral causes the integral to converge faster. This means that it is almost impossible to simulate dynamical processes.

Strongly coupled systems are also common in condensed matter physics. Here again there is a standard approach for some models: the *Landau–Fermi liquid* theory [31]. A Landau–Fermi liquid successfully models the normal state of many metals at low temperature. It rests on two key ideas, the Pauli exclusion principle and the notion of adiabaticity. Consider a system of non-interacting fermions at low temperature. By the exclusion principle, they occupy all the momentum states $p < p_F$, where p_F is the Fermi momentum. The higher momentum states are not occupied. Now we adiabatically switch on interactions between the particles. This should induce a continuous change in some of the dynamic properties of the particles, such as their effective mass, since their dynamics is altered by interactions. The new, effective particles are known as *quasiparticles*. Provided there are no singularities in the total energy of the system as we switch on interactions — the process is adiabatic — the new system should be similar to the old system. There should be a one-to-one correspondence between particles in the non-interacting theory and quasiparticles in the interacting theory. This one-to-one correspondence is however far from clear in a strongly coupled system, where the notion of quasiparticles is not even well-defined. As a result, there are strongly-coupled theories where the Landau–Fermi liquid description is, unsurprisingly, not applicable.

One example of strongly-coupled systems where the Landau–Fermi liquid description breaks down is in *high-temperature superconductors*. These are materials, such as the famous cuprates [32], that behave as superconductors with a critical temperature above 30 Kelvin. Conventional superconductors, described by BCS theory and its extensions, have critical temperatures that are far lower, typically of the order a few Kelvin. There is so far no satisfying theoretical explanation for high-temperature superconductivity.

Perhaps even more important than providing a rare theoretical insight into the behaviour of strongly-coupled matter is that gauge/gravity duality also addresses

the question of the universal behaviour of field theories. That is, it helps us to find whether there are any properties that large classes of field theories are likely to share. The most celebrated result is the ratio of shear viscosity to entropy density [33],

$$\frac{\eta}{s} = \frac{1}{4\pi}\frac{\hbar}{k_B}. \tag{1.1}$$

It has been shown that for a broad class of strongly coupled field theories with a gravity dual, the matter content of the theory will respect this relation. Moreover, it is conjectured that this value of η/s is a lower bound for a wide class of thermal quantum field theories.

The quark-gluon plasma, a phase of quark matter at high temperature, high density or both, is the perfect candidate for a test of the η/s prediction. This is because it is a strongly coupled fluid. Quark-gluon plasma can be observed slightly above the confinement/deconfinement temperature, that is, between temperatures of 175 MeV and 250 MeV, in heavy ion collisions. And indeed, experiments at Brookhaven National Laboratory's Relativistic Heavy Ion Collider (RHIC) have found that quark-gluon plasma has a small value of η/s [34]. This agrees very well with the gauge/gravity prediction, a result which cannot be replicated with perturbative methods. The RHIC results also indicate that η/s for the quark-gluon plasma is slightly above $1/4\pi$ — the conjectured universal bound holds!

The concept of a shear viscosity is only defined for fluids. In order to get an effective description of a strongly coupled field theory as a fluid, we need to take the *hydrodynamic limit*. In this limit we consider only the behaviour of the system over long distances and long times and neglect the microscopic details. Fluids are described in terms of temperature, pressure and density — thermodynamic variables. But thermodynamics applies to systems in equilibrium. The trick is to coarse-grain the space over which the field theory is defined. We break it up into patches and assume each patch is an equilibrium system with specific values of the thermodynamic variables. At long distance and time scales, this is realistic. We then zoom out of the picture even further and promote the thermodynamic variables to functions of space and time, effectively obtaining a "temperature field" $T(x)$.

This procedure is usually carried out in field theories, but in gauge/gravity duality it is done on the gravity side [35]. The result is startling. The coarse-graining procedure is done over tube-like patches of the AdS bulk spacetime stretching from the black hole horizon to the boundary. Each of these tubes corresponds to a patch with a different temperature, so the black hole horizon radius varies from tube to tube. To find the precise variation of the background geometry, we need to use Einstein's equations. And when imposing Einstein's equations on the metric coefficients dual to velocity vector fields in the boundary theory, we see the emergence of the relativistic Navier–Stokes equations. Gravity, we find, contains knowledge of fluid dynamics!

From toy models of QCD and the quark-gluon plasma to Navier–Stokes equations hidden within Einstein's, we have found that exploring what is hidden by a black hole's entropy can reveal a lot of physics. This thesis continues the process with the author's own original work. We study superconductors using holography and find one with a peculiar twist. We show how this is related to an old question about the QCD ground state. We then move on and discuss a different model,

based on a condensed matter system, and show how gauge/gravity duality can help us understand time-dependent processes there.

An important concept to understand during these discussions is that of a *holographic superconductor* [36, 37]. We turn to these next.

Holographic superconductors and magnetic fields

Superconductivity is a result of symmetry breaking. The presence of a $U(1)$ electromagnetic gauge symmetry, dynamically broken down to a discrete subgroup, is all a field theory needs in order to exhibit the spectacular phenomenology of a superconductor. This fact has been known for a long time but is clearly explained by Weinberg for high energy theorists in [38]. From electromagnetic gauge invariance we get that the system must have an infinite DC (zero frequency) conductivity and must expel magnetic fields. The latter feature is known as the *Meissner–Ochsenfeld effect* [39]. Due to this effect, magnetic fields decay exponentially at the boundary of a superconducting sample, and if the field gets too strong the sample is forced back into its normal phase. Magnetic fields and superconductors, according to this conventional wisdom, should not coexist.

Given the minimality of the circumstances that create a superconductor, it should perhaps not be surprising that we can find holographic dualities where the field theory has a superconducting phase. We just need a spontaneously broken $U(1)$ group. What this means on the gravity side, however, is somewhat surprising and it caused people to think more deeply about black hole no-hair conjectures. The gravity dual to a condensed operator that breaks the $U(1)$ at low temperature, it turns out, is a hairy black hole solution. The operator is dual to a field that is part of a stable, static black hole configuration. No-hair conjectures claim that such a configuration is impossible for certain backgrounds.

Unsurprisingly, holographic superconductors have the same properties as the usual field theory superconductors. They can be set up so that above a critical temperature, the system is in the normal, unbroken phase. Below the critical temperature the $U(1)$ symmetry is dynamically broken. On the gravity side this means that a stable non-vanishing field configuration is possible below a certain black hole horizon radius but not above. And by examining small electric field fluctuations about the gravity background it is possible to determine the optical (frequency dependent) conductivity in the field theory and find its DC divergence. Turning on a magnetic field has the effect of making the stable field configuration energetically unfavourable, destroying the superconducting phase.

It is natural to think that holographic superconductors can help lead to an understanding of high-temperature superconductivity. They are models of superconductivity in strongly coupled theories. They abandon the quasiparticle description completely; there is no need to describe electrons that come together in Cooper pairs. There is only an operator condensing below a critical temperature. These are powerful ideas, and while holography has not yet solved the problem of high-temperature superconductivity, as always it improves our understanding of strongly coupled matter.

As an example of what we can learn, consider the phase diagram in figure 1.1, taken from [40]. The authors of this figure were studying a gauge/gravity model where the field theory at finite temperature has an $SU(2)$ isospin symmetry and a $U(1)$ baryon symmetry. On the gravity side this corresponds to adding D7-branes

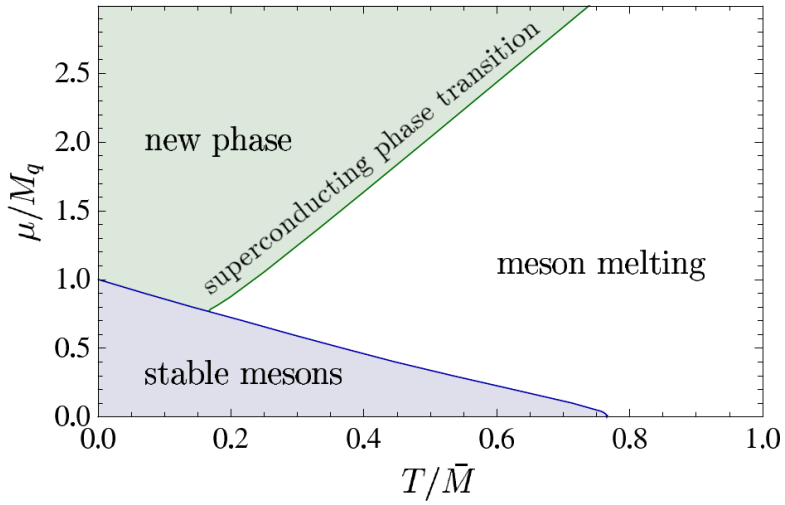

Figure 1.1: The phase diagram in chemical potential μ and temperature T of a gauge/gravity model with $SU(2) \times U(1)$ flavour symmetry, studied in [40]. For small temperature and chemical potential, the mesons are stable. At large temperatures they "melt" into the background soup of particles. At large chemical potential the system is superconducting. This model served as inspiration for one of the main results of this thesis.

aligned in a particular way so that the setup is stable. Studying fluctuations of the branes yields results about the bound states formed by the two flavours of particles in the isospin group spectrum. Using the language of QCD, these bound states are naturally seen as mesons. By studying the mesons at different values of the chemical potential, implemented in the boundary conditions of a gauge field on the gravity side, and temperature, coming from the black hole, the phase diagram in figure 1.1 is found. It shows that the mesons are stable at low temperature and chemical potential, that they "melt" into the background particle soup at high temperatures, and that they undergo a superconducting phase transition at high chemical potential. So we learn that there are superconducting phases, in what can be seen as a toy model for QCD, that are reached by making the chemical potential large enough. Are there other ways to obtain a superconducting phase?

If we are willing to entertain the idea that magnetic fields are not always incompatible with superconductors, we find that the startling answer is yes! This is one of the main results of this thesis, being an outcome of the study of a simple gauge/-gravity model — slightly simpler than the one in [40]. The gravity side has an $SU(2)$ Yang–Mills [41] field and a black hole. In the field theory this corresponds to an $SU(2)$ global symmetry and a finite temperature. Treating a $U(1)$ subgroup as an electromagnetic component, we switch on an external magnetic field. When that magnetic field is strong, above some critical value B_c, the $U(1)$ electromagnetic subgroup is spontaneously broken by other components of the Yang–Mills field. The system undergoes a superconducting phase transition because of the magnetic field, rather than the magnetic field suppressing superconductivity.

We can complete the picture, studying the interplay between chemical potential and magnetic field. The resulting phase diagram, figure 1.2, shows how the border between the superconducting and normal phases changes as μ and B are varied.

Our model is a little different from the one in [40], but the two theories agree on the presence of a superconducting phase at large chemical potential. And the magnetic field helps to bring down the value of chemical potential required to enter the superconducting phase.

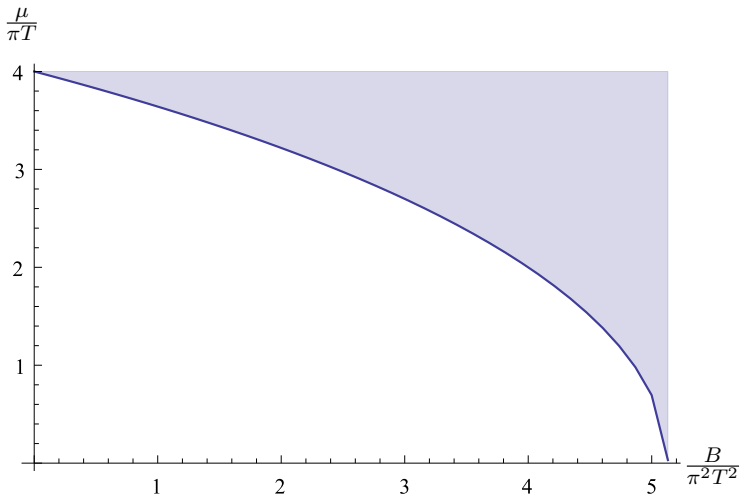

Figure 1.2: The B-μ phase diagram. The white region is the normal, uncondensed phase. The shaded region is the condensed phase. This result is calculated in chapter 6.

This exotic effect has an equally exotic ground state. By focusing on a region of the phase diagram where the condensing fields are still small, that is, near the phase transition line, we can find the precise form of the energy-minimising state. The surprise is that the ground state in *inhomogeneous*, in stark contrast with the homogeneous ground state found when only μ is non-zero. The magnetic field induces a condensate that not only breaks a $U(1)$ symmetry, but also translation symmetry. The magnitude of the condensed field, and thus the magnitude of the operator condensate in the field theory, is shown in figure 1.3. It forms a triangular lattice of Abrikosov vortices. The lattice spacing is determined by the strength of the magnetic field B; the stronger B, the more tightly the vortices are bound. When B vanishes the lattice spacing diverges, leaving a homogeneous ground state.

Abrikosov vortices were first discovered in certain superconductors called *type-II superconductors* [42,43]. They are due to the interaction between the superconducting condensate and an external magnetic field, but the mechanism is different from the one in this thesis. In type-II superconductors a small magnetic field pokes holes in the scalar condensate, each hole corresponding to a quantum of magnetic flux. Magnetic flux is conserved, so dialling up the strength of the field leads to more flux tubes forced through the condensate. Eventually the entire superconducting sample vanishes, replaced by a homogeneous magnetic field. But right before the critical point at which that happens, the flux tubes get packed tightly throughout the sample. They exert a repulsive force on each other, so they do not overlap. The configuration that minimises the ground state is the triangular lattice, the same configuration found in the very different model in this thesis.

Abrikosov vortices show up in many more superconducting systems. The type-II example above is what happens in BCS superconductors [44, 45]. The vortex

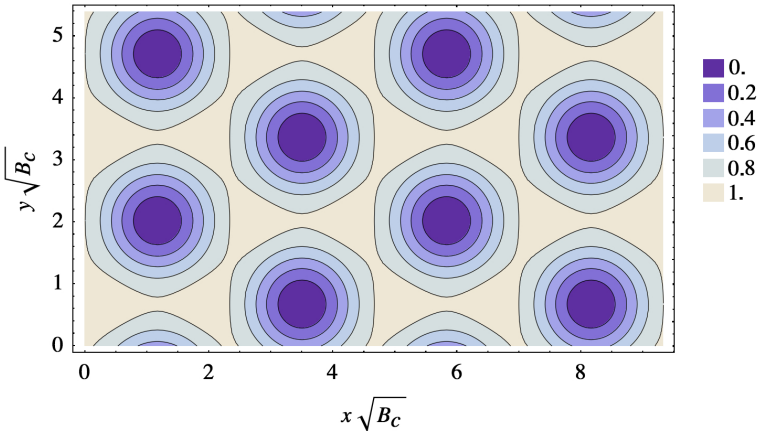

Figure 1.3: The magnitude of the condensed operator in the field theory of the simple gauge/gravity model with $SU(2)$ symmetry that we study in this thesis. At the centre of the dark vortices, the condensate vanishes. Lighter values correspond to larger values of the condensate. The magnitude is normalised to the maximum value it takes. The dimensions are displayed in units of the critical magnetic field strength at zero chemical potential. This result is calculated in chapter 5.

lattice is described well by Ginzburg–Landau theory [46] and its relativistic generalisation, the Higgs model. But they also appear in phenomenological models of QCD. The simplest such toy model is $SU(2)$ Yang–Mills theory in $(3+1)$-dimensions, where a gluon field condenses to form a triangular lattice in the presence of a magnetic field [47–51]. A similar effect is seen in the Nambu–Jona-Lasinio model and the DSGS model [52–57]. Electroweak theory also contains vortex lattice solutions. [58–61]

But just because vortex lattices appear in different models does not mean that their rediscovery in gauge/gravity duality is not interesting. Their appearance in our model as a result of a strong magnetic field shows that the effect is more general. It survives the large N limit that gauge/gravity duality requires. It has a gravity dual given by a novel black hole solution. And finally, the model is so simple that it seems likely we should see the effect in a broad class of theories, a hint at the universality of vortex lattice solutions.

The Kondo effect

Take a Landau–Fermi liquid of electrons and add a single magnetic spin impurity. At high energies, this is not interesting: the system behaves as an ensemble of free electrons decoupled from a magnetic impurity. Lower the temperature, however, and the impurity starts to couple to the electrons. The coupling increases as the temperature is lowered until, at the *Kondo temperature*, it diverges. The impurity forms a strongly coupled state bound to the electrons. In this state, the impurity's spin is completely screened. This strongly coupled phenomenon is known as the *Kondo effect* [62].

The Kondo effect is an example of a condensed matter system to which we can apply gauge/gravity duality [63]. We can in particular use it to learn more about the strongly coupled regime. But it can also help us learn about the duality itself, because the Kondo model has been studied in detail for decades and a solution

based on numerical renormalisation group methods exists [64]. It is rare that we find a strongly coupled field theory with known results that we can use as independent confirmation of a gauge/gravity model.

In this thesis we are particularly interested in studying time-dependent phenomena in a holographic Kondo model, and the associated technical challenges to be overcome. The Kondo coupling depends on the temperature and has a definite value once the system is in thermal equilibrium. But there are experiments in systems analogous to the Kondo setup where it is possible to effectively alter the value of the coupling for a short time, then watch it relax back to its equilibrium value. In this thesis we study this problem. We quench the effective Kondo coupling in the holographic Kondo model presented in [63]. On the gravity side, this involves implementing time-dependent boundary conditions in a scalar field. The resulting partial differential equations must be solved using techniques from numerical relativity.

The work is ongoing, but there are some preliminary results, calculated in a limit where the scalar field does not backreact onto the background geometry.

Achievements of this thesis

The original results in this thesis focus on holographic superconductors. Both the vortex lattice solutions and the strongly-coupled phase of the holographic Kondo model come about through superconducting phase transitions. The focus is specifically on inhomogeneous ground states. This is interesting from the perspective of both condensed matter physics and black hole physics. The inhomogeneous ground states correspond to novel black hole solutions.

In particular, for our study of inhomogeneous ground states we focus on a simple holographic model where the gravity theory is on an asymptotically AdS_5 background. We consider two different models, described in section 5.1. In the first, the AdS_5 contains a black hole horizon at a fixed radial distance. This models a finite-temperature field theory. In the second the geometry is cut off at a fixed radial distance, yielding a confining field theory. In both models we also include an $SU(2)$ Yang–Mills field and switch on a magnetic component B. We find:

1. **A black hole instability from the magnetic field**
   Increasing the strength of the magnetic field induces an instability in the background solution. We find this instability through the use of a *quasinormal mode* analysis in section 5.3.2. The instability indicates that the black hole background with a single magnetic component of the Yang–Mills field is not stable when B is above a critical value B_c. Additional components of the Yang–Mills field need to be switched on as well.

   This result was published in [1, 3].

2. **The new ground state forms a triangular vortex lattice**
   Finding the new ground state requires a perturbative expansion. This is only accurate when the condensate is small, which is the case at values near B_c. We perform the perturbative analysis, solving the equations up to third order. At first order we can tell that the ground state should be a lattice. To find the precise form of the lattice, whether it is for example square, triangular, rhombic or parallelogrammic, we need to calculate the free energy of each configuration. This we can only do by going to third

order in the expansion. The results are presented in sections 5.8 and 5.9. The triangular lattice has the smallest total energy.

This result was published in [2, 4].

3. **The μ-B phase diagram**
   In section 6.1 we augment the model by including a finite chemical potential μ as well. We repeat the stability analysis to find the μ-B phase diagram. We again calculate the free energy to third order with μ nonzero and find that the triangular lattice is the minimal energy solution near the phase transition line.

In chapter 7 we shift focus to a different model, the holographic Kondo model developed in [63]. It is set in AdS_3, dual to a $(1 + 1)$-dimensional field theory. The spatial dimension in the field theory is bisected by an impurity, modelled on the gravity side as a brane stretching from the AdS_3 boundary into its bulk. The brane spans an AdS_2 subspace of the AdS_3. It contains a scalar field which lets us determine the Kondo coupling.

4. **Time-dependent problems in the holographic Kondo model**
   In section 7.4 we give the Kondo coupling a time-dependent quench while working in the probe limit. We numerically calculate the response of the system. This involves solving a numerical relativity problem with a bulge in a scalar field propagating into the black hole. We present the results of the computation done in two different ways.

Structure of this thesis

The outline of this thesis is as follows.

Chapter 2 We give motivation for the AdS/CFT correspondence and then discuss its original "derivation" by Maldacena in terms of a D-brane construction. We then show how the correspondence can be generalised.

Chapter 3 We discuss magnetic vortex solutions, first in the context of Ginzburg–Landau superconductors and their relativistic generalisation, then in the context of phenomenological models of QCD. We discuss how they can be created by external magnetic fields.

Chapter 4 We explain what a holographic superconductor is and present the construction of some simple holographic superconductor models. We also explain how the more realistic models have inhomogeneous ground states, and give examples.

Chapter 5 We present original work by the author showing that a strong $SU(2)$ magnetic field can lead to a superconducting phase transition in a simple holographic superconductor model. We go on to find the ground state in the superconducting phase and show that it forms a triangular Abrikosov lattice.

Chapter 6 Continuing the original work of the preceding chapter, we present two possible extensions to the model. The first includes a finite chemical potential. We find that the minimum energy state is also a triangular Abrikosov lattice.

Chapter 7 After a brief introduction to the Kondo problem and the various approaches to solving it, we discuss a holographic Kondo model from the literature. We then do an original study of time-dependent phenomena in this model.

Chapter 8 We give concluding remarks and an outlook on future work.

Conventions

In this thesis we set $c = \hbar = k_B = 1$. We always use the "mostly plus" metric convention, where only the time component of the metric has a minus sign. The word *vev* is an acronym for *vacuum expectation value.*

Chapter 2

Gauge/gravity duality

In 1997 Juan Maldacena published a landmark paper [24] conjecturing a duality between $\mathcal{N} = 4$ Super Yang–Mills theory in 4 dimensions and a type IIB superstring theory on $\mathrm{AdS}_5 \times S^5$. Through this *AdS/CFT correspondence* it suddenly became clear how a specific quantum field theory and general relativity on a given background could be viewed as two sides of the same coin. This new understanding not only gives insight into quantum gravity, but is also the first concrete example of the *holographic principle*, first proposed by Gerard 't Hooft [7] and Leonard Susskind [8]. Most importantly for this thesis however is that the correspondence gives new insight into strongly coupled field theories. In its simplest form, it provides a model relating a strongly coupled gauge theory to a weakly coupled gravity theory. By solving Einstein's equations it is possible to calculate properties — such as operator dimensions and expectation values — in a strongly coupled regime where perturbation theory is not applicable. And by generalising the original correspondence to field theories other than $\mathcal{N} = 4$ Super Yang–Mills, applications to strongly-coupled condensed matter systems or toy models of QCD become possible.

In a 2010 lecture series Joseph Polchinski presented an intuitive motivation for the AdS/CFT duality [65]. Polchinski starts by asking a question: Is it possible to form a spin-2 graviton as a bound state of two spin-1 gauge bosons? The answer turns out to be no. It comes in the form of a no-go theorem due to Weinberg and Witten [66]. The no-go theorem applies to an arbitrary field theory with a Lorentz-covariant energy-momentum tensor $T_{\mu\nu}$ and a massless spin-2 particle in the spectrum. Consider the matrix element

$$\langle \text{massless spin } 2, k | T_{\mu\nu} | \text{massless spin } 2, k' \rangle. \tag{2.1}$$

Weinberg and Witten show that this matrix element cannot exist — it has contradictory properties. The intuitive reasoning behind this is that it represents a local observable, and it is known that in general relativity it is impossible to define local observables. This is because there is no invariant local way of specifying a position in general relativity.

As we learned from the classic example of the Coleman–Mandula theorem, however, a no-go theorem is only as strong as its assumptions. And by relaxing one of the assumptions, there is still a way to make this idea work. The trick is in the holographic principle — we introduce an extra dimension. A black hole's entropy is proportional to its area in Planck units, not its volume [5, 6]. This is a hint

that the number degrees of freedom in a given volume in a gravitational theory is proportional to the surface area of the volume, and that a quantum gravity theory should be formulated in terms of degrees of freedom on a lower-dimensional surface. So the hidden assumption in the Weinberg–Witten theorem is that the spin-2 bound state exists in the same number of dimensions as its constituents. If we follow the hint from the black hole entropy formula, we can postulate that this graviton actually lives in a spacetime with one higher dimension.

The hidden extra dimension actually appears in some places in QCD phenomenology. One example comes from the BFKL analysis of the pomeron. In this analysis a gluon pair is described in terms of its centre of mass coordinates and the separation z. It turns out that the gluon pair wave function satisfies a 5-dimensional wave equation — one dimension higher than its constituent quarks — and interactions are approximately local in z. So the separation z behaves like an extra spacetime dimension.

It is natural to ask what this 5-dimensional space could be. To answer this, let us consider a field theory that is easy to deal with — a conformal field theory. In such a theory, all distance scales look the same. In particular, if we rescale the gluon pair, the centre of mass coordinates and separation scale z should scale in the same way. The most general space that is invariant under both this rescaling symmetry and 4-dimensional Minkowski symmetry is described by the metric

$$ds^2 = L^2 \frac{dz^2 + \eta_{\mu\nu} dx^\mu dx^\nu}{z^2}. \tag{2.2}$$

This is the metric for the Poincaré patch of 5-dimensional *Anti-de Sitter space* (AdS_5).

The intuition we have so far is the following. We are trying to see if a spin-2 graviton can emerge as a bound state of gauge bosons. In order to sidestep the Weinberg–Witten theorem, we claim that the resulting graviton lives in a space with one more dimension by appealing to the holographic principle. For a 4-dimensional CFT, the higher dimensional space is AdS_5. The CFT can be thought of as living on the boundary of the AdS_5. The CFT is also dual to the gravity theory, by which we mean that it should exactly describe the gravity theory in the AdS_5 bulk and vice versa.

In order for this picture to make sense, we need to enforce two limits. The first is that the field theory coupling is strong. Only then can we be sure that the two gauge bosons are bound tightly enough that they really behave like a graviton. The second is that we want to use classical Einstein gravity, so the AdS radius L must be large compared to the Planck length.

Using the holographic principle, it is simple to show that large L means that the dual field theory has a large number of degrees of freedom per site. We do the calculation for a d-dimensional field theory dual to a $(d+1)$-dimensional gravity theory. Firstly, the holographic principle says that

$$\frac{\text{Area of boundary}}{4G_N} \equiv N_d, \tag{2.3}$$

where N_d is the number of degrees of freedom in the field theory and G_N is the $(d+1)$-dimensional Newton constant. Both sides of this equation are infinite, so we need to regulate by putting the boundary on a lattice. Suppose that the boundary is a d-dimensional box of side length R and that each site has side length

ε. Then if we have a gauge theory with gauge group $SU(N)$, so there are roughly N^2 gluons, the total degrees of freedom in the theory goes like

$$N_d \sim \left(\frac{R}{\varepsilon}\right)^{d-1} N^2. \tag{2.4}$$

On the gravity side, we need to calculate the area of the boundary, A. It is

$$A = \int_{\mathbb{R}^{d-1}, z\to 0} d^{d-1}x\sqrt{-g} = \int_{\mathbb{R}^{d-1}, z\to 0} d^{d-1}x \frac{L^{d-1}}{z^{d-1}}, \tag{2.5}$$

where g is the determinant of the AdS_{d+1} metric. The area diverges in two ways. The first is from the integration over $\mathbb{R}^{d-1}$, and the second is from integrating too close to the boundary. We again put the boundary on a box of side length R, and we integrate only until $z = \varepsilon$. This ε is roughly the same as the one in the field theory picture, because it also imposes a minimum separation length z. We then have

$$A = \int_0^R d^{d-1}x \frac{L^{d-1}}{\varepsilon^{d-1}} = \left(\frac{RL}{\varepsilon}\right)^{d-1}. \tag{2.6}$$

Using this result with equations (2.3) and (2.4) then gives

$$N^2 \propto \frac{L^{d-1}}{G_N}, \tag{2.7}$$

which was what we claimed. A large AdS radius means that there are a large number of fields in the dual field theory. In fact, we will see in the more precise motivation for the AdS/CFT correspondence that the field theory is a *large N* field theory when the gravity theory is classical. Appendix A contains a brief introduction to the large N limit.

In this intuitive motivation for the AdS/CFT correspondence we have not mentioned anything about string theory. However, Maldacena's original 1997 publication used a D-brane construction to motivate the correspondence. In the next section we look at that motivation in some detail and in the process make the formulation more precise. We describe a detailed matching of parameters on both sides of the duality, as well as introducing the AdS/CFT dictionary for calculating operator expectation values from fields in the gravity theory. In section 2.3 we then show that the correspondence can be generalised, beyond AdS space and conformal field theory, to what should more appropriately be called *gauge/gravity duality*. This sets us up for the discussion of holographic superconductors in chapter 4, after a detour to discuss vortex line solutions in field theory without holography in chapter 3.

2.1 The original AdS/CFT correspondence

The motivation in the previous section gives an intuitive overview of why we can expect the AdS/CFT correspondence is true. In this section we make that intuition more precise by presenting Maldacena's original argument [24]. There are two excellent early reviews of this topic, a set of lecture notes by D'Hoker and Freedman [67] and an article known as the "MAGOO" review after its authors

Aharony, Gubser, Maldacena, Ooguri and Oz [68]. We follow a combination of both of these reviews in this section.

The picture to start with is that of a stack of N D3-branes in (9+1)-dimensional asymptotically Minkowski space in type IIB string theory. The branes are parallel and directly on top of each other in a $(3+1)$-dimensional subspace of the full spacetime. By taking the low energy limit of this setup in two different ways, we will find two different theories, which we then identify. One of these theories is $\mathcal{N}=4$ super Yang–Mills (SYM) theory in $(3+1)$-dimensions, and the other is type IIB string theory compactified on $\mathrm{AdS}_5 \times S^5$.

There are two kinds of perturbative excitations of string theory in this asymptotically Minkowski spacetime, open strings and closed strings. Looking at the setup from the perspective of these different types of strings will give the two different dual theories. The closed strings are excitations of empty space and give rise to spin-2 modes, that is, they give rise to gravity. At low energies, below the string scale $1/l_s$, only the gravity multiplet of type IIB supergravity remains. Open strings on the other hand have their endpoints on the D3-branes and describe excitations of the D-branes. Since these strings live on the worldvolume of the branes, they give rise to the SYM gauge theory. Below we make this description more detailed, and end up with the precise formulation of the AdS/CFT correspondence.

2.1.1 The open string picture

The open string picture focuses on the D-brane worldvolume theory, although closed strings are also considered. In general an open string stretched between two D-branes has a minimum length and thus a minimum mass. Since we are considering a stack of coincident D-branes, however, massless open string excitations exist. If we consider energies below the string scale, then only these massless modes are excited. An effective Lagrangian for both open and closed massless string states can be written down. It takes the form

$$S = S_{\text{bulk}} + S_{\text{brane}} + S_{\text{int}}. \tag{2.8}$$

The term S_{bulk} describes the dynamics of the closed strings. It is the action of $(9+1)$-dimensional type IIB supergravity plus some higher curvature corrections. The term S_{brane} is defined on the D3-brane worldvolume, since it only includes open string modes. It is the action of $\mathcal{N}=4$ super Yang–Mills theory with gauge group $SU(N)$. It also contains higher order corrections such as $\alpha'^2 \mathrm{tr}\left(F^2\right)$, but these vanish in the low energy ($\alpha' \to 0$) limit. The term S_{int} represents interactions between the brane modes and the bulk modes.

To see why the action term S_{brane} should give $\mathcal{N}=4$ super Yang–Mills, consider the open strings on the stack of branes. If the stack has only one brane, so that $N=1$, a massless open string excitation brings a $U(1)$ gauge symmetry on what is effectively (3+1)-dimensional flat space. The brane is a 1/2 BPS object, so it breaks half of the supersymmetries to yield $\mathcal{N}=4$. We thus have a $U(1)$ gauge theory with $\mathcal{N}=4$ Poincaré supersymmetry. In the low energy approximation, this theory is free.

Now consider $N>1$ D3-branes in the stack. Open string states attached to these branes now have labels corresponding to the branes on which they end. These labels are known as *Chan–Paton factors*. Since the branes are all indistinguishable

(they are on top of each other), the Chan–Paton brane labels can be reassigned between the branes according to a $U(N)$ symmetry group. This explains why the effective theory on the brane has a $U(N) = SU(N) \times U(1)$ gauge group. The $U(1)$ factor can be ignored, however; it corresponds to the overall position of the branes so it may be neglected when considering only the worldvolume theory.

The bulk term S_{bulk} describes a free supergravity theory. The part of the action containing the graviton can be expanded schematically as

$$S_{\text{bulk}} \sim \frac{1}{2\kappa^2} \int d^{10}x\sqrt{-g}R \sim \int (\partial h)^2 + g_s(\alpha')^2(\partial h)^2 h + \dots, \tag{2.9}$$

where we have written the action as $g = \eta + \kappa h$ and used that $\kappa \sim g_s(\alpha')^2$. In the low energy limit, $\kappa \to 0$ and so the interaction terms drop out. The same thing happens for the parts of the action containing the other supergravity fields.

In the same way, the interaction term S_{int} also vanishes in the low energy limit. In the open string picture we thus have a worldvolume SYM gauge theory decoupled from a free $(9+1)$-dimensional supergravity theory in the low energy limit.

2.1.2 The closed string picture

The low energy limit from the closed string point of view involves studying the supergravity setup in more detail. The metric for the stack of N D3-branes in $(9+1)$-dimensional type IIB supergravity can be written as

$$ds^2 = \left(1 + \frac{L^4}{y^4}\right)^{-\frac{1}{2}} \eta_{\mu\nu} dx^\mu dx^\nu + \left(1 + \frac{L^4}{y^4}\right)^{\frac{1}{2}} \left(dy^2 + y^2 d\Omega_5^2\right). \tag{2.10}$$

The x^μ are the brane worldvolume coordinates. y and Ω_5 are the transverse coordinate, with y providing a measure of radial distance from the branes. L is the *radius* of the D3-branes, and it can be shown to satisfy the relation

$$L^4 = 4\pi g_s N (\alpha')^2. \tag{2.11}$$

In addition the solution contains a self-dual 5-form field strength

$$F_5 = (1 + *) dt \wedge dx^1 \wedge dx^2 \wedge dx^3 \wedge dH^{-1}, \tag{2.12}$$

where $H(y) = 1 + \frac{L^4}{y^4}$.

We see from the metric component g_{tt} that the energy E_y of an object measured at y is related to the energy E measured at infinity by $E = \left(1 + \frac{L^4}{y^4}\right)^{-\frac{1}{4}} E_y$, which is the observed redshift. In other words, the same object would look to an observer at infinity as if it had lower and lower energy as it gets moved closer to the branes. This means that there are two kinds of low energy excitations that an observer at infinity sees. The first is from excitations that are brought arbitrarily close to the branes at $y = 0$. The second is from massless excitations with wavelengths much larger than the brane radius L and are thus blind to the branes. These two types of excitations decouple from each other in the low energy limit, because the long wavelength excitations do not see the brane and the near horizon excitations cannot escape the brane's gravitational potential.

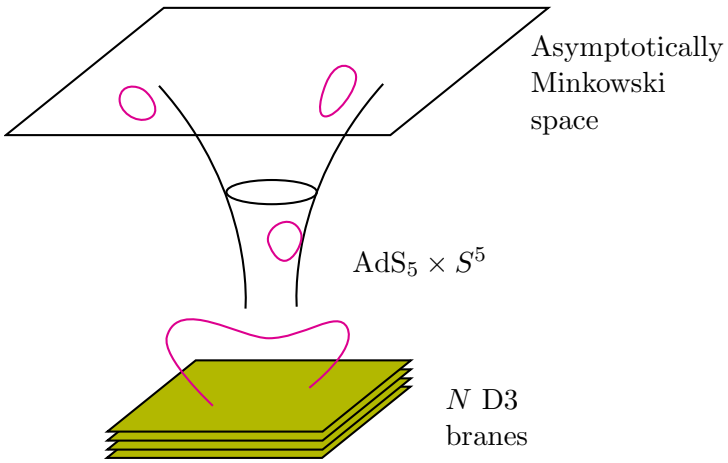

Figure 2.1: A visual representation of the near-brane limit. Asymptotically the spacetime is Minkowski. Near the branes it tends to AdS$_5 \times S^5$. In the open string picture, the region on the branes becomes $\mathcal{N} = 4$ super Yang–Mills theory with gauge group $SU(N)$. This led Maldacena to propose that there is a duality between the two theories.

To examine the system near the branes, we define the coordinate $u = \frac{L^2}{y}$ and take the limit where $u \gg L$. The metric becomes

$$ds^2 = \frac{L^2}{u^2}\eta_{\mu\nu}dx^\mu dx^\nu + \frac{L^2}{u^2}du^2 + L^2 d\Omega_5^2. \tag{2.13}$$

This is the metric for the space AdS$_5 \times S^5$, with AdS radius L and radius coordinate u. The boundary of the AdS space is at $u = 0$. This setup is illustrated in figure 2.1.

2.1.3 Maldacena's conjecture

The previous sections presented two pictures of the low energy limit. From the open string point of view there is a free supergravity theory in $(9+1)$-dimensions and an $\mathcal{N} = 4$ super Yang–Mills gauge theory. From the closed string point of view there is the same free supergravity theory $(9 + 1)$-dimensions and a type IIB supergravity theory on AdS$_5 \times S^5$. The Maldacena conjecture is that these two theories are *dual*, meaning that they are exactly equivalent descriptions of the same physical system.

The full AdS/CFT conjecture is slightly more general than the motivation described above. It comes in three different forms.

The strongest form

The *strongest* form of the AdS/CFT correspondence states that there is an equivalence between $\mathcal{N} = 4$ super Yang–Mills theory in (3+1)-dimensions with gauge group $SU(N)$ and full type IIB superstring theory on AdS$_5 \times S^5$. There is a matching of parameters, with the Yang–Mills coupling constant related to the string coupling constant by $g_{YM}^2 = 4\pi g_s$, and the AdS radius L given by $L^4 = 4\pi g_s N(\alpha')^2$.

The field-operator map, to be explained below, holds. In addition, the flux of the F_5 form over the S^5 is constrained by $\int_{S^5} F_5 = N$. This form of the correspondence holds for all values of the parameters L, g_s, α' and N. For this reason it is difficult to test. In particular, when g_s and α' are not small, we are in the regime of full non-perturbative quantised type IIB superstring theory.

The strong form

The *strong* form of the conjecture is obtained by taking the 't Hooft limit of the theory in the strongest form. The 't Hooft limit [69] is defined by sending $N \to \infty$ while keeping $\lambda = g_{YM}^2 N$ fixed. It has the effect of suppressing all non-planar Feynman diagrams in a perturbative expansion of the gauge theory. Since $g_s = \frac{\lambda}{N} \ll 1$, the superstring theory becomes classical, and α' remains finite.

The weak form

The *weak* form of the conjecture is obtained by taking the additional large λ-limit. Taking these two limits together is known as the Maldacena limit. The correspondence turns into one between an $\mathcal{N} = 4$ super Yang–Mills theory at strong coupling ($\lambda \gg 1$) with gauge group $SU(N)$ for N large in (3+1)-dimensions and a classical type IIB supergravity in the bulk. The large λ limit is equivalent to the small α' limit through the relation $L^4 = \lambda(\alpha')^2$, which turns the string theory into a supergravity theory.

Soon after Maldacena proposed the conjecture, Edward Witten expanded upon it in [25]. He introduced a precise matching between fields in the bulk $\mathrm{AdS}_5 \times S^5$ and operators in the dual field theory. The idea is that the bulk fields tend to a specific value on the boundary of the AdS space. Conceptually one can think of the boundary as where the field theory "lives"[1]. The boundary values of the fields become sources for operators in the dual field theory. More precisely, for a bulk theory with fields ϕ,

$$Z_{\text{bulk}}\left[\phi(u,\vec{x})|_{u\to 0} = \phi_0(\vec{x})\right] \equiv \left\langle e^{\int d^4x \phi_0(\vec{x})\mathcal{O}(\vec{x})} \right\rangle, \tag{2.14}$$

where the Z is the partition function of the bulk theory, and the correlator is calculated in the dual field theory. $\mathcal{O}$ is an operator in the field theory. This is known as the field-operator map. It makes it possible to do actual calculations using the correspondence, and will be very useful in this thesis.

The AdS/CFT correspondence is a holographic duality. This means that all the degrees of freedom of a theory with gravity in $(4+1)$-dimensions can be described by a theory in $(3+1)$-dimensions — one dimension lower. The most famous evidence that a theory of quantum gravity is expected to have this behaviour comes from the *Bekenstein bound*, which states that the maximum entropy of a volume of space is $S_{\max} = \text{Area}/4G_N$ [70]. The intuitive argument for this is simple. Suppose that this bound was violated and there is some volume of space with entropy higher than $S_{\max}$. Then throw in more matter. The entropy should not decrease. When enough matter is thrown in, the volume should turn into a black hole, which has entropy $S_{\max}$. Provided that the second law of thermodynamics is

[1] Be careful though — in the near-brane limit (2.13), the brane worldvolume is actually at $u = \infty$, deep in the bulk!

not violated, this is a contradiction. Therefore the Bekenstein bound holds. And notice what this implies — the number of degrees of freedom of a system scales like the area of the boundary of the region, not as its volume. Standard quantum field theories do not behave in this way. The holographic principle is a way of understanding this result.

The weak form of the correspondence is the one that has been studied the most and for which the most evidence has accumulated. It is a strong/weak coupling duality, making it very useful. We can find results in a strongly coupled field theory by doing calculations in a weakly coupled gravity theory. It can also be generalised to what should more appropriately be called *gauge/gravity duality*. Extensions to the correspondence include adding a black hole to the bulk, which induces a finite temperature in the dual field theory. It is also possible to add a chemical potential. This is done by specifying a boundary value for a bulk gauge field. Both of these ingredients are important for this thesis' main results.

2.1.4 Matching symmetries

A first simple test of the correspondence is that the symmetries on both sides of the duality should be identical. This is indeed the case, as we now show, following [67].

$\mathcal{N} = 4$ super Yang–Mills theory in (3+1)-dimensions has the continuous global symmetry group $SU(2,2|4)$.[2] This group is made up of the following ingredients.

Conformal symmetry is generated by translations P^μ, Lorentz transformations $M_{\mu\nu}$, dilations D and special conformal transformations K^μ. They form the group $SO(2,4) \sim SU(2,2)$.

Poincaré supersymmetries are generated by the supercharges Q^a_α and their conjugates $\bar{Q}_{\dot{\alpha}a}$, where $a = 1 \ldots 4$.

R-symmetry is the symmetry under which the supercharges transform among each other. It forms the group $SU(4)_R \sim SO(6)$.

Conformal supersymmetries are needed to close the algebra. The Poincaré supersymmetries and the special conformal transformations K^μ do not commute. Their commutators give the conformal supersymmetry supercharges $S_{\alpha a}$ and their conjugates $\bar{S}^a_{\dot{\alpha}}$.

These global symmetries also exist on the gravity side. The maximal bosonic subgroup of $SU(2,2|4)$ is $SU(2,2) \times SU(4)_R \sim SO(2,4) \times SO(6)$. But $SO(2,4)$ is the isometry group of AdS_5 and $SO(6)$ is the isometry group of S^5, so the bosonic subgroups match easily. The matching of the supersymmetries works as follows. Half of the 32 Poincaré supersymmetry generators of type IIB superstring theory are broken by the stack of N D3-branes. In the AdS limit, however, the 16 remaining supersymmetries are supplemented by another 16 conformal symmetries that are not preserved in the full D3-brane background. The result is an $SU(2,2|4)$ global symmetry group on the gravity side.

Note that only global symmetries match. Gauge symmetries are redundancies of the description, so they are not relevant to the physics of the two theories. This

[2] $\mathcal{N} = 4$ super Yang–Mills theory also has an S-duality symmetry. In the 't Hooft limit this is no longer consistent, however. Since we are only interested in the weak form of the correspondence in this thesis, we will neglect this symmetry.

fact has practical importance. In later sections when we consider holographic superconductors, we look at spontaneous gauge symmetry breaking on the gravity side. On the field theory side however, because only the global part of the gauge symmetries is mapped, this corresponds to the breaking of a global symmetry.

2.2 Practicalities

How do we use the holographic dictionary (2.14) to do practical calculations? The main difficulty with the dictionary is that it has the partition function of a gravity theory on $\mathrm{AdS}_5 \times S^5$ on one side of the equation. But this is actually easy to address. If we focus on the weak form of the correspondence, the gravity theory is classical so the partition function is described well by the saddle point approximation,

$$Z_{\mathrm{bulk}} \approx e^{-S_{\mathrm{on-shell}}}, \tag{2.15}$$

where $S_{\mathrm{on-shell}}$ is the on-shell gravity action. This means that we should be able to calculate field theory correlation functions by taking functional derivatives of $e^{-S_{\mathrm{on-shell}}}$.

2.2.1 Example with a gauge field

Let us see how this works in practice with an example. In chapter 5 we consider a model with an $SU(2)$ gauge field in the bulk gravity theory. The classical gravity background is AdS_5; we have integrated out the S^5. The model exhibits spontaneous symmetry breaking, which results in some of the gauge field components becoming nonzero spontaneously, without a source. We can calculate the resulting vev in the field theory by making use of the dictionary relation

$$e^{-W_{\mathrm{CFT}}[\mathcal{A}^{(0)}]} = \langle e^{\int_{\partial AdS} \mathcal{A}^{(0)}_\mu J^\mu} \rangle = e^{-S_{\mathrm{on-shell}}}. \tag{2.16}$$

The minus sign on the right-hand side is because we have Wick-rotated to Euclidean space. W_{CFT} is the field theory effective action. Here $\mathcal{A}^{(0)}$ is the value of the gauge field $\mathcal{A}$ at the AdS boundary. It acts as a source in the boundary field theory. In the setup of chapter 5, the only source we want in the field theory comes from the component $\mathcal{A}^3_y = xB$, producing the magnetic field. For the other gauge field components there should be no explicit source.

The vev is found through the variation

$$\langle J^\mu \rangle = \left. \frac{\delta W_{\mathrm{CFT}}}{\delta \mathcal{A}^{(0)}_\mu} \right|_{\mathcal{A}^{(0)}_\mu = 0} = \left. \frac{\delta S_{\mathrm{on-shell}}}{\delta \mathcal{A}^{(0)}_\mu} \right|_{\mathcal{A}^{(0)}_\mu = 0}. \tag{2.17}$$

The second equality makes use of the gauge/gravity dictionary.

The trick to solving equation (2.17) for the vev is to recall the Hamilton–Jacobi equation from classical mechanics. This equation involves variations of the boundary value of a field. We reproduce the relevant part of that derivation here. Consider a general action

$$S = \int d^d x \int_{u_i}^{u_f} du \; \mathcal{L}(\mathcal{A}_\mu, \partial_\mu \mathcal{A}_\nu). \tag{2.18}$$

The x-directions are unbounded, while $u_i \leq u \leq u_f$. We assume that this action is on-shell, and consider what happens when we vary the value of $\mathcal{A}_\mu$ at u_i by a small amount, while keeping $\mathcal{A}_\mu$ fixed at the other boundary, $u = u_f$. Since the action is on-shell, $\mathcal{A}_\mu$ satisfies the equations of motion, so in general $\mathcal{A}_\mu(u)$ changes for all $u_i \leq u < u_f$ as we change its value at u_i. The variation is thus

$$\begin{aligned} \mathcal{A}_\mu(u) &\to \mathcal{A}_\mu(u) + \delta\mathcal{A}_\mu(u), \\ \delta\mathcal{A}_\mu(u_i) &= \delta\mathcal{A}_{i,\mu}, \qquad \delta\mathcal{A}_\mu(u_f) = 0. \end{aligned} \tag{2.19}$$

Under this variation, the on-shell action changes as

$$\begin{aligned} \delta S_{\text{on-shell}} &= \int d^d x \int_{u_i}^{u_f} du \left(\frac{\partial \mathcal{L}}{\partial A_\nu} \delta\mathcal{A}_\nu + \frac{\partial \mathcal{L}}{\partial\left(\partial_\mu \mathcal{A}_\nu\right)} \delta\left(\partial_\mu \mathcal{A}_\nu\right) \right) \\ &= \int d^d x \int_{u_i}^{u_f} du \left(\partial_\mu \frac{\partial \mathcal{L}}{\partial\left(\partial_\mu \mathcal{A}_\nu\right)} \delta\mathcal{A}_\nu + \frac{\partial \mathcal{L}}{\partial\left(\partial_\mu \mathcal{A}_\nu\right)} \partial_\mu \delta\mathcal{A}_\nu \right) \\ &= \int d^d x \int_{u_i}^{u_f} du\ \partial_\mu \left(\frac{\partial \mathcal{L}}{\partial\left(\partial_\mu \mathcal{A}_\nu\right)} \delta\mathcal{A}_\nu \right) \\ &= \int d^d x\ \left. \frac{\partial \mathcal{L}}{\partial\left(\partial_u \mathcal{A}_\nu\right)} \delta\mathcal{A}_\nu \right|_{u_i}^{u_f} \\ &= -\int d^d x\ \frac{\partial \mathcal{L}}{\partial\left(\partial_u \mathcal{A}_\nu\right)}(u_i) \delta\mathcal{A}_\nu(u_i). \end{aligned} \tag{2.20}$$

We used the Euler–Lagrange equations (because the action is on-shell) to get to the second line. This completes our formula for the vev:

$$\langle J^\mu \rangle = \left. \frac{\delta W_{\text{CFT}}}{\delta \mathcal{A}_\mu^{(0)}} \right|_{\mathcal{A}_\mu^{(0)}=0} = \left. \frac{\delta S_{\text{on-shell}}}{\delta \mathcal{A}_\mu^{(0)}} \right|_{\mathcal{A}_\mu^{(0)}=0} = -\int d^4 x \left. \frac{\partial \mathcal{L}}{\partial\left(\partial_u \mathcal{A}_\mu\right)} \right|_{u=0}. \tag{2.21}$$

It is interesting to note that the above derivation holds even though the on-shell Yang–Mills action can be written as

$$\begin{aligned} S_{\text{on-shell}} &= -\frac{1}{4\hat{g}^2} \int d^{d+1} x \sqrt{-g} F^a_{\mu\nu} F^{a\mu\nu} \\ &= -\frac{1}{2\hat{g}^2} \int_{\partial AdS} d^d x \sqrt{-\gamma} n_\mu A^a_\nu F^{a\mu\nu} \\ &\quad + \frac{1}{4\hat{g}^2} \int_{AdS} d^{d+1} x \sqrt{-g} \epsilon^{abc} A^a_\mu A^b_\nu F^{c\mu\nu}, \end{aligned} \tag{2.22}$$

where we integrated by parts and substituted in the equations of motion. n^μ is the normal vector to the boundary at $u = \epsilon$, pointing outwards, and thus given by $n = -\frac{1}{\sqrt{g_{uu}}} \frac{\partial}{\partial u}$. The second term on the right-hand side, the bulk term, is not present in non-interacting theories. This bulk term should seemingly influence the calculation of the condensate when varying with respect to the boundary value. It turns out that it makes no contribution, which is due to the derivation (2.20).

Expanding the gauge field near the AdS boundary, equations (2.16) and (2.21) tell us that we should get

$$\mathcal{A}^a_\mu(u, x)\big|_{u\to 0} = s^a_\mu(x) + v^a_\mu(x) u^2 + \ldots, \tag{2.23}$$

where $s^a_\mu(x)$ is the field theory source and $v^a_\mu(x)$ is the field theory vacuum expectation value.

One subtlety that we glossed over in equation (2.17) is that the on-shell action is not necessarily finite. This is due to the infinite volume of AdS space. In order to get finite quantities it is therefore necessary to regulate the action. This is a complex subject, and a good set of lecture notes on the topic is [71]. Here we simply point out that for the $SU(2)$ Yang–Mills action, the necessary counterterm to add is

$$S_{\mathrm{CT}} = -\frac{L}{4\hat{g}^2}\int d^dx\sqrt{-\gamma}\log(\varepsilon)F^a_{\mu\nu}F^{a\mu\nu}. \tag{2.24}$$

where γ is the (determinant of the) induced metric on the surface at $z=\varepsilon$. In the limit $\varepsilon\to 0$, the total action including this counterterm is finite.

2.2.2 More general operators

$\mathcal{N}=4$ super Yang–Mills is conformal with superconformal symmetry group $SU(2,2|4)$, so its operators can be characterised by the way they transform under this group. In particular, an operator $\mathcal{O}$ in a conformal theory is labelled by its scaling dimension Δ. Through the AdS/CFT correspondence, an operator's scaling dimension is related to the mass of a dual field ϕ.

To see this, consider a scalar field ϕ in the gravity theory dual to the operator $\mathcal{O}$. The scalar field satisfies the wave equation

$$\left(\Box_g - m^2\right)\phi = 0, \tag{2.25}$$

where $\Box_g$ is the Laplacian associated to the metric g defined in (2.13). The asymptotic solution for ϕ in these coordinates is

$$\phi(r) \sim u^{4-\Delta}A + u^{\Delta}B + \ldots, \tag{2.26}$$

where the quantity we have labelled as Δ is given by $\Delta = 2+\sqrt{4+L^2m^2}$. For $m^2>0$, the first term is non-normalisable while the second term is normalisable. This situation is slightly more complicated than the one for the gauge field, because now the boundary value of ϕ (as $u\to 0$) does not exist. Instead we need to define the field theory source by

$$\phi_0 = \lim_{u\to 0} u^{\Delta-4}\phi(u) = A. \tag{2.27}$$

We can then use the dictionary (2.14) to find that $B=\langle\mathcal{O}\rangle$. Since ϕ is a scalar, it has scaling dimension zero. This implies that A has scaling dimension $4-\Delta$ and $\langle\mathcal{O}\rangle$ has scaling dimension Δ.

This analysis can be repeated for fields of arbitrary spin. Because the gravity equations of motion are different for fields of different spin, the boundary asymptotics also changes. The relations between masses on the AdS_5 gravity side and scaling dimensions on the $(3+1)$-dimensional field theory side are [67]

scalars	$m^2L^2 = \Delta(\Delta-4)$
spin 1/2, 3/2	$\lvert m\rvert L = \Delta - 2$
p-form	$m^2L^2 = (\Delta-p)(\Delta+p-4)$
spin 2	$m^2L^2 = \Delta(\Delta-4)$.

	0	1	2	3	4	5	6	7	8	9
D3	×	×	×	×						
D7	×	×	×	×	×	×	×	×		

Table 2.1: The alignment of the D-branes in the D3/D7 setup in (9+1)-dimensional flat space. The integers in the first row represent the coordinate directions x^0–x^9. The time coordinate is x^0. This setup is stable.

These relations only hold in AdS_5 and for when the field is normalised in such a way that it satisfies the Klein–Gordon equation. For scalar fields this is automatic, but for fields with other spins this does not necessarily hold. The easiest way to see when a field will satisfy the Klein–Gordon equation is to look at its kinetic term in the action. For a scalar, there is one metric factor in $g^{\mu\nu}\partial_\mu\phi\partial_\nu\phi$. For a vector there are two: $g^{\mu\nu}g^{\sigma\tau}\partial_\mu\mathcal{A}_\sigma\partial_\nu\mathcal{A}_\tau$. So in (2.23) we got that $\Delta = 0, 2$ for the gauge field. To get the scalar's normalisation, we would have to absorb a factor of L/u into each of the two $\mathcal{A}$'s. This extra factor has the effect of changing $\Delta \to \Delta - 1$ in the boundary expansion of $\mathcal{A}$, in agreement with the formula for 1-forms in the table above.

2.3 Extensions

Ever since Maldacena discovered the original AdS/CFT correspondence with a gravity theory on $AdS_5 \times S^5$, a number of other holographically dual theories have been found. The simplest extension is to start from a stack of extremal black D3-branes, which amounts to generalising the AdS_5 part of the metric to AdS_5–Schwarzschild, adding a black hole. The black hole adds a temperature to the SYM theory. This was already done by the time Witten elucidated the correspondence in [25]. With a finite temperature it is possible to study thermodynamics in the field theory. A natural next step was to add a chemical potential, which is easily implemented in the boundary conditions of the gravity gauge field.

In 2002 Karch and Katz proposed another extension [72] that added flavour to the field theory. The idea is to add a stack of N_f probe D7-branes to the original stack of N D3-branes. The probe limit is a valid approximation when $N_f \ll N$. The setup is stable when the branes are aligned as in table 2.1. The near-D3-brane limit is then taken as before to give a gravity theory on $AdS_5 \times S^5$ with D7-branes spanning the AdS_5 and an S^3 subspace of the S^5. The D7-branes break the S^5 rotational symmetry.

On the field theory side, the D3-D7 setup gives an $\mathcal{N} = 2$ supersymmetry $SU(N)$ gauge theory that has N_f hypermultiplets in the fundamental representation of the gauge group as well as the usual $\mathcal{N} = 4$ super Yang–Mills degrees of freedom. The $\mathcal{N} = 4$ fields arise from the massless open string modes with endpoints only on the D3-branes (3-3 strings) as before. The $\mathcal{N} = 2$ fundamental hypermultiplets come from open strings stretched between the D3 and D7 branes (3-7 strings). The 7-7 strings decouple in the Maldacena limit and the $U(N_f)$ gauge group becomes a global flavour group. Using this setup, it becomes possible to model fields with the same symmetries as quarks and mesons, see [27].

In 2004 Tadakatsu Sakai and Shigeki Sugimoto proposed a holographic setup that can be thought of as describing (3+1)-dimensional large N QCD with massless

	0	1	2	3	(4)	5	6	7	8	9
D4	×	×	×	×	×					
D8-$\overline{\text{D8}}$	×	×	×	×		×	×	×	×	×

Table 2.2: The alignment of the D-branes in the Sakai–Sugimoto setup in $(9+1)$-dimensions. The integers in the first row represent the coordinate directions x^0–x^9. The time coordinate is x^0. The x^4 direction is compactified on a circle.

flavours [73, 74]. It is constructed in a type IIA superstring theory with N_f probe D8- and $\overline{\text{D8}}$-branes in a background containing a stack of N D4-branes with the x^4 direction compactified on a circle. There are anti-periodic boundary conditions for the fermions on the circle, which cause the fermions arising from the 4-4 strings to gain masses of order the inverse circle radius, breaking supersymmetry. The brane alignment is indicated in table 2.2.

The field theory interpretation of the Sakai–Sugimoto duality comes from the worldvolume theory on the D4-branes. In the UV it is a $(4+1)$-dimensional theory with quarks living on defects (the D8- and $\overline{\text{D8}}$-branes). In the IR the theory is $(3+1)$-dimensional, though. The most important feature of this model however is that it exhibits chiral symmetry breaking. The D8- and $\overline{\text{D8}}$-branes provide a $U(N_f) \times U(N_f)$ symmetry group. This is spontaneously broken when the branes join into a single curved D8-brane, leaving only a single $U(N_f)$ subgroup. The symmetry breaking results in a Nambu–Goldstone boson that can be identified with the pion.

Because it is more similar to QCD than other holographic models, the Sakai–Sugimoto model also has many applications. Relevant to this thesis is the work by [75], in which a similar instability at large magnetic field to the one presented in chapter 5 was found.

As a final example of a holographic duality arising from a string theory brane setup, we briefly discuss the ABJM model, first presented by Ofer Aharony, Oren Bergman, Daniel Louis Jafferis and Juan Maldacena in 2008 [76]. The field theory side of this duality is a $(2+1)$-dimensional $\mathcal{N}=6$ superconformal Chern–Simons matter theory with gauge group $U(N) \times U(N)$ and Chern–Simons levels k and $-k$. The gravity side, valid in the large N limit, is M-theory on $\text{AdS}_4 \times S^7/\mathbb{Z}_k$. It is also possible to take the 't Hooft limit where N becomes large but the ratio N/k remains fixed. Then the gravity side becomes type a IIA string theory on $\text{AdS}_4 \times \mathbb{CP}^3$. The brane construction motivating this theory is a stack of M2-branes placed at the singularity of the conifold $\mathbb{C}^4/\mathbb{Z}_k$. The conifold singularity is necessary to create the $S^7/\mathbb{Z}_k$ compact space. Otherwise, for M2-branes in asymptotically flat space, the near horizon solution is simply $\text{AdS}_4 \times S^7$.

The ABJM model sparked a mini-revolution in the field as researchers rushed to uncover the implications of the new duality. With more than 10 years of hindsight since the original AdS/CFT correspondence, it was clear which were the right questions to ask and understanding of the ABJM duality progressed rapidly. In [77], the author of this thesis and collaborators had a hand in uncovering some of the properties of dual giant gravitons in the gravity model. These are D2-branes wrapping an $S^2 \subset \text{AdS}_4$. We give the giants an angular momentum in the compact $\mathbb{CP}^3$, and analyse the stability of the setup. As $\frac{1}{2}$-BPS objects, the giants are protected against strong coupling corrections and so form an excellent set of states for probing the non-perturbative sector of type IIA string theory. They are

dual to Schur polynomials of scalar fields on the field theory side.

The extensions we have mentioned so far are all examples of what are known as *top-down models*. These are models that are motivated from explicit brane constructions in string theory. They are seen as more rigorous because they provide a precise matching of parameters between the two dual theories and the full Lagrangians on both the field theory and the supergravity theory are known. Another approach is to study *bottom-up models*. In these we aim to model a strongly coupled field theory holographically by describing the properties it should have. We then produce an ad hoc construction of a gravity dual by implementing the specific properties we would like the field theory to have. For example, suppose we wish to study a finite-temperature field theory in $(2+1)$-dimensions with vector fields transforming under a global $SU(2)$ symmetry. We would then choose a gravity dual on an asymptotically AdS_4–Schwarzschild background with an action that includes an F^2 term for an $SU(2)$ Yang–Mills gauge field.

Bottom-up models have the advantage that we can choose exactly what ingredients we want the field theory to have and construct the gravity action accordingly. The disadvantage though is that we do not know the precise Lagrangian of the field theory, or indeed whether the field theory dual is well-defined. The motivation for studying such models is that we can search for universal properties that hold for broad classes of field theories. A famous example is the Kovtun, Son and Starinets result [33] for the universality of the shear viscosity over entropy density ratio $\eta/s = \frac{\hbar}{4\pi k_B}$. This was shown to hold in a broad class of strongly interacting field theories that have a particular type of gravity dual. The dual theory must be isotropic[3] Einstein gravity in an asymptotically Anti-de Sitter black hole background. The authors of [33] conjecture that this result for η/s is a lower bound for a wide class of systems.[4] So even though a bottom-up model was studied, the result was profound and conjectured to be applicable to many different systems. For most of the rest of this thesis we work mainly with bottom-up models.

In the remainder of this section we review the description of field theories at finite temperature and chemical potential, and then show how these properties can be added to a holographic system. This prepares the discussion for the study of holographic superconductors in chapter 4.

2.3.1 Finite temperature in field theory and chemical potentials

There is a relationship between the generating functional of quantum field theory and the partition function of statistical mechanics that makes it possible to use quantum field theory techniques to calculate thermodynamic properties of a system. In this section we review this relationship briefly.

The first concept we need to introduce is the statistical density matrix, which can be represented by an operator that we call $\hat{\rho}$. It is used to describe a system with an uncertain preparation history — all that is known is the probability with which the system is in a certain pure quantum state. We illustrate its definition with an example. Suppose a system is in a state $|\psi\rangle$. We know that the expected value of an operator $\mathcal{O}$ is given by $\langle\mathcal{O}\rangle = \langle\psi|\mathcal{O}|\psi\rangle$. Now suppose the system is

[3] Note that in Einstein gravity with spontaneously broken rotational symmetry, the ratio η/s is non-universal; see [78].

[4] Interestingly, it is also possible to find a fermionic analogue of this universal bound. This was done in [79].

prepared in such a way that it could be in state $|\psi_1\rangle$ with probability p or state $|\psi_2\rangle$ with probability $(1-p)$. The two states are orthonormal. In general it is not possible to find a single state $|\xi\rangle$ such that the expectation value of $\mathcal{O}$ is given by $\langle\xi|\mathcal{O}|\xi\rangle$. The way to find the expectation value is by using the density matrix operator, and then

$$\langle\mathcal{O}\rangle = \frac{\mathrm{tr}\mathcal{O}\hat{\rho}}{\mathrm{tr}\hat{\rho}}. \tag{2.28}$$

The trace is defined as the sum over basis states, that is,

$$\mathrm{tr}\hat{A} = \sum_i \langle\psi_i|\hat{A}|\psi_i\rangle, \tag{2.29}$$

where $\{|\psi_i\rangle\}$ forms a complete orthonormal basis for the Hilbert space. In this example, we see that the density matrix operator must be given by

$$\hat{\rho} = p|\psi_1\rangle\langle\psi_1| + (1-p)|\psi_2\rangle\langle\psi_2|. \tag{2.30}$$

To check,

$$\begin{aligned}
\langle\mathcal{O}\rangle &= \frac{\mathrm{tr}\mathcal{O}\hat{\rho}}{\mathrm{tr}\hat{\rho}} && (2.31)\\
&= \frac{p\langle\psi_1|\mathcal{O}|\psi_1\rangle\langle\psi_1|\psi_1\rangle + (1-p)\langle\psi_2|\mathcal{O}|\psi_2\rangle\langle\psi_2|\psi_2\rangle}{p\langle\psi_1|\psi_1\rangle\langle\psi_1|\psi_1\rangle + (1-p)\langle\psi_2|\psi_2\rangle\langle\psi_2|\psi_2\rangle} && (2.32)\\
&= p\langle\psi_1|\mathcal{O}|\psi_1\rangle + (1-p)\langle\psi_2|\mathcal{O}|\psi_2\rangle, && (2.33)
\end{aligned}$$

which is what we want. From this it is clear that a general definition for the density matrix operator in a Hilbert space with basis $\{|\psi_i\rangle\}$ is

$$\hat{\rho} = \sum_i p_i|\psi_i\rangle\langle\psi_i|, \tag{2.34}$$

and thus an element of the density matrix is given by $(\rho)_{ij} = \langle\psi_i|\hat{\rho}|\psi_j\rangle$. Some restrictions on this definition are that [80]

1. $\mathrm{tr}\rho = 1$, which says that the total probability $\sum_i p_i = 1$,
2. $\rho = \rho^\dagger$, the hermiticity condition,
3. $p_i \geq 0$, so all the eigenvalues (probabilities) are non-negative.

The statistical density matrix operator is the fundamental object in equilibrium statistical mechanics. For the grand canonical ensemble, it is defined as

$$\hat{\rho} = \exp\left[-\beta\left(H - \mu_i\hat{N}_i\right)\right], \tag{2.35}$$

where H is the Hamiltonian of the system, μ_i are the chemical potentials and $\hat{N}_i$ are the number operators associated with those chemical potentials. If $\{|\psi_n\rangle\}$ form a complete set of orthonormal energy eigenstates, then the grand canonical partition function is given by

$$\begin{aligned}
Z = \mathrm{tr}\hat{\rho} &= \sum_n \langle\psi_n|\exp\left[-\beta\left(H - \mu_i\hat{N}_i\right)\right]|\psi_n\rangle && (2.36)\\
&= \sum_n e^{-\beta(E_n - \mu_i N_i)}\langle\psi_n|\psi_n\rangle && (2.37)\\
&= \sum_n e^{-\beta(E_n - \mu_i N_i)}. && (2.38)
\end{aligned}$$

Now consider a scalar field theory. Recall that, using the path integral formalism, we have that [81]

$$\langle\psi_a|e^{-iHt_f}|\psi_a\rangle = \int[d\pi]\int_{\psi(\vec{x},0)=\psi_a(\vec{x})}^{\psi(\vec{x},t)=\psi_a(\vec{x})}[d\psi]e^{i\int_0^{t_f}dt\int d^dx[\pi(x)\partial_t\psi(x)-\mathcal{H}(\pi,\psi)]} \tag{2.39}$$

for some state $|\psi_a\rangle$, where $\psi(x)$ is a field with conjugate momentum $\pi(x)=\partial_t\psi(x)$ and $H=\int_0^{t_f}\int d^dx\mathcal{H}$. The integration over $\psi(x)$ must begin and end with $\psi(\vec{x})$ while the integration over $\pi(x)$ has no restrictions. The partition function (with no chemical potentials) is given by

$$Z = \text{tr } e^{-\beta H} = \sum_a \int d\psi_a\langle\psi_a|e^{-\beta H}|\psi_a\rangle. \tag{2.40}$$

If we identify $\beta = t_f$ and switch to an imaginary time variable, $\tau = it$, then we get

$$Z = \int[d\pi]\int_{\text{PBC}}[d\psi]\exp\left\{\int_0^\beta d\tau\int d^dx\left[i\pi(x)\partial_\tau\psi(x)-\mathcal{H}(\pi(x),\psi(x))\right]\right\}, \tag{2.41}$$

where "PBC" stands for "periodic boundary conditions" and means that the integration over $\psi(x)$ is constrained such that $\psi(\vec{x},0)=\psi(\vec{x},\beta)$, but because of the trace the initial condition is not fixed and must take all values.

Let us now see how to add a chemical potential. The thermodynamic dual of the chemical potential is the charge, and in order to have charge we need to augment this theory to a complex scalar field theory. We can consider a simple theory with a Hamiltonian given by

$$\mathcal{H} = \pi^\dagger\pi + \nabla\psi^\dagger\cdot\nabla\psi + V(\psi^\dagger,\psi), \tag{2.42}$$

where the canonical momentum $\pi=\partial_t\psi^\dagger$ and a conserved current density

$$j_\mu = i(\psi^\dagger\partial_\mu\psi - \psi\partial_\mu\psi^\dagger). \tag{2.43}$$

The conserved charge is the time component of the current,

$$N = \int d^dx\mathcal{N} = \int d^dx\ i(\psi^\dagger\pi^\dagger - \psi\pi). \tag{2.44}$$

We can use this and the definition (2.36) to write the grand canonical partition function as

$$Z = \int[d\pi^\dagger][d\pi]\int_{\text{PBC}}[d\psi^\dagger][d\psi]e^{\int_0^\beta d\tau\int d^dx\left[i\pi^\dagger\partial_\tau\psi^\dagger+i\pi\partial_\tau\psi-\mathcal{H}(\pi,\psi)+\mu\mathcal{N}(\pi,\psi)\right]}, \tag{2.45}$$

where we replaced $\mathcal{H}\to\mathcal{H}-\mu\mathcal{N}$, with μ the chemical potential. If we now expand the integrand in the exponential, it can be written as

$$\begin{aligned}&-\left[\pi^\dagger - i(\partial_\tau-\mu)\psi\right]\left[\pi - i(\partial_\tau+\mu)\psi^\dagger\right]\\&\quad-(\partial_\tau+\mu)\,\psi^\dagger\,(\partial_\tau-\mu)\,\psi - \nabla\psi^\dagger\cdot\nabla\psi - V(\psi^\dagger,\psi).\end{aligned} \tag{2.46}$$

Only the first term depends on the conjugate momenta. If we think of the contributions $-i(\partial_\tau-\mu)\psi$ and $-i(\partial_\tau+\mu)\psi^\dagger$ as nothing more than shifts in the integration

variables, we can integrate out the first term to get some constant factor. We will ignore this constant factor because normalising the partition function will make it go away. Restoring the Minkowski time variable, we get

$$Z = \int [d\psi^\dagger][d\psi] e^{i\int_0^{t_f} dt \int d^d x \left[(\partial_t + i\mu)\psi^\dagger(\partial_t - i\mu)\psi - \nabla\psi^\dagger\cdot\nabla\psi - V(\psi^\dagger,\psi)\right]}. \tag{2.47}$$

We recognise the integrand of the exponent to be an effective Lagrange density. The μ has the effect of changing the time derivative to $\partial_t - i\mu$. This is exactly the covariant derivative one gets when switching on a gauge field with time component $A_t = \mu$! This trick comes in handy for introducing a chemical potential to a holographic theory. Note however that the chemical potential only requires switching on the time component, and that there is no kinetic term for A in the Lagrangian. It is thus not the same as having a theory with a dynamical field.

The above explanation was general, but we can now apply it to the AdS/CFT correspondence. By considering a bulk theory that contains a gauge field A, we can switch on a chemical potential in the dual field theory by setting $A_t = \mu$. As we saw in (2.23), according to the gauge/gravity dictionary the expansion of A in $(4+1)$-dimensions is

$$A_t \sim \mu + \langle J^t \rangle u^2 + \ldots, \tag{2.48}$$

since A_μ is a source for a vector operator J^μ. The time component of a vector current is a density. We also know J^t must be a density because it couples to the chemical potential. Thus, in switching on a gauge field and calculating its asymptotic behaviour, we can create a dual gauge theory with both a chemical potential and a finite density that we can calculate from the gravitational side.

2.3.2 Black holes and thermal field theories

Having reviewed how to describe a field theory with a finite temperature, we show how in the dual gravity theory finite temperature is described by a black hole. We focus on the simple example where the gravity dual is AdS–Schwarzschild, but the basic idea generalises to other black hole backgrounds.

If we repeat Maldacena's argument using a stack of extremal black D3-branes instead, we can extend the AdS metric (2.13) to the metric for AdS_5–Schwarzschild space crossed with S^5. Let us take the bottom-up philosophy and neglect the compact S^5 space because we are not interested in the field theory $SU(4)_R$ symmetry. This is a consistent truncation to states with vanishing S^5 angular momentum on the gravity side. Let us also generalise the setup to $(d+1)$-dimensions, which is dual to a d-dimensional field theory. The metric we are interested in is

$$ds^2 = \frac{L^2}{u^2}\left(-f(u)dt^2 + \frac{du^2}{f(u)} + \delta_{ij}dx^i dx^j\right), \tag{2.49}$$

where $f(u) = 1 - \frac{u^d}{u_H^d}$ is a blackening factor and $i = 1, \ldots, d-1$.

We now do a Wick rotation by defining $\tau = it$ and also define the new coordinate $\rho^2 = u - u_H$. If we take the near-horizon limit, then $\rho^2/u_H \ll 1$, and we can expand $f(u) = f(u_H) + \rho^2 f'(u_H) = \rho^2 f'(u_H)$. The metric becomes

$$ds^2 = \frac{L^2}{u^2}\frac{4}{f'(u_H)}\left[\rho^2\left(\frac{f'(u_H)}{2}\right)^2 d\tau^2 + d\rho^2 + \frac{f'(u_H)}{4}\delta_{ij}dx^i dx^j\right]. \tag{2.50}$$

If we define $\phi = \frac{f'(u_H)}{2}$, the first two terms in the brackets are nothing but the metric on a two-dimensional flat surface. If $0 \leq \phi \leq \phi_{max} < 2\pi$, this surface is a cone, if $0 \leq \phi < \phi_{max} > 2\pi$, the surface is a saddle, and if $0 \leq \phi \leq 2\pi$ then the surface is a 2-plane. The space we started out with is regular everywhere on the horizon, so in these new coordinates it must be as well. Demanding regularity, we must choose the 2-plane because the other flat surfaces have a singularity at $\rho = 0$. This means we must choose that $0 \leq \tau < \frac{4\pi}{f'(u_H)}$, which translates to making the identification $\tau \sim \tau + \pi u_H$.

As we learned in the previous section, making a periodic identification in an imaginary time variable $\tau \sim \tau + \beta$ is the way to produce the partition function of a field theory at a finite temperature $T = 1/\beta$. We thus see that introducing a black hole in the AdS space is equivalent to making the boundary theory a finite temperature field theory. The temperature is $T = \frac{d}{4\pi u_H}$. This is the Hawking temperature of the black hole.

Now that we have a temperature, we can do more thermodynamics. We stay in the Euclidean signature. The gravity setup is described by the action

$$S_E = -\frac{1}{2\kappa^2}\int d^{d+1}x\sqrt{g}\,(R - 2\Lambda) + \frac{1}{2\kappa^2}\int_{u\to 0} d^d x\sqrt{\gamma}\left(-2K + \frac{2(d-1)}{L}\right). \tag{2.51}$$

The action is split into a bulk part integrating over the full space with metric g and a boundary part with induced metric γ. κ^2 is the gravitational coupling in $(d+1)$-dimensions. The bulk integral contains the Einstein–Hilbert term and the cosmological constant, which is $\Lambda = -\frac{d(d-1)}{2L^2}$ in Anti-de Sitter space. There are also two boundary terms. The first is the Gibbons–Hawking–York boundary term [82, 83]. This is necessary so that the variational principle is well-defined on manifolds with a boundary. K is the trace of the extrinsic curvature, $K = P^{\mu\nu}\nabla_\mu n_\nu$, where $P^{\mu\nu} = g^{\mu\nu} - n^\mu n^\nu$ is a projector onto the boundary and n^μ is the outward-pointing normal to the boundary surface. The final term is a local counterterm. It is necessary for holographic renormalisation, so that the on-shell action is finite. It serves the same purpose as the counterterm (2.24).

Plugging the Euclidean version of the metric (2.49) into the action, we find

$$S_E = -\frac{(4\pi)^d L^{d-1}}{2\kappa^2 d^d} V_{d-1} T^{d-1}, \tag{2.52}$$

where V_{d-1} is the spatial volume of the field theory. One thing to be careful about when doing this calculation is that the bulk integral goes from $u = 0$ to $u = u_H$, that is, the integral does not reach beyond the horizon. Now we can use the gauge/gravity dictionary to calculate the CFT partition function,

$$Z_{CFT} = e^{-S_E}. \tag{2.53}$$

From the partition function we can calculate the free energy

$$F = -T\ln Z = -\frac{(4\pi)^d L^{d-1}}{2\kappa^2 d^d} V_{d-1} T^d, \tag{2.54}$$

and the entropy

$$S = -\frac{\partial F}{\partial T} = \frac{(4\pi)^d L^{d-1}}{2\kappa^2 d^{d-1}} V_{d-1} T^{d-1}. \tag{2.55}$$

This calculation made use of the gauge/gravity dictionary. But it agrees with the Bekenstein–Hawking entropy formula, as we can check. The area of the black hole event horizon is simply given by the volume integral

$$A = \int_{u=u_h, t=\text{fixed}} d^{d-1}x\sqrt{-g} = \left(\frac{L}{u_H}\right)^{d-1} V_{d-1}. \tag{2.56}$$

Using the entropy formula and $T = \frac{d}{4\pi u_H}$ we get

$$S = \frac{A}{4G_N} = \frac{2\pi A}{\kappa^2} = \frac{(4\pi)^d L^{d-1}}{2\kappa^2 d^{d-1}} V_{d-1} T^{d-1}. \tag{2.57}$$

As promised, the gauge/gravity dictionary reproduces the results known from the Bekenstein–Hawking entropy formula!

2.4 Summary

Maldacena's conjecture gave us the foundations on which to build gauge/gravity duality. In its original, weak form it claims that there is a duality between $\mathcal{N} = 4$ super Yang–Mills theory with gauge group $SU(N)$ at large N and classical type IIB supergravity theory on $\mathrm{AdS}_5 \times S^5$. But we can generalise the duality. We can add a finite temperature, chemical potential or flavour. We can also build bottom-up models where we choose the number of dimensions or the matter content. The result is a recipe for constructing strongly coupled field theories in which it is possible to calculate results by solving Einstein's equations.

In the following chapters we use this powerful recipe to learn about strongly coupled systems. The original results in chapter 5 concern Abrikosov vortices in holographic superconductors, while the results in chapter 7 focus on a particular holographic Kondo model. In preparation for these chapters, we first discuss Abrikosov vortices in chapter 3 and holographic superconductors in chapter 4.

Chapter 3

Magnetic vortex lines

Vortex lines were the first of the topological objects discovered in gauge theories with spontaneously broken symmetry. They are found in the Ginzburg–Landau model of superconductivity in type-II superconductors, in the work by Ambjørn, Nielsen and Olesen resulting from a gluon instability [47–51] or a W-boson instability [58–61], and in various phenomenological models of QCD from a ρ-meson instability [52–57]. The original work presented in this thesis adds to the list: they also show up in holographic superconductors where the instability is triggered by an $SU(2)$ magnetic field.

In this chapter, however, we review what is known about vortex lines. We give an overview of how vortex lines arise in Ginzburg–Landau theory in section 3.1. This overview serves the additional purpose of introducing conventional superconductors, providing background for the study of holographic superconductors in chapter 4. In section 3.2 we make the Ginzburg–Landau model relativistic and encounter the Nielsen–Olesen vortex. We explore the structure of the vortex; at its core, the superconducting condensate vanishes and at its border the magnetic field decays exponentially. Section 3.3 defines what a type-II superconductor is and explains that it can exhibit a full lattice of vortices. Finally, in section 3.4 we pick two QCD toy models and study the instabilities that lead to similar vortex lattices there. These instabilities are especially relevant to the original work in this thesis because they are also induced by a magnetic field.

3.1 Ginzburg–Landau effective field theory model

The first microscopic theory of superconductors was developed in 1957. It provides a good description of low-temperature superconductors and is known as BCS theory, after John Bardeen, Leon Cooper and John Schrieffer [44, 45]. The theory describes the condensation of Cooper pairs of electrons at low enough temperatures into a boson-like state. The presence of this state acts as an order parameter for superconductivity. The theory was so successful that it won its discoverers the Nobel prize in physics in 1972. The full microscopic theory of superconductivity is however too complex for our needs, so instead we focus on an effective theory that hides the unnecessary details. This theory is Ginzburg–Landau theory.

Ginzburg–Landau theory was developed by Vitaly Ginzburg and Lev Landau [46] in 1950, before the microscopic theory was understood. In a showcase of startling physical intuition, Ginzburg and Landau gave the central role of the

theory to a "pseudowavefunction" $\phi(\vec{x})$. $\phi(\vec{x})$ acts as the order parameter for the onset of superconductivity. When Gor'kov showed in 1959 [84] that the theory is a limiting case of BCS theory, it became clear that $\phi(\vec{x})$ is the wavefunction of the Cooper-paired electrons, with $n_s(\vec{x}) = |\phi(\vec{x})|^2$ representing their local density.

Ginzburg–Landau theory is a generalisation of the earlier London theory of superconductivity in that it can deal with non-linear responses to n_s and n_s can vary in space. It also reproduces the London equations. At temperatures near T_c, where the superconducting phase transition occurs, the theory best approximates BCS theory since here the spatial variations of $\phi(\vec{x})$ and the gauge field $\mathbf{A}(\vec{x})$ are small. As such it is useful for describing the macroscopic behaviour of a superconducting system where free energy rather than the detailed spectrum of excitations is important. Moreover, it is simpler than BCS theory for dealing with spatially inhomogeneous ground states.

The main postulate of Ginzburg–Landau theory is that if $\phi(\vec{x})$ varies slowly in space and is small, its free energy density can be written as an expansion

$$f_s = f_n + \tilde{\alpha}|\phi|^2 + \frac{\beta}{2}|\phi|^4 + \frac{1}{2m}\left|(\nabla - ie\mathbf{A})\,\phi\right|^2 + \ldots, \tag{3.1}$$

where f_n and f_s are the free energy density in the normal and superconducting phases, respectively. m and e are the effective mass and charge of ϕ. Given that β is positive, the idea is that $\tilde{\alpha} < 0$ below T_c and $\tilde{\alpha} > 0$ above T_c, and so the mechanism behind superconductivity is nothing but the Higgs mechanism. For this reason it makes sense to define $\tilde{\alpha} = \alpha(T - T_c)$, where α is a positive constant with dimensions of mass. The linear dependence of $\tilde{\alpha}$ on T makes sense when considering the series expansion of $\tilde{\alpha}(T)$ near T_c.

Notice that the model written above is non-relativistic. One way of generalising to the relativistic case indeed gives the Higgs model. From a modern field theory perspective, Ginzburg–Landau theory is easier to understand via the Higgs model, from which f_s can be derived. We thus consider the Abelian Higgs Lagrangian,

$$\mathcal{L} = -(\partial_\mu - ieA_\mu)\phi(\partial^\mu + ieA^\mu)\phi^* - m^2|\phi|^2 - \lambda|\phi|^4 - \frac{1}{4}F_{\mu\nu}F^{\mu\nu}. \tag{3.2}$$

We can easily obtain f_s from this Lagrangian. Assume that the system is static, so that $\partial_t\phi = 0$. We also go to Coulomb gauge, $\nabla \cdot \mathbf{A} = 0$, which in the absence of source charges means that $A_t = 0$. Lagrangian (3.2) then becomes

$$-\mathcal{L} = \frac{1}{2}(\nabla \times \mathbf{A})^2 + |(\nabla - ie\mathbf{A})\phi|^2 + m^2|\phi|^2 + \lambda|\phi|^4 + \ldots. \tag{3.3}$$

Setting $m^2 = \alpha(T - T_c)$ and $\lambda = \beta/2$ gives the expression for f_s above.

The equations of motion for this theory are

$$(\partial_\mu - ieA_\mu)^2\phi = m^2\phi + 2\lambda|\phi|^2\phi, \tag{3.4}$$

$$\partial^\nu F_{\mu\nu} = ej_\mu \equiv -ie(\phi^*\partial_\mu\phi - \phi\partial_\mu\phi^*) - 2e^2A_\mu|\phi|^2. \tag{3.5}$$

Spontaneous symmetry breaking occurs when $m^2 < 0$. Then the minimum of the potential is at

$$n_s \equiv |\phi_0|^2 = -\frac{m^2}{2\lambda} = \frac{\alpha}{2\lambda}(T_c - T). \tag{3.6}$$

Clearly ϕ is an order parameter for the onset of superconductivity: when $T > T_c$, $\phi = 0$ and when $T < T_c$, $\phi \neq 0$. Note also the mean field behaviour, $\phi \sim (1 - T/T_c)^{\frac{1}{2}}$, where the critical exponent is $\frac{1}{2}$.

Now consider the current (3.5) associated to the $U(1)$ symmetry of (3.2). When $T < T_c$ and the field ϕ varies only slightly over the distance of the system, the second term dominates and

$$\mathbf{j} = \frac{em^2}{\lambda}\mathbf{A} = -2e|\phi_0|^2\mathbf{A} \equiv -k^2\mathbf{A}. \tag{3.7}$$

This is one of the *London equations*, first written down in 1935 by the London brothers [85], relating the superconducting current and the surrounding electromagnetic field.[1] Since $\mathbf{E} = -\partial_t\mathbf{A} = 0$ and Ohm's law tells us that $\mathbf{E} = R\mathbf{j}$, we have found that $R = 0$. This is one of the defining characteristics of a superconductor.

One effect of great importance to this thesis was discovered experimentally in 1933. The *Meissner–Ochsenfeld effect*, named after the experimenters [39], is that superconductors expel magnetic fields. The Higgs model explains it as follows. We start from Ampère's law,

$$\nabla \times \mathbf{B} = \mathbf{j}, \tag{3.8}$$

and take the curl of both sides. Using $\nabla \cdot \mathbf{B} = 0$ and applying the London equation (3.7) gives

$$\nabla^2\mathbf{B} = k^2\mathbf{B}. \tag{3.9}$$

According to this equation, the background magnetic field outside a superconducting sample decays exponentially inside the sample. As we show in the next section, the characteristic decay length is $1/k = 1/\sqrt{2}e|\phi_0|$. What we learn is that any weak enough external magnetic field is effectively expelled from a superconducting sample. Moreover, it turns out that when the magnetic field is strong enough the superconducting state is destroyed completely.

3.2 The Nielsen–Olesen vortex

We saw in the previous section that, in certain circumstances to be detailed later, a magnetic field completely destroys a superconducting phase. This is the situation in what are known as *type-I superconductors*. In *type-II superconductors*, however, it is possible to have a relatively weak magnetic field coexist with the superconducting condensate. The magnetic field can poke a hole in the condensate, with this "hole" filled instead with a magnetic field vortex. This section is devoted to describing such a vortex.

The *Abrikosov vortex* of type-II superconductors was first discovered by Alexei Abrikosov in 1956 [42]. These vortices are present in Ginzburg–Landau theory. The vortices in the relativistic model of the previous section are known as *Nielsen–Olesen vortices*. In this section we carefully follow [86], the original work by Nielsen and Olesen that first constructed these vortices in the Higgs model in 1973.

[1] Note that this equation is not gauge invariant. This comes from the approximation that the derivative terms in the definition (3.5) of j_μ is small. Remember that when using the London equations we have to be in the Coulomb gauge, $\nabla \cdot \mathbf{A} = 0$.

When [86] was published, the dual resonance model of string-like hadronic matter based on [87] was still popular. This stringy model was later abandoned as a model of hadrons with the rise of QCD, but ultimately provided the seeds for the growth of string theory. Nevertheless, it did have some experimental success; it explained the Regge trajectory in meson scattering experiments.

Even with a string model, Nielsen and Olesen pointed out it was however still reasonable to expect that relativistic physics is described by field theory. They therefore tried to cook up a field theory with string-like structures. It turns out to be relatively easy to find vortex line solutions in the Higgs model with equations of motion identical to those of the Nambu dual string in a certain limit. This limit is that the string's radius of curvature is much larger than the width of the string.[2]

To find vortex solutions, we start by writing the scalar from (3.2) as

$$\phi = |\phi| e^{i\chi}. \tag{3.10}$$

From equation (3.5) we then get

$$A_\mu = -\frac{j_\mu}{2e|\phi|^2} + \frac{1}{e}\partial_\mu \chi. \tag{3.11}$$

We consider a magnetic field $B = F_{xy}$ in the z-direction. Assume there is no current. The magnetic flux going through a unit square in the xy-plane is given by

$$\Phi = \int F_{\mu\nu} d\sigma^{\mu\nu} = \oint A_\mu dx^\mu = \frac{1}{e}\oint \partial_\mu \chi dx^\mu, \tag{3.12}$$

where $d\sigma^{\mu\nu}$ is a two-dimensional surface element. Now we learn something interesting. Since ϕ is single-valued, χ changes by $2\pi n$ as we go around a closed loop, for integer n. Thus,

$$\Phi = n\Phi_0, \qquad \Phi_0 = \frac{2\pi}{e}. \tag{3.13}$$

The flux lines are quantised! This leads to a new interpretation of B: it is a measure of the number of flux lines passing through a unit square in the xy-plane.

Each flux line corresponds to a string-like vortex. Let us find a vortex solution from the equations of motion. We look for a cylindrically symmetric solution with z the axis of rotation. Choosing the gauge $A_t = 0$, this means we are looking for solutions of the type $A_\theta \equiv A(r)$, and $A_r = A_z = 0$. r is the radial coordinate and θ is the angular coordinate. From (3.12) we see that the flux is thus

$$\Phi(r) = 2\pi r A(r), \tag{3.14}$$

so that the magnetic field is

$$B = \frac{1}{2\pi r}\frac{d}{dr}\Phi(r) = \frac{1}{r}\frac{d}{dr}\left(rA(r)\right). \tag{3.15}$$

[2]While Nielsen and Olesen tried to obtain string-like behaviour from field theory, the author of this thesis hopes to obtain field theories from string theory. Interestingly, in both approaches we end up at the Nielsen–Olesen vortex line.

With this ansatz the equations of motion (3.4) and (3.5) become

$$-\frac{1}{r}\frac{d}{dr}\left(r\frac{d}{dr}|\phi|\right)+\left[\left(\frac{1}{r}+eA\right)^2+m^2+2\lambda|\phi|^2\right]|\phi|=0, \tag{3.16}$$

$$-\frac{d}{dr}\left(\frac{1}{r}\frac{d}{dr}(rA)\right)+2|\phi|^2\left(e^2A+\frac{e}{r}\right)=0. \tag{3.17}$$

An analytic solution to these equations is not available, but we can make some approximations. The vortex is localised near the origin, $r=0$. For large r, we expect A to decay and ϕ to be constant. Solving (3.16) under these assumptions, it is easy to show that

$$|\phi|\approx\phi_0=\sqrt{\frac{-m^2}{2\lambda}}. \tag{3.18}$$

This corresponds to the minimum of the Higgs potential, (3.6), as expected. Moreover, at large r we get that the magnetic field decays as

$$B\sim\sqrt{\frac{\pi\phi_0}{\sqrt{2}er}}e^{-\sqrt{2}e\phi_0 r}. \tag{3.19}$$

The picture that is emerging so far agrees with what we discussed in the previous section. At low energies, in the superconducting phase, we find a constant condensate ϕ_0. When we introduce a magnetic field, it penetrates the condensate and decays with the characteristic length λ_P given by

$$\frac{1}{\lambda_P}=\sqrt{2}e\phi_0. \tag{3.20}$$

This is known as the *penetration depth* of the magnetic field. We mentioned that a magnetic field destroys the superconducting phase, so we should find that the condensate also decays inside the magnetic vortex. To investigate this, we look at fluctuations ρ of ϕ about the vacuum solution ϕ_0. We write

$$|\phi|=\phi_0+\rho(x) \tag{3.21}$$

and look at the potential $V(\phi)=m^2\phi^2+\lambda\phi^4$. Its quadratic order term in ρ is $-2m^2\rho^2$. This implies that ρ has a Yukawa-type solution of the form

$$\rho(x)\sim e^{-\sqrt{-m^2}r}. \tag{3.22}$$

From this we can define the new characteristic length, known as the *coherence length*, by

$$\xi=\frac{1}{\sqrt{-m^2}}. \tag{3.23}$$

ξ is the approximate distance over which ϕ recovers its vacuum value.

Figure 3.1 summarises what we have learned about the vortex solution. In the next section we describe how this relates to type-II superconductors.

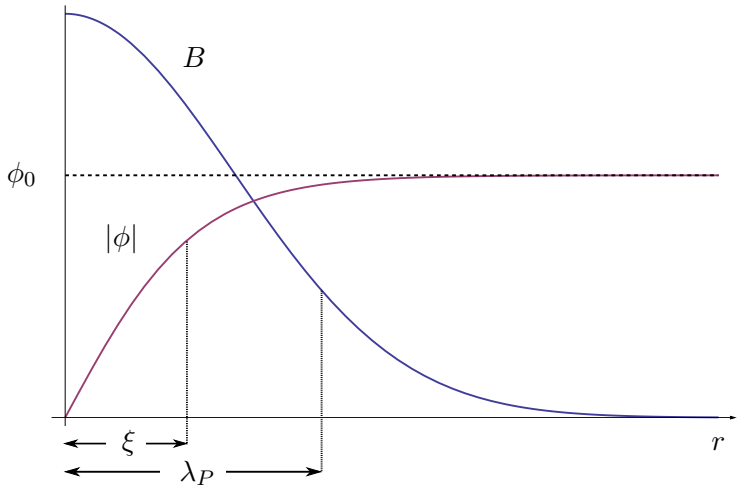

Figure 3.1: The approximate radial profile of the vortex solution. $|\phi|$ goes to a constant at large r and vanishes within the vortex. B decays with penetration depth λ_P and $|\phi|$ decays back to the vacuum solution with coherence length ξ.

3.3 A vortex lattice in type-II superconductors

We now have enough information to define the difference between type-I and type-II superconductors. We need to define the *Ginzburg–Landau parameter*, which is simply the ratio $\kappa = \lambda_P/\xi$ between the penetration depth and the coherence length. In the (non-relativistic) Ginzburg–Landau theory, it was shown that the behaviour of the superconductor changes depending on κ. For $0 < \kappa < 1/\sqrt{2}$ the system is known as a *type-I superconductor*. For $\kappa > 1/\sqrt{2}$ it is a *type-II superconductor*.

Type-I superconductors do not have magnetic vortex solutions in the standard Ginzburg–Landau treatment. At low temperature, in a superconducting sample where $\phi = \phi_0$, turning on an external magnetic field with large enough magnitude B would return the system to the normal phase. That is, there exists some critical value B_c of the external magnetic field above which the superconductivity is destroyed and $\langle\phi^2\rangle = 0$. The magnetic flux lines are expelled from the sample until they are strong enough to destroy the whole condensate.

Type-II superconductors are different. There are two critical values of the magnetic field. Increase an external magnetic field beyond the first, B_{c_1}, and the magnetic flux lines start to pierce the condensate, forming vortex line solutions throughout the sample. Each of these vortices is described by the solution depicted in figure 3.1. As we described earlier, each vortex has a unit of magnetic flux, so increasing B increases the number of vortices. Eventually, at the second critical value B_{c_2}, the magnetic field has poked so many holes in the condensate that it vanishes completely. Above B_{c_2} we are again in the normal phase.

The difference between the behaviours of the two superconductors can be traced to the surface energy of the condensate. Type-I superconductors have a positive surface energy. The qualitative argument for this is that there is an energy cost $\sim \xi B_c^2$ for the change of ϕ from its superconducting value to zero, with a gain of only $\sim \lambda_P B_c^2$ from reducing the magnetic field energy. Since the boundary between the superconducting state and the normal state costs energy, type-I su-

perconductors try to minimise the boundary length. For type-II superconductors, on the other hand, the argument is reversed. They have a negative surface energy so the boundary length is maximised for every unit of magnetic flux. This means that every flux tube is surrounded by superconducting condensate.

It is particularly interesting and relevant for this thesis to look at the ground state of a type-II superconductor at a magnetic field B beneath but very close to B_{c_2}. In this parameter regime, the maximum number of magnetic flux tubes have penetrated the condensate without destroying it. The flux tubes are parallel and arranged regularly. It turns out that the arrangement that minimises the total free energy of the setup is a triangular lattice. Next we present some of the calculations that substantiate these claims. We follow the presentation in [51]. In chapter 5 we show that in a simple holographic model, we find the same triangular lattice ground state.

To derive the vortex lattice solution we start with equations (3.4) and (3.5). As before, we choose an external magnetic field $B = F_{xy}$ pointing in the z-direction. The gauge choice is that $A_\mu = Bx\delta_{y\mu}$. B is smaller than, but very close to, B_{c2}. Then we are close to the transition point to the normal phase, so the quantity $|\phi|^2$ is very small. This means we can work with an expansion in small $|\phi|$ so that

$$F_{xy} = B + \mathcal{O}(|\phi|^2), \qquad F_{\mu\nu} = \mathcal{O}(|\phi|^2) \quad \text{otherwise}, \tag{3.24}$$

and we can linearise the equations of motion to give

$$\left(\partial_\mu - ieBx\delta_{y\mu}\right)^2 \phi = m^2\phi, \tag{3.25}$$

$$\partial^\nu F_{\mu\nu} = 2e^2|\phi|^2 \left(\frac{1}{e}\partial_\mu\chi - Bx\delta_{y\mu}\right). \tag{3.26}$$

In the second equation we used the decomposition (3.10). Using the Fourier transform and factoring out the t and z dependence,

$$\phi = \int \frac{dk}{2\pi} e^{iky} h(x) f(t,z), \tag{3.27}$$

we get a shifted quantum harmonic oscillator equation for h given by

$$-\frac{1}{2}\partial_x^2 h + \frac{e^2B^2}{2}(x - \frac{k}{eB})^2 h = -\frac{m^2}{2}h. \tag{3.28}$$

Here $\frac{k}{eB}$ is the x-position of the center of the classical Larmor orbital. The spectrum is discrete; there are solutions only for certain values $B = B_N$, where $N = 0, 1, 2, \ldots$. These values are given by

$$\left(N + \frac{1}{2}\right) eB_N = -\frac{m^2}{2} \tag{3.29}$$

We are interested in the ground state, so it makes sense to focus only on the lowest energy state where $B = B_0$. The solution for ϕ then becomes

$$\phi = \int \frac{dk}{2\pi} c(k) \exp\left\{iky - \frac{1}{2}eB\left(x - \frac{k}{eB}\right)^2\right\} f(t,z). \tag{3.30}$$

Here $c(k)$ is an arbitrary function of k. Using equation (3.26) it is then possible to show that

$$F_{xy} = B - e|\phi|^2. \tag{3.31}$$

To derive these solutions, we have made use of only the linear order equations. This is why the solution (3.30) is so general. To find the ground state of the system, we need to determine the function $c(k)$. This can only be done by going to higher order. The calculation is somewhat involved so we postpone the discussion to chapter 5, where we encounter this problem again. In that case we solve it for a simple holographic model by minimising the free energy of the system.

In this Higgs model, $c(k)$ is found by minimising the Gibbs free energy [51]. As mentioned above, the result is a triangular lattice of vortex flux lines; it is identical to the result depicted in figure 5.8.

3.4 Quantum chromodynamics and strong magnetic fields

There is a remarkable similarity between Abrikosov vortices in type-II superconductors and the ground state of various phenomenological models of quantum chromodynamics at strong magnetic fields. It was pointed out in the 1970's that in the presence of a background colour-magnetic field, a non-abelian gauge theory forms an unstable gluon mode [47]. There quickly ensued a flurry of papers exploring what this instability means for QCD [48–51]. These showed a number of interesting results, one of which is that in a popular phenomenological model of QCD, $SU(2)$ Yang–Mills theory, the ground state in the presence of a background colour-magnetic field contains randomly distributed vortex lines that are similar to Abrikosov vortices. These vortices were again discovered in studying electroweak theory [58–61], where it is the W-boson that condenses. Recently a series of papers by Maxim Chernodub and collaborators, working in a different model, presented similar results for a $U(1)$ magnetic field and ρ-meson condensate in various QCD models [52–57]. Since one of the main results of this thesis is that simple holographic models exist that contain vortex lattices as a ground state in the presence of a strong flavour-magnetic field, it is useful to review the earlier work here.

3.4.1 $SU(2)$ Yang–Mills

We start with the instability found in pure $SU(2)$ Yang–Mills theory in $(3+1)$-dimensional flat space by Ambjørn and Olesen, closely following [47,51]. Defining the new field

$$W_\mu = \frac{1}{\sqrt{2}}\left(A^1_\mu + iA^2_\mu\right), \qquad A_\mu = A^3_\mu, \tag{3.32}$$

the Lagrangian can be written as

$$\begin{aligned}\mathcal{L}_{YM} = &-\frac{1}{2}\left(\bar{D}_\mu \bar{W}_\nu - \bar{D}_\nu \bar{W}_\mu\right)\left(D^\mu W^\nu - D^\nu W^\mu\right) \\ &- \bar{D}_\mu \bar{W}^\mu D_\nu W^\nu - \frac{1}{4}F_{\mu\nu}^2 - \frac{1}{2}\left(\partial_\mu A^\mu\right)^2 \\ &- ig\left(\partial_\mu A_\nu - \partial_\nu A_\mu\right)\bar{W}^\mu W^\nu \\ &+ \frac{1}{4}g^2\left(W_\mu \bar{W}_\nu - W_\nu \bar{W}_\mu\right)^2,\end{aligned} \tag{3.33}$$

where

$$\begin{aligned}D_\mu &= \partial_\mu - igA_\mu, \\ F_{\mu\nu} &= \partial_\mu A_\nu - \partial_\nu A_\mu.\end{aligned} \tag{3.34}$$

The authors then switch on a homogeneous colour-magnetic field B in the 3-direction, choosing the gauge such that $A_y = Bx$. The linearised equations of motion for W_μ then become

$$-\left(\partial_\nu - igA_\nu\right)^2 W_\mu + 2igF^{\mu\nu}W_\nu = 0. \tag{3.35}$$

The second term in these equations is the crucial one. It is due to the magnetic moment of the gluon, and is responsible for an imaginary component of the vacuum energy. From [47], the vacuum energy can be written as a sum over energy modes of W_μ as

$$E_{\text{vac}} = \frac{VgB}{4\pi^2}\int_{-\infty}^{\infty} dk_z \sum_{n=0}^{\infty}\left\{\sqrt{2gB\left(n+\frac{3}{2}\right)+k_z^2} + \sqrt{2gB\left(n-\frac{1}{2}\right)+k_z^2}\right\}, \tag{3.36}$$

where V is the volume of all space and k_z is the z-momentum. The two terms in the integrand correspond to the different spin modes $S_3 = \pm 1$ of the W_μ field. The instability comes from the second term, when $n = 0$ and E_{vac} becomes imaginary.

In [47], the vacuum energy is also calculated for a scalar field and a fermion. In those cases there is no unstable mode. For the scalar this is due to its lack of spin. For the fermion this is due to an extra sign that comes in because of Fermi statistics.

For the spin-1 field W_μ, however, the unstable mode $W_\mu^{(0)}$ is present. It is stabilised when it takes the particular form

$$W_x^{(0)} = -iW_y^{(0)} \equiv W^{(0)}, \tag{3.37}$$

where $W^{(0)}$ takes the same form as the quantum harmonic oscillator wave function. This is given by

$$W^{(0)} = \int \frac{dk}{2\pi} c(k) \exp\left\{-\frac{1}{2}gB\left(x - \frac{k}{gB}\right)^2 + iky\right\} f(t,z), \tag{3.38}$$

where f is an arbitrary function of t and z and c is an arbitrary function of k. This is exactly the same function that one obtains for the condensate in type-II superconductors to linear order, the solution (3.30). Again, it is also the same

function that we obtain to linear order in chapter 5. When imposing the appropriate conditions on f, which come from the higher order equations and a physical argument, this function represents the condensate in a magnetic vortex lattice.

The physical argument works as follows. From the vacuum energy (3.36) we can see that the zero mode is only unstable for $k_z^2 < gB$. This means that the vacuum energy becomes imaginary when the external colour-magnetic field is constant over too large a distance. This means that it can't be constant. The next simplest thing is that the field is periodic — a lattice. Assuming periodicity and a state that minimises the energy, it is possible to put some constraints on f, and the end result is a lattice of Abrikosov vortices. We explain how this works in detail in section 5.4 for our holographic setup.

How is it that this solution is so similar to type-II superconductors? This is easy to see with a bit more work. It's possible to show that, to this order, the only vanishing part of the field strength tensor F up to anti-symmetry is

$$F_{xy}^3 = B - 2g|W^{(0)}|^2. \tag{3.39}$$

From this the authors of [51] show that the classical energy is

$$\begin{aligned} E &= \frac{1}{2}\int d^3x \left(F_{xy}^3\right)^2 \\ &= \int d^3x \left[\frac{1}{2}B^2 - 2gB|W^{(0)}|^2 + 2g^2|W^{(0)}|^4\right]. \end{aligned} \tag{3.40}$$

As noted in [48], this is very similar to the Higgs potential. The term $-2gB|W^{(0)}|^2$, coming from the gluon's magnetic moment, is seen to yield something like a Higgs mass term.

Based on the calculations that we have only roughly summarised above, the picture of the QCD vacuum at the beginning of the 1980's was different from our understanding today. Asymptotic freedom had already been discovered, so it was known that such weak coupling calculations could hold at small distance scales. The proposal by [48–51] was therefore that at short distances QCD is dominated by the "spaghetti vacuum". This colourful name is an apt description of the long tubes of intertwined colour-magnetic vortices, not entirely static or z-independent due to quantum fluctuations. The spaghetti vacuum is also divided up into domains in which the vortices have roughly the same orientation in both coordinate and colour space. The domains are distributed randomly, so at large scales there is sufficient disorder that Lorentz and colour symmetries of the vacuum are effectively present.

This picture can explain quark confinement. The idea is that as a single quark moves through the vacuum it collides with vortices. This process adds a random phase to the quark as it moves through the domains. When summing over all the paths, a single quark would build up a very large free energy compared to quarks travelling in colour singlets. This effectively prohibits quarks in isolation. Quark–anti-quark pairs are confined by a linear potential due to a colour-electric string between the two charges [48].

3.4.2 The DSGS model

The next model we look at is the DSGS model, constructed by Djukanovic, Schindler, Gegelia and Scherer in [88]. It is an effective model of ρ-mesons in

quantum electrodynamics. We see a similar pattern. A vector mode, in this case a ρ-meson, becomes unstable at large magnetic field. The ground state is again a triangular vortex lattice, described to linear order by a solution with the same form as (3.30). It was first shown that the triangular lattice is the ground state in [52]. Since the linear order lattice solution is again obtained by solving a quantum harmonic oscillator equation as before, we do not repeat the calculation. We only show the instability.

The DSGS Lagrangian is given by

$$\begin{aligned}\mathcal{L} = &-\frac{1}{4}F_{\mu\nu}F^{\mu\nu} - \frac{1}{2}\left(D_\mu\rho_\nu - D_\nu\rho_\mu\right)^\dagger\left(D^\mu\rho^\nu - D^\nu\rho^\mu\right) + m_\rho^2\rho_\mu^\dagger\rho^\mu \\ &- \frac{1}{4}\rho^{(0)}_{\mu\nu}\rho^{(0)\mu\nu} + \frac{m_\rho^2}{2}\rho^{(0)}_\mu\rho^{(0)\mu} + \frac{e}{2g_s}F^{\mu\nu}\rho^{(0)}_{\mu\nu}.\end{aligned} \tag{3.41}$$

Here $D_\mu = \partial_\mu + ig_s\rho^{(0)}_\mu - ieA_\mu$ is the covariant derivative, g_s is the $\rho\pi\pi$ coupling, A_μ is the photon field that has field strength $F_{\mu\nu} = \partial_\mu A_\nu - \partial_\nu A_\mu$, the fields $\rho_\mu = \left(\rho^{(1)}_\mu - i\rho^{(2)}_\mu\right)/\sqrt{2}$ and $\rho^{(0)} \equiv \rho^{(3)}$ are charged and neutral vector mesons with mass m_ρ and $\rho^{(0)}_{\mu\nu} = 2\partial_{[\mu}\rho^{(0)}_{\nu]} - 2ig_s\rho^\dagger_{[\mu}\rho_{\nu]}$.

The last term in (3.41) describes a coupling between the electromagnetic field and the ρ-mesons. It plays an important role in the creation of a superconducting phase.

In [89] the energy density was calculated to second order. The quadratic part is

$$\epsilon^{(2)}(\rho_\mu) = \sum_{i,j=x,y}\rho_i^\dagger M_{ij}\rho_j + m_\rho^2\left(\rho_t^\dagger\rho_t + \rho_z^\dagger\rho_z\right), \tag{3.42}$$

with

$$M = \begin{pmatrix} m_\rho^2 & ieB \\ -ieB & m_\rho^2 \end{pmatrix}. \tag{3.43}$$

The mass terms for ρ_t and ρ_z do not change with B. For ρ_x and ρ_y this is not the case — these components have a non-diagonal mass matrix M that depends on B. The eigenvalues and eigenvectors of M are

$$\mu_\pm^2 = m_\rho^2 \pm eB, \qquad \rho_\pm = \frac{1}{\sqrt{2}}\left(\rho_x \mp i\rho_y\right). \tag{3.44}$$

We see that the ρ_- state is unstable at sufficiently strong magnetic field. When $B > B_c = m_\rho^2/e$, the state has a negative effective mass, producing a tachyonic mode. The tachyonic mode then leads to a spontaneous symmetry breaking of the QCD vacuum, producing a ρ-meson condensate. The condensate consists of charged mesons.

The physical picture of what is happening goes like this. The quantum vacuum is a seething soup of virtual particles. In the presence of a strong magnetic field, some of these virtual particles become real. Real quarks emerge from the vacuum. They consist of both positive and negative charges, but the net charge is zero. As well as the electromagnetic charge, quarks have colour, and the colour force causes them to form a bound state of charged ρ-mesons. It is the interplay between the colour force binding the quarks and the electromagnetic force enabling the flow of current that produces the superconductivity. That is why the last interaction term

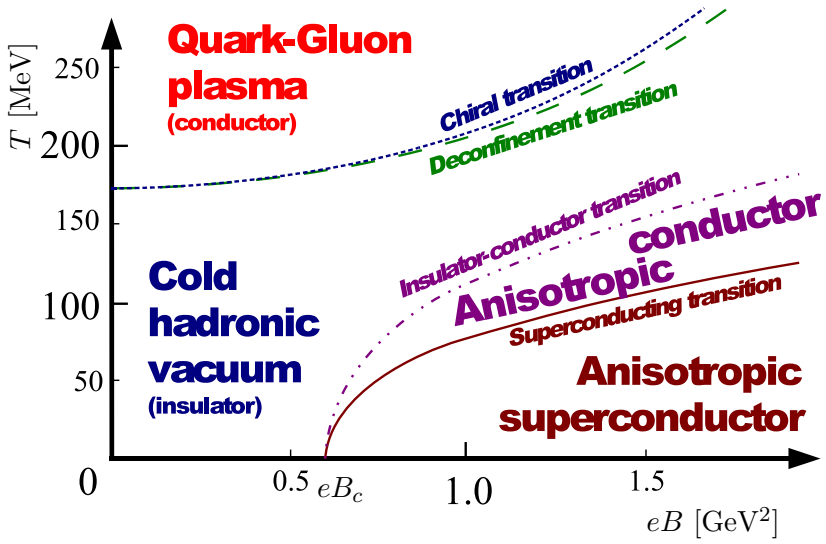

Figure 3.2: A qualitative phase diagram for the QCD vacuum as a function of temperature T and magnetic field B, according to [89]. The region of interest is the one labelled "Anisotropic superconductor". This figure was taken from [89].

in (3.41) is important. The ρ-mesons play the role of the Cooper pairs in BCS theory. In BCS theory there is also an interplay between two forces. From the photons there is a repulsive interaction between electrons and from the phonons there is an attractive interaction causing the formation of Cooper pairs. There is thus an analogy between the QCD superconductivity and conventional BCS superconductivity.

If these ideas are correct, the QCD vacuum becomes superconducting at magnetic field values of the order 10^{16} Tesla, which is around the hadronic scale. At the Large Hadron Collider in Geneva it is expected that magnetic fields of this order should be created in heavy ion collisions [56]. Such strong magnetic fields are the result of off-center ion collisions. An experimental signature would be an excess in the production of ρ-mesons.

This model does however approximate the ρ-mesons as pointlike particles, which is not accurate. ρ-mesons have a radius of roughly $r_\rho \sim 0.5$ fm, which is of the same order as the radii of the lowest Landau levels at the critical magnetic field strength. This problem is overcome in [89] by investigating a model going beyond the point-like approximation as well and finds qualitatively similar results.

The author of [89] also makes a prediction about what the phase diagram of finite-temperature QCD should look like. It is shown in figure 3.2. The region of interest is the one labelled "Anisotropic superconductor". It shows that when the magnetic field is large compared to the temperature, the QCD vacuum condenses and becomes superconducting. In chapter 6 we present the analogous phase diagram for our model.

Chapter 4

Holographic superconductors

In the previous chapter we saw some of the basic properties of a superconductor: it exhibits spontaneous symmetry breaking at low temperature, resulting in a non-vanishing vacuum expectation value of some operator. Infinite DC conductivity and the Meissner–Ochsenfeld effect then follow as a result of electromagnetic gauge invariance. The spontaneous symmetry breaking typically, although as this thesis shows, not always, follows from the lowering of the temperature beneath a critical value. In this chapter we review some of the early and simplest holographic superconductor models. They are bottom-up holographic models, constructed with the goal of reproducing all the properties a superconductor must have. In section 4.3 we discuss the possibility of making holographic superconductors more realistic by breaking translation invariance in the ground state. Inhomogeneous ground states are actively being studied and have shown some startling agreement with experiment.

How do we go about building a superconductor holographically? There are two essential requirements, a finite temperature and an order parameter. As we explained in section 2.3.2, creating a finite-temperature field theory requires placing a black hole in the gravity dual. The temperature T of the field theory is then the Hawking temperature of the black hole. The second requirement, the field theory order parameter, is a quantity that is zero in the normal phase and nonzero in the superconducting phase. This quantity is provided by the vev of the operator that undergoes spontaneous symmetry breaking as the system enters the superconducting phase. The simplest operator $\mathcal{O}$ to include in the field theory is a scalar operator, which is dual to a scalar field ϕ in the gravity theory. When the superconducting order parameter is a scalar condensate, it is known as an s-wave superconductor. On the other hand, if the order parameter is a vector, the superconductor is a p-wave, and if it is a spin-2 order parameter then the superconductor is a d-wave. We give examples of s-wave and p-wave superconductors below.

As we mentioned, a black hole is one of the crucial ingredients in a holographic superconductor. AdS black holes are different from black holes in asymptotically flat space in that they have a positive specific heat, similar to objects we experience every day. This means that their temperature increases when matter is added to them. In other words, the temperature of an AdS black hole is proportional to its radius, as we saw in section 2.3.2. So in order to produce a gravitational system that behaves like a superconductor, we need to create an AdS black hole with a critical radius. When it is above that critical radius in size, the ground state

solution outside the horizon should be vacuum AdS. When the size is below the critical radius, the (static) ground state should contain a field with non-trivial profile. In other words, the black hole solution should have "hair".

In 2008, Steven Gubser [36], followed by Sean Hartnoll, Christopher Herzog and Gary Horowitz [37], were the first to give explicit examples of a holographic s-wave superconductor. The gravity setup contains an AdS–Reissner–Nordström black hole and a scalar field. Soon after in [90, 91] Steven Gubser and Silviu Pufu presented a holographic p-wave superconductor using an $SU(2)$ Yang–Mills field instead of a scalar. For the holographic d-wave there is still no really satisfactory model. A bottom-up approach was first used in [92], where the authors used a charged spin-2 field. This model had problems with the equations for the spin-2 field, which were not consistent and had issues with causality. There have been a number of attempts to address these issues, including an attempt to construct a top-down model of the d-wave superconductor in [93].

There is one point worth mentioning before we review these holographic superconductor models. Technically, the field theory dual is not a superconductor but rather a *superfluid*. A superconductor is the result of the spontaneous breaking of a gauge symmetry, whereas in a superfluid it is a global symmetry that is broken. In all the examples we look at we will indeed be breaking a gauge symmetry spontaneously in the bulk, but as we have seen, in gauge/gravity duality gauge symmetries in the gravity theory map to global symmetries in the field theory. However, the field theory can still be thought of as a *weakly gauged* superconductor, which means that the gauge field coupling is small[1]. Moreover, the term *holographic superconductor* has become the established way of referring to gauge/gravity models with spontaneous symmetry breaking, so we will continue to use it in this thesis.

4.1 A holographic s-wave superconductor

To create a simple holographic s-wave superconductor, we need an AdS–black hole background where the black hole has scalar hair when it has a radius below a critical value and no hair above that value. In flat space there are "no-hair" theorems explaining why this is impossible. The essence of the argument is that any scalar field present would either fall into the black hole or radiate away to infinity — there is no stable middle ground. In asymptotically AdS space however, this is possible. To get the scalar field remaining static outside the horizon, the gravitational attraction is overcome by using a charged *Reissner–Nordström* black hole. And thanks to the AdS geometry, matter cannot radiate away to infinity. Intuitively one can imagine that there is a balance between the attractive gravitational force and the repulsive electrostatic force. This makes it possible for a stable non-trivial scalar field profile to form. Moreover, the stability of this system depends on the size of the black hole, since making the black hole size too large relative to its charge would destabilise it. This is precisely the effect we need. Figure 4.1 shows an intuitive picture of the geometry before and after the condensate forms.

[1] This point is subtle, because although we do strictly have a broken global $U(1)$, there are ways of seeing the Meissner–Ochsenfeld effect in holography [94]. This effect depends on there being a massive photon, a result of gauge symmetry breaking.

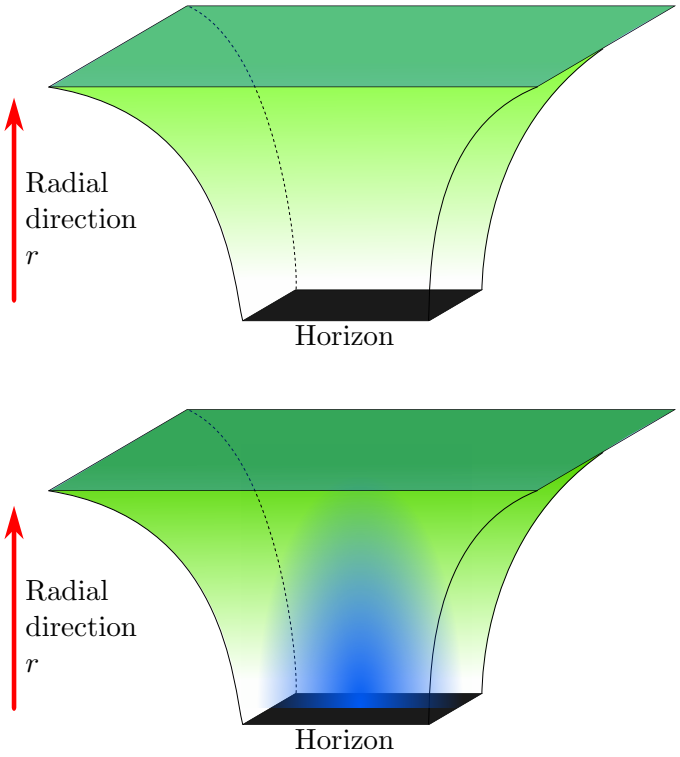

Figure 4.1: An intuitive picture of the holographic superconductor. Anti-de Sitter space is represented with the radial coordinate increasing upwards. The horizon is the limit in the IR of the geometry. The field theory can be thought of as living on the boundary, the plane at the top. The green shade is meant to depict the electric field, sourcing a chemical potential at the boundary. The blue shaded area is the scalar condensate. The top picture shows the uncondensed phase. The bottom picture shows the condensed phase.

Let us make this intuition more precise. We closely follow the exposition of [37, 95]. We consider a simple system with a superconductor in 2+1 dimensions dual to a 3+1-dimensional planar Schwarzschild anti-de Sitter black hole. The action is

$$S = \int d^4x\sqrt{-g}\left(R + \frac{6}{L^2} - \frac{1}{4}F_{\mu\nu}F^{\mu\nu} - \frac{1}{2}|\nabla_\mu\phi - iqA_\mu\phi|^2 - \frac{1}{2}m^2|\phi|^2\right). \quad (4.1)$$

This is just general relativity with an added scalar field ϕ coupled to electromagnetism. The cosmological constant is negative and given by $\Lambda = -3/L^2$, as is usual for AdS space.

To make this simple example even simpler, we work in the *probe limit*. Notice that we can rescale the matter fields to $A_\mu = \tilde{A}_\mu/q$ and $\phi = \tilde{\phi}/q$. Then the matter part of the action has an overall factor of $1/q^2$ in front. The probe limit is when we take $q \to \infty$, so that the matter part of the action is infinitesimal compared to the geometry part. The effect is that the fields can feel the influence of the geometry, but they do not influence the geometry in return. In other words, there is no *metric backreaction*. The problem simplifies in this limit, but most of the interesting physics remains. From now on we work with the rescaled fields but drop the tildes.

The metric for the AdS_4–Schwarzschild black hole, which remains fixed in the probe limit, is

$$ds^2 = -f(r)dt^2 + \frac{dr^2}{f(r)} + r^2(dx^2 + dy^2). \tag{4.2}$$

In these coordinates the AdS boundary is at $r \to \infty$. Here the blackening factor is

$$f(r) = \frac{r^2}{L^2}\left(1 - \frac{r_H^3}{r^3}\right), \tag{4.3}$$

with L the AdS radius and r_H the Schwarzschild radius. The Hawking temperature of the black hole can be calculated to be

$$T = \frac{3r_H}{4\pi L^2}. \tag{4.4}$$

We specialise to the case where $m^2 = -2/L^2$. This is negative, but perfectly allowed in AdS space because it is still above the *Breitenlohner–Freedman bound* [96]. Breitenlohner and Freedman showed that a gravity solution with scalars in AdS_{d+1} spacetime is stable as long as the mass satisfies

$$m^2 \geq m_{BF}^2 = -\frac{d^2}{4L^2}. \tag{4.5}$$

In flat space m^2 should always be positive, but in AdS space there is a lot of volume at large radius that allows positive gradient energy to compensate for negative m^2.

Which gauge field components do we want to switch on? We can invoke gauge redundancy to set one of the components to zero. In fact this is something we must always do because there is no field theory dual to the gauge redundancy — only physical symmetries are mapped. This is in particular seen from how the gauge/gravity dictionary treats boundary values $A_\mu^{(0)}$ of the gauge field as the source term $A_\mu^{(0)} J^\mu$ in the field theory dual. On the gravity side μ runs over more dimensions than on the field theory side[2]. The canonical choice is to set $A_r = 0$. The only gauge field components we can consider switching on are then A_t, A_x and A_y. It turns out to be enough to switch on A_t. We also assume that the fields depend only on r, that is, the plane symmetry

$$\phi = \phi(r), \qquad A_t = A_t(r). \tag{4.6}$$

We chose to turn on $A_t(r)$ because its boundary value is the field theory chemical potential associated to the global $U(1)$ symmetry dual to A_μ's gauge symmetry on the gravity side. However, it results in a nonzero field strength component F_{tr}, which means there is a radial electric field. What sources this electric field? If we were not neglecting backreaction, we would have needed a charged Reissner–Nordström black hole. In the probe approximation, however, an infinitesimal (that is, negligible) charge on the black hole is sufficient to source the electric field.

[2]This of course makes sense because when you take the pullback of A_μ to the boundary, there is no A_r component.

Using the ansatz (4.6), the equations of motion become

$$\phi'' + \left(\frac{f'}{f} + \frac{2}{r}\right)\phi' + \left(\frac{(A_t)^2}{f^2} + \frac{2}{L^2 f}\right)\phi = 0, \tag{4.7}$$

$$A_t'' + \frac{2}{r}A_t' - \frac{2\phi^2}{f}A_t = 0. \tag{4.8}$$

In the second of these equations we can see that a non-zero ϕ means that the A_t equation has a mass term. ϕ in this way triggers a Higgs mechanism.

To impose boundary conditions, consider the following. At the horizon we need $g^{\mu\nu}A_\mu A_\nu = g^{tt}(A_t)^2$ to remain finite, which of course means we need to set $A_t(r_H) = 0$. It is not obvious why we need to stop the vector potential from diverging when all that should really matter is that the physical electromagnetic field remains finite. Perhaps the divergence can be gauged away. This cannot be done, however, because with our gauge choice $A_r = 0$ comes the restriction that a gauge transformation λ can no longer depend on r [3]. Thus the r-dependence of A_t cannot be changed with a gauge transformation, and it must be zero at the horizon. Another boundary condition comes from multiplying (4.7) by f and evaluating it at $r = r_H$. One finds that $\phi(r_H)$ and $\phi'(r_H)$ are not independent.

For boundary conditions at the AdS boundary, we can expand the field asymptotically to get the form that should be familiar from section 2.2.2,

$$\phi = \frac{\phi^{(1)}}{r} + \frac{\phi^{(2)}}{r^2} + \dots \tag{4.9}$$

$$A_t = \mu - \frac{\rho}{r} + \dots. \tag{4.10}$$

Usually ϕ has a normalisable and an non-normalisable mode. Since the mass is negative, however, both modes are normalisable. We impose a boundary condition by choosing one of these to be zero, say $\phi^{(1)} = 0$. It is necessary to have this zero so that no explicit source term is added to the boundary theory Lagrangian. Now $\phi^{(2)} = \mathcal{O}_2$ is the expectation value of the scalar operator that we want to be the order parameter for the transition into the superconducting phase. In the expansion for A_t, μ is the chemical potential of the boundary theory, as usual, and ρ is the charge.

With these boundary conditions fixed, there is now just one free parameter, an overall scale. This can be chosen arbitrarily to solve the equations numerically. We are not interested in the exact form these solutions take, but rather how the order parameter $\mathcal{O}_2$ changes with temperature. Here one has to be careful when plotting the dependence, because the boundary theory is conformal so the temperature can be rescaled to any value. This is reflected in the bulk theory by the way we can scale the coordinates $r \to ar$ and $(t, x, y) \to (t, x, y)/a$ to leave the metric invariant and the field $A_t \to aA_t$ to leave the field equations invariant. To avoid this scaling symmetry it makes sense to plot dimensionless quantities, such as $\sqrt{\mathcal{O}_2}/\mu$ versus T/μ. What one finds is precisely that there is a critical temperature T_c such that $\mathcal{O}_2$ vanishes when $T > T_c$ and is non-zero when $T < T_c$. This is the behaviour that we want from superconductivity. Due to this critical temperature T_c, it makes sense to plot $\sqrt{\mathcal{O}_2}/T_c$ versus T/T_c, which is equivalent to the scaling by μ. This is what is done in figure 4.2. Near T_c, we see there

[3] See chapter 5 for more information.

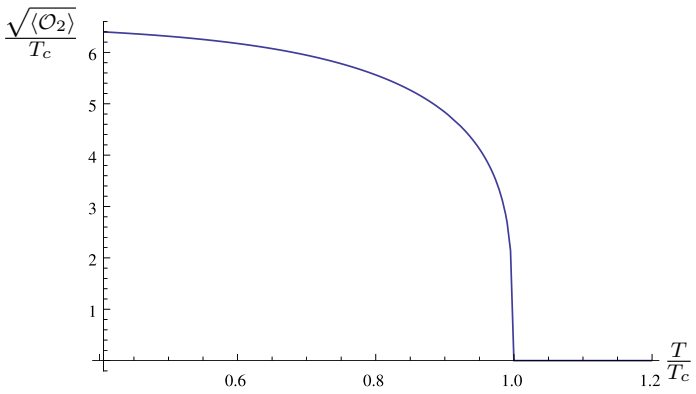

Figure 4.2: The condensate $\mathcal{O}_2$ as a function of T near the critical temperature T_c. Near T_c there is a square root behaviour $\mathcal{O}_2 \sim T_c^2(1 - T/T_c)^{1/2}$.

is a square root behaviour $\mathcal{O}_2 \sim T_c^2(1 - T/T_c)^{1/2}$, which is as predicted by the Ginzburg–Landau model.

The reason we see this behaviour comes from looking more closely at the equation for ϕ, (4.7). It has an effective mass term that looks like $\left((A_t)^2/f^2 + 2/L^2 f\right)\phi$. Keeping in mind that we have chosen the mass of the scalar field to be negative, because the first term has the same sign as the mass term we can tell that it is also negative. When A_t grows (as it has to when we're decreasing T/μ) the effective squared mass becomes more and more negative. Eventually, at $T = T_c$, it is negative enough for ϕ to be unstable, at which point a second solution becomes possible with non-zero ϕ. We say that ϕ *condenses*. The order parameter $\mathcal{O}_2$ for this second solution is also nonzero. This idea is key to all the examples of superconductivity we will be looking at in this thesis.

The nonzero condensate is scalar hair developed by the black hole. One can calculate the free energy of the boundary field theory for both solutions, with the condensate and without, at the same temperature below T_c, and find that it is always lower in the case with scalar hair. It is thus an energetically favoured state.

It may seem strange that this superconductor has a nonzero charge (ρ in the expansion for A_t above) when superfluids normally are supposed to be neutral. This comes from the way in which we are building the bottom-up model of the superconductor, since we can not specify a detailed microscopic description of the dual field theory. The best way to think about it is that the field theory models the electrons in the superconductor but not the lattice [95]. Indeed, the theory is invariant under translations. In section 4.3 we discuss the efforts to break translation invariance in the field theory, which give rise to more realistic superconductor models.

4.1.1 The optical conductivity

Of course, we cannot be sure that a system is a superconductor unless we calculate its optical conductivity and find a δ-function peak at zero frequency. To do this we need some spatial component of the current. It does not matter which because the theory is symmetric under spatial rotations. We pick J_x. To find this quantity in the boundary field theory we should of course switch on the field A_x in the

bulk. Since we need a current with a frequency dependence, we give A_x a time dependence of the form $e^{-i\omega t}$. Its equation of motion is then

$$A_x'' + \frac{f'}{f}A_x' + \left(\frac{\omega^2}{f^2} - \frac{2\phi^2}{f}\right)A_x = 0. \tag{4.11}$$

An important boundary condition for the field A_x at the horizon is that it be propagating into the black hole. This is important not only for physical reasons (nothing comes out of a black hole), but also because, as Son et al. showed in [97], this boundary condition means that the Green's function calculated in the dual field theory is the retarded Green's function, corresponding to causal propagation. We look at this in detail in chapter 5.

The asymptotic behaviour of A_x at large AdS radius is

$$A_x = A_x^{(0)} + \frac{A_x^{(1)}}{r} + \dots. \tag{4.12}$$

$A_x^{(1)}$ is of course the vacuum expectation value of the current that we are looking for, $\langle J_x \rangle$. The gauge/gravity dictionary also tells us that $A_x^{(0)}$ is a source field in the boundary theory. The electric field in the boundary theory is thus $E_x = \partial_x A_t^{(0)} - \partial_t A_x^{(0)} = -\dot{A}_x^{(0)} = i\omega A_x^{(0)}$. Now we can use Ohm's law to find the conductivity,

$$\sigma(\omega) = \frac{\langle J_x \rangle}{E_x} = -\frac{iA_x^{(1)}}{\omega A_x^{(0)}}. \tag{4.13}$$

One can solve equation (4.11) numerically. The real part of the conductivity as a function of frequency is plotted in figure 4.3 for various temperatures. The figure was taken from [37].

When $T > T_c$, the conductivity is nonzero and independent of frequency. The thing to notice is the formation of a gap where the conductivity vanishes for low frequencies. This is a common feature in superconductors [98]. Importantly, there is also a delta function in σ at $\omega = 0$. This is difficult to see from the numerical calculations, but is more obvious when one looks at the imaginary part of the conductivity, plotted in figure 4.4. The imaginary part shows a pole. There is a mathematical relationship between the real and imaginary parts of a complex function that is analytic in the upper half-plane. Moreover, we know that the conductivity is such a complex function because Toll proved in [99] that response functions are analytic in the upper half-plane if and only if they are causal. The relationship that they fulfil is given by the Kramer-Kronig relations, one of which is

$$\operatorname{Im}\sigma(\omega) = -\frac{1}{\pi}\mathcal{P}\int_{-\infty}^{\infty}\frac{\operatorname{Re}\sigma(\omega')}{\omega' - \omega}d\omega'. \tag{4.14}$$

$\mathcal{P}$ denotes the Cauchy principle value. From this relation it is easy to see that there is a pole in the imaginary part of the conductivity if and only if there is delta function at the same ω in the real part of the conductivity. We easily see this pole in figure 4.4.

The overall result is thus that we see the behaviour of a superconductor in the dual field theory — it has an infinite DC conductivity and a gap in which there is

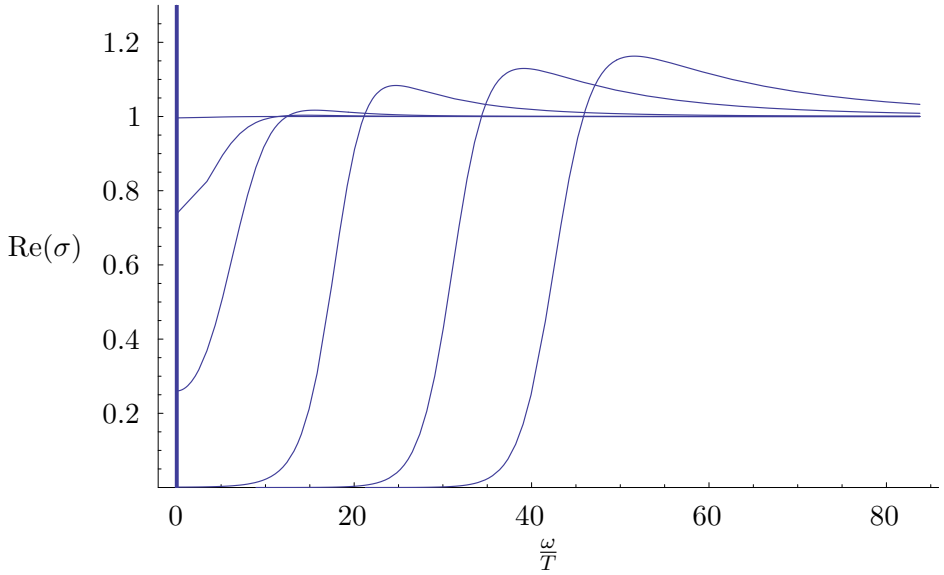

Figure 4.3: The real part of the conductivity σ as a function of frequency, rescaled by the critical temperature T_c, for various values of the temperature. The top flat line is the conductivity for all values of $T > T_c$, where there is no condensate. As the temperature decreases, a gap forms and becomes wider. This figure was taken from [37].

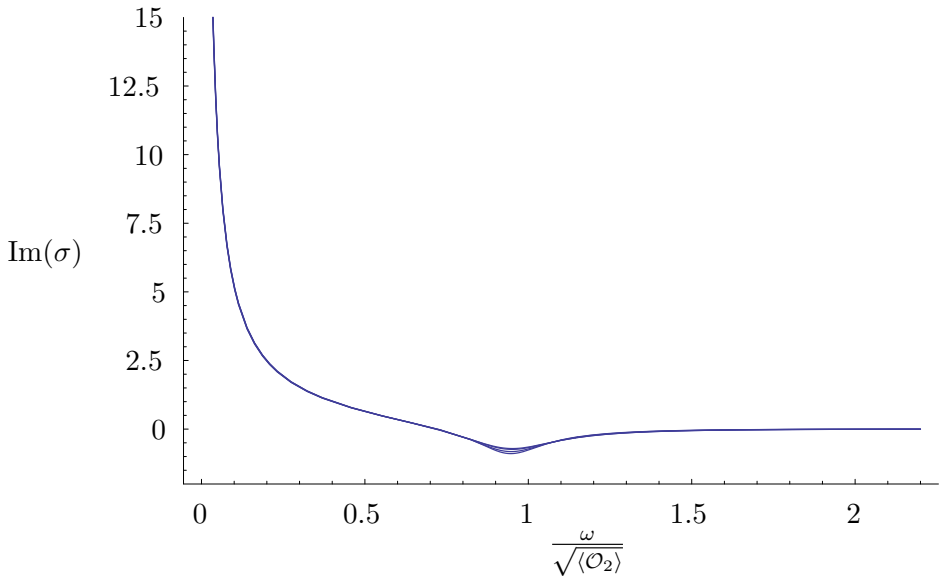

Figure 4.4: The imaginary part of the conductivity σ as a function of frequency, this time rescaled by the condensate $\sqrt{\langle \mathcal{O}_2 \rangle}$, for various values of the temperature. The pole at $\omega = 0$ is easy to see. This figure was taken from [37].

no conductivity for low frequencies. This is neatly explained by the gravity dual, encoding all this information in the form of a black hole with a gauge field that is stable at zero frequency. At higher frequencies, where we see finite conductivity in the field theory, there must be dissipation. Dissipation is represented in the gravity theory by the gauge field falling into the black hole and losing energy. If we were not using the probe approximation and had included back reaction, this process would cause the black hole to grow, increasing the temperature. An increase in temperature is exactly what is expected in the field theory when dissipation occurs, so the interpretation is consistent.

4.2 A holographic p-wave superconductor

It was shown in [90, 91] that it is also possible to construct a holographic p-wave superconductor, where the condensate breaks rotation invariance by singling out a direction in space. In this section we review some of the ideas of [91]. They are essentially the same ideas as for the s-wave, the main difference being that instead of a scalar field condensing, we have an $SU(2)$ gauge field. We also consider the setup in $(4+1)$-dimensions, instead of the $(3+1)$-dimensional model of [91], to bring it closer to the author's main work in chapter 5.

Although technically this model is bottom-up, it can still be viewed as a certain low-energy limit of the D3-D7 brane model described in section 2.3. The $SU(2)$ Yang–Mills action is the low-energy effective action on the $N_f = 2$ probe D7 branes. It comes from taking the small field strength limit of the DBI action. The $SU(2)$ gauge symmetry maps to an $SU(2)$ global symmetry on the field theory, which can be viewed as an isospin symmetry. Similar to the s-wave model where we switched on a $U(1)$ chemical potential, here we switch on an isospin chemical potential for the $U(1)_3$ subgroup of $SU(2)$.

In this section we use the background and action from chapter 5. Further details about the convention are given there. The $(4+1)$-dimensional theory on AdS_5–Schwarzschild space is specified by the action

$$S = \int d^5x\sqrt{-g}\left\{\frac{1}{2\kappa^2}\left(R + \frac{d(d-1)}{L^2}\right) - \frac{1}{4\hat{g}^2}F^a{}_{\mu\nu}F^{a\mu\nu}\right\}. \tag{4.15}$$

As before we take the probe limit, so that $\frac{1}{4\hat{g}^2}F^2 \to 0$ and we can neglect backreaction on the geometry. The fixed background metric is then the same as before,

$$ds^2 = \frac{L^2}{u^2}\left(-f(u)dt^2 + dx^2 + dy^2 + dz^2 + \frac{du^2}{f(u)}\right), \tag{4.16}$$

with $f(u) = 1 - \frac{u^4}{u_H^4}$. The AdS boundary is at $u \to 0$. The Hawking temperature of the black hole is $T = 1/\pi u_H$. We use the scaling symmetry of the background to set $u_H = 1$.

The $SU(2)$ gauge field is $\mathcal{A} = \mathcal{A}^a_\mu \tau^a dx^\mu$, for $a = 1 \ldots 3$. The Lie algebra basis is given by $\tau^a = \frac{\sigma^a}{2i}$, with σ^a the Pauli matrices. The simple gauge field ansatz

$$\mathcal{A} = \Phi(u)\tau^3 dt + w(u)\tau^1 dx \tag{4.17}$$

is enough to ensure the non-trivial dynamics that we need. The boundary value of Φ, the $\mathcal{A}^3_t$ component, is equal to the isospin chemical potential. Its presence

explicitly breaks the $SU(2)$ gauge symmetry of the theory to $U(1)$. The function w is the one that condenses, breaking the remaining $U(1)$ symmetry. Additionally, it separates out the x-direction as special, breaking $SO(3)$ rotational symmetry. When the temperature is high, $w(u) = 0$. Below a critical temperature T_c, w is a nontrivial function that is non-vanishing at the horizon. It vanishes at the boundary though because we are modelling a spontaneously broken symmetry in the field theory, that is, the breaking happens without a source.

The equations of motion are

$$0 = \Phi'' - \frac{\Phi'}{u} - \frac{\Phi w^2}{f}, \tag{4.18}$$

$$0 = w'' + \left(\frac{f'}{f} - \frac{1}{u}\right) w' + \frac{\Phi^2 w}{f^2}. \tag{4.19}$$

These are similar to the s-wave equations (4.7)–(4.8), so it is no surprise that we get the same superconductor behaviour. Also, we can see now why it is important to have a non-abelian gauge field. The component w has an effective mass term Φ^2/f^2 that comes from the coupling of the gauge field components among themselves. This would not have been present in the equation of an abelian gauge field. We again see that as Φ^2 gets larger, corresponding to higher chemical potential or lower temperature, the effective mass-squared of w gets more negative, eventually resulting in an instability.

The components have boundary expansions

$$\Phi = \mu + \Phi_2 u^2 + \mathcal{O}(u^6), \tag{4.20}$$

$$w = w_2 u^2 + \mathcal{O}(u^4). \tag{4.21}$$

Here μ is the isospin ($U(1)_3$) chemical potential, and so Φ_2, as the subleading term, is proportional to the charge density associated with the $U(1)_3$ symmetry. In other words, by the gauge/gravity dictionary, vev of the current component $\langle J^3_t \rangle \propto \Phi_2$. Similarly we have $\langle J^1_x \rangle \propto w$. In chapter 5 we calculate the proportionality constants for these quantities exactly.

Because we are in a bottom-up model, it is impossible to know the precise form of the current J^a_μ. But by comparing to the D3-D7 setup we can make a rough guess [100]. The D7-branes add an $\mathcal{N} = 2$ supersymmetric hypermultiplet to the field theory with fermions ψ_i and scalars ϕ_j. There are $N_f = 2$ flavours, which we label u and d, which transform under the $SU(2)$ global isospin group. The chemical potential is then a source for the operator

$$\begin{aligned} J^3_t &\propto \bar{\psi}\sigma^3\gamma_0\psi + \phi\sigma^3\partial_t\phi \\ &= \bar{\psi}_u\gamma_0\psi_u + \phi_u\partial_t\phi_u - \bar{\psi}_d\gamma_0\psi_d - \phi_d\partial_t\phi_d \\ &= n_u - n_d. \end{aligned} \tag{4.22}$$

The σ^i are Pauli matrices acting as a basis for the flavour symmetry and γ_μ are the Dirac matrices. $\psi = (\psi_u, \psi_d)$ and $\phi = (\phi_u, \phi_d)$ and so n_u and n_d are the respective charge densities of the isospin fields. Similarly, the condensate takes the form

$$J^1_z \propto \bar{\psi}\sigma^1\gamma_z\psi + \phi\sigma^1\partial_z\phi. \tag{4.23}$$

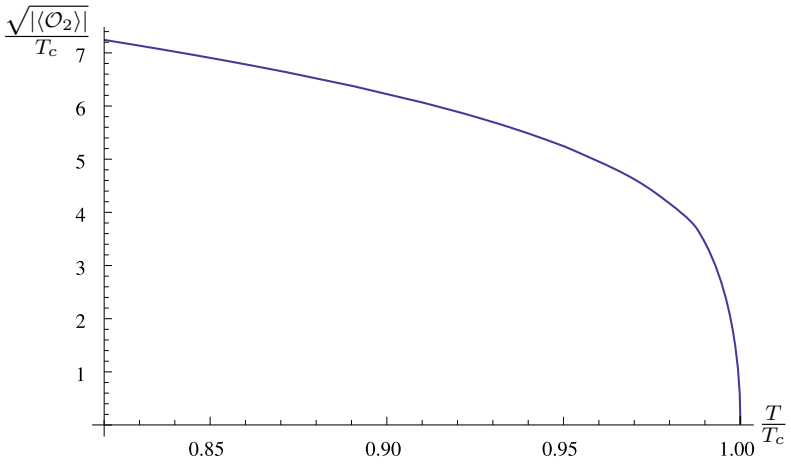

Figure 4.5: The condensate $\mathcal{O}_2$ as a function of T near the critical temperature T_c. Near T_c there is a square root behaviour $\mathcal{O}_2 \sim T_c^2(1 - T/T_c)^{1/2}$. This plot is similar to the case of the s-wave, figure 4.2.

If a microscopic Lagrangian could be written down for our bottom-up model's field theory, it would probably be similar to this.

As in the previous section, we can calculate the form of the condensate as a function of the temperature. The result is plotted in figure 4.5. We see that the condensate has the usual mean field behaviour where it scales as $(T_c - T)^{\frac{1}{2}}$ near $T = T_c$.

The other choice we could have made for the gauge field ansatz is

$$\mathcal{A} = \Phi(u)\tau^3 dt + w(u)\left(\tau^1 dx + \tau^2 dy\right). \tag{4.24}$$

The equations of motion become

$$0 = \Phi'' - \frac{\Phi'}{u} - \frac{2\Phi w^2}{f}, \tag{4.25}$$

$$0 = w'' + \left(\frac{f'}{f} - \frac{1}{u}\right)w' + \frac{\Phi^2 w}{f^2} - \frac{w^3}{f}. \tag{4.26}$$

They are similar to equations (4.18)–(4.19) and w also condenses at low enough temperatures. In this case as w condenses it means that both $\langle J_x^1\rangle$ and $\langle J_y^2\rangle$ condense simultaneously in the field theory. In [91] this is called a $p + ip$-wave superconductor to distinguish it from the p-wave above.

When $w = 0$, the equation for Φ is the same for both the p-wave and the $p+ip$-wave. Moreover, when doing a stability analysis by considering fluctuations about the $w = 0$ solution in both setups, the equations of motion for the fluctuations are also identical. This means that the fluctuations become exponentially growing at identical values of T, so that the critical temperature T_c when a condensate forms is the same for both the p-wave and the $p + ip$-wave setups.

Of the two different condensates that can exist at the same temperature, which one is the real ground state? According to [91], the p-wave. There the authors did a standard stability analysis by investigating fluctuations about the $p + ip$-wave background above and below T_c and found that the fluctuations were exponentially

growing. See figure 7 of [91]. This fact is important for the models of chapters 5 and 6. In those models we switch on a magnetic field and find the stable ground state. As the magnetic field tends to zero, the ground state tends towards the $p + ip$-wave state, so we know that it cannot be stable.

4.3 Inhomogeneous ground states

The hairy black hole solutions of the previous section act as an inspiration to search for even more novel black hole backgrounds. And it turns out there is a very rich landscape of solutions if one looks for inhomogeneous ground states. This has been a subject of intense study over recent years, not only for its intrinsic interest but also for the tantalising prospect of applications to strongly coupled field theories such as QCD and real-world condensed matter systems. Condensed matter systems typically do not have translation invariance — the superconductor models of the previous system would be more realistic if they contained a lattice. Finding out when inhomogeneous ground states emerge *spontaneously* is also of interest. We saw in chapter 3 that an early model of the QCD vacuum has spontaneously emerging vortex lattices. Since this effect also exists in further models with non-abelian gauge fields, the question of the universality of spontaneously emerging lattices arises.

4.3.1 Explicit symmetry breaking

We start the exploration of holographic models with inhomogeneous ground states by considering the work of Gary Horowitz, Jorge Santos, David Tong in [101]. Their motivation was to build a more realistic condensed matter model by including what many prior models had left out — a lattice. The translation invariance of the field theory directions means that the real part of the optical conductivity has a delta peak at zero frequency (infinite DC conductivity) for all temperatures, even outside the superconducting phase[4]. The authors of [101] chose the simplest way to overcome the translation invariance and introduce a lattice by imposing one explicitly in the boundary conditions. Their model is similar to the one from section 4.1. They use Einstein–Maxwell theory with a neutral scalar field that has $m^2 = -2/L^2$. They also do not neglect backreaction, so they have a charged black hole and numerically solve for the effect of the matter fields on the geometry. The lattice boundary conditions are imposed in the source of the scalar Φ. For the boundary expansion

$$\Phi = u\phi_1 + u^2\phi_2 + \mathcal{O}(u^3), \tag{4.27}$$

(where u is the radial coordinate) the source was chosen to be

$$\phi_1(x) = A\cos(kx), \tag{4.28}$$

for some amplitude A and wave number k. As in the earlier s-wave model, there is an electric field coming from the A_t component that provides a field theory

[4] We did not see this in the example of section 4.1. In that example the conductivity is finite and independent of frequency for $T > T_c$. The reason for this is the probe limit, which made the scalar decouple from the geometry and so the electric and energy currents decouple. This implicitly breaks translation invariance. Going away from the probe limit gives infinite DC conductivity in the normal phase; see [94].

chemical potential. In [101] it is chosen to be constant. Earlier work however considered a modulated chemical potential instead of a modulated scalar source, such as [102, 103].

With the boundary conditions chosen, the first step is to solve the Einstein–Maxwell equations numerically. This yields solutions for Φ, the gauge field $\mathcal{A}$ and the metric g in two variables, u and x, due to Φ imprinting its modulated form on $\mathcal{A}$ and g. Next the authors calculate the optical conductivity, which is done by considering fluctuations of the gauge field about the background. This is an involved numerical computation, but the results in the end are striking. Instead of an infinite DC conductivity, the delta peak in broadened into a Drude peak,

$$\sigma(\omega) \approx \frac{K\tau}{1 - i\omega\tau}, \tag{4.29}$$

at low frequencies. Here K is an overall constant determined from the numerical data. τ is relaxation time of the system. In the Drude model, it would correspond to the typical time scale it would take electrons in the material to stop moving after the applied electric field has been switched off. In real materials the relaxation is typically due to impurities and finite temperature effects.

At high frequencies, the optical conductivity rises to a positive constant. This is not something that is measured experimentally, but in the high frequency limit the lattice can be neglected. The constant conductivity is a property of $(2 + 1)$-dimensional conformal field theories.

Intermediate frequencies, however, hold the biggest surprise. There the optical conductivity takes the form

$$|\sigma(\omega)| \approx \frac{B}{\omega^{2/3}} + C, \tag{4.30}$$

for constants B and C. This power-law falloff is remarkable because experimental measurements of certain cuprate high-temperature superconductors yield the same result. For example, figure 3 of [104] shows the power law behaviour of the optical conductivity measured in $Bi_2Sr_2Ca_{0.92}Y_{0.08}Cu_2O_{8+\delta}$, a cuprate. It is measured to be $|\sigma(\omega)| = C\omega^{-0.65}$, agreeing very well with the holographic result.

The authors continued studying the effect of lattices in later work. In [105] they consider, among others, a model in asymptotically AdS_5 space. This model has a different scaling behaviour at intermediate frequencies. There $|\sigma(\omega)| \approx C\omega^{-\sqrt{3}/2}$. In [106] they are back in AdS_4, but then they also work out properties of the system in the superconducting phase, which they did not do in their earlier work. They find that the system has a normal fluid component in addition to the superfluid component. The normal fluid displays an optical conductivity Drude peak at low frequencies and the same $\omega^{-2/3}$ scaling at intermediate frequencies.

4.3.2 Spontaneous symmetry breaking

It is more surprising when inhomogeneous ground states emerge spontaneously. Over the years a number of mechanisms that lead to dynamically generated inhomogeneities have been uncovered. The first approach involved a Yang–Mills–Chern–Simons theory in an AdS_5 QCD model in [107]. The key feature of this bottom-up model is the Chern–Simons term. Its presence causes the emergence of an anisotropic ground state of vector mesons that breaks both rotation and translation symmetry, reminiscent of the smectic phase of liquid crystals.

A number of other works have made use of the Chern–Simons term in various gravitational backgrounds to produce models that exhibit spontaneous inhomogeneous ground states [108–111]. Some of the ground states are helical, such as in [112–115]. One interesting aspect of these results is the simple but powerful *quasinormal mode* analysis used to uncover them. We explain quasinormal modes in more detail in section 5.3.2.

As an example, we look at the model by Shin Nakamura, Hirosi Ooguri and Chang-Soon Park in [112]. It Einstein–Maxwell–Chern–Simons theory with action given by

$$S = \frac{1}{16\pi G_N}\int d^5x\left\{\sqrt{-g}\left(R + \frac{12}{L^2} - \frac{L^2}{4}F_{\mu\nu}F^{\mu\nu}\right) + \alpha L^3 F\wedge F\wedge A\right\}. \quad (4.31)$$

L is the AdS radius which we set to unity. The gravity background is the Reissner–Nordström black hole in asymptotically AdS_5 spacetime with metric

$$ds^2 = -f(r)dt^2 + \frac{dr^2}{f(r)} + r^2 d\vec{y}^2, \quad (4.32)$$

where the blackening factor is given by

$$f(r) = r^2\left[1 - \left(1 + \frac{\mu^2}{3r_+^2}\right)\left(\frac{r_+}{r}\right)^4 + \frac{\mu^2}{3r_+^2}\left(\frac{r_+}{r}\right)^6\right]. \quad (4.33)$$

In addition, the black hole sources a field strength given by

$$F = -\frac{2\mu r_+^2}{r^3}dt\wedge dr. \quad (4.34)$$

There are several adjustable parameters in this model. The field theory temperature is given by

$$T = \frac{r_+}{2\pi}\left(2 - \frac{\mu^2}{3r_+^2}\right), \quad (4.35)$$

and the chemical potential μ can be used to define dimensionless ratios such as T/μ as usual. α, the Chern–Simons coupling, can also be adjusted and in [112] they do precisely that. They find that for $\alpha > \alpha_c$, there is a critical temperature $T_c(\alpha)$ below which the background becomes unstable. The remarkable thing about the instability is that it only happens at finite momentum k. This suggests a new ground state that breaks translation invariance.

More precisely, consider fluctuations of the metric and the gauge field about the background. The fluctuations should be small so that the equations of motion can be linearised. They have time and space dependence $\sim e^{-i\omega t + ikx}$. The equations of motion thus depend explicitly on ω and k. Pick a value of k and the adjustable parameters T and α and determine the value ω needs to take to satisfy the equations of motion. It turns out that for α big enough and T small enough, there are nonzero values of k that require ω to have a positive imaginary part, leading to exponentially growing fluctuations. This is the instability. It does not occur at $k = 0$.

This simple analysis, which involves solving linear differential equations in a single variable r, leads to a more interesting field theory condensate than we

have seen so far in this chapter. The condensate, related in the usual way to the subleading term in the boundary expansion of the gauge field, takes the form

$$\langle \vec{J}(x) \rangle = \mathrm{Re}\left(\vec{u}e^{ikx}\right), \tag{4.36}$$

for a chosen value of k, where $\vec{u}$ is a polarisation vector obeying

$$\vec{k} \times \vec{u} = \pm i|k|\vec{u}. \tag{4.37}$$

The analysis in [112] indicates that the sign on the right-hand side should be the same as the sign of $-\alpha\mu$. In other words, the sign of the Chern–Simons coupling determines whether the circular polarisation of the expectation value is counter-clockwise or clockwise. Chern–Simons terms are parity violating, so it is not surprising that α should have this effect. The condensate is a helix; it breaks both translation and rotation symmetry but preserves a combination of the two. This configuration is similar to the cholestric phase of liquid crystals.

In the follow-up work [113], the authors go beyond the linearised analysis to find the form of the ground state more precisely. They also show that in the limit of large α, the phase transition is second order.

4.3.3 Magnetic fields

The early studies of magnetic fields in s-wave superconductors were simply aiming to see whether the Meissner–Ochsenfeld effect could be reproduced. In [116, 117] it was found that it could. In simple s-wave models turning on a magnetic field has the tendency to reduce the overall magnitude of the condensate in the superconducting phase. There is also a critical value B_c of the magnetic field above which no condensate would form.

But even in these simple models there are signs of a much richer ground state structure. In [116] it was found that the s-wave in asymptotically $(3+1)$-dimensional AdS space has a charged scalar condensate that is inhomogeneous in the boundary directions. The effective mass of the scalar has a contribution from the square of the magnetic field with the opposite sign to the electric field contribution, so that it tends to inhibit the formation of the superconducting phase. The condensate shares the solution of the quantum harmonic oscillator wavefunction in one dimension. The magnetic field has the effect of localising the charged condensate into Landau levels. The lowest of these levels has a Gaussian profile, or "droplet".

The study of this system's ground state was made more precise in [118, 119]. There it was revealed that the droplet is not the only type of solution for the charged scalar condensate at finite magnetic field. There is also a vortex solution. The vortex solution is strikingly similar to the solution of figure 3.1. The condensate is zero at the origin, the centre of the vortex, and constant at spatial infinity, while the magnetic field is finite at the centre and decays at infinity. The authors argue that the two types of solution appear at different regions in the (B, T) phase diagram. They claim that the droplets appear only above a critical value of B and thus do not appear in the superconducting phase. It is doubtful whether they then form an energetically favourable ground state. The vortices however do form in the superconducting phase, at low enough B. They trap the magnetic flux into tubes, as is familiar from type-II superconductors.

With the single vortex solution in hand, the next step was to find out whether holographic superconductors support vortex lattice solutions like those in type-II superconductors and whether they form a ground state. The challenge was taken up by Kengo Maeda, Makoto Natsuume and Takashi Okamura in [120]. They studied a (3+1)-dimensional gravity model of a holographic s-wave superconductor and, following an analysis similar to Abrikosov's, found that it behaves as a type-II superconductor.

The Maeda et al. model is Einstein–Maxwell with a complex scalar. The effective action is

$$S = \int d^4x\sqrt{-g}\left(-\frac{1}{4}F^{\mu\nu}F_{\mu\nu} - |\left(\nabla_\mu - iA_\mu\right)\Psi|^2 - m^2|\Psi|^2\right). \tag{4.38}$$

The action is effective because the gravitational part is ignored; we are in the probe limit. $F_{\mu\nu}$ is the field strength of the $U(1)$ gauge field A_μ. The background is AdS_4–Schwarzschild with metric

$$ds^2 = \frac{L^2\alpha^2}{u^2}\left(-h(u)dt^2 + dx^2 + dy^2\right) + \frac{L^2}{u^2}\frac{du^2}{h(u)}, \tag{4.39}$$

where $\alpha(T) = \frac{4\pi T}{3} = \frac{u_H}{L^2}$, L is the AdS radius, u_H is the horizon radius, T is the field theory temperature, and $h(u) = 1 - u^3$. We set $u_H = 1$ for simplicity. The complex scalar has mass $m^2 = -\frac{2}{L^2}$, as in section 4.1. With this choice, the equations of motion yield the boundary expansion

$$\Psi = \psi_1 u + \psi_2 u^2 + \mathcal{O}(u^3). \tag{4.40}$$

Because m^2 is negative and so there is no unnormalisable mode, either ψ_1 or ψ_2 can be interpreted as the vev of the scalar operator in the dual theory, with scaling dimensions $\Delta = 1$ or $\Delta = 2$, respectively. We choose to interpret ψ_1 as the source and set it to zero for spontaneous symmetry breaking. Finally, there should be an electric and a magnetic field. The electric field determines the field theory chemical potential by $\mu = A_t|_{u=0}$, as usual, and the magnetic field gives the field theory external magnetic field by $B = F_{xy}|_{u=0}$.

As explained in section 3.3, type-II superconductors have two critical magnetic field values B_{c_1} and B_{c_2}. The aim is to model the ground state of the holographic superconductor just below B_{c_2}, where the condensate is small and we expect to find a vortex lattice. We know from [118, 119] that B_{c_2} exists in holographic models, because they found a critical magnetic field above which the vortices cease to exist. The approach is thus to fix a value for T, which corresponds to fixing μ, small enough so that the system is in the superconducting phase. Then adjust the magnetic field B such that $B < B_{c_2}$ and $\varepsilon = (B_{c_2} - B)/B_{c_2} \ll 1$. The small ε allows us to make an expansion about the normal phase solution,

$$\Psi(x, y, u) = \varepsilon^{1/2}\psi_1(x, y, u) + \varepsilon^{3/2}\psi_2(x, y, u) + \ldots \tag{4.41}$$

$$A_\mu(x, y, u) = A_\mu^{(0)}(x, y, u) + \varepsilon A_\mu^{(1)}(x, y, u) + \ldots, \tag{4.42}$$

where the zeroth order solution is given by

$$A_t^{(0)} = \mu(1 - u), \qquad A_x^{(0)} = 0, \qquad A_y^{(0)} = B_{c_2}x, \tag{4.43}$$

and $\Psi = 0$. This expansion was first made by Abrikosov in [42], and is also what we do in chapter 5.

Solving the equations to linear order, one finds the general solution

$$\psi_1(x,y,u) = \frac{1}{L^2}\sum_{l,m,n} C_{l,m,n} e^{inky - \frac{B_{c2}}{2}\left(x - \frac{nk}{B_{c2}}\right)^2} H_m\left[\sqrt{2B_{c2}}\left(x - \frac{nk}{B_{c2}}\right)\right] \rho_l(u). \tag{4.44}$$

This should be reminiscent of the solution (3.30), and we encounter it again in chapter 5. The x-dependent part of the exponent times the Hermite polynomials H_m is nothing but the quantum harmonic oscillator solution found in [116]. Focusing only on the lowest energy solution with $m = 0$, we again get the droplet form. In the radial direction, the general solution also contains a tower of modes given by $\rho_l(u)$. There is no closed form solution for the ρ_l, so they have to be solved for numerically. Since we are looking for the ground state, we can again focus on the lowest energy solution ρ_0. The $C_{l,m,n}$ and k are constants that need to be fixed by solving the equations to higher order in ε and calculating the free energy. Maeda et al. do this, and it turns out that they take values that yield the triangular lattice vortex solution in the x- and y-directions for ψ_1, which means a triangular lattice condensate in the field theory.

There are some remarks to be made about this model. Firstly, it shows that one of the simplest holographic superconductor models, the s-wave, behaves like a type-II superconductor rather than a type-I. The Meissner–Ochsenfeld effect is present; the magnetic field reduces the size of the condensate and eventually destroys it completely. Also, right beneath the critical magnetic field B_{c2}, an vortex lattice forms.

Secondly, this model is microscopic, not effective as with Ginzburg–Landau. The gravity setup is exactly dual to a field theory where there are no electrons being bound into Cooper pairs. There are no quasiparticles whatsoever because the theory is strongly coupled. What there is is a strongly coupled theory with a scalar operator that condenses below a certain temperature. The gravitational description looks like an effective description at long wavelength like the Ginzburg–Landau model because of the large N limit.

Finally, given that all our intuition about the Ginzburg–Landau model is being verified by studying the s-wave holographic superconductor, it is quite surprising that the result is so different for the p-wave. As we show in chapter 4, the magnetic field contributes to the effective mass of a non-abelian gauge field with the opposite sign. The magnetic field tends to induce superconductivity rather than destroy it. The vortices are still present, but they appear *above* the critical magnetic field value that induces superconductivity. And indeed, the ground state is a triangular lattice.

Before we move to considering the p-wave, the main original work of this thesis, we consider the broader context of magnetic field-induced ground states. Vortex lattices are not the only exotic ground states that make an appearance in holography. Various striped phases have been found for example in [121] and [122]. These works consider top-down brane models from 11-dimensional supergravity. The latter shows that there is an infinite family of solutions from supergravity that exhibit a magnetically induced instability resulting in an inhomogeneous ground state. This sort of work is important because it shows that inhomogeneous ground states do not only arise from bottom-up models.

Finally, translation invariance can also be broken with magnetic monopoles. This was studied in an AdS_4 background in [123] and [124]. The magnetic monopoles are solutions of Yang–Mills–Higgs theory with gauge group $SU(2)$. In a certain limit where the monopole magnetic charge becomes large, a "monopole wall" is formed. This is a monopole solution where the radius of the monopole is large enough to be treated as a plane. It was shown in [123] that there is a W boson instability in this background. In [124] the new ground state resulting from the instability was found numerically, and it was shown to be a hexagonal lattice.

Chapter 5

Holographic lattice ground states from a magnetic field

Take a simple gauge/gravity model on AdS_5 with either a black hole or a hard wall cutoff in the bulk. Add an $SU(2)$ gauge field and switch on a magnetic component with magnitude B. For small B, this is a stable, normal phase solution. It is invariant under a $U(1)$ gauge symmetry, a subset of the full $SU(2)$ symmetry present when B vanishes. Increase B, however, and the remaining gauge symmetry is broken. For B above a critical value B_c, the solution is unstable. For a solution to be stable when $B > B_c$, other components of the gauge field must be nonzero. These other components are analogous to W-bosons. For B near B_c, they form a triangular vortex lattice ground state. This is the superconducting phase. In the dual strongly coupled field theory, the vortex lattice is present in the expectation value of a vector condensate.

This model is important in the context of chapter 4. As a holographic superconductor, it tells us that the superconducting phase transition can be triggered by a large enough non-abelian magnetic field. In addition, it features the spontaneous production of an inhomogeneous lattice ground state. Lattice ground states are crucial for the development of more realistic holographic condensed matter models so it is important to understand how they can come about. A holographic superconductor without a lattice tends to have infinite DC conductivity simply because of translation invariance of the ground state.

Moreover, our model might have implications for QCD. As we saw in chapter 3, there are various toy models of QCD that have vector particle condensates — either gluons, W-bosons or ρ-mesons — in the presence of strong magnetic fields. In this chapter we provide evidence that the effect is more general since it appears in two simple holographic models. We should thus not exclude the possibility that QCD itself has such lattice ground states.

This chapter is devoted to the details of the calculation in this model. It is based on the author's original work in [2]. We first describe the holographic model in section 5.1. We move on to the perturbative strategy needed to find the ground state in section 5.2. In section 5.3 we study the equations to linear order, where we show that an instability exists using both a quasinormal mode analysis and a Schrödinger potential analysis. Section 5.4 describes the possible lattice solutions that are valid at linear order. Identifying the triangular lattice as the ground state requires going to higher order. We show the reason for this by discussing

the field theory's ground state energy in section 5.5. We then solve the equations and present the results.

The instability in the normal phase solution was first found by the author and collaborators in [1, 3], while the ground state of the superconducting phase was found in [2, 4].

5.1 Holographic Setup

5.1.1 Geometry

The system we study is an Einstein–Yang–Mills theory on the (Poincaré patch of) an asymptotically AdS_5 with an $SU(2)$ gauge field. The action is given by

$$S = \int d^5x\sqrt{-g}\ \left\{\frac{1}{16\pi G_N}(R+\Lambda) - \frac{1}{4\hat{g}^2}\mathrm{tr}(F_{\mu\nu}F^{\mu\nu})\right\}, \tag{5.1}$$

where $\hat{g}$ is the Yang–Mills coupling, G_N in the 5D gravitational constant and L is the AdS_5 radius. R is the Ricci scalar and F is the Yang–Mills field strength.

We consider the probe approximation, where the Yang–Mills term is small compared to the Einstein–Hilbert term, so that the backreaction of the gauge fields onto the geometry can be neglected. We thus choose a fixed 5-dimensional AdS-Schwarzschild background geometry. The metric is

$$ds^2 = \frac{L^2}{u^2}\left(-f(u)dt^2 + dx^2 + dy^2 + dz^2 + \frac{du^2}{f(u)}\right), \tag{5.2}$$

where the asymptotically AdS region is at $u \to 0$.

We study two different models that turn out to have very similar properties. The first is a finite temperature model first proposed in [25]. In this case f is a blackening factor given by $f(u) = 1 - \frac{u^4}{u_H^4}$, which results in the AdS–Schwarzschild geometry. u_H the location of the planar black hole horizon. The Hawking temperature of the black hole is $T = 1/\pi u_H$.

The second model was introduced in [125, 126] as a simple attempt to model confinement holographically. The idea is to simply terminate the AdS geometry at a finite radial distance $u = u_C$ and impose Neumann boundary conditions on the fields there. It is therefore called the hard wall cutoff model. In this model we set $f(u) = 1$, so it corresponds to a zero-temperature theory if we let $u_C \to \infty$. The reason why this can be thought of as a crude model of confinement is that the part of the geometry corresponding to the IR of the field theory is absent. This constrains the fields to live in the UV, effectively confining them to a small space. Matching this model with QCD means choosing the cutoff scale such that $u_C \sim 1/\Lambda_{QCD}$.

In both models the geometry has a scaling symmetry. The metric is unchanged if each coordinate is rescaled by $x^\mu \to \lambda x^\mu$ for constant λ, as long as we also scale u_H and u_C. This means that, without loss of generality, we can set $u_H = u_C = 1$. This is simply a choice of units. Factors of u_H and u_C can be restored by dimensional analysis.

Unless otherwise noted, the following discussion will be independent of the particular model we are using. We specialise to the AdS–Schwarzschild model when performing the stability analysis because that involves features specific to

finite-temperature field theory. Also, when we get to the numerics, results from the two models are presented separately.

5.1.2 The Yang–Mills action

The relevant part of the action simplifies to

$$S = -\frac{1}{4\hat{g}^2}\int d^5x\sqrt{-g}\ \mathrm{tr}\left(F_{\mu\nu}F^{\mu\nu}\right), \tag{5.3}$$

with the equations of motion

$$\nabla^\mu F^a_{\mu\nu} + \epsilon^{abc}\mathcal{A}^{b\mu}F^c_{\mu\nu} = 0. \tag{5.4}$$

The $SU(2)$ gauge field is $\mathcal{A} = \mathcal{A}^a_\mu \tau^a dx^\mu$, for $a = 1\ldots 3$. We use the convention where the Lie algebra basis is given by $\tau^a = \frac{\sigma^a}{2i}$, with σ^a the Pauli matrices, and the structure constants f^{abc} are defined by $[\tau^a, \tau^b] = \epsilon^{abc}\tau^c$ so that $f^{abc} = \epsilon^{abc}$. With these definitions, the components of the field-strength tensor $F = d\mathcal{A}+\mathcal{A}\wedge\mathcal{A}$ become

$$F^a_{\mu\nu} = \partial_\mu \mathcal{A}^a_\nu - \partial_\nu \mathcal{A}^a_\mu + \epsilon^{abc}\mathcal{A}^b_\mu \mathcal{A}^c_\nu. \tag{5.5}$$

As mentioned at the start of the chapter, the main aim of this chapter is to look at the effect of a strong (flavour-)magnetic field given by $F^3_{xy} = B$, with all other components of $F^a_{\mu\nu}$ vanishing. We will see that when B becomes large[1], other components of F become non-zero dynamically. To get a consistent set of equations we therefore consider a gauge field $\mathcal{A}$ of the form

$$\mathcal{A} = \sum_{a=1,2,3,\mu=x,y} \mathcal{A}^a_\mu(t,x,y,u)\tau^a dx^\mu. \tag{5.6}$$

It turns out that we could turn off the t and z dependence of the gauge field and still have consistent equations. This simplifies the equations. Turning off the t dependence guarantees a static solution. Turning off the z dependence, where the z direction is parallel to the magnetic field, yields a lattice in the x, y-plane. For the moment we leave the t-dependence in the ansatz. This allows us to consider time-dependent perturbations while discussing the linearised solutions to the equations. When going to higher order, however, we turn the t-dependence off.

The action (5.3) has an $SU(2)$ gauge freedom. For the ansatz above to make sense, we need to specify how the gauge is fixed. It is therefore important to understand how gauge transformations affect the system. Under a gauge transformation $e^{i\Lambda(x^\mu)}$, $\mathcal{A}$ transforms as

$$\mathcal{A}_\mu \to \mathcal{A}_\mu + \delta\mathcal{A}_\mu = e^{i\Lambda}\mathcal{A}_\mu e^{-i\Lambda} - i\partial_\mu e^{i\Lambda}e^{-i\Lambda}. \tag{5.7}$$

When $\Lambda(x^\mu)$ is an infinitesimal transformation, this becomes

$$\delta\mathcal{A}^a_\mu = \mathcal{D}_\mu\Lambda^a = \partial_\mu\Lambda^a + \epsilon^{abc}\mathcal{A}^b_\mu\Lambda^c. \tag{5.8}$$

[1]Since we have chosen the units where $u_H = 1$ or $u_C = 1$, B is a dimensionless quantity. Restoring the units, the statement is that $Bu_H^2 = B/(\pi T)^2$ or $Bu_C^2 \sim B/\Lambda^2_{QCD}$ is large, or that B is large compared to the radial scale of the background.

The gauge transformations give us the freedom to fix the gauge $\mathcal{A}^a_u = 0$. We work in this gauge from now on. This does not, however, fix all the gauge symmetry. There are still gauge transformations that leave the choice $\mathcal{A}^a_u = 0$ intact. From (5.8) we see that for gauge transformations $\delta\mathcal{A}^a_u = 0$, we can still choose $\Lambda = \Lambda(t, x, y, z)$.

Choosing the solution $F^3_{xy} = B$, with all other components vanishing, breaks this remaining gauge symmetry. Only $U(1)$ transformations of the form $\Lambda = \Lambda^3(t, x, y, z)\tau^3$ leave the choice for F invariant. For B large enough, all the components in (5.6) become nonzero due to the dynamics; this breaks the remaining symmetry. We thus claim to have a superconductor, because the $U(1)$ symmetry is broken dynamically[2]. Taking the linear combinations $\mathcal{E}^\pm_\mu = \mathcal{A}^1_\mu \pm i\mathcal{A}^2_\mu$ gives fields that transform in the fundamental of the remaining gauge symmetry. It can be checked from (5.8) that $\mathcal{E}^\pm_\mu \to (1 \mp i\Lambda^3)\mathcal{E}^\pm_\mu$ whenever $\Lambda = \Lambda^3\tau^3$. Later on we work only with the fields $\mathcal{E}^+$, which we rename to $\mathcal{E}$.

5.1.3 Reading off field theory quantities

We learned in section 2.2.1 how to find the dual field theory source and expectation value from the boundary data of the gauge field. Equations (2.16) and (2.21) imply that in an expansion of the gauge fields near the AdS boundary, the leading term is the source and the subleading term is proportional to the vev. The field $\mathcal{A}^3_{x,y}$ has a boundary expansion given by

$$\mathcal{A}^3_{x,y}\big|_{u\to 0} = s^{(3)}_{x,y} + v^{(3)}_{x,y}u^2 + \dots, \tag{5.9}$$

where $s^{(3)}_{x,y}$ is the value of the source, which in this case is the externally applied magnetic field potential. $v^{(3)}_{x,y}$ is proportional to the vev, corresponding to the magnetisation. We set the boundary conditions so that the applied magnetic field is not corrected by the higher order perturbations in ε, whereas the magnetisation will obtain a non-zero value.

Similarly, the fields $A^{1,2}_{x,y}$ have a boundary expansion given by

$$\mathcal{A}^{1,2}_{x,y}\big|_{u\to 0} = s^{(1,2)}_{x,y} + v^{(1,2)}_{x,y}u^2 + \dots, \tag{5.10}$$

where $s^{(1,2)}_{x,y}$ corresponds to the source of the operator that will condense to break the $U(1)$ symmetry. We adjust the boundary conditions in such a way that this vanishes. This means that the symmetry breaking is spontaneous. $v^{(1,2)}_{x,y}$ is proportional to the vacuum expectation value of this operator, which we read off to find the resulting supercurrent in the superconducting phase.

Boundary conditions are also imposed on the fields in the IR. In the case of the black hole background, we impose regularity at the horizon and in the case of the hard wall model we impose Neumann boundary conditions.

5.2 Perturbative strategy

Substituting the ansatz (5.6) into equation (5.4) yields nine coupled partial differential equations in the variables t, x, y and u. Of these nine equations of

[2] Technically the field theory dual to this model is a superfluid, not a superconductor. This is because the $U(1)$ gauge symmetry in the bulk theory gets mapped to a global symmetry in the field theory. We can think of it as a "weakly-gauged" superconductor.

motion, six are dynamical equations for each field $\mathcal{A}^{1,2,3}_{x,y}$, and three equations are constraints. The constraint equations arise from the equations of motion for the components $\mathcal{A}^{1,2,3}_{u}$, which were chosen to be zero using gauge symmetry. A general solution to these equations is presumably not available in closed form. We make a perturbative ansatz and solve them order by order, as Abrikosov first did to find vortices in type II superconductors. Our strategy is based on Abrikosov's and is explained in the current section.

5.2.1 The comparison to Ginzburg–Landau theory

For clarity we rewrite the Ginzburg–Landau equations (3.4)–(3.5) as

$$(-i\nabla - \mathbf{A})^2 \phi - \phi + |\phi|^2\phi = 0, \tag{5.11}$$

$$\nabla \times \nabla \times \mathbf{A} = -i\left(\phi^*\nabla\phi - \phi\nabla\phi^*\right) - |\phi|^2\mathbf{A}. \tag{5.12}$$

Only the structure of these equations is important, so we have ignored constant factors. Here ϕ is the wave function of Cooper pairs, and $\mathbf{A}$ is the electromagnetic vector potential. The nine equations of motion in our system can be split into two groups that roughly correspond to the two equations above.

The first of the two groups, hereafter called the condensate equations, contains the six equations for the fields $\mathcal{A}^{1,2}_{x,y,u}$. The superconducting condensate of the dual field theory, which is like ϕ above, is found by differentiating the on-shell action with respect to the boundary values of $\mathcal{A}^{1,2}_{x,y}$, as in equation (2.21). Of the six equations in this group, the dynamical equations are for $\mathcal{A}^{1,2}_{x,y}$ and the constraint[3] equations are for $\mathcal{A}^{1,2}_{u}$. So this first group is analogous to equation (5.11).

The analogy can be made more clear. As mentioned above, we can make the field definitions $\mathcal{E}_{x,y} = \mathcal{A}^1_{x,y} + i\mathcal{A}^2_{x,y}$. Doing so allows us to combine the six real equations into three complex equations, two dynamical and one constraint. The constraint equation relates $\mathcal{E}_x$ and $\mathcal{E}_y$ such that there is only one complex degree of freedom left, which is analogous to the state ϕ. All this is hard to see at the non-perturbative level, but it illustrates the strategy we follow for solving the equations at each order: we use the constraint equation to reduce the two dynamical equations into one, and then solve it.

The second group of equations, which we call the magnetic field equations, is for the fields $\mathcal{A}^3_{x,y,u}$, corresponding to $\mathbf{A}$ in equation (5.12) above. There are three such equations, one of which is a constraint. At each order we will be able to use the constraint to separate the equations into one for $\mathcal{A}^3_x$ and one for $\mathcal{A}^3_y$.

5.2.2 The gauge field perturbative expansion

Our strategy works as follows. We first choose a constant external magnetic field, B, by setting $A^3_y = xB$ and $A^3_x = 0$. For B less than some critical value B_c, this configuration with all other components zero solves the equations of motion. This is the normal phase of the superconductor. We will show that the system enters a superconducting phase when the magnetic field is increased beyond some critical value B_c. In this phase, the ground state has a non-trivial profile for all the fields in the ansatz equation (5.6). We look for this configuration at some

[3]Recall that we have set $\mathcal{A}^a_u = 0$. However, its equations of motion still impose constraints on the other fields.

value of B infinitesimally above B_c, where the condensate is still small. This lets us do a perturbative expansion in a small parameter $\varepsilon \sim \frac{B-B_c}{B_c}$. To make the exposition clearer we leave this parameter ε explicit when studying the expansion. However, it will be absorbed into the definition of the perturbative corrections to the fields when we come to minimising the energy. We thus write an ansatz for the expansion in the form

$$\begin{aligned} \mathcal{A}^3_y &= xB_c + \varepsilon A^3_y + \varepsilon^2 a^3_y + \dots, \\ \mathcal{A}^a_\mu &= \varepsilon A^a_\mu + \varepsilon^2 a^a_\mu + \dots \qquad \text{for } (a,\mu) \neq (3,y), \end{aligned} \tag{5.13}$$

and solve the equations order by order in ε.

Having defined the ansatz for our gauge potential in equation (5.13) we can learn more about the perturbative expansion by studying the non-linear structure of the equations of motion. The equation for $\mathcal{A}^3_u$ is

$$-\mathcal{A}^2_x\partial_u\mathcal{A}^1_x - \mathcal{A}^2_y\partial_u\mathcal{A}^1_y + \mathcal{A}^1_x\partial_u\mathcal{A}^2_x + \mathcal{A}^1_y\partial_u\mathcal{A}^2_y + \partial_y\partial_u\mathcal{A}^3_y + \partial_x\partial_u\mathcal{A}^3_x = 0. \tag{5.14}$$

We see that the magnetic field components appear in the linear terms, while the condensate components appear in quadratic terms. This suggests that a contribution to the condensate components that is first order in the perturbative expansion influences a second order contribution in the magnetic field components. More generally, an odd order contribution to the condensate components influences an even order contribution to the magnetic field components.

This structure is common throughout all the equations of motion. It turns out that terms in the perturbative expansion of the magnetic field components that have an odd order vanish. The even order terms in the condensate components can then also be set to zero. We can thus constrain the expansion ansatz of equation (5.13) to

$$\begin{aligned} \mathcal{E}_{x,y} &= \varepsilon E_{x,y} + \varepsilon^3 e_{x,y} + \mathcal{O}(\varepsilon^5), \\ \mathcal{A}^3_y &= xB_c + \varepsilon^2 a^3_y + \mathcal{O}(\varepsilon^4), \\ \mathcal{A}^3_x &= \varepsilon^2 a^3_x + \mathcal{O}(\varepsilon^4). \end{aligned} \tag{5.15}$$

Here the calligraphic letters denote the non-perturbative fields. $E_{x,y}$ and $e_{x,y}$ are first and third order contributions to the condensate components, respectively, while $a^3_{x,y}$ are second order corrections to $\mathcal{A}^3_{x,y}$.

Because of this convenient expansion of the fields, the condensate components and the magnetic components decouple at each order. That means that at each order, we only need to work with fields we have already solved at previous orders. Our strategy is thus to solve for the fields in the following sequence:

$$\begin{array}{lcccccl} \mathcal{E}_{x,y} = & & \boxed{\varepsilon E_{x,y}} & + & \boxed{\varepsilon^3 e_{x,y}} & + \mathcal{O}(\varepsilon^5), \\ \mathcal{A}^3_y = & xB_c & + & \boxed{\varepsilon^2 a^3_y} & & + \mathcal{O}(\varepsilon^4), \\ \mathcal{A}^3_x = & & & \boxed{\varepsilon^2 a^3_x} & & + \mathcal{O}(\varepsilon^4). \end{array}$$

In the next section we start with the linear order solution, which will shed more light on the procedure that must be implemented at higher orders.

5.3 The linearised equations

We can extract many interesting features of the physics of the system by solving the equations to linear order. The most remarkable thing we find at linear order is that the equations have a nontrivial solution in a certain parameter range — when B is *larger* than some critical value, B_c. This nontrivial solution, as we show in a later section by going beyond linear order, represents a state with lower free energy than the trivial solution and so it is the preferred state.

Another remarkable feature is the precise form of the solutions. At linear order the equations are separable. This means our work is divided between two components — the form of the solution in the boundary field theory's spatial directions and the radial profile of the solution. Both components tell an interesting story. The spatial component tells us that the field theory condensate is made up of vortices. At this order the vortices do not interact, but we eventually show by going to higher order that they form a triangular lattice in their ground state.

From the radial component we can tell the renormalisation behaviour of the dual field theory. The fields' radial profile vanishes at the boundary, in the field theory's UV, and is nonzero in the bulk, the field theory's IR. The new ground state thus shows the emergence of a lattice at low energies.

In this section we first use the linearised equations to show that the trivial solution is not stable. This is done by considering small fluctuations of the fields about the trivial solution. These fluctuations grow exponentially above a critical value B_c of the magnetic. This indicates an instability of the trivial solution and suggests the presence of a different ground state. This stability analysis goes hand-in-hand with finding the general form of the new ground state. In the next section we show how to obtain vortices distributed in a lattice from this general form.

5.3.1 Separating the equations

To study fluctuations about the trivial solution, we assume that the fields have time dependence proportional to $e^{-i\omega t}$. Using the expansion (5.15), we then find that the linear order equations of motion (in complex form) are

$$0 = iBx\partial_u E_y + \partial_y\partial_u E_y + \partial_x\partial_u E_x, \tag{5.16}$$

$$0 = \left(B^2x^2 - \frac{\omega^2}{f}\right)E_x - iBE_y + \left(\frac{f}{u} - f'\right)\partial_u E_x - f\partial_u^2 E_x - 2iBx\partial_y E_x - \partial_y^2 E_x + iBx\partial_x E_y + \partial_x\partial_y E_y, \tag{5.17}$$

$$0 = \left(2iB - \frac{\omega^2}{f}\right)E_x + \left(\frac{f}{u} - f'\right)\partial_u E_y - f\partial_u^2 E_y + iBx\partial_x E_x + \partial_x\partial_y E_x - \partial_x^2 E_y. \tag{5.18}$$

Here, as above, $f(u) = 1 - u^4$ for the AdS Schwarzschild model and $f(u) = 1$ for the hard wall model.

These equations can be solved by following Abrikosov [43], where he uses a rather elegant trick. First we assume that the solution is independent of y, which gets rid of all the terms with y-derivatives in the equations. This allows us to solve for E_y in terms of E_x, giving the solution

$$E_y = \frac{i}{Bx}\partial_x E_x. \tag{5.19}$$

The next thing to notice is that the equations are separable, so we make the ansatz $E_x = X(x)\mathcal{U}(\omega, u)$. We then solve the equations for X and $\mathcal{U}$, and afterwards restore the y-dependence using a cunning observation about our gauge choice. We chose the gauge where $\mathcal{A}_y^3 = xB$, but we could equally well have chosen that $\mathcal{A}_y^3 = xB - k$, for some constant k. This gives the same physical magnetic field, namely $F_{xy} = B$. Since the equations of motion now have $x - k/B$ everywhere that x appeared, the solution to E_x in this different gauge is now $E_x = X(x - k/B)\mathcal{U}(\omega, u)$. From (5.7) we see that the change $\mathcal{A}_y^3 = xB \to xB - k$ is the result of the gauge transformation $\Lambda^3 = -yk$. But also notice from the gauge transformations that this transforms

$$E_x \to e^{-i\Lambda^3} E_x = e^{iky} E_x. \tag{5.20}$$

In terms of the solution functions,

$$E_x = X(x)\mathcal{U}(\omega, u) \to e^{iky} X(x)\mathcal{U}(\omega, u) = X(x - k/B)\mathcal{U}(\omega, u). \tag{5.21}$$

In other words, once we have the solution $X(x)\mathcal{U}(\omega, u)$ in our original gauge, we know that $e^{-iky} X(x - k/B)\mathcal{U}(\omega, u)$ is also a solution. In general, since the equations of motion are linear PDE's (to this order), the solution is

$$E_x = \sum_n e^{-inky} X\left(x - \frac{nk}{B}\right)\mathcal{U}(\omega, u). \tag{5.22}$$

The y-dependence is restored!

The next step is then to find X and $\mathcal{U}$. Here there are no elegant tricks and the equations have to be solved by brute force. The constraint equation (5.16) fixes E_y in terms of E_x, and then the equation of motion for E_y, (5.18), becomes the x-derivative of equation (5.17). So there is only one separable equation to solve. It yields the equations for $X(x)$ and $\mathcal{U}(\omega, u)$,

$$-C = B^2x^2 + \frac{\frac{2X'}{x} - X''}{X}, \tag{5.23}$$

$$C = -\frac{\omega^2}{f} + \frac{\left(\frac{f}{u} - f'\right)\mathcal{U}' - f\mathcal{U}''}{\mathcal{U}}, \tag{5.24}$$

where C is the separation constant and prime denotes differentiation with respect to u.

The X equation

The X equation is identical to the one for the quantum harmonic oscillator. To solve it, first define a function $Y(x)$ such that $X(x) = e^{-\frac{B}{2}x^2} Y(x)$. We will assume that $B > 0$. This analysis will be slightly modified for $B < 0$ but should still work. Then (5.23) becomes

$$xY''(x) - 2(Bx^2 + 1)Y' + x(B - C)Y = 0. \tag{5.25}$$

Now we change variables to $y = Bx^2$ to get

$$yY''(y) + \left(-\frac{1}{2} - y\right)Y' - \frac{C - B}{4B}Y = 0. \tag{5.26}$$

This is the confluent hypergeometric differential equation, also known as Kummer's differential equation. It has solutions

$$Y(x) = \mathcal{A}\ {}_1F_1\left(\frac{C-B}{4B}; -\frac{1}{2}; Bx^2\right) + \mathcal{B}\ U\left(\frac{C-B}{4B}; -\frac{1}{2}; Bx^2\right). \tag{5.27}$$

${}_1F_1(a;b;z)$ and $U(a;b;z)$ are the confluent hypergeometric functions of the first and second kind, respectively. We need to analyse the asymptotic behaviour of these functions to find out when they will produce physical solutions that are regular for all x. As $x \to \infty$,

$$\begin{aligned} {}_1F_1(a;b;Bx^2) \sim\ & e^{Bx^2}(Bx^2)^{a-b}\left(\frac{\Gamma(b)}{\Gamma(a)} + \mathcal{O}\left(\frac{1}{x^2}\right)\right) \\ & + \frac{(-Bx^2)^{-a}\Gamma(b)}{\Gamma(b-a)}\left(1 + \mathcal{O}\left(\frac{1}{x^2}\right)\right). \end{aligned} \tag{5.28}$$

Looking at the first term, it is clear that this function will blow up exponentially at infinity, except in the special case where the $1/\Gamma(a)$ diverges and cancels out the exponential. This happens whenever $a = -n$ for $n \in \mathbb{N}$. (Recall that in $X(x)$, this term is multiplied by $e^{-\frac{B}{2}x^2}$, which is not enough to cancel the exponential divergence.) So for $a = -n$, this expansion does not hold. There is another identity we can use for $a = -n$, and in fact it shows that ${}_1F_1$ becomes the polynomial

$${}_1F_1\left(-n; b; Bx^2\right) = \frac{n!}{(b)_n} L_n^{b-1}(Bx^2), \tag{5.29}$$

where L_n^{b-1} is the n^{th} generalized Laguerre polynomial and $(\cdot)_n$ the Pochhammer symbol.

Using an identity we can write the second term in $Y(x)$ as

$$\begin{aligned} U\left(a; -\frac{1}{2}; Bx^2\right) = & \frac{\Gamma(\frac{3}{2})}{\Gamma(a+\frac{3}{2})}{}_1F_1\left(a; -\frac{1}{2}; Bx^2\right) \\ & + \frac{\Gamma(-\frac{3}{2})}{\Gamma(a)}(Bx^2)^{\frac{3}{2}}{}_1F_1\left(a+\frac{3}{2}; \frac{5}{2}; Bx^2\right). \end{aligned} \tag{5.30}$$

This shows that $U(a; -\frac{1}{2}; Bx^2) \sim e^{Bx^2}$ as $x \to \infty$ unless $a = -n$ or $a = -n - \frac{3}{2}$, and it is indeed possible to show that U is a polynomial for these values of a. To do this, we use the identities

$$U\left(a; -\frac{1}{2}; z\right) = \frac{-\frac{1}{2}+z}{-\frac{1}{2}-a}U\left(a; \frac{1}{2}; z\right) - \frac{z}{-\frac{1}{2}-a}U\left(a; \frac{3}{2}; z\right), \tag{5.31}$$

$$U\left(-\frac{n}{2}; \frac{1}{2}; z\right) = 2^{-n}H_n\left(\sqrt{z}\right) \qquad \text{for } n \in \mathbb{N}, \tag{5.32}$$

$$U\left(\frac{1}{2} - \frac{n}{2}; \frac{3}{2}; z\right) = \frac{2^{-n}}{\sqrt{z}}H_n\left(\sqrt{z}\right) \qquad \text{for } n \in \mathbb{N}, \tag{5.33}$$

where H_n are the Hermite polynomials, to show that, for $a = -n - \frac{3}{2}$,

$$\begin{aligned} U\left(-n-\frac{3}{2}; -\frac{1}{2}; Bx^2\right) = & \frac{z-\frac{1}{2}}{n+1}2^{-2n-3}H_{2n+3}\left(\sqrt{Bx^2}\right) \\ & - \frac{\sqrt{z}}{n+1}2^{-2n-4}H_{2n+4}\left(\sqrt{Bx^2}\right). \end{aligned} \tag{5.34}$$

This is a polynomial and thus regular for all x. For $a = -n$, we simply need the identity

$$U\left(-n; c; Bx^2\right) = (-1)^n n! L_n^{c-1}(Bx^2) \tag{5.35}$$

to see that U reduces to a polynomial.

We thus see that the solutions for $X(x)$ blow up exponentially for large x, unless a takes some particular values. At these particular values $X(x)$ becomes an exponentially suppressed polynomial. These solutions are physical. We would like the physical solution with least energy, since this is the state that will condense first. Since the energy of a quantum state increases with the number of roots, this means we need to pick the polynomial solution with no roots. This corresponds to choosing $a = 0$. In our case, $a = \frac{C-B}{4B}$, or $B = \frac{C}{1+4a}$. This means that the constraint we have on a to produce physical solutions translates to a constraint on C. Since $B > 0$, this means $C > 0$. Note that higher values of a cannot then be chosen, since they would change the sign of B.

The $\mathcal{U}$ equation

Choosing the lowest Landau level solution for X gives that the separation constant $C = B$. This turns equation (5.24) into

$$\mathcal{U}'' + \left(\frac{f'}{f} - \frac{1}{u}\right)\mathcal{U}' + \left(\frac{B}{f} + \frac{\omega^2}{f^2}\right)\mathcal{U} = 0. \tag{5.36}$$

The thing to notice here is that the equation has an effective mass term for $\mathcal{U}$, and that the square of the mass is negative for large B and ω. This suggests that when we solve the equation, we will find a non-trival profile for $\mathcal{U}$ at large B. In the next subsection we will investigate that further. In this subsection we look at the behaviour of the $\mathcal{U}$ equation at its domain boundaries.

The equation is most subtle for the AdS–Schwarzschild model, when $f(u) = 1 - u^4$. It has regular singular points at $u = 1$, the location of the black hole horizon. The way to get around the singular points and solve the equation is to use the Frobenius method. We write $\mathcal{U}(\omega, u) = (1-u)^\nu F(u)$, and assume that $\mathcal{U}(\omega, u) \sim (1-u)^\nu$ at $u \approx 1$, which is the same as requiring $F(u) \to 1$ as $u \to 1$. In this limit the equation becomes

$$\begin{aligned} 0 = \nu(\nu-1)(1-u)^{\nu-2} + \nu\frac{3u^3 + \frac{1}{u}}{1-u^4}(1-u)^{\nu-1} \\ + \left(\frac{B}{1-u^4} + \frac{\omega^2}{(1-u^4)^2}\right)(1-u)^\nu \end{aligned} \tag{5.37}$$

$$\Rightarrow 0 = \nu(\nu-1) + \frac{\nu\left(3u^3 + \frac{1}{u}\right)}{(1+u^2)(1+u)} + \frac{B(1-u)}{(1+u^2)(1+u)} + \frac{\omega^2}{(1+u^2)^2(1+u)^2}. \tag{5.38}$$

Evaluating this at the horizon gives $\nu = \pm\frac{i\omega}{4}$. The two possible solutions correspond to waves travelling into or out of the horizon. Since it is a black hole, the physical option would be to have waves propagating only into the horizon. This also agrees with the prescription for calculating retarded Green's functions

that was proposed by [97]. We see which solution is ingoing by looking at the near-horizon behaviour of the field, given by

$$E_x(t,x,u) \sim e^{-i\pi T\omega t}\mathcal{U}(u) \tag{5.39}$$
$$= e^{-i\pi T\omega t \pm i\frac{\omega}{4}\ln(1-u)}. \tag{5.40}$$

From this it is clear that the ingoing wave, going to larger u, is given by the solution $\mathcal{U} = (1-u)^{-i\frac{\omega}{4}}F(u)$.

In the hardwall model, the geometry ends at $u = 1$ but is otherwise entirely regular there. We impose the boundary condition $U'(1) = 0$.

It is also instructive to look at the behaviour of equation (5.36) near the boundary. The boundary behaviour is identical for both models. At $u \approx 0$, it becomes

$$\mathcal{U}'' - \frac{\mathcal{U}'}{u} + (\omega^2 + B)\mathcal{U} = 0. \tag{5.41}$$

Using the ansatz that $\mathcal{U} \sim u^\Delta$ near the boundary, we get

$$\Delta(\Delta-1)u^{\Delta-2} - \Delta u^{\Delta-2} + (\omega^2+B)u^\Delta = 0, \tag{5.42}$$

which has solutions for $\Delta = 0$ and $\Delta = 2$.

5.3.2 Fluctuation stability analysis

Since X is independent of ω, we can focus only on the radial equation to analyse the fluctuations. We also focus only on the AdS–Schwarzschild model, because the finite temperature makes it more interesting and realistic. Note however that this stability analysis is not strictly necessary, so we do not need to repeat it for the hard wall model. In later sections we find the new ground state directly, so its existence does not need to be proved first. The stability analysis does however introduce some interesting physical concepts, so we include it here.

We analyse the instability of the system for various values of B in two ways. The first is by using *quasinormal modes*, which we first introduced in section 4.3. As we have mentioned, the correct boundary conditions for the radial equation (5.36) are the infalling condition at the horizon and vanishing condition at the boundary. When these are imposed, equation (5.36) has solutions only for particular values of ω. It was shown in [127] that when $B = 0$, the possible values of ω are $\omega_n = n(\pm 2 - 2i)$. The fact that these frequencies can be imaginary should not be surprising. Recall that the fluctuations have a time dependence that goes like $e^{-i\omega t}$. When ω is purely real the fluctuation is a standing wave, also known as a normal mode. When ω has a negative imaginary part, the fluctuation gets exponentially smaller. This dissipation of the energy of the fluctuation comes from the ingoing boundary conditions at the horizon — energy is falling into the black hole. Because of the dissipation, this is no longer a normal mode but is rather called a quasinormal mode. The (complex) frequency of a quasinormal mode is its *quasinormal frequency*. When the quasinormal frequencies have a positive imaginary part, the fluctuations blow up. This indicates an instability in the gauge field, and is the signal we are looking for that a non-trivial profile of the gauge field (and thus a condensate in the dual theory) is forming.

The easiest way to investigate the quasinormal frequencies is by looking at the retarded Green's function dual to the fluctuations. This is because the quasinormal

frequencies are the locations of the poles of the Green's function. We thus first look at Son et al.'s prescription for calculating the retarded Green's function to see why this is, and then analyse the motion of the quasinormal frequencies in the complex plane as a function of the background magnetic field.

The second approach we use is a Schrödinger potential analysis, where we rewrite the radial equation as a Schrödinger equation and look for the formation of bound states. This we do in section 5.3.4.

5.3.3 The poles of the retarded Green's function

The first part of the prescription from [97] requires choosing infalling boundary conditions for the bulk field near the black hole horizon. We have already imposed those conditions above. Now we work out the retarded Green's function dual to the fluctuations by using the AdS/CFT dictionary described in chapter 2.

First we Fourier transform the gauge field in the boundary directions,

$$A^a_\mu(x,u) = \int \frac{d^4k}{(2\pi)^4} e^{ik^i x_i} \tilde{A}^a_\mu(k^i,u), \tag{5.43}$$

and substitute it into the on-shell action (2.22) to give

$$S_{\text{on-shell}} = -\frac{1}{2\hat{g}^2}\int \frac{d^4k}{(2\pi)^4}\sqrt{-\gamma}n^u\Big(\tilde{A}^{a\nu}(-k^i,u)\partial_u\tilde{A}^a_\nu(k^i,u) - \tilde{A}^{a\nu}(-k^i,u)\partial_\nu\tilde{A}^a_u(k^i,u)\Big)\Big|_{u=\epsilon}. \tag{5.44}$$

We ignored the bulk term in (2.22) because it vanishes at linear order. In our case $\tilde{A}_u = 0$, so the second term disappears. The next step is to write the bulk field in momentum space as

$$\tilde{A}^a_\mu(k^i,u) = p^a_\mu(k^i,u)\tilde{A}^a_{0\mu}(k^i) \qquad \text{(no sum)}, \tag{5.45}$$

where $A^a_{0\mu}(k^i)$ is the boundary ($u=\epsilon$) value of $A^a_\mu(k^i,u)$, and $p^a_\mu(k^i,u)$ gives its u-dependence, with $\lim_{u\to 0} p^a_\mu(k^i,u) = 1$. Then,

$$S_{\text{cl}} = -\frac{1}{2\hat{g}^2}\int \frac{d^4k^i}{(2\pi)^4}\sqrt{-\gamma}n^u g^{\mu\nu}\tilde{A}^a_{0\mu}(-k^i)p^a_\mu(-k^i,u)\partial_u p^a_\nu(k^i,u)\tilde{A}^a_{0\nu}(k^i)\Big|_{u=\epsilon}. \tag{5.46}$$

According to the recipe proposed by [97], we now know that the retarded Green's function in the boundary theory is given by

$$\begin{aligned}(G^R)^{ab}_{\mu\nu}(k^i) &= -i\int d^4x e^{-ik^i x_i}\theta(t)\langle[J^a_\mu(k^i),J^b_\nu(0)]\rangle \\ &= -\int d^4x e^{-ik^i x_i}\theta(t)\frac{\delta^2 S_{\text{cl}}}{\delta A^{a\mu}_0(x)\delta A^{b\nu}_0(0)} \\ &= \frac{1}{\hat{g}^2}\sqrt{-\gamma}n^u\delta^{ab}g_{\mu\nu}p^a_\mu(-k^i,u)\partial_u p^b_\nu(k^i,u)\Big|_{u\to 0},\end{aligned} \tag{5.47}$$

with no sum over the indices. Using equation (5.45), we can rewrite this as

$$(G^R)^{ab}_{\mu\nu}(k^i) = \frac{1}{g^2}\sqrt{-\gamma}n^u\delta^{ab}g_{\mu\nu}\frac{\tilde{A}^a_\mu(-k^i,u)}{\tilde{A}^a_\mu(-k^i,0)}\frac{\partial_u\tilde{A}^b_\nu(k^i,u)}{\tilde{A}^b_\nu(k^i,0)}\Big|_{u\to 0}. \tag{5.48}$$

Now, we changed variables to the $E^{\pm}_{\mu}$ fields, so we should write the Green's function in terms of these fields as well. A change of variables gives

$$\begin{aligned}(G^R)^{+-}_{\mu\nu}(k^i) &= -i\frac{\delta^2 S_{\rm cl}}{\delta E^{+\mu}(k^i)\delta E^{-\nu}(0)} \\ &= -\frac{i}{4}\frac{\delta^2 S_{\rm cl}}{\delta A^{1\mu}(k^i)\delta A^{1\nu}(0)} - \frac{i}{4}\frac{\delta^2 S_{\rm cl}}{\delta A^{2\mu}(k^i)\delta A^{2\nu}(0)} \\ &\qquad - \frac{1}{4}\frac{\delta^2 S_{\rm cl}}{\delta A^{2\mu}(k^i)\delta A^{1\nu}(0)} + \frac{1}{4}\frac{\delta^2 S_{\rm cl}}{\delta A^{1\mu}(k^i)\delta A^{2\nu}(0)} \\ &= \frac{1}{4}(G^R)^{11}_{\mu\nu}(k^i) + \frac{1}{4}(G^R)^{22}_{\mu\nu}(k^i), \end{aligned} \tag{5.49}$$

where we used (5.47) to get to the last line. The other components are

$$(G^R)^{-+}_{\mu\nu}(k^i) = \frac{1}{4}(G^R)^{11}_{\mu\nu}(k^i) + \frac{1}{4}(G^R)^{22}_{\mu\nu}(k^i), \tag{5.50}$$

$$(G^R)^{++}_{\mu\nu}(k^i) = 0, \tag{5.51}$$

$$(G^R)^{--}_{\mu\nu}(k^i) = 0. \tag{5.52}$$

Since $E^{\pm}_x$ is separated as $E^{\pm}_x = \mathcal{U}(\omega,u)\tilde{X}(q)$, where $k^i = (\omega, q, 0, 0)$, we can focus solely on the u (and ω) dependence of the Green's function to get

$$(G^R)^{+-}_{xx}(\omega) \sim \left.\frac{\mathcal{U}'(\omega,u)}{\mathcal{U}(\omega,0)}\right|_{u\to 0}. \tag{5.53}$$

We see that zeroes of $\mathcal{U}(\omega,0)$ give poles in the retarded Green's function. But these zeroes are precisely the vanishing Dirichlet boundary conditions we need to impose for fluctuations. Thus, since the physical modes fluctuate at the quasinormal frequencies, we have shown that the quasinormal frequencies are at the locations of the poles in the retarded Green's function.

There is a nice way of interpreting poles in the Green's function with a negative imaginary part. Consider a pole in the Green's function at $\omega_0 - i\Gamma$, with $\omega_0, \Gamma > 0$. It looks like

$$G^R(\omega) \sim \frac{1}{\omega - \omega_0 + i\Gamma}. \tag{5.54}$$

Since the spectral density is $\mathfrak{R}(\omega) = -2\ \mathrm{Im}\, G^R(\omega)$, this pole gives a spectral density that looks like

$$\mathfrak{R}(\omega) \sim \frac{2\Gamma}{(\omega-\omega_0)^2 + \Gamma^2}, \tag{5.55}$$

which is a peak located at ω_0 with a width given by Γ. Thus, in the spectral density where one only looks at real ω, it makes sense to interpret these peaks as quasi-particles with a lifetime of $1/\Gamma$. Of course, this applies only when the imaginary part of the frequency ω is negative, because the fluctuations blow up otherwise.

We can plot the Green's function in equation (5.53) as a function of the frequency ω. For this it is required to calculate $\mathcal{U}(\omega,u)$ and $\mathcal{U}'(\omega,u)$ at the AdS boundary. We do this by integrating numerically from the horizon to the boundary. To avoid numerical infinities, the idea is to start at just outside the horizon,

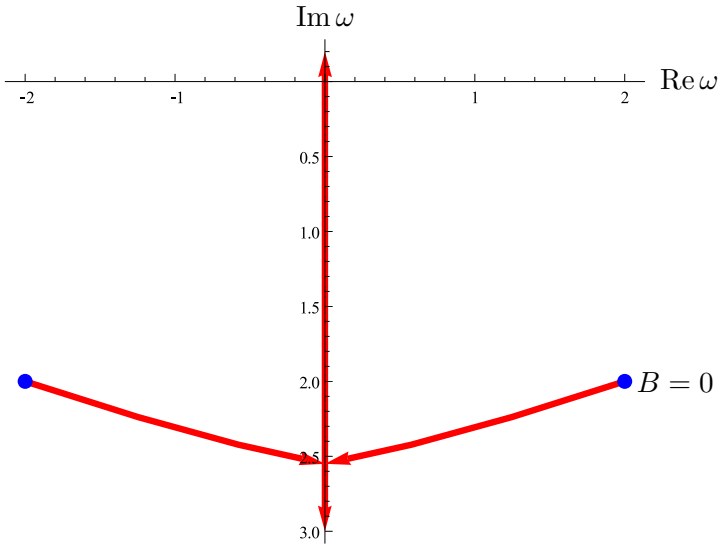

Figure 5.1: The movement of the poles of the Green's function at increasing B. The two lowest order poles (with imaginary part closest to zero) start at $\omega = \pm 2 - 2i$. They move towards the imaginary axis, merge, then split again. The merging happens when $B \approx 1.92$. One pole then moves downward, away from 0 and outside the range of the figure. The other, which is drawn, moves towards 0 and eventually crosses the real axis into the upper half-plane when $B = B_c \approx 5.15$.

$u_{\text{start}} = 1 - 10^{-5}$, and integrate to just before the boundary at $u_{\text{end}} = 10^{-5}$. We then of course need to find $\mathcal{U}(\omega, u_{\text{start}})$. This is done by expanding $\mathcal{U}(\omega, u)$ in a Taylor series near $u = 1$ and fixing $\mathcal{U}(\omega, 1) = 1$, and then we can calculate the series coefficients that satisfy the equation of motion. $\mathcal{U}(\omega, u)$ looks like

$$\mathcal{U}(\omega, u) = (1-u)^{-i\frac{\omega}{4}} \left(1 + \frac{-2\omega + (3\omega^2 + 4B)i}{8(\omega + 2i)}(u-1) + \dots\right), \tag{5.56}$$

which can be used to find $\mathcal{U}(\omega, u_{\text{start}})$. We then plot the result for various values of ω and B to find the poles and how they move as B changes. The result for the two lowest-order poles is plotted in figure 5.1.

When $B = 0$, the lowest-order poles start off at $\omega = \pm 2 - 2i$. Increasing B, they move towards the imaginary axis until they merge. They then split again as B is increased further, with one pole moving towards negative imaginary values and the other moving towards positive imaginary values. Eventually the pole moving upwards crosses the real axis at a critical value of the magnetic field, B_c. This is the instability we were looking for. This instability means that the field gains a nontrivial profile, producing the condensate in the dual field theory.

Note also that the instability happens at $\omega = 0$. This means we can switch off the time-dependence of the equations and find a static new ground state. Also, every time a higher order pole ω_n reaches the origin we have a solution $\mathcal{U}$ with $\omega = 0$. These are however higher energy solutions to $\mathcal{U}$. Since we wish to find a new ground state, we focus on the lowest energy case, which is when the first pole reaches the origin.

5.3.4 Schrödinger potential analysis

The second qualitative way of understanding the instability comes from rewriting the radial equation (5.36) as a Schrödinger equation of the form

$$-\partial_{R_*}^2\psi + V_S\psi = E\psi. \tag{5.57}$$

The Schrödinger potential V_S then determines the possible values of the energy spectrum $E = \omega^2$. R_* is a coordinate that we define below. To rewrite equation (5.36) as a Schrödinger equation, we follow the procedure described in the appendix of [128].

We first switch to the radial AdS coordinate $r = \frac{1}{u}$. Recall that with this coordinate, the horizon is at $r = 1$ while the boundary is at $r = \infty$. Making the replacement, equation (5.36) becomes

$$\left(2 - \frac{1}{r^4} - r^4\right)U'' + \left(\frac{1}{r^5} + \frac{2}{r} - 3r^3\right)U' + B\left(-1 + \frac{1}{r^4}\right)U = \omega^2 U. \tag{5.58}$$

Using the definitions

$$H_0 = \left(r^2 - \frac{1}{r^2}\right)^2, \tag{5.59}$$

$$H_1 = \frac{1}{r} - r^3, \tag{5.60}$$

$$H_2 = -B + \frac{B}{r^4}, \tag{5.61}$$

this becomes

$$-\frac{H_0}{H_1}\partial_r\left(H_1\partial_r U\right) + H_2 U = \omega^2 U. \tag{5.62}$$

Next we write U as the product of two functions of r, $U(\omega, r) = h(r)\psi(\omega, r)$. Then

$$-H_0\psi'' - H_0\left(2\frac{h'}{h} + \frac{H_1'}{H_1}\right)\psi' + \left[H_2 - H_0\left(\frac{h''}{h} + \frac{H_1'}{H_1}\frac{h'}{h}\right)\right]\psi = \omega^2\psi. \tag{5.63}$$

By introducing a new coordinate

$$R_* = \int_r^\infty \frac{d\bar{r}}{\sqrt{H_0(\bar{r})}} = \frac{1}{4}\left(\pi + 2\text{arccoth } r - 2\arctan r\right), \tag{5.64}$$

the first term becomes $-H_0\psi'' = -\partial_{R_*}^2\psi + \frac{\partial_{R_*}H_0}{2H_0}\partial_{R_*}\psi$. We can then set

$$h = \frac{H_0^{\frac{1}{4}}}{H_1^{\frac{1}{2}}}, \tag{5.65}$$

which will eliminate all terms in ψ'. The resulting equation is

$$-\partial_{R_*}^2\psi + V_S\psi = \omega^2\psi \tag{5.66}$$

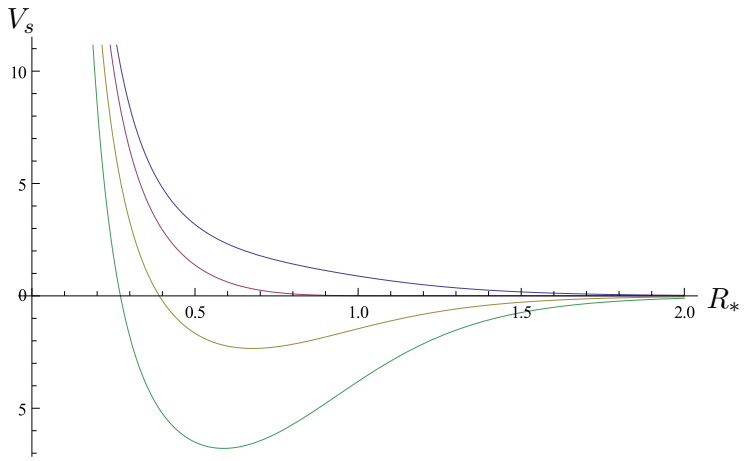

Figure 5.2: The Schrödinger potential at different values of B. It is helpful to compare this with figure 5.1. From top to bottom, the curves show the potential at the values $B = 0,\ 1.92,\ 5.15$ and 10. The first curve shows the potential when there is no magnetic field, the second one is for the value of B at which the poles merge on the imaginary axis, the third is for the value at which the first pole crosses the real axis, and the final value is to see what the potential does at higher B. We see that a potential well forms with negative potential energy. The value $B = 1.92$ is roughly where the curve first dips below zero, which is where the poles in figure 5.1 merge.

where

$$V_S = H_2 - H_0\left(\frac{h''}{h} + \frac{H_1'}{H_1}\frac{h'}{h}\right) \tag{5.67}$$

$$= \frac{\left(-1+r^4\right)\left(5-4Br^2+3r^4\right)}{4r^6} \tag{5.68}$$

$$= \frac{\left(1-u^4\right)\left(3-4Bu^2+5u^4\right)}{4u^2}. \tag{5.69}$$

This is the potential in the Schrödinger equation.

The coordinate R_* is like the "tortoise" coordinate from Schwarzschild spacetime. Near the event horizon, as $r \to 1$, $H_0 \approx (r-1)^2$, which gives $R_* \sim -\ln(r-1)$ and so $R_* \to +\infty$. For large r, $H_0 \sim r^4$, giving $R_* \sim \frac{1}{r} \to 0$. H_0 is positive everywhere whenever $r > 1$, so R_* is a monotonic function.

Equation (5.64) needs to be inverted numerically to get r as a function of R_*. It requires a simple root-finding algorithm. Once this is done, we can plot the potential for various values of B, as in figure 5.2.

Solving the Schrödinger problem that we have set up with the appropriate boundary conditions, we can analyze the quasinormal modes. The appropriate boundary condition, as before, is that we choose infalling waves at the horizon, $R_* \to \infty$. We see that there is an infinite potential wall at $R_* = 0$, which makes sense since this corresponds to the AdS boundary. We thus need to impose vanishing boundary conditions at this potential wall.

Infalling boundary conditions at the horizon, as we calculated before, mean

that

$$U \sim e^{-i\frac{\omega}{4}\ln(1-u)} \tag{5.70}$$

$$\sim e^{-i\frac{\omega}{4}\ln(r-1)} \tag{5.71}$$

$$\Rightarrow h\psi \sim e^{i\frac{\omega}{4}R_*}. \tag{5.72}$$

The definition of h in equation (5.65) shows that it does not depend on ω, so it must be that $\psi \sim e^{i\frac{\omega}{4}R_*}$ as $R_* \to \infty$.

For small values of B, the potential is monotonically decreasing. Generally in such a case we expect the energy eigenvalues to be complex. We thus suppose that $\omega = \Omega + i\Gamma$, for Ω and Γ real. The energy becomes $E = \omega^2 = \Omega^2 - \Gamma^2 + 2i\Omega\Gamma$. The imaginary part of the energy can be positive or negative, describing either a growing or a decaying mode. The growing modes might appear to be a problem, but since the Schrödinger potential analysis is just an analytical tool, one should not assign these modes any physical significance.

For B big enough, a potential well forms, and eventually it becomes possible for ψ to form a bound state. For such a bound state, ψ should decay exponentially towards the horizon. Given the boundary condition there, $\psi \sim e^{i\frac{\omega}{4}R_*} \sim e^{-\frac{\Gamma}{4}R_*}$, this means that we expect $\Gamma > 0$. In other words, a bound state in a negative-energy well is a sign that a quasinormal mode has crossed the real axis to positive imaginary values. This agrees with our previous analysis of the quasinormal modes.

5.4 Lattice solutions

In the process of showing the existence of a new ground state, we have also found the general form that this ground state takes to linear order and at low energy. We have shown that the lowest Landau level solution is given by

$$E_y = -iE_x, \tag{5.73}$$

$$E_x = \sum_{n=-\infty}^{\infty} C_n e^{-inky - \frac{1}{2}B_c\left(x - \frac{nk}{B_c}\right)^2} \mathcal{U}(u), \tag{5.74}$$

where k and the C_n are constants and $\mathcal{U}$ satisfies equation (5.36) with $\omega = 0$. As mentioned earlier, there are multiple such functions $\mathcal{U}$, but we take the lowest energy one. For the AdS Schwarzschild model we get $B_c \approx 5.1$ and for the hard wall model we get $B_c \approx 5.8$[4].

It should be noted that the solution (5.74) for E_x agrees (except for the factors of $\mathcal{U}(u)$ and $f(t,z)$) with the linear order solutions we found for the various models in chapter 3. In equations (3.30) and (3.38) however we chose the continuous form of the solution, whereas here we replaced the integral with a sum. This is so that we only have discrete coefficients C_n to deal with rather than functions $c(k)$.

Depending on the values of the parameters C_n and k (to be determined by the higher order equations in the perturbative expansion), E_x corresponds to different inhomogeneous functions in the x, y-plane. We are particularly interested in finding those with lattice symmetries that represent evenly spaced vortices running in the z direction in the gauge theory.

[4]This is the zero of the Bessel function of the first kind $J_0(\sqrt{B})$.

Before going beyond linear order, we discuss the possible solutions we can expect. The number of coefficients specifying a configuration can make the problem of finding the lowest energy solution unmanageable without making use of some symmetries. We can argue that, since nothing in the setup is explicitly breaking translational invariance in the x, y-directions, the solution should be a highly symmetric lattice. How this comes about and what lattice shapes are possible is the subject of this section.[5]

5.4.1 The Abrikosov lattice solution

The key step is to assume that, in order for $|E_x|$ to be a lattice solution, the coefficients C_n must have the same magnitude $|C_n|$. Moreover they should be periodic in some integer P, that is, $C_n = C_{n+P}$.

In [42], Abrikosov first studied the simplest solution, a square lattice. In this case, $P = 1$, implying that $C_n = C$ for all n, and $k = \sqrt{2\pi B_c}$. Later Kleiner et al. in [130] generalised the analysis by looking at $P = 2$, with $C_1 = \pm iC_0 = \pm iC$. This choice of coefficients specifies a general rhombic lattice, with the shape of the rhombus controlled by varying k. In particular, a square lattice can be obtained by choosing $k = \sqrt{\pi B_c}$. This square lattice is the same as Abrikosov's solution with $P = 1$, but it is rotated by $\pi/4$ and translated. A triangular lattice is obtained by choosing $k = 3^{\frac{1}{4}}\sqrt{\pi B_c}$.

To show how this works, we first substitute $P = 2$ and $C_1 = iC_0 = iC$ into the solution for E_x, which simplifies to

$$E_x = C \sum_{n=-\infty}^{\infty} e^{i\frac{\pi}{2}n^2 - inky - \frac{1}{2}B_c\left(x - \frac{nk}{B_c}\right)^2} U(u). \tag{5.75}$$

It is then easy to see the symmetries $|E_x(x+[m+\frac{1}{2}q]L_x, y+[n+\frac{1}{2}q]L_y)| = |E_x(x,y)|$ for integers m, n and q. L_x and L_y are the lengths of the lattice cell in the x and y directions, and are given by $L_x = 2k/B_c$ and $L_y = 2\pi/k$. See figure 5.3.

We follow the approach of [130], which is to compute the energy density of the lattice for a range of values of the ratio $L_x/L_y = k^2/\pi B_c$. This essentially means that we vary k. The energy is computed numerically from the analytic expressions we obtain at each order in the following sections. What we find agrees with their result that the triangular lattice has the lowest energy of the $P \leq 2$ solutions. When doing this, magnetic flux conservation is an important constraint. The total applied magnetic field per unit area is constant, and each lattice cell corresponds to a vortex with a single quantum of magnetic flux. This means that when comparing the energy of different lattices, we should make sure that they have the same magnetic flux per unit area, which in turn means that their lattice cells have the same area. Fortunately with this ansatz that is always the case since the area $L_xL_y = 4\pi/B_c$ is independent of k.

In the following sections we calculate analytic expressions for the higher order corrections to the gauge field. We keep P and the coefficients C_n general, except for imposing the periodicity condition $C_n = C_{n+P}$.

[5] A review of this topic is given in [129].

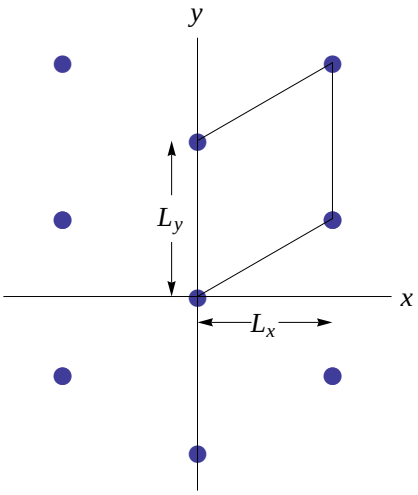

Figure 5.3: A lattice cell, illustrating the meanings of L_x and L_y for a fixed area cell.

5.5 The gauge theory ground state energy

At this stage we have a linear order solution with the free parameters k, P and C_n for $n = 0 \dots P-1$. As we saw in the previous subsection, we can change these parameters to fix different lattice configurations. The reason they are free is because at linear order the different vortices do not interact. Ideally we would like to include interactions and find the ground state solution. The question we therefore wish to answer is, "Which lattice solution minimises the energy?"

To calculate the energy, we appeal to the holographic dictionary. In the AdS Schwarzschild model we have a finite temperature field theory with no chemical potential. This implies we are in the canonical ensemble. The holographic dictionary then tells us that the free energy is given by $\mathcal{F}/T = -\ln \mathcal{Z} = -S_{\text{on-shell}}$. In the hard wall case, we are simply calculating the energy of the field configuration, which is defined in terms of the classical action in the same way.

Since we are only interested in whether the energy of a particular superconducting solution is lower than that of the normal phase solution, we can simply calculate the difference $\Delta\mathcal{F} = \mathcal{F}_s - \mathcal{F}_n$ and thus do not need to implement holographic renormalisation. Here $\mathcal{F}_s$ is the energy of the superconducting phase, while $\mathcal{F}_n$ is the normal phase energy with $\mathcal{A}_y^3 = xB$ and all other components zero. We also need to take care of the fact that $S_{\text{on-shell}}$ diverges when we perform the integral over the Minkowski directions. This is easy to fix by considering the energy density[6] Ω, which is obtained by integrating $S_{\text{on-shell}}$ only over the world volume of one lattice cell and dividing by its volume.

To which order do we need to go to calculate the minimum energy state? Ω has terms that are quadratic and quartic in the gauge potential. To linear order we can only calculate the quadratic order terms. We need the quartic terms however because they ensure that the energy is bounded from below — they have an overall positive coefficient. The quartic terms have lowest perturbative contributions of order ε^4. One might expect contributions of order ε^3 coming from the zeroth order

[6] We divide the free energy by T in the finite temperature model to get a dimensionless Ω. This means that in both models, our total dimensionless energy is simply -$S_{\text{on-shell}}$.

magnetic field contribution multiplied by three first order corrections. However, from equation (5.15) it can be shown that such terms do not arise. Thus we should expect to expand to third order in $\mathcal{A}^{1,2}_{x,y}$ and fourth order in $\mathcal{A}^{3}_{x,y}$. However, it turns out that going to fourth order is not necessary because inserting ansatz (5.15) into the action of equation (5.3), we find that the only fourth order terms from $\mathcal{A}^{3}_{x,y}$ that appear at the fourth order of the action are proportional to $\sim \partial_y a_x^{(4)3} - \partial_x a_y^{(4)3}$. Here $a_x^{(4)3}$ and $a_y^{(4)3}$ are the fourth order corrections to $\mathcal{A}^3_x$ and $\mathcal{A}^3_y$, respectively. This term respects the lattice symmetries, thus on performing the integration over the lattice cell to get the energy density, it vanishes by Stokes' theorem. So in order to obtain an energy functional that is bounded from below and includes vortex interactions, we need to complete the calculation to third order. We do this in the following section.

5.6 Solving the equations to higher orders

In this section we solve the equations of motion up to third order in the perturbation parameter, with some of the more technical details left for the appendix.

The second order corrections to the gauge fields contribute to the potentials $\mathcal{A}^3_x$ and $\mathcal{A}^3_y$, that is, a^3_x and a^3_y in (5.15). These fields source the external magnetic field and the magnetisation. We impose that these corrections must vanish at the AdS boundary, so that the dual field theory has a constant applied magnetic field. We find however that they do not vanish throughout the bulk. In particular they develop non-vanishing subleading terms in the boundary expansion, representing a magnetisation in the field theory.

In appendix B.1 we explain how the equations for the Fourier modes of the fields a^3_x and a^3_y can be decoupled. This yields the following equations

$$u\partial_u\left(\frac{f}{u}\partial_u \hat{a}^3_{x,y}(m,n,u)\right) - \left(k^2n^2 + \frac{4B_c^2m^2\pi^2}{k^2P^2}\right)\hat{a}^3_{x,y}(m,n,u) + T_{x,y}e^{-\frac{k^2n^2}{4B_c}+\frac{inm\pi}{P}-\frac{B_cm^2\pi^2}{k^2P^2}}\left(\sum_{l=0}^{P-1} e^{\frac{2ilm\pi}{P}}\bar{C}_l C_{l+n}\right)\mathcal{U}^2 = 0, \tag{5.76}$$

where

$$T_x = -i\frac{\sqrt{B_c\pi}}{P}n, \quad T_y = 2i\frac{\pi^{3/2}B_c^{3/2}}{k^2P^2}m, \tag{5.77}$$

and

$$a^3_{x,y}(x,y,u) = \sum_m\sum_n e^{-i\frac{2\pi mB_c}{Pk}x - inky}\ \hat{a}^3_{x,y}(m,n,u). \tag{5.78}$$

As before, P defines the periodicity in the C_n. The parameters m and n correspond to the Fourier space levels of these fields. In order to calculate the solution $a^3_{x,y}(x,y,u)$ we will in theory need to solve these equations for all values of m and n. However, it will turn out to be sufficient to only study the first few Fourier modes. The numerical procedure for solving these is explained in section 5.7

At third order we are studying the perturbative corrections to the condensate. Here we calculate the corrections e_x and e_y. It is reasonable to assume that the

answer is of the form

$$\varepsilon E_x + \varepsilon^3 e_x = \varepsilon \sum_{n=-\infty}^{\infty} \left(C_n \mathcal{U}(u) + \varepsilon^2 c_{x,n}(u)\right) e^{-inky - \frac{1}{2}B_c\left(x - \frac{nk}{B_c}\right)^2}, \tag{5.79}$$

$$\varepsilon E_y + \varepsilon^3 e_y = \varepsilon \sum_{n=-\infty}^{\infty} \left(-iC_n \mathcal{U}(u) + \varepsilon^2 c_{y,n}(u)\right) e^{-inky - \frac{1}{2}B_c\left(x - \frac{nk}{B_c}\right)^2}, \tag{5.80}$$

where we have made use of equation (5.73) to relate the first order terms $C_n\mathcal{U}(u)$ in $\mathcal{E}_x$ and $\mathcal{E}_y$. $c_{(x,y),n}(u)$ is the first perturbative correction to the condensate where the u dependence is a function of n in contrast to the first order term.

We can write e_x and e_y in Fourier space, then use the three condensate equations discussed in section 5.2.1 to calculate these corrections. The one constraint equation can be used to decouple the other two equations. We then have one equation for $c_{x,n}(u)$ and one for $c_{y,n}(u)$. Further details are provided in appendix B.2.

5.7 Numerical solutions

Having separated the equations into ordinary differential equations in u by the method outlined in the appendices, we can now solve them numerically. Both the second and third order equations take the same general form, given by

$$u\partial_u\left(\frac{f}{u}\partial_u\phi\right) + G(m,n)\phi + H(m,n,u) = 0. \tag{5.81}$$

This equation can be solved numerically by picking some parameters for C_n and k that give a particular lattice and then using a shooting method to integrate from $u = 1$ (the horizon/hard wall cutoff) to $u = 0$ (the AdS boundary). It is an inhomogeneous second order differential equation, so there are two integration constants. The first is fixed by imposing regularity at the horizon or Neumann boundary conditions at the hard wall cutoff. This fixes the value of $\partial_u\phi(1)$. The second constant is obtained by demanding that $\phi(0) = 0$, so that the fields vanish at the AdS boundary. This vanishing corresponds to both the magnetic field strength corrections and the source for the condensate being set to zero. We fulfil this boundary condition by adjusting $\phi(1)$. Unlike in the case of the first order equations, the equations here are not homogeneous and thus the source sets a scale with which the value $\phi(1)$ can be compared. Changing $\phi(1)$ in this case thus acts as more than just a scaling for the solution and so is used as the tuning parameter to satisfy the UV constraint.

For all of the equations, we can implement this procedure for arbitrary integers m and n, corresponding to the different Fourier modes of the gauge fields. This will then give a Fourier coefficient $\hat{a}^3_{x,y}(m,n,u)$ that can be used to determine $a^3_{x,y}(x,y,u)$. Fortunately we do not have to do the calculation for many different values of m and n, because as the values get large, the source term gets suppressed exponentially. This can be seen in equation (5.76) for the second order terms and is true also for the third order equation. For a vanishing source, the equations for $\hat{a}^3_x$ or $\hat{a}^3_y$ have only the trivial solution. This means that $\hat{a}^3_{x,y}(m,n,u)$ is negligibly small for large m or n, and we can therefore truncate the Fourier series for $a^3_{x,y}$ beyond $m, n \approx 3$.

5.8 Results

5.8.1 Finding the minimum energy state

As explained above, we wish to find the values of the parameters k, P and $C_n = C_{n+P}$ that give the minimum energy state. These parameters define the shape of the lattice. Our analysis is only valid for B slightly above B_c, where B_c is determined by a stability calculation such as the one in section 5.3.3. The first step is thus to pick a value for B in this vicinity. We then choose a set of lattice parameters that give us the lattice solution we wish to consider. As mentioned in [129], for lattice solutions all the C_n must have the same magnitude C. We can therefore fix C_n up to the normalisation C, along with a value of k, according to the discussion in section 5.4.1. We then substitute these values into the energy density that was defined in section 5.5. It takes the form $\Delta\Omega = a_1\varepsilon C + a_2\varepsilon^2 C^2 + \dots$. At this point we see that we can redefine C by absorbing a factor of ε, which we call C_ε. C_ε is the only parameter left unfixed up to this point in the analysis. Here the a_i are values that are calculated numerically from substituting the solutions to the equations of motion into the expression for the energy derived in appendix B.3. $\Delta\Omega$ forms a Mexican hat potential, which is easy to minimise numerically. An illustration of this procedure is shown in figure 5.4. The plot in figure 5.5 shows

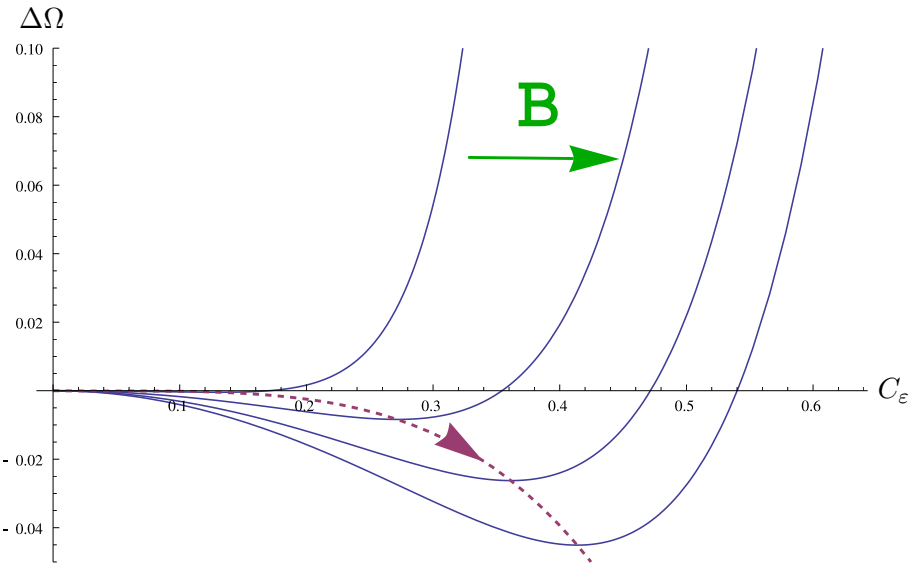

Figure 5.4: The change in energy density in units of temperature as a function of C_ε, the overall condensate scale. The leftmost curve corresponds to $B = B_c$, which is never negative for nonzero condensate. Curves for $B < B_c$ are similar. Increasing B beyond B_c yields the curves to the right, and we see the formation of a clear minimum of the energy that is lower than the energy of the normal phase. The dashed line traces out the minimum of each of these curves, which corresponds to the energetically preferred size of the condensate as a function of B. This plot was generated in the AdS Schwarzschild model for $P = 2$ and $k = 3^{\frac{1}{4}}\sqrt{\pi B}$, corresponding to a triangular lattice. B takes the values $B \approx B_c, 1.04B_c, 1.07B_c, 1.1B_c$ from left to right. Changing P and k to correspond to different lattices or using the hard wall model yields qualitatively similar results.

the energy-minimising value of C_ε as a function of magnetic field near the phase

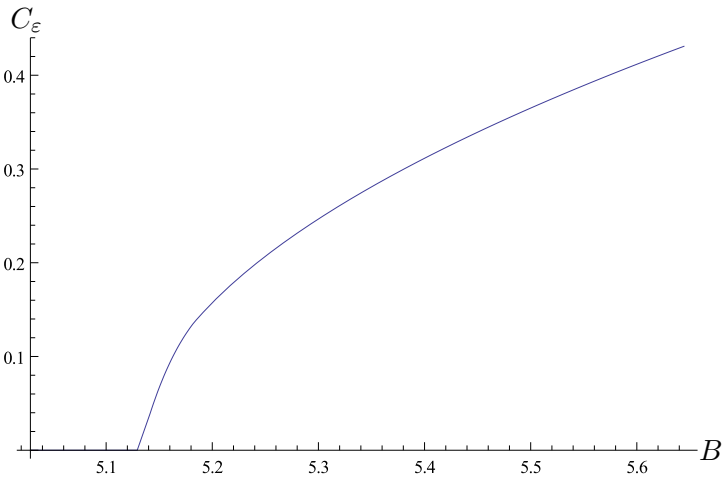

Figure 5.5: $C_\varepsilon \sim$ the overall condensate size for the AdS Schwarzschild solution in units of the temperature, as a function of the external magnetic field B. For $B < B_c$, the condensate is zero, and for B slightly above B_c, we see a $(B - B_c)^{\frac{1}{2}}$ scaling behaviour. This plot was generated for $P = 2$ and $k = 3^{\frac{1}{4}}\sqrt{\pi B}$, corresponding to a triangular lattice. The plot for different lattices in both the AdS Schwarzschild and hard wall models is the same, up to a scaling of the B and C_ε axes. For the triangular lattice, the AdS Schwarzschild model has scaling behaviour $C_\varepsilon = 0.58(B - 5.1)^{\frac{1}{2}}$ and the hard wall model has $C_\varepsilon = 0.53(B - 5.8)^{\frac{1}{2}}$.

transition at B_c. It shows that $C_\varepsilon \sim (B - B_c)^{\frac{1}{2}}$, so the condensate[7] has a critical exponent of 1/2. A fit to the numerical data for the triangular lattice gives that $C_\varepsilon = 0.58(B - B_c)^{\frac{1}{2}}$ in the AdS Schwarzschild model and $C_\varepsilon = 0.53(B - B_c)^{\frac{1}{2}}$ in the hard wall model.

Having minimised with respect to C_ε for a given value of B and a given lattice configuration, we can plot the difference in the energy between the normal and superconducting states. Figure 5.6 shows $\Delta\Omega$, the difference between the energy density in the superconducting and normal phases, as a function of external magnetic field for two different lattices. The first lattice is square, and the second is triangular. Both are described in section 5.4.1.

The curves plotted in figure 5.6 are the result of calculations in the AdS Schwarzschild model, but we get the same results up to a rescaling of the axes for the hard wall model. In the AdS Schwarzschild model, the critical magnetic field $B_c \approx 5.1$, while in the hard wall model $B_c \approx 5.8$. Each curve shows that the free energy density is proportional to $(B - B_c)^2$. This shows that the phase transition is second order, as expected if one looks at the analogous case in Ginzburg-Landau theory. There one can show ([98]) that the free energy is proportional to $(T - T_c)^2$, where T_c is the phase transition critical temperature.

5.9 An analysis of $P = 2$ solutions

We now specialise to the case where the periodicity of the C_n is $P = 2$. This describes a general rhombic lattice solution which includes both the triangular and

[7]Note that only the combination εC is physically relevant, not C or ε independently.

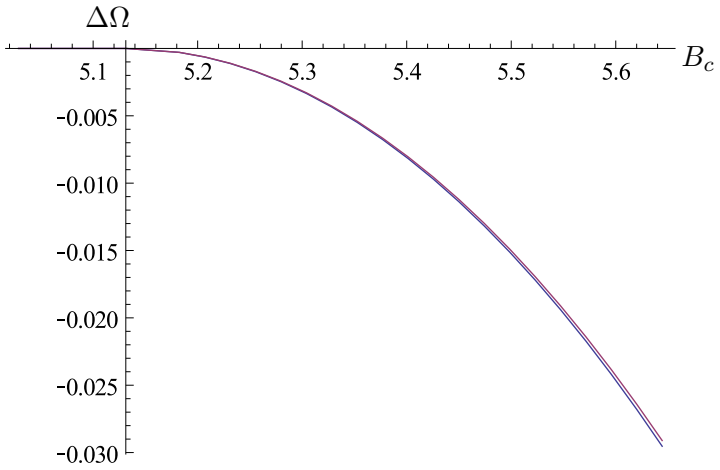

Figure 5.6: The change in energy density (compared to the normal phase) for the triangular and square lattices as the external applied magnetic field is varied. The phase transition happens at $B_c \approx 5.1$, which is where the coordinate axes are centred. $\Delta\Omega_{\text{square}} - \Delta\Omega_{\text{triangle}}$ is so small that the two plots are almost on top of each other. This is for the AdS Schwarzschild model, but the plots for the hard wall model are identical except for the scale on the axes. In the hard wall model, $B_c \approx 5.8$.

square lattices. The $P = 1$ square lattice can be found within the $P = 2$ solutions up to translation and rotation. We here perform the analysis done in [130] as described at the end of section 5.4.1.

The energy difference as a function of R is plotted in figure 5.7. By looking at the form of equation (5.75), it is possible to see that the triangular lattice occurs for $R = L_x/L_y = \sqrt{3}$ and $R = 1/\sqrt{3}$. In general, R and $1/R$ give the same lattice but with the x and y directions flipped. This is why figure 5.7 displays the symmetry $\Delta\Omega(R) = \Delta\Omega(1/R)$. The triangular lattice corresponds to a global minimum of the energy as a function of R, as seen from the figure. There is a local maximum for the square lattice, which is when $R = 1$. As $R \to \infty$ (or $R \to 0$), the free energy increases. Intuitively one can understand this by making use of the properties of Abrikosov vortices that we understand from type II superconductors. These vortices repel. Since $R \to \infty$ and $R \to 0$ correspond to elongating the rhombic lattice cell (while keeping the area constant) neighbouring vortices are squeezed together, and since they repel, this is energetically unfavourable.

We can calculate the condensate in the minimum energy state using equation (2.21). The result, to linear order in ε, is

$$\langle J_x^+ \rangle \equiv \frac{\delta S_{\text{on-shell}}}{\delta E_x^{(0)}} = \frac{L}{2\hat{g}^2} U_{\text{sub}} C_\varepsilon \sum_{n=-\infty}^{\infty} e^{-i\frac{\pi}{2}n^2 + inky - \frac{1}{2}B_c\left(x - \frac{nk}{B_c}\right)^2} \tag{5.82}$$

The AdS radius can be related to field theory quantities through the relation $L^4 = 2\lambda\alpha'^2$, where λ is the 't Hooft coupling and α' the string tension. The factor U_{sub} is equal to the subleading term in the boundary expansion of $U(u)$. Using equation (5.36) it is possible to show that

$$U_{\text{sub}} = B_c \int_0^{u_H} \frac{U(u)}{u} du, \tag{5.83}$$

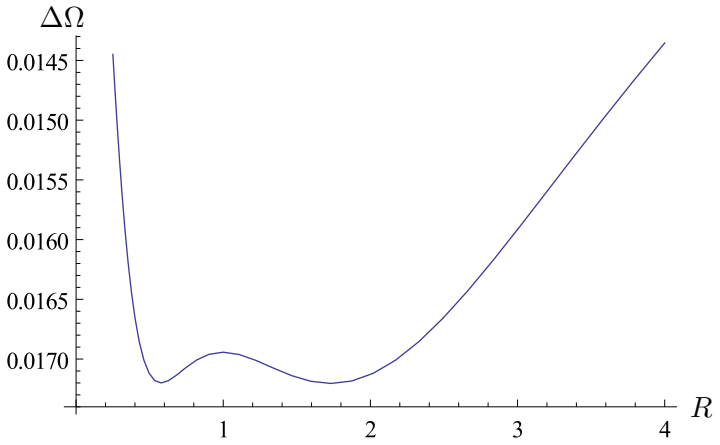

Figure 5.7: The change in free energy density as a function of $R = L_x/L_y$, the ratio of side lengths of a constant area lattice cell. This plot is for the AdS Schwarzschild model, but the plot for the hard wall model is identical up to a rescaling of the axes. When $R = 1$, the lattice is square and the free energy achieves a local maximum. When $R = \sqrt{3}$ and $1/\sqrt{3}$, the lattice is triangular and the free energy is at a global minimum. Note that the plot has the symmetry $\Delta\Omega(R) = \Delta\Omega(1/R)$, which simply corresponds to swapping the x, y-axes.

so it can be determined numerically. In figure 5.8 we present the contour plot of $3^{\frac{1}{4}}\sqrt{8}\frac{\hat{g}^4}{L^2U_{\rm sub}^2C_\varepsilon^2}\,|\langle J_x^+\rangle|^2$, the modulus squared of the condensate in the x, y-plane for the minimum energy solution corresponding to the triangular lattice. The factors are chosen so that the maximum value is 1. Inserting the numerical values, we find that the maximum value the condensate takes is $|\langle J_x^+\rangle| = 1.0\frac{L}{\hat{g}^2}\,(B - B_c)^{\frac{1}{2}}$ for the AdS Schwarzschild model, where $B_c \approx 5.1$, and $|\langle J_x^+\rangle| = 1.3\frac{L}{\hat{g}^2}\,(B - B_c)^{\frac{1}{2}}$ for the hard wall model, where $B_c \approx 5.8$.

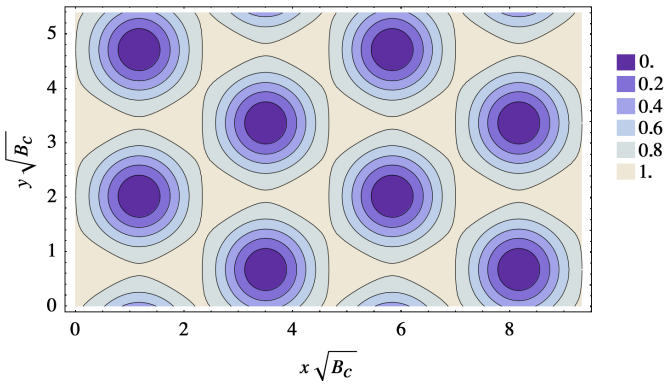

Figure 5.8: A contour plot of $3^{\frac{1}{4}}\sqrt{8}\frac{\hat{g}^4}{L^2U_{\rm sub}^2C_\varepsilon^2}\,|\langle J_x^+\rangle|^2$, the modulus squared of the field theory condensate dual to E_x in the ground state triangular lattice. At the center of the dark vortices, the condensate vanishes.

We could also plot the magnetisation of the ground state, which is found from the normalisable term in the boundary value expansion of $\partial_x a_y^3 - \partial_y a_x^3$. However, it takes the same form as the absolute value of the condensate and the numerics

indicates that it differs only up to a scale.

5.10 Conclusion

In this chapter we have shown that two simple asymptotically AdS gravity models with an $SU(2)$ Yang–Mills field are unstable when a magnetic component of that field becomes large enough. This instability indicates that there exists a new ground state. We showed that this new ground state contains vortex lines. To find the minimum energy configuration of these vortex lines, we argued that there was nothing influencing the large scale translation symmetry of the setup, so they must be aligned in a lattice pattern. We then enumerated various lattice configurations and calculated the energy of each. Of the lattice configurations we tried, we found that the triangular lattice has the lowest energy. This must be the ground state. This result agrees with the case for type-II superconductors [130].

This solution is potentially interesting for condensed matter models, where, as we have already argued, a lattice is essential for getting realistic phenomenology. It could also have implications for QCD. Since very strong magnetic fields are present in highly off-centre collisions at heavy ion colliders, perhaps it is possible to observe an effect such as an excess in ρ-meson production, as predicted by [53].

It is important to understand how universal the result is. We saw it in two different holographic models. In the next chapter we see it still holds even when we switch on a chemical potential. We also know that it appears in many other models. In all these cases, the ground state is a triangular lattice. Finding a proof of universality would require investigating the phenomenon in more gravity backgrounds to see at which point it breaks down.

Another avenue for investigation is to find out how matter interacts with the vortex lattice. In the second half of the next chapter we show how to approach this question by adding fermion zero modes.

Chapter 6

Extending the holographic lattice ground state model

The gauge/gravity model of the previous chapter is beautifully simple. A single $SU(2)$ Yang–Mills gauge field is robust enough to act as both magnetic field order parameter and condensate. But this simplicity means that it can easily be extended. The goal of the present chapter is to consider two possible extensions: we add a finite chemical potential in section 6.1 and we add probe fermions in section 6.2.

6.1 Adding the chemical potential

The first extension is to switch on a chemical potential μ in addition to the magnetic field B. We repeat the perturbative analysis of the previous chapter, finding the values of μ and B at which the system becomes unstable. This allows us to draw a two-dimensional phase diagram showing the normal and superconducting phases. We also give a picture of how the lattice changes at various points in the phase diagram in figure 6.3. At second order we compute the corrections to the charge density, showing how the vortices squeeze $U(1)$ charge to the side. This could not be done in the previous chapter; it is derived from the corrections to the gauge field component providing the chemical potential. Finally, in section 6.1.6 we calculate the free energy of the system and show that the triangular lattice is still the ground state even for finite chemical potential.

This is work that was done by the author, but was never published due to the appearance of similar work by Kenny Wong in [131]. Wong's work is based on [1, 2], but uses an AdS_4 instead. He does not continue the calculation to third order, though, and has no results for the free energy. This chapter contains the only calculation showing that the triangular lattice is still a ground state it finite chemical potential that the author is aware of.

6.1.1 The ansatz

Consider the AdS–Schwarzschild model of chapter 5. The geometry is still described by the metric

$$ds^2 = \frac{L^2}{u^2}\left(-f(u)dt^2 + dx^2 + dy^2 + dz^2 + \frac{du^2}{f(u)}\right), \tag{6.1}$$

with $f(u) = 1 - u^4$ and we still look at the action in the probe limit given by

$$S = -\frac{1}{4\hat{g}^2}\int d^5x\sqrt{-g}\ \mathrm{tr}\left(F_{\mu\nu}F^{\mu\nu}\right), \tag{6.2}$$

with equations of motion

$$\nabla^\mu F^a_{\mu\nu} + \epsilon^{abc}\mathcal{A}^{b\mu}F^c_{\mu\nu} = 0. \tag{6.3}$$

The difference is that the ansatz is slightly modified to include a chemical potential. In addition to the magnetic field B, we add a chemical potential by imposing it as a boundary condition to the $\mathcal{A}^3_t$ component. This means that the ansatz (5.13) becomes

$$\begin{aligned}
\mathcal{A}^3_t &= \mu_c - u^2\mu_c + \varepsilon A^3_t + \varepsilon^2 a^3_t + \ldots,\\
\mathcal{A}^3_y &= xB_c + \varepsilon A^3_y + \varepsilon^2 a^3_y + \ldots,\\
\mathcal{A}^a_\mu &= \varepsilon A^a_\mu + \varepsilon^2 a^a_\mu + \ldots \qquad \text{for } (a,\mu) \neq (3,y) \text{ or } (3,t),
\end{aligned} \tag{6.4}$$

where the form of $\mathcal{A}^3_t$ at zeroth order was chosen because it satisfies the equations of motion when $\varepsilon = 0$.

The goal is similar to before. We perform a perturbative expansion in ε, which is a parameter proportional to the overall condensate size. This means that we restrict our view to the parameter range in which the condensate is small — we start exactly at the superconducting phase transition that occurs at $B = B_c$ and $\mu = \mu_c$ and calculate small corrections in ε going into the superconducting region of the phase diagram.

One motivation for the ansatz (6.4) is based on what we know from [91]. There it was shown that the field theory dual to the $SU(2)$ Yang–Mills holographic model above undergoes a phase transition at small temperature and zero magnetic field. The new phase has the same symmetries as a p-wave superfluid. Small temperature corresponds to large chemical potential, since conformal symmetry means that only the ratio T/μ is physically relevant. This means that, at $B = 0$, the system we are considering is in a superconducting phase for μ above a critical value μ_c. So we know that we are in the superconducting phase for $\mu > \mu_c$ when $B = 0$ and for $B > B_c$ when $\mu = 0$. What does the phase diagram look like for both B and μ nonzero? In other words, what is the shape of the curve described by (B_c, μ_c)? To answer this we turn to the linearised equations of motion.

6.1.2 The linear order equations of motion

Substituting ansatz (6.4) into the equations of motion (6.3) yields

$$\begin{aligned}
0 &= i\mu_c u^2\partial_u E_t - i\mu_c\partial_u E_t - 2i\mu_c u E_t\\
&\quad + iB_c x f\partial_u E_y + f\partial_y\partial_u E_y + f\partial_x\partial_u E_x
\end{aligned} \tag{6.5}$$

$$\begin{aligned}
0 &= -B_c^2x^2E_t + 2iB_cx\partial_yE_t - B_c\mu_cu^2xE_y + B_c\mu_cxE_y\\
&\quad + \partial_y^2E_t + \partial_x^2E_t + i\mu_cu^2\partial_xE_x - i\mu_c\partial_xE_x + i\mu_cu^2\partial_yE_y - i\mu_c\partial_yE_y\\
&\quad - \frac{f\partial_uE_t}{u} + f\partial_u^2E_t
\end{aligned} \tag{6.6}$$

$$
\begin{aligned}
0 = {} & B_c^2 x^2 E_x - 2iB_c x\partial_y E_x + iB_c x\partial_x E_y - iB_c E_y \\
& + \frac{i\mu_c u^2 \partial_x E_t}{f} - \frac{i\mu_c \partial_x E_t}{f} - f'\partial_u E_x - f\partial_u^2 E_x + \frac{f\partial_u E_x}{u} - \partial_y^2 E_x \\
& - \frac{\mu_c^2 u^4 E_x}{f} + \frac{2\mu_c^2 u^2 E_x}{f} - \frac{\mu_c^2 E_x}{f} + \partial_x\partial_y E_y
\end{aligned} \tag{6.7}
$$

$$
\begin{aligned}
0 = {} & -\frac{B_c\mu_c\left(u^2-1\right)xE_t}{f} + iB_c x\partial_x E_x + 2iB_c E_x + \frac{i\mu_c\left(u^2-1\right)\partial_y E_t}{f} \\
& + \partial_x\partial_y E_x + \left(\frac{f}{u} - f'\right)\partial_u E_y - f\partial_u^2 E_y - \partial_x^2 E_y - \frac{\mu_c^2\left(u^2-1\right)^2 E_y}{f}
\end{aligned} \tag{6.8}
$$

$$
\begin{aligned}
0 = {} & \frac{E_z\left(B_c^2 x^2 f - \mu_c^2\left(u^2-1\right)^2\right)}{f} - 2iB_c x\partial_y E_z + \left(\frac{f}{u} - f'\right)\partial_u E_z \\
& - f\partial_u^2 E_z - \partial_y^2 E_z - \partial_x^2 E_z
\end{aligned} \tag{6.9}
$$

to linear order. We would like to find a ground state so we search only for static solutions.

We kept fluctuations in all the components of the gauge field (except of course $\mathcal{A}_u$) so that it is possible to analyse how the equations couple. The first thing to notice is that E_z clearly decouples from the other components. This means that we can consistently set it to zero. The only thing that needs to be checked is that E_z does not condense in regions of the phase diagrams where the other components have not already condensed. If E_z condenses first, then the new ground state is given by its profile, and we should not have set it to zero. However, by solving the equation (6.9) using separation of variables, we checked that E_z does not condense for small B and μ before the components E_x and E_y do.

E_t couples to E_x and E_y, but it can also be consistently set to zero. The reason for doing this can be understood by looking at the equations of motion. Whenever μ_c is small or E_x and E_y describe the lattice solution from chapter 5, E_t effectively decouples from E_x and E_y. So we can solve for E_t as if the other components were zero. Doing that, we find that E_t does not depend on μ_c, only on B_c. And in fact, there is no solution for E_t, for any value of B_c, that satisfies the boundary conditions. The boundary conditions are that E_t vanishes at the horizon by regularity and vanishes at the AdS boundary because we do not want a field theory chemical potential. This motivates us to ignore the effect of E_t and set it to zero.

6.1.3 Results from first order

The equations for E_x and E_y are again separable, and the solution is given by

$$E_y = -iE_x, \tag{6.10}$$

$$E_x = \sum_{n=-\infty}^{\infty} C_n e^{-inky - \frac{1}{2}B_c\left(x - \frac{nk}{B_c}\right)^2}\mathcal{U}(u), \tag{6.11}$$

as before. The difference is in the equation for $\mathcal{U}(u)$, which is slightly modified. It is now

$$0 = \frac{\left(B_c f + \mu_c^2\left(u^2-1\right)^2\right)}{f^2}\mathcal{U} + \left(\frac{f'}{f} - \frac{1}{u}\right)\mathcal{U}' + \mathcal{U}''. \tag{6.12}$$

Exploring the phase diagram is now as simple as solving this ordinary differential equation numerically. The boundary conditions are that $\mathcal{U}$ vanishes at the AdS boundary ($u = 0$) and is regular at the horizon ($u = 1$ in dimensionless units). B_c and μ_c are two adjustable parameters. Previously we only had the one adjustable parameter B_c that we adjusted until we found a lowest order solution $\mathcal{U}$ that respects the boundary conditions. Now we can choose any value of B_c and adjust μ_c until $\mathcal{U}$ respects the boundary conditions. As usual, the key point here is that we choose the lowest order solution for $\mathcal{U}$ — the one with no roots except at the boundary — so that we get the lowest energy solution, which corresponds to the first mode that will condense.

We solve equation (6.12) using the shooting method, shooting from $u = 1$ to $u = 0$. This is done by choosing values for B_c between 0 and 5.1[1] and then varying μ_c. The aim is to find the value of μ_c that makes $\mathcal{U}$ vanish at $u = 0$. The boundary condition at the horizon is that $\mathcal{U}' = 1$, as described in chapter 5. Due to the singularities in equation (6.12) at the boundary and horizon, the numerical integration is done from $u = 1 - 10^{-5}$ to $u = 10^{-5}$. We also calculate the horizon expansion of $\mathcal{U}$ to third order in order to get an accurate analytical expression for $\mathcal{U}$ at $u = 1 - 10^{-5}$.

A representative plot of $\mathcal{U}(u)$ is given in figure 6.1. The resulting phase diagram is given in figure 6.2. The white region of the diagram depicts the normal phase, while the shaded region contains the condensed phase. The linearised solution to the equations (6.10) and (6.11) is valid along the phase transition line. The most striking feature of the phase diagram is that it indicates that the critical temperature for the onset of superconductivity is increased — since μ is decreased – for stronger magnetic field.

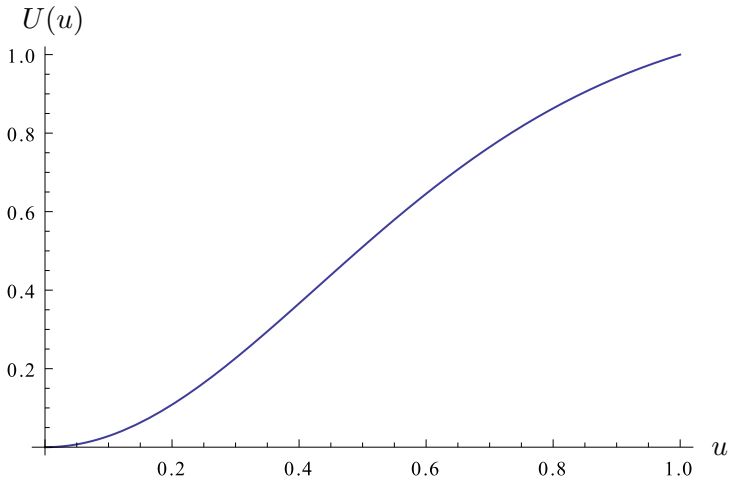

Figure 6.1: A representative plot of $\mathcal{U}$ as a function of u. The AdS boundary is at $u = 0$ and the horizon is at $u = 1$. The parameters chosen are $B_c = 2$ and $\mu_c \approx 3.2$.

It is worth considering the ground state along the phase transition line in more detail. We know that at $\mu = 0$ the magnitude of the vector condensate vev for the ground state solution in the field theory has the contours shown in figure 5.8. This Abrikosov lattice solution depends only on B_c, since μ_c only influences the shape

[1]Recall from chapter 5 that the phase transition occurs at approximately 5.1 for $\mu = 0$.

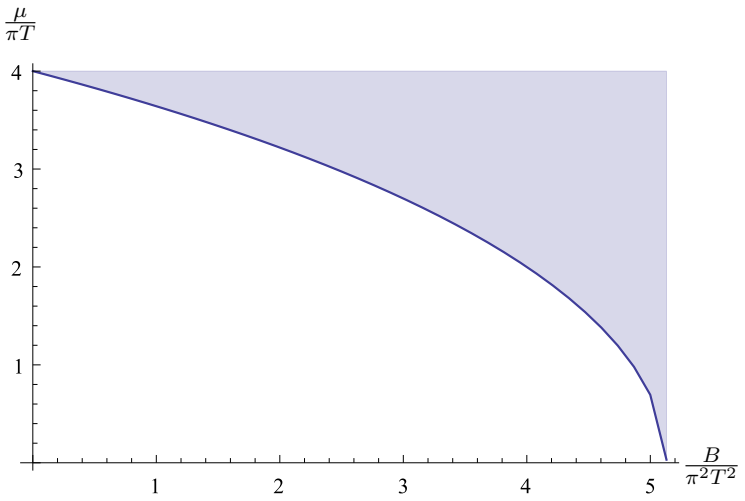

Figure 6.2: The B-μ phase diagram. The white region is the normal, uncondensed phase. The shaded region is the condensed phase. The ground state solutions (6.10) and (6.11) are approximately correct on the phase transition line (B_c, μ_c).

of $\mathcal{U}$. This means that as we trace the phase transition line up towards greater μ_c, so that B_c decreases, the lattice spacing and the vortex radius both increase. This makes sense: as the magnetic field is decreased, the individual vortices are no longer bound together as tightly. When B vanishes, the vortex radius diverges. Then the solutions (6.10) and (6.11) reduce to the $p + ip$-wave solution from [91]; they become homogeneous. Figure 6.3 shows these expanding vortices for various values of B.

This intuition is confirmed by calculating the free energy of the triangular lattice ground state as we vary B_c and μ_c. To do this we continue the calculation to third order.

6.1.4 Results from second order

The second order equations of motion are the same as those from chapter 5 with one key difference: as expansion (6.4) shows, there is now an a_t^3 component. Serendipitously, this component decouples from the rest. Its equation of motion is

$$0 = f\partial_u^2 a_t^3 - \frac{f\partial_u a_t^3}{u} + \partial_y^2 a_t^3 + \partial_x^2 a_t^3 + 2\mu_c \left(u^2 - 1\right) \bar{E}_x E_x. \tag{6.13}$$

The boundary conditions are simple. By regularity at the horizon, a_t^3 must vanish there. At the AdS boundary, we do not wish for it to make a contribution to the chemical potential, so we set it to zero there as well.

When $\mu_c = 0$, the source of the equation vanishes. For vanishing source there is no nontrivial solution for a_t^3 satisfying the boundary conditions. a_t^3 should therefore be set to zero when there is no chemical potential. This is consistent with chapter 5.

Equation (6.13) is a partial differential equation. We can solve it as before by making use of the lattice periodicity that we know the full background solution

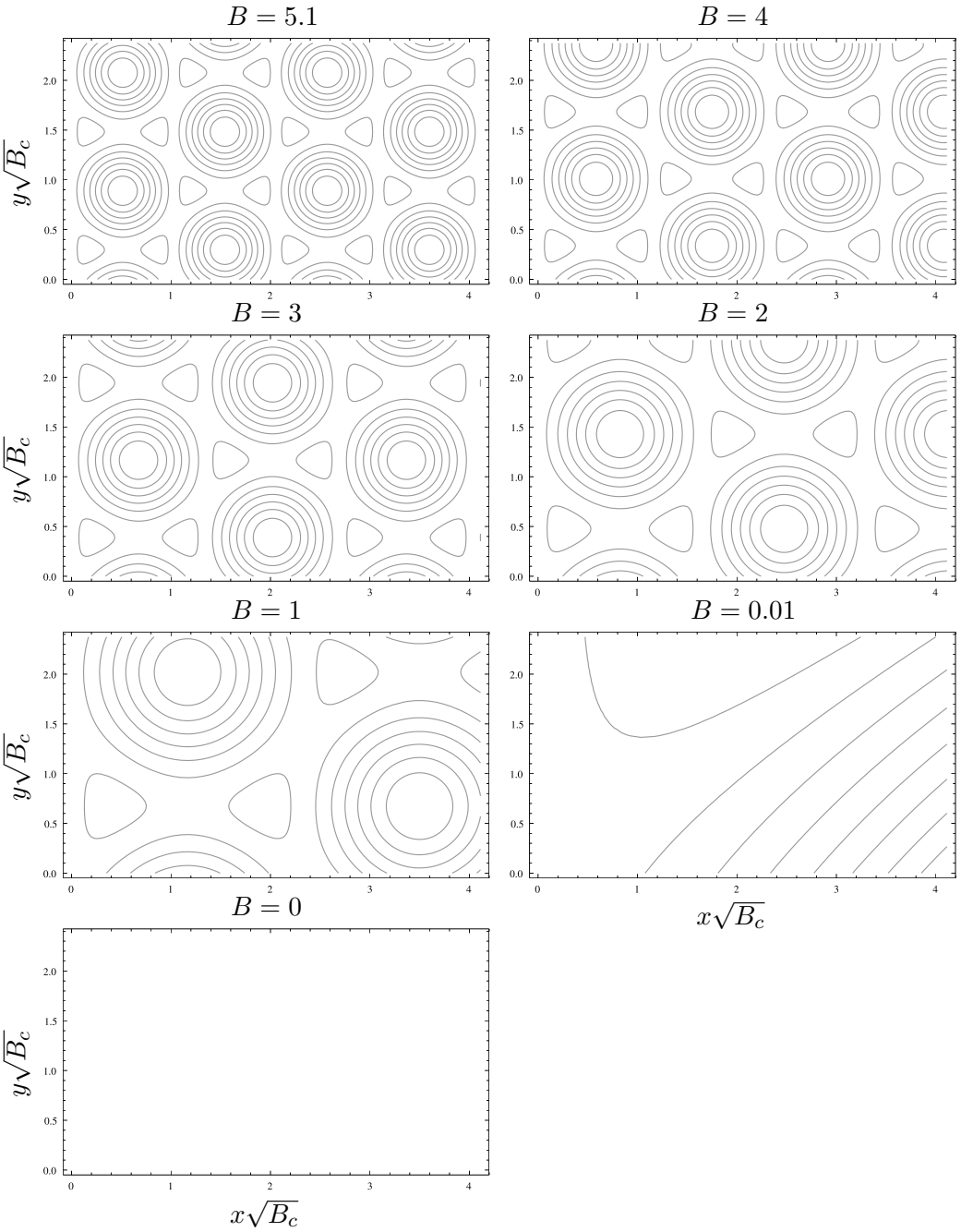

Figure 6.3: The contour lines of the magnitude of the vector condensate for various values of B. The x and y directions are presented in units of $\sqrt{B_c}$, where B_c is the critical magnetic field value when $\mu = 0$. From the numerics, $B_c \approx 5.1$ in our model. The entire vortex lattice gets bigger as B decreases, which makes sense because the vortices are not as tightly bound in a weaker magnetic field.

must have. This lets us use the Fourier series decomposition

$$a_t^3(x, y, u) = \sum_m \sum_n e^{-i\frac{2\pi m B_c}{Pk}x - inky}\ \hat{a}_t^3(m, n, u), \tag{6.14}$$

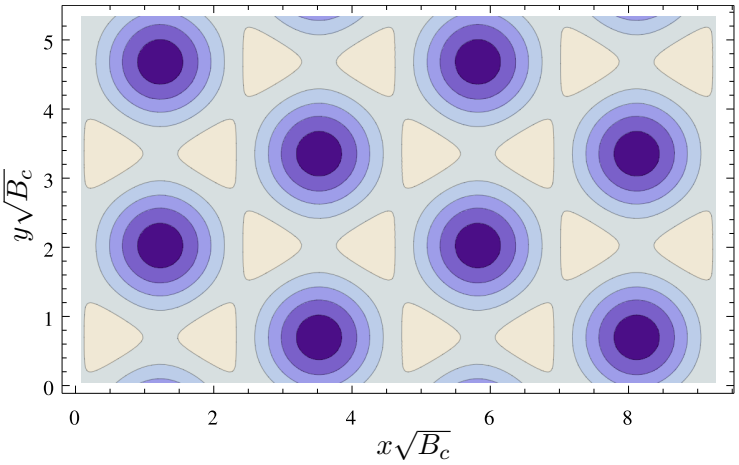

Figure 6.4: The structure of the corrections to the charge density $\langle J_t^3 \rangle$. Darker regions are where the charge density has smaller magnitude. We see that there is less charge inside the vortex cores.

the equation of motion for $\hat{a}_t^3$ becomes

$$f\partial_u^2 \hat{a}_t^3 - \frac{f}{u}\partial_u \hat{a}_t^3 - \left(k^2 n^2 + \frac{4B_c^2 m^2 \pi^2}{k^2 P^2}\right)\hat{a}_t^3(m,n,u) + \frac{2\sqrt{\pi B_c}}{kP}\mu_c\left(u^2-1\right)e^{-\frac{k^2n^2}{4B_c}+\frac{inm\pi}{P}-\frac{B_c m^2\pi^2}{k^2P^2}}\left(\sum_{l=0}^{P-1} e^{\frac{2ilm\pi}{P}}\bar{C}_l C_{l+n}\right)\mathcal{U}^2 = 0. \quad (6.15)$$

To solve for $\hat{a}_t^3$ we therefore have to pick values of B_c and μ_c, solve for $\mathcal{U}$, and finally pick a lattice solution by fixing P and C_l. $\hat{a}_t^3$ must vanish at the horizon and the AdS boundary, so we use the shooting method by varying $\partial_u \hat{a}_t^3\big|_{u=1}$. The numerical integration is done from $u = 1 - 10^{-5}$ to $u = 10^{-5}$.

From the gauge/gravity dictionary we know that the boundary falloff of $\mathcal{A}_t^3$ gives the field theory charge density,

$$\mathcal{A}_t^3 \sim \mu + u^2 \langle J_t^3 \rangle + \mathcal{O}(u^4). \quad (6.16)$$

From (6.4) we know that the zeroth order contribution to $\langle J_t^3 \rangle$ is $-\mu_c$. By doing a fit to our numerical solutions for $\hat{a}_t^3$ and putting everything together using (6.14), we can thus find the $\mathcal{O}(\varepsilon^2)$ corrections. The result is plotted in figure 6.4 for a representative value of B_c and μ_c and a triangular lattice.

The result for the magnetisation, from the $\mathcal{A}_x^3$ and $\mathcal{A}_y^3$ components, is precisely the same as in chapter 5. There is not even a factor of μ_c entering the $\mathcal{A}_x^3$ and $\mathcal{A}_y^3$ equations of motion. It only enters implicitly; the value of B_c is different, of course, depending on μ_c.

6.1.5 Results from third order

As in chapter 5, we continue the expansion to third order with the ansatz

$$\mathcal{E}_{x,y} = \varepsilon E_{x,y} + \varepsilon^3 e_{x,y} + \mathcal{O}(\varepsilon^5). \quad (6.17)$$

There are four equations of motion at this order. There is a constraint equation, which is identical to (B.13). There are equations of motion for both e_x and e_y.

These are similar to (B.14) and (B.15) except that they also contain source terms proportional to μ_c or a_t^3. Finally there is a second constraint equation, which would have been the equation of motion for e_t if e_t were not set to zero. It can be checked that this constraint equation is equivalent to the first.

6.1.6 The free energy results

The calculation of the free energy proceeds as in section 5.8. We find the free energy density $\Delta\Omega$, which we define to be the free energy $-TS_{\text{on-shell}}$ divided by the volume of a lattice cell (given by $\frac{4\pi}{B_c}$) and also divided by the temperature T. As before, the process is very similar to that in appendix B.3. The difference is that now there are terms including μ_c and a_t^3 in the expression for the free energy. In addition, in the normal phase the on-shell action is given by

$$\begin{aligned} S_{\text{on-shell}} &= \frac{1}{4\hat{g}^2}\int d^5x\sqrt{-g}F^a_{\mu\nu}F^{a\mu\nu} \\ &= \frac{\mathcal{L}\mathcal{V}}{4\hat{g}^2}\int_0^1 du\left(\frac{B_c^2}{u}-4u\mu_c^2\right), \end{aligned} \tag{6.18}$$

where $\mathcal{V}$ is the volume of the boundary directions. The renormalisation counterterm (2.24) gets rid of the term $\frac{B_c^2}{u}$, cancelling the divergence as it should. The other term is finite, but we still subtract it because we are only interested in the free energy difference compared to the normal phase.

Having established the analytical form of $\Delta\Omega$ as in appendix B.3, we can do the numerical integration to find $\Delta\Omega$ near the phase transition line in the (B,μ) phase diagram (figure 6.2). We know that the triangular lattice is the ground state configuration for B slightly above B_c when $\mu = 0$, so it is natural to check whether it remains a thermodynamically preferred state for $\mu \neq 0$. As figure 6.5 shows, it does. There we plot $\Delta\Omega$ near the phase transition line, at $(B,\mu) = 1.01(B_c,\mu_c)$, once as a function of both B and once as a function of μ. The important thing to notice is that $\Delta\Omega$ remains negative.

Now that we know that the triangular lattice solution is preferred to the normal state solution, the next question to ask is whether the triangular lattice solution is preferred to other lattice solutions. To find the answer we repeat the calculation of section 5.9. That is, we choose a value of B_c, which gives a corresponding value of μ_c. This gives us the point in the phase diagram $(B,\mu) = 1.01(B_c,\mu_c)$ near the critical line. At this point, we adjust k such the the ratio R of the lattice side lengths changes. We calculate $\Delta\Omega$ for every value of B, μ and R. The result is plotted in figure 6.6. In the plot, B runs from 0 to approximately 5.1, and R runs from 1 to 4. Values of R less than 1 are excluded because they can be obtained by symmetry, since $\Delta\Omega(R) = \Delta\Omega(1/R)$. To make the presentation clearer, we have subtracted $\Delta\Omega|_{R=1}$ so that the left edge of the figure is normalised to zero. The black line in the figure is the line of minimum $\Delta\Omega$ as a function of B. It is always at $R \approx \sqrt{3}$. The ground state when including a chemical potential is still a triangular lattice!

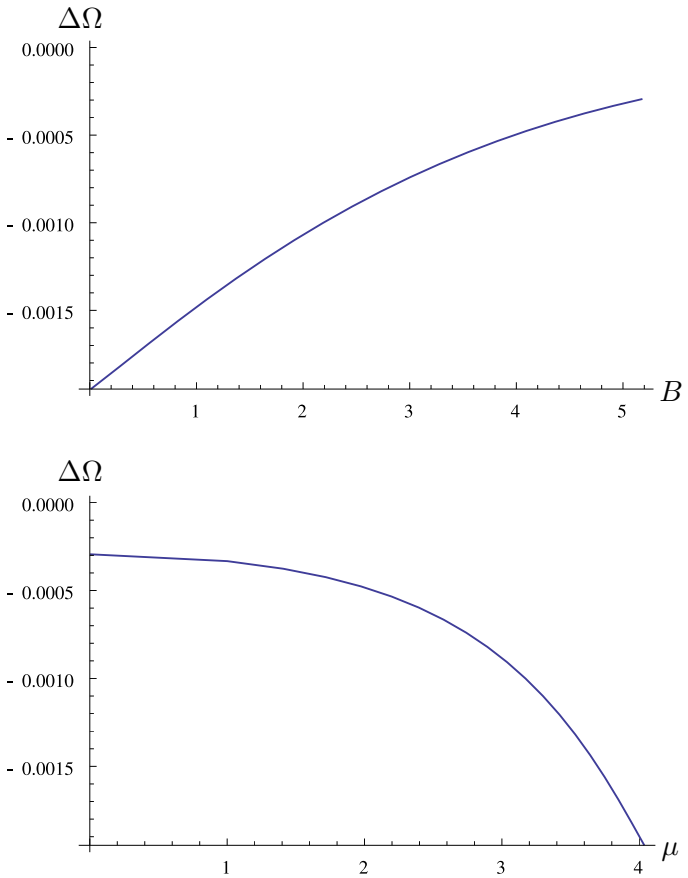

Figure 6.5: The change in free energy density compared to the normal phase solution, $\Delta\Omega$. It was calculated for the triangular lattice solution near the critical (B_c, μ_c) line in the phase diagram. More specifically, this plot shows $\Delta\Omega$ calculated at $(B, \mu) = 1.01(B_c, \mu_c)$. The important thing to notice is that $\Delta\Omega$ is negative, so the triangular lattice solution is preferred to the normal phase. The two plots contain the same information, but with respect to different parameters.

6.2 Adding probe fermions

No physically realistic system is complete without fermions. Their presence gives rise to a range of fascinating phenomena, from chiral symmetry breaking in QCD to novel topological properties in condensed matter systems. In this section we explain how to investigate their effect on the holographic vortex lattices from section 6.1.

In the context of Nielsen–Olesen vortex strings in abelian gauge theory, the presence of fermions was already studied in the early 1980's [132, 133]. It was discovered that massless fermions split into left- and right-moving modes that travel back and forth along the vortex cores. If they are given some electric charge and an electric field is switched on, the electric field breaks the balance. A net dissipationless electric current is produced along the vortex core. In [133] it was called a "superconducting string". Interestingly, one motivation for studying such strings was astrophysical; it was hoped that they could be observed passing through galactic magnetic fields.

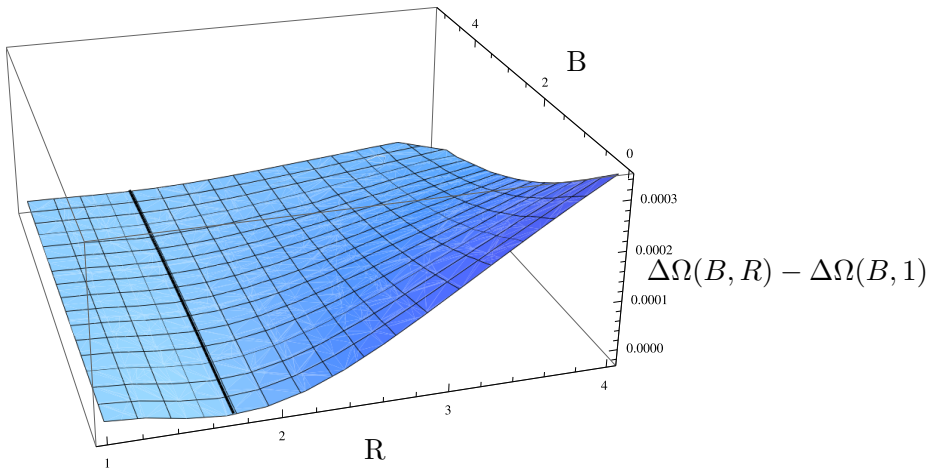

Figure 6.6: The change in free energy density $\Delta\Omega$ as a function of $B(\mu)$ and R, normalised by subtracting $\Delta\Omega|_{R=1}$ so that the left edge of the plot is fixed to zero. This subtraction does not change the location of the minimum line, which is indicated in black on the figure. $\Delta\Omega(B,R)$ itself is negative over the whole domain. The minimum is at $R=\sqrt{3}$, the value for the triangular lattice.

Fermion zero modes have also been studied more recently in vortex lattice backgrounds. In [134] a simple $SU(2)$ Yang–Mills theory in $(2+1)$-dimensional flat space was coupled to fundamental Dirac fermions. As we know from section 3.4, turning on an $SU(2)$ magnetic field in this setup yields a magnetic vortex lattice ground state. Starting from this lattice, the authors of [134] studied the spectrum of fermion zero modes and found that it contains two Dirac points per fermion flavour. A Dirac point is a point in the Brillouin zone where the fermion dispersion relation is linear, meaning it is described by the Dirac equation. A similar study is done in [135] where the authors consider a $(3+1)$-dimensional phenomenological model of QCD instead. They find an exact solution for the fermion zero modes and study its properties.

It would be interesting to find the holographic perspective on these results. What, if anything, changes when we consider fermions in a holographic model instead? With the vortices in a gravitational background, how does that influence the fermions' behaviour? In this chapter we present the setup and process needed to study these questions.

6.2.1 Holographic setup

Fermion representations are simpler to deal with in a $(3+1)$-dimensional holographic model than a $(4+1)$-dimensional model. We therefore consider the model presented in [131] with an AdS_4 background. Here the dual field theory is $(2+1)$-dimensional so that fundamental fermions are represented by 2-component spinors.

The bosonic part of the action is $SU(2)$ Einstein–Yang–Mills,

$$S_{\text{bosonic}} = \int d^4x\sqrt{-g}\,\left\{\frac{1}{2\kappa^2}\left(R+\frac{6}{L^2}\right) - \frac{1}{4\hat{g}^2}F^a_{\mu\nu}F^{a\mu\nu}\right\}, \tag{6.19}$$

where $\hat{g}^2$ is now dimensionless since we are in $(3+1)$-dimensions and L is the AdS radius. As before, we consider a black hole background with a magnetic field and a

chemical potential. One advantage of working in the lower number of dimensions is that we can now find an exact solution away from the probe approximation. If we define the dimensionless ratio

$$\gamma = \frac{2\hat{g}^2 L^2}{\kappa^2}, \tag{6.20}$$

the background solution has geometry given by the metric

$$ds^2 = \frac{L^2}{u^2}\left(-f(u)dt^2 + \frac{du^2}{f(u)} + dx^2 + dy^2\right). \tag{6.21}$$

Here $f(u)$ is given by

$$f(u) = 1 - (4 - 4\pi T u_H)\frac{u^3}{u_H^3} + (3 - 4\pi T u_H)\frac{u^4}{u_H^4}, \tag{6.22}$$

where u_H is the horizon radius and T is the field theory temperature. T and u_H satisfy the relation

$$T = \frac{1}{4\pi u_H}\left(3 - \frac{1}{\gamma}\left(B^2 u_H^4 + \mu^2 u_H^2\right)\right), \tag{6.23}$$

for magnetic field B and chemical potential μ in the field theory. The $U(1)$ subset of the $SU(2)$ gauge field A_μ^a describing the background electric and magnetic fields is given by

$$A_y^3 = Bx, \qquad A_t^3 = \mu(1 - u/u_H). \tag{6.24}$$

We rescale the coordinates to set $u_H = 1$, as before.

This AdS_4 model has a phase diagram similar to the one in figure 6.2, as shown in [131]. In particular, for certain values of B and μ the equations of motion induce the condensation of a triangular vortex lattice, given to linear order by

$$E_x = C\sum_{n=-\infty}^{\infty} \exp\left\{i\frac{\pi}{2}n^2 - inky - \frac{1}{2}B\left(x - \frac{nk}{B}\right)^2\right\}\mathcal{U}(u), \tag{6.25}$$

$$E_y = -iE_x, \tag{6.26}$$

$$C_n = C_{n+2}, \quad k = 3^{1/4}\sqrt{\pi B}, \tag{6.27}$$

where $E_{x,y} \equiv A^1_{x,y} + iA^2_{x,y}$ and $\bar{E}_{x,y} \equiv A^1_{x,y} - iA^2_{x,y}$. $\mathcal{U}(u)$ is determined by solving

$$\frac{\left(Bf + \mu^2(u-1)^2\right)}{f}\mathcal{U} + \frac{f'}{f}\mathcal{U}' + \mathcal{U}'' = 0, \tag{6.28}$$

subject to the boundary conditions $\mathcal{U}(1) = 1$ and $\mathcal{U}(0) = 0$.

One thing to note about the solution above is that, although we are considering metric backreaction, we are only considering it for the influence of A_y^3 and A_t^3. The lattice components E_x and E_y are treated as probes; we have not been able to find a way of expressing their effect on the geometry analytically. As such, the overall scale C should be kept small for this to be a valid approximation. This is equivalent to saying that we should not venture too far into the superconducting part of the phase diagram in figure 6.2, otherwise the approximation breaks down.

Now we add fermions. They are also taken to be in the probe limit. We add the term

$$S_{\text{fermion}} = \int d^4x\sqrt{-g}i\bar{\psi}\left(\not{D} - m\right)\psi + S_{\text{bdy}} \tag{6.29}$$

to the action, where $\not{D}$ is defined as

$$\not{D} = \Gamma^M D_M = \Gamma^M\left(\partial_M - iA_M + \frac{1}{4}\omega_M^{ab}\Gamma_{ab}\right). \tag{6.30}$$

Γ^M are the gamma matrices in $(3+1)$-dimensions and ω_M^{ab} is the spin connection, defined by

$$\omega_{Mab} = e_{Nb}\partial_M e_a^N + e_{Nb}\Gamma^N_{MP}e_a^P, \tag{6.31}$$

with e_N^μ the vielbeins[2].

It is not clear from the gauge/gravity dictionary (2.14) how exactly to extract field theory information from the bulk fermions. For one thing, in the bulk theory fermions are represented by 4-component Dirac spinors, while in the boundary theory Dirac spinors have only 2 components. In addition, the Dirac equation is first order, so one needs to be careful in imposing Dirichlet boundary conditions for the fermions. There is however a prescription that we follow, first proposed by [136], and later refined by [137, 138].

The first step is to form the projectors

$$\Gamma_\pm = \frac{1}{2}\left(1 \pm \Gamma^{\underline{u}}\right) \tag{6.32}$$

from the gamma matrices so that $\psi_\pm = \Gamma_\pm\psi$ and we can write

$$\psi = \begin{pmatrix} \psi_+ \\ \psi_- \end{pmatrix}. \tag{6.33}$$

If we calculate the canonical momenta in r-slicing from the action (6.29), we find that

$$\Pi_+ = -\sqrt{-gg^{rr}}\bar{\psi}_-, \quad \Pi_- = \sqrt{-gg^{rr}}\bar{\psi}_+. \tag{6.34}$$

In other words, ψ_+ and ψ_- are conjugate to each other. Fixing both of them would fix the solution everywhere, which would clearly be incorrect since, for example, we could end up with a solution that is irregular in the interior. The solution is to fix the boundary value of only half of the components. We choose to fix ψ_+ and then determine ψ_- from the Dirac equation and regularity in the interior. Now ψ_+ has the correct number of components to act as a source for the field theory fermionic operator.

The action (6.29) has a boundary term. It is necessary for the variational principle to be well-defined on a spacetime with boundary. In our case it is given by

$$S_{\text{bdy}} = i\int d^3x\sqrt{-\gamma}\ \left(\bar{\psi}_+\psi_-\right)\Big|_{u\to 0}, \tag{6.35}$$

[2] Conventions: M, N, ... run over the spacetime directions. a, b, ... run over the tangent directions. If we refer to a specific tangent-space gamma matrix, the component will be underlined, as in $\Gamma^{\underline{u}}$.

where γ is the determinant of the boundary metric. This term is crucial for calculating fermionic correlators.

Now we specialise to a specific basis. The gamma matrices we use are

$$\Gamma^{\underline{u}} = \begin{pmatrix} 1 & 0 \\ 0 & -1 \end{pmatrix}, \quad \Gamma^{\underline{i}} = \begin{pmatrix} 0 & \gamma^i \\ \gamma^i & 0 \end{pmatrix}, \tag{6.36}$$

where the superscript index i denotes t, x, y and

$$\gamma^t = i\sigma_3, \quad \gamma^x = \sigma_1, \quad \gamma^y = \sigma_2, \tag{6.37}$$

with σ_i the Pauli matrices.

The fermions and gauge field can be split up by their colour components as

$$\psi = \begin{pmatrix} \psi^1 \\ \psi^2 \end{pmatrix}, \quad A_M = \sum_a A_M^a t_a, \quad \text{with} \quad t_a = \frac{1}{2}\sigma_a, \quad a = 1, 2, 3. \tag{6.38}$$

These two fermion components couple to the 3-component of the gauge field with opposite charge. Note that this choice of generators τ^a is different from that chosen in the previous chapters, but it does not change the equations of motion for each gauge field component.

6.2.2 Solving the Dirac equation

From the action (6.29) we derive the Dirac equation

$$\left(\not{D} - m\right)\psi = 0. \tag{6.39}$$

Substituting in the metric and gauge field, this gives

$$\begin{aligned} \Bigg(\sqrt{f(u)}\Gamma^u \left(\frac{f'(u)}{4f(u)} - \frac{3}{2u} + \partial_u\right) + \frac{\Gamma^t}{\sqrt{f(u)}}\left(\partial_t \mp \frac{i\Phi(u)}{2}\right) \\ + \Gamma^x\partial_x + \Gamma^y\left(\partial_y \mp \frac{1}{2}iBx\right) - \frac{m}{u}\Bigg)\psi^{1,2}(t,x,y,u) \\ = \frac{1}{2}\left(\mp\Gamma^y + i\Gamma^x\right)\left(A_x^1(x,y,u) \mp iA_x^2(x,y,u)\right)\psi^{2,1}(t,x,y,u). \end{aligned} \tag{6.40}$$

In these equations we have absorbed the factor of the AdS radius L into the fermion mass m and $\Phi(u) = A_t^3 = \mu(1-u)$. We see that ψ^1 and ψ^2 are oppositely charged under the magnetic $U(1)$ subgroup.

Solving with no lattice

In general the partial differential equations (6.40) are hard to solve, so we start with a simple case: the lattice is not present. If we assume the lattice vanishes, the equations become separable,

$$\left(U_\mp(t,u) + V_\mp(x,y)\right)\psi^{1,2}(t,x,y,u) = 0 \tag{6.41}$$

where

$$U_\mp(t,u) = \sqrt{f(u)}\Gamma^u\left(\frac{f'(u)}{4f(u)} - \frac{3}{2u} + \partial_u\right) + \frac{\Gamma^t}{\sqrt{f(u)}}\left(\partial_t \mp \frac{i\Phi(u)}{2}\right) - \frac{m}{u}, \tag{6.42}$$

$$V_\mp(x,y) = \Gamma^x\partial_x + \Gamma^y\left(\partial_y \mp \frac{1}{2}iBx\right). \tag{6.43}$$

These equations were solved in [139]. The solution is

$$\psi^{1,2}(t,x,y,u) = \int \frac{d\omega}{2\pi}\frac{dq}{2\pi} e^{-i\omega t - iqy - \frac{1}{4}B(x+\frac{2q}{B})^2} \sum_n \tilde{\psi}^{1,2}_n(\omega,x,q,u), \tag{6.44}$$

where we defined

$$\tilde{\psi}^1_{n\geq 0} = \begin{pmatrix} \hat{H}_n(x,q)R^1_+ \\ \hat{H}_{n-1}(x,q)R^1_+ \\ \hat{H}_n(x,q)R^1_- \\ -\hat{H}_{n-1}(x,q)R^1_- \end{pmatrix} \qquad \tilde{\psi}^1_{n<0} = \begin{pmatrix} \hat{H}_{-n}(x,q)R^1_+ \\ -\hat{H}_{-n+1}(x,q)R^1_+ \\ \hat{H}_{-n}(x,q)R^1_- \\ \hat{H}_{-n+1}(x,q)R^1_- \end{pmatrix} \tag{6.45}$$

$$\tilde{\psi}^2_{n\geq 0} = \begin{pmatrix} \hat{H}_{n-1}(x,q)R^2_+ \\ -\hat{H}_n(x,q)R^2_+ \\ \hat{H}_{n-1}(x,q)R^2_- \\ \hat{H}_n(x,q)R^2_- \end{pmatrix} \qquad \tilde{\psi}^2_{n<0} = \begin{pmatrix} \hat{H}_{-n+1}(x,q)R^2_+ \\ \hat{H}_{-n}(x,q)R^2_+ \\ \hat{H}_{-n+1}(x,q)R^2_- \\ -\hat{H}_{-n}(x,q)R^2_- \end{pmatrix} \tag{6.46}$$

with

$$\hat{H}_n(x,q) = \frac{2^{-n/2}}{\sqrt{n!}} H_n\left(\frac{Bx-2q}{\sqrt{2B}}\right) \qquad n \geq 0, \tag{6.47}$$

$$\hat{H}_{-1}(x,q) = 0, \tag{6.48}$$

and H_n are the Hermite polynomials. The $R^{1,2}_\pm$ are functions of ω, u, and n that can be solved for numerically.

These solutions tell a familiar story. The fermions are trapped in a background magnetic field pointing in the radial direction. The magnetic field holds the fermions in localised bundles in the shape of quantum harmonic oscillator wavefunctions. These bundles are Landau levels and they have discrete energy levels E_n. Because of this trapping, the fermions have fewer degrees of freedom. The momenta k_x and k_y they would have in the absence of a magnetic field is replaced by a single discrete parameter n, the Landau level.

The energy levels are $E^2_n = \frac{1}{2}B\,(2n+1+2s)$, where the spin takes values $s = \pm\frac{1}{2}$. The term dependent on s is analogous to Zeeman splitting of the energy levels. The spin down part for $n = 0$ exactly cancels the zero-point energy, so the resulting lowest Landau level has vanishing energy.

The full solution is a sum over the Landau levels as well as a sum over the radial components $R^{1,2}_\pm$. The two components $\hat{H}_n$ and R are related to each other via a constant $L_n = \sqrt{nB}$. L_n appears as a separation constant in the equations. If we focus on zero modes as in [135], we should neglect the higher order terms. It is however also possible to keep the higher order terms as was done in [139]. There the authors treat L_n as a continuous parameter and calculate the Green's function as a function of frequency ω and L_n. This is a good approximation at large values of n, where the spacing between the levels goes like $\frac{1}{\sqrt{n}}$.

Ansatz with lattice

Since the system without a lattice background has already been solved in [139], we focus instead on including the lattice. We specialise on the zero modes, so select only the $n = 0$ case, and use an ansatz similar to the one from [134],

$$\psi^{1,2}(t,x,y,u) = \int \frac{d\omega}{2\pi}\frac{dq}{2\pi} e^{-i\omega t \mp iqy - \frac{1}{4}B(x+\frac{2q}{B})^2} \xi^{1,2}(\omega,q,u), \tag{6.49}$$

where the $-iqy$ is for ψ_1 and the $+iqy$ is for ψ_2. This relative sign comes from the fact that they have opposite charges under the 3-component of the gauge field. The motivation for this ansatz is that it is the same as the solution for the zero mode in the absence of the lattice, except that ξ has a q-dependence. The q-dependence is meant to capture the lattice effects on ψ.

Substituting the ansatz (6.49) into the equation (6.40) gives

$$\begin{aligned}\int \frac{dq}{2\pi}\Bigg[&\sqrt{f(u)}\Gamma^u\left(\frac{f'(u)}{4f(u)}-\frac{3}{2u}+\partial_u\right)-i\frac{\Gamma^t}{\sqrt{f(u)}}\left(\omega\pm\frac{\Phi(u)}{2}\right)\\&-\left(q+\frac{1}{2}Bx\right)(\Gamma^x\pm i\Gamma^y)-\frac{m}{u}\Bigg]e^{\mp iqy-\frac{1}{4}B(x+\frac{2q}{B})^2}\xi^{1,2}(\omega,q,u)\\&=\int\frac{dq}{2\pi}\frac{i}{2}(\Gamma^x\pm i\Gamma^y)\times\\&\qquad(A^1_x(x,y,u)\mp iA^2_x(x,y,u))e^{\pm iqy-\frac{1}{4}B(x+\frac{2q}{B})^2}\xi^{2,1}(\omega,q,u),\end{aligned}\tag{6.50}$$

where we have acted on both sides with $\int dt\ e^{i\omega' t}$ and replaced $\omega'\to\omega$, so we are now working in frequency space. Next we do the inverse Fourier transform in the y-direction. Acting with $\int dy\ e^{\pm iq'y}$ and replacing $q'\to q$ gives

$$\begin{aligned}\Bigg[&\sqrt{f(u)}\Gamma^u\left(\frac{f'(u)}{4f(u)}-\frac{3}{2u}+\partial_u\right)-i\frac{\Gamma^t}{\sqrt{f(u)}}\left(\omega\pm\frac{\Phi(u)}{2}\right)\\&-\left(q+\frac{1}{2}Bx\right)(\Gamma^x\pm i\Gamma^y)-\frac{m}{u}\Bigg]e^{-\frac{1}{4}B(x+\frac{2q}{B})^2}\xi^{1,2}(\omega,q,u)\\&=\frac{i}{2}\mathcal{U}(u)(\Gamma^x\pm i\Gamma^y)\times\\&\qquad C\sum_n e^{\mp i\frac{\pi}{2}n^2-\frac{1}{2}B(x-\frac{nk}{B})^2}e^{-\frac{1}{4}B\left(x-\frac{2(q+nk)}{B}\right)^2}\xi^{2,1}(\omega,-q-nk,u).\end{aligned}\tag{6.51}$$

If this equation were separable in the usual way, we would now be able to divide by the part of the solution that depends only on x and throw away that part of the equation. In this equation however we use a different trick. Instead of dividing out by an x-dependent factor, we integrate the whole equation with respect to x; that is, we apply the operation $\int_{-\infty}^{\infty}dx$. We then obtain

$$\begin{aligned}\Bigg[&\sqrt{f(u)}\Gamma^u\left(\frac{f'(u)}{4f(u)}-\frac{3}{2u}+\partial_u\right)-i\frac{\Gamma^t}{\sqrt{f(u)}}\left(\omega\pm\frac{\Phi(u)}{2}\right)-\frac{m}{u}\Bigg]\xi^{1,2}(\omega,q,u)\\&=\frac{i}{2}\mathcal{U}(u)(\Gamma^x\pm i\Gamma^y)\frac{C}{\sqrt{3}}\sum_n e^{\mp i\frac{\pi}{2}n^2-\frac{(kn+2q)^2}{6B}}\xi^{2,1}(\omega,-q-nk,u).\end{aligned}\tag{6.52}$$

Now consider an expansion in small condensate, where $C\to\varepsilon C$ for small $\varepsilon>0$ and $\xi^{1,2}=\xi^{1,2}_{(0)}+\varepsilon\xi^{1,2}_{(1)}+\dots$. This is similar to the expansion done in chapter 5. Let us also write the equation schematically as

$$L\xi^{1,2}(\omega,q,u)=\hat{A}\ \varepsilon C\sum_n e^{\mp i\frac{\pi}{2}n^2-\frac{(kn+2q)^2}{6B}}\xi^{2,1}(\omega,-q-nk,u).\tag{6.53}$$

Perturbatively, equation (6.52) becomes

$$L\xi^{1,2}_{(0)}(\omega,q,u)=0, \tag{6.54}$$

$$L\xi^{1,2}_{(i+1)}(\omega,q,u)=\hat{A}\ C\sum_n e^{\mp i\frac{\pi}{2}n^2-\frac{(kn+2q)^2}{6B}}\xi^{2,1}_{(i)}(\omega,-q-nk,u). \tag{6.55}$$

Because the operator L is independent of q, so is $\xi^{1,2}_{(0)}$. In particular this means that $\xi^{1,2}_{(0)}(\omega,q,u)=\xi^{1,2}_{(0)}(\omega,q+k,u)$. By induction one can prove that this holds at all orders. If we assume it holds at order i, then

$$L\xi^{1,2}_{(i+1)}(\omega,q+k,u)=\hat{A}\ C\sum_n e^{\mp i\frac{\pi}{2}n^2-\frac{(k(n+2)+2q)^2}{6B}}\xi^{2,1}_{(i)}(\omega,-q-(n+1)k,u) \tag{6.56}$$

$$=\hat{A}\ C\sum_n e^{\mp i\frac{\pi}{2}n^2-\frac{(k(n+2)+2q)^2}{6B}}\xi^{2,1}_{(i)}(\omega,-q-(n+2)k,u) \tag{6.57}$$

$$=\hat{A}\ C\sum_n e^{\mp i\frac{\pi}{2}n^2-\frac{(kn+2q)^2}{6B}}\xi^{2,1}_{(i)}(\omega,-q-nk,u) \tag{6.58}$$

$$=L\xi^{1,2}_{(i+1)}(\omega,q,u). \tag{6.59}$$

Since this holds for all ω, q and u, we conclude that $\xi^{1,2}(\omega,q+k,u)=\xi^{1,2}(\omega,q,u)$ to all orders. Then equation (6.52) becomes

$$\left[\sqrt{f(u)}\Gamma^u\left(\frac{f'(u)}{4f(u)}-\frac{3}{2u}+\partial_u\right)-i\frac{\Gamma^t}{\sqrt{f(u)}}\left(\omega\pm\frac{\Phi(u)}{2}\right)-\frac{m}{u}\right]\xi^{1,2}(\omega,q,u)$$

$$=\frac{i}{2}\mathcal{U}(u)\left(\Gamma^x\pm i\Gamma^y\right)\xi^{2,1}(\omega,-q,u)\frac{C}{\sqrt{3}}\sum_n e^{\mp i\frac{\pi}{2}n^2-\frac{(kn+2q)^2}{6B}} \tag{6.60}$$

$$=\frac{i}{2}\mathcal{U}(u)\left(\Gamma^x\pm i\Gamma^y\right)\xi^{2,1}(\omega,-q,u)\frac{Ce^{\frac{\mp 2iq^2}{(\sqrt{3}\pm 3i)B}}}{\sqrt{\frac{1}{2}\left(\sqrt{3}\pm 3i\right)}}\times$$

$$\vartheta_3\left(\frac{2\sqrt[4]{3}\sqrt{\pi}q}{\left(\pm 3i+\sqrt{3}\right)\sqrt{B}},e^{-\frac{6\pi}{\pm 3i+\sqrt{3}}}\right). \tag{6.61}$$

and we can evaluate it numerically.

The action's boundary term, from which we calculate the Green's function, is then given by

$$S_{\text{bdy}}=i\int_\partial d^3x\sqrt{-\gamma}\ \left(\bar{\psi}^1_+\psi^1_-+\bar{\psi}^2_+\psi^2_-\right)\Big|_{u\to 0}$$

$$=i\sqrt{-\gamma}\sqrt{\frac{2\pi}{B}}\int\frac{d\omega}{2\pi}\frac{dq}{2\pi}\ \left(\bar{\xi}^1_+\xi^1_-+\bar{\xi}^2_+\xi^2_-\right)\Big|_{u\to 0}. \tag{6.62}$$

The boundary expansion, derived from the equations of motion, is

$$\xi^{1,2}_+(\omega,q,u)\sim u^{\frac{3}{2}+m}A^{1,2}(\omega,q)+u^{\frac{3}{2}-m+1}B^{1,2}(\omega,q),$$

$$\xi^{1,2}_-(\omega,q,u)\sim u^{\frac{3}{2}-m}D^{1,2}(\omega,q)+u^{\frac{3}{2}+m+1}C^{1,2}(\omega,q). \tag{6.63}$$

The horizon expansion is

$$\xi=(1-u)^{-\frac{1}{4}-\frac{i\omega}{4\pi T}}\left(\xi^{(0)}+\sqrt{1-u}\xi^{(1)}+\mathcal{O}(1-u)\right). \tag{6.64}$$

Taking the functional derivative of S_{bdy}, it can be shown that the Green's function is

$$G^{R\ (\alpha\beta)(ab)} = -i\mathcal{M}^{(\alpha\delta)ab}(\gamma^t)^{\delta\beta}, \tag{6.65}$$

where we have suppressed the spinor and $SU(2)$ indices. $\mathcal{M}$ is obtained from

$$D^{(\alpha)(a)} = \mathcal{M}^{(\alpha\beta)(ab)}A^{(\beta)(b)}. \tag{6.66}$$

6.2.3 Outlook

In this section we have only set up the equations. We showed that without the lattice background, the problem reduces to one already solved in a similar system in [139]. With the lattice background, we can do a perturbative expansion. We found that, assuming the answer can be described perturbatively, it is possible to solve for all orders at once by solving a single equation numerically. Of course, since we expect topological effects to play a role, the validity of this assumption is not entirely clear.

We could also decide to take not only the lowest Landau level solution. Then the ansatz would turn into the solution (6.44), but with the $R_{\pm}^{1,2}$ upgraded to be functions of q as well. As before, the q-dependence of these radial functions is supposed to make up for the presence of the lattice. This is exactly the same procedure as in [134]; the only difference is that they only consider the lowest Landau level solutions. Note that in that case, half of the components are zero.

In this case it might be possible to repeat the calculation of the previous section with this more general ansatz. The Hermite polynomials have nice orthogonality properties that should allow us to project out all but one Landau level at a time. If that works, all the other tricks we use should work out as well. We leave this for future work.

Chapter 7

The holographic Kondo model

Consider a Landau–Fermi liquid of electrons with a single magnetic impurity. Both the electrons and the impurity are in a fundamental representation of $SU(2)$ and have spin $\frac{1}{2}$. This is known as the *Kondo model* and was introduced by Jun Kondo in 1964. The model was a theorist's answer to an outstanding experimental puzzle. Measurements of the resistivity ρ of gold with iron impurities in 1934 by [140] indicated a pronounced minimum in the temperature-dependent $\rho(T)$ at low temperatures. Standard Landau–Fermi liquid theory predicts that ρ is monotonically increasing with temperature. This feature of the resistivity having a minimum is known as the *Kondo effect*, since Kondo showed in [62] that his model reproduces the resistivity minimum. But his calculation was done perturbatively and his result also predicts that the resistivity diverges as $T \to 0$, a regime where the perturbative expansion breaks down. Experimentally the resistivity stays finite at small temperature. Understanding what happens in the Kondo model when $T \to 0$ became known as the *Kondo problem*.

The Kondo model fascinated theorists because it is a very simple example of a strongly coupled system. It is asymptotically free, so in the UV the impurity is effectively decoupled from the fermions. But lower the temperature and the *Kondo coupling* of the impurity to the conduction electrons increases. At the *Kondo temperature* T_K, a temperature lower than where the resistivity minimum is found, the Kondo coupling diverges. The conduction electrons bind strongly to the impurity, forming a *Kondo singlet*.

Because of the strong coupling, a variety of techniques were developed in an attempt to extract exact results from the Kondo model. However, none of these approaches were reliable until Kenneth Wilson developed the renormalisation group. The Kondo model was one of renormalisation group theory's first big successes [64].

The Kondo model can be seen as a toy model for QCD as well. The divergence of the Kondo coupling at a given temperature is an example of dimensional transmutation that generates an energy scale. Below this scale there is a strongly coupled bound state. This is reminiscent of quark confinement. The asymptotic freedom completes the analogy.

The Kondo model is also interesting because it can easily be extended. In the 1990's a series of papers by Affleck and Ludwig [141–146] emerged that study the Kondo model in the particular limit where it can be described by a CFT. It is also possible to promote the $SU(2)$ spin group to $SU(N)$ and take the large N limit. These two limits make the model a candidate for the application of gauge/gravity duality, if a suitable gravity dual can be constructed.

Such a holographic model was constructed in [63]. There the authors first take a top-down approach. They present a D-brane construction and take the Maldacena limit, resulting in a large N conformal field theory. By aligning the branes in the appropriate way, they can arrange for an impurity and a scalar operator, the condensation of which indicates the formation of the Kondo singlet. The authors then take the salient features of this D-brane construction and build a bottom-up model. The bottom-up model has the advantage of being less complicated for calculations. They find the Kondo coupling as a function of temperature, and then investigate the transition to the Kondo singlet state at low temperatures.

With a holographic Kondo model in hand, it makes sense to investigate the properties that use the correspondence's strengths. These include the calculation of entanglement entropy and the study of time-dependent phenomena. In this chapter we choose the latter. We consider what happens when the Kondo coupling at a given temperature is given a time-dependent quench. Using numerical techniques for solving partial differential equations, we then investigate the time scale it takes for the system to return to equilibrium.

This study is related to a recent experiment by [147]. There the authors study a system with a *quantum dot*, where the dot is similar to the Kondo impurity. Initially the dot has no net spin, but by hitting it with photons of the right wavelength, they can knock an electron out, decreasing the dot's occupation number. This "quenches" the system, suddenly putting it in a state where there is a net spin impurity localised in the conduction band. This amounts to effectively turning on a Kondo coupling. The subsequent evolution of the system can then be measured.

This chapter is divided into the following sections. We first give a review of the Kondo model in section 7.1. We then present the holographic Kondo models from [63]. The top-down model is discussed in section 7.2. A review of the bottom-up model as well as the superconducting solutions found in the static setup is then presented in section 7.3. The sections thereafter contain original work by the author of this thesis and collaborators. Section 7.4 discusses time-dependence. We add a Gaussian quench to the Kondo coupling, then find the evolution of the system. In the final section we summarise the results and outline future work.

7.1 Introduction to the Kondo model

As mentioned at the start of the chapter, the Kondo model describes a Fermi liquid of free electrons and a single magnetic impurity. As an example, in the experiment done in [140] the setup was gold with iron impurities. More recently the Kondo effect has also been seen in *quantum dots* [148]. A quantum dot is an isolated island of electrons within a material that has a magnetic spin.

The Kondo model is a special case of the *Anderson model*. The picture to have in mind is depicted in figure 7.1. It represents an impurity in the conduction band of electrons. The Fermi energy of the electrons is given by ϵ_F. The impurity has energy levels filled with various levels of electrons. Levels with more electrons have higher energy thanks to the Coulomb interaction between the electrons. The energy of the level with one electron is ϵ_d and the energy of one level higher is $\epsilon_d + U$, where U is the Hubbard energy, the typical strength of the Coulomb interaction between two electrons. To get the Kondo model, the energies ϵ_F, ϵ_d

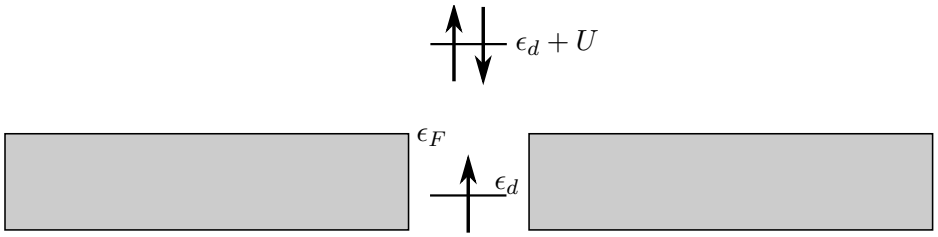

Figure 7.1: The illustration to have in mind for the Anderson model. The impurity is shown in the centre and the conduction band electrons with Fermi energy ϵ_F are on either side. Two energy levels in the impurity with energies ϵ_d and $\epsilon_d + U$ are shown. The lower is occupied by a single electron and the upper by an electron pair. The energies are adjusted for this material so that $\epsilon_d < \epsilon_F < \epsilon_d + U$. To obtain the Kondo model we assume U is large enough that all energy levels except the one with a single electron can be neglected.

and U are chosen in such a way that $\epsilon_d < \epsilon_F < \epsilon_d + U$, so that only the energy level with a single electron comes into play. The other energy levels are neglected. The single electron provides the magnetic impurity.

Following [63, 149], we can describe the Kondo model with the Hamiltonian

$$H_K = \psi_\alpha^\dagger \frac{-\nabla^2}{2m} \psi_\alpha + \hat{\lambda}_K \delta(\vec{x}) \vec{S} \cdot \psi_\alpha^\dagger \vec{\tau}_{\alpha\beta} \psi_\beta. \tag{7.1}$$

The first term is the kinetic term for the fundamental $SU(2)$ conduction band electrons ψ_α with spins $\alpha = \uparrow$ or $\alpha = \downarrow$. m is the electron mass. $\psi_\alpha^\dagger$ is a creation operator and ψ_α an annihilation operator. The second term describes interactions between the electrons and the impurity. The δ-function localises the impurity at $\vec{x} = 0$. The vector $\vec{\tau}$ is a basis for the $SU(2)$ generators given by $\tau^a = \frac{1}{2}\sigma^a$, where σ^a are the Pauli matrices. $\vec{S}$ is the spin of the impurity. Finally, $\hat{\lambda}_K$ is the Kondo coupling. The coupling is called anti-ferromagnetic if $\hat{\lambda}_K > 0$ and ferromagnetic if $\hat{\lambda}_K < 0$.

By using perturbation theory, Jun Kondo showed in [62] that the temperature-dependence of this system's resistivity is

$$\rho \sim \rho_0 + aT^5 + \hat{\lambda}_K \log\left(\frac{T}{T_F}\right). \tag{7.2}$$

Here $aT^5 > 0$ is a term that comes from the effect of lattice vibrations and T_F is the Fermi temperature of the system. In a Fermi liquid without the impurity, the resistivity would be monotonically increasing with temperature. Thanks to the log term coming from the impurity, however, we find that the resistivity has a local minimum at

$$T_{\min} \sim -\left(a/\hat{\lambda}_K\right)^{1/5} \tag{7.3}$$

and diverges at low temperatures. The minimum agrees with the experimental findings of [140]. The low-temperature divergence, however, does not agree with experiment and is interpreted as coming from the breakdown of perturbation theory in the low-temperature regime. What experiments show is that the resistivity actually approaches a finite value at low temperatures.

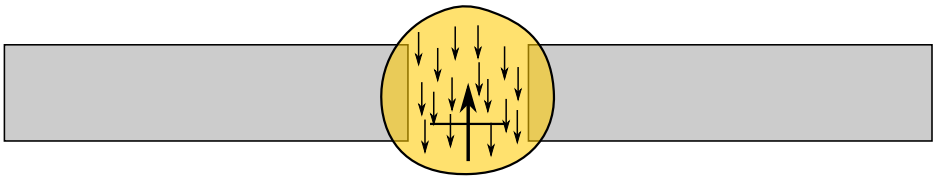

Figure 7.2: The magnetic impurity at temperatures below T_K, where the Kondo coupling is large. The impurity and the conduction electrons form a strongly coupled spin singlet, screening the magnetic moment of the impurity completely.

Kondo also showed that the coupling $\hat{\lambda}_K$ runs with temperature scale. The perturbative result is

$$\hat{\lambda}_K(T) = \frac{\hat{\lambda}_{K0} n_e}{1 + n_e \hat{\lambda}_{K0} \log(T/T_F)}, \tag{7.4}$$

where n_e is proportional to the conduction electron density. When $\hat{\lambda}_{K0} < 0$, the ferromagnetic case, we see that $\hat{\lambda}_K$ goes to zero at low temperature so the ground state is a free fermion system. When $\hat{\lambda}_{K0} > 0$, however, the situation is far more interesting. The coupling goes to zero in the UV, so it exhibits asymptotic freedom. There is also a divergence at the dynamically generated scale

$$T_K = T_F e^{-1/n_e \hat{\lambda}_{K0}}, \tag{7.5}$$

the Kondo temperature. This shows that at low energies the conduction electrons are strongly coupled to the impurity, as in figure 7.2, forming the Kondo singlet. It also turns out that at low energies the Kondo singlet's spin is absent due to being completely screened, and the remaining unbound electrons form a Fermi liquid with the boundary condition that the electron wavefunction must vanish at the impurity. Also, the transition to this new state at the Kondo temperature is a crossover, not a phase transition. For diverging coupling, perturbation theory should definitely no longer hold, so we have the Kondo problem: what is the solution of the Kondo model at low temperatures when $\hat{\lambda}_K > 0$?

We already know that gauge/gravity duality is helpful for solving problems at strong coupling. But the Kondo model as described is still not in a form amenable to AdS/CFT techniques. For that we need to generalise it first. We generalise it in two ways in the next two sections. First we explain how it can be turned into a conformal field theory, and then we take the large N limit.

The CFT approach

The CFT approach to the Kondo model was developed in the 1990's in a series of papers by Ian Affleck and Andreas Ludwig [141–146]. The idea is to reduce the problem to one dimension by doing a partial wave decomposition of the electrons. We retain only the s-wave state, so there is spherical symmetry centred at the impurity and the angular coordinates can be integrated out, leaving only the radial direction. The next step is to linearise the dispersion relation about the Fermi momentum k_F. This is valid at energies far below k_F. We are left with only in-going and out-going s-wave fermions. These can be described as left-moving and right-moving. But we can get rid of the right-movers with a trick. We extend

the radial axis to negative values and reflect the right-movers about the origin, turning them into left-movers. The resulting Hamiltonian is then

$$H = \frac{v_F}{2\pi}\psi_L^\dagger i\partial_x\psi_L + v_F\lambda_K\delta(x)\vec{S}\cdot\psi_L^\dagger\vec{\tau}\psi_L. \tag{7.6}$$

Here ψ_L are the left-moving fermions, v_F is the Fermi velocity $v_F = k_F/m$ and $\lambda_K = \frac{k_F^2}{2\pi^2 v_F}\hat{\lambda}_K$. From now on we choose $v_F = 1$ for simplicity. This model is in (1+1)-dimensions, so the Kondo coupling λ_K is dimensionless, $\delta(x)$ has dimension one, $\vec{S}$ is dimensionless and ψ_L has dimension 1/2.

The symmetry group of this new reduced model is now much larger. In particular, in the UV and the IR, the model is conformal and their symmetry groups match. This larger symmetry group can be used to calculate the complete spectrum of the theory, giving a complete solution to the Kondo problem.

The large N approach

Let us enhance the symmetry group of the Kondo model. In the original model the impurity transforms under the spin $SU(2)$ group. We promote this to $SU(N)$. In addition we can consider multiple *channels* of electrons. A channel is what particle physicists call "flavour". If there are k channels, the total gauge symmetry group becomes $SU(N)\times SU(k)\times U(1)$, where $SU(k)$ is the channel symmetry and $U(1)$ the charge symmetry.

Having generalised to $SU(N)$, we can take the large N limit. This is well-defined if we simultaneously send $N\to\infty$ and $\lambda_K\to 0$, keeping $N\lambda_K$ fixed. In this limit, the Kondo model gets another dynamically-generated temperature scale T_c, below which the system is in a superconducting phase. Let us explain how this works.

We represent the impurity spin $\vec{S}$ in terms of *slave fermions* χ. This is a technique where we artificially increase the number of degrees of freedom in the Hilbert space by decomposing physical fields into multiple unphysical fields. We choose that the slave fermions χ transform in the fundamental representation of $SU(N)$ and that

$$S^a = \chi^\dagger T^a\chi, \quad a = 1,2,\ldots,N^2-1. \tag{7.7}$$

T^a are the generators of $SU(N)$ in fundamental representation. Rotating the phase of χ leaves S^a invariant, so the theory gains an additional $U(1)$ symmetry. With the additional symmetry and artificial degrees of freedom, we should introduce a constraint to project onto the physical states in the Hilbert space. The constraint is simple: we choose $\chi^\dagger\chi = q$. q is fixed by the representation that we choose for $SU(N)$. For a totally anti-symmetric representation of $SU(N)$ where the Young tableau is a single column, that column has q boxes.

Now we can rewrite the interaction term of the Hamiltonian (7.6). We make use of the identity

$$\sum_a T^a_{\alpha\beta}T^a_{\gamma\delta} = \frac{1}{2}\left(\delta_{\alpha\delta}\delta_{\beta\gamma} - \frac{1}{N}\delta_{\alpha\beta}\delta_{\gamma\delta}\right), \quad \alpha,\beta,\gamma,\delta = 1,\ldots,N \tag{7.8}$$

for $SU(N)$ group generators. This gives

$$\begin{aligned}\lambda_K \delta(x) \left(\psi_L^\dagger T^a \psi_L\right) S^a &= \lambda_K \delta(x) \left(\psi_L^\dagger T^a \psi_L\right) \left(\chi^\dagger T^a \chi\right) \\ &= \frac{1}{2} \lambda_K \delta(x) \left[\mathcal{O}\mathcal{O}^\dagger - \frac{q}{N} \left(\psi_L^\dagger \psi_L\right)\right], \end{aligned} \tag{7.9}$$

where we defined the operator $\mathcal{O} \equiv \psi_L^\dagger \chi$ and used $\chi^\dagger \chi = q$. The operator $\mathcal{O}$ is a function of time only because χ cannot propagate away from the impurity. It transforms under the bifundamental of $SU(k) \times U(1)$ and has minus the $U(1)$ charge of the electron. It is also a singlet of $SU(N)$, which is why the authors of [63] decide to call $\mathcal{O}\mathcal{O}^\dagger$ a double-trace deformation even though it is not really the trace of a matrix. $\mathcal{O}$ has classical mass dimension $1/2$.

In the large N limit, it turns out that the system undergoes a second-order mean field phase transition at a temperature T_c, which is on the order of T_K. $\langle \mathcal{O} \rangle$ is an order parameter for this phase transition. When $T \geq T_c$, $\langle \mathcal{O} \rangle = 0$, and it is nonzero for $T < T_c$. This condensation represents the fermions ψ_L getting stuck to the impurity fermions χ, creating the Kondo singlet. In other words, in the large N limit the Kondo effect, where a Kondo singlet gets formed, is a phase transition into a superconducting phase.

One interesting point to note is that the condensation of $\mathcal{O}$ is a spontaneous breaking of the gauge symmetry, which should be impossible in $(1+1)$-dimensions due to the Mermin–Wagner theorem [150]. The reason it works here is because of the large N limit. If $1/N$ corrections are taken into account, the effect is changed from a sharp phase transition at T_c to a smooth crossover transition around T_c.

It should also be pointed out that the large N approximation is only valid at low temperatures. This is because when $T > T_c$, the model reduces to a system of free chiral fermions ψ_L. Calculating anything at high temperatures requires taking $1/N$ corrections into account.

Summary

The Kondo model describes an impurity carrying a net spin in a Fermi liquid of fermions, typically the conduction band of a metal. In the UV, the impurity is effectively decoupled from the fermions since the system exhibits asymptotic freedom. Lowering the temperature, the coupling gets stronger. Eventually a minimum in the resistivity is reached, which is one experimental signature of the Kondo effect. As the temperature is lowered further, the Kondo coupling eventually diverges at the Kondo temperature T_K. Below this scale the impurity is in a strongly coupled bound state with the conduction band electrons, known as the Kondo singlet. In the limit where $T \to 0$, the singlet's spin vanishes because it is completely screened. The conduction band electron wavefunction vanishes at the singlet. This is intuitively because the singlet is so strongly bound that it needs an infinite amount of energy for the electrons to penetrate it.

We can make the Kondo model amenable to gauge/gravity techniques by turning it into a conformal field theory with gauge group $SU(N)$ at large N. This is done by taking a partial wave decomposition of the electrons and retaining only the s-wave states, yielding an effective $(1+1)$-dimensional theory, and linearising the dispersion relation about k_F. The $SU(2)$ spin group of the impurity is promoted to $SU(N)$ and the large N limit is taken. Now the Kondo model is a

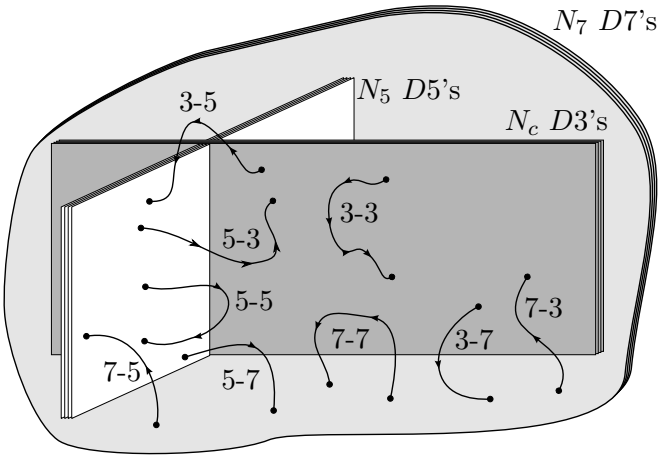

Figure 7.3: A sketch of the top-down holographic Kondo model from [63]. There are N_c D3-branes, N_5 D5-branes and N_7 D7-branes, with $N_5 \ll N_c$ and $N_7 \ll N_c$. The different kinds of open strings stretching between the branes are also shown. This figure was taken with permission from [149].

superconductor. There is a critical temperature T_c of the same order as T_K below which a "double-trace" operator $\mathcal{O}$ condenses. The condensation of this operator indicates the onset of superconductivity as well as the formation of the Kondo singlet.

With the Kondo model understood, it is possible to construct a holographic dual. There are two approaches we can take, and both are described in [63]. In their top-down approach, the authors present a D-brane construction and take the Maldacena limit, resulting in a large N field theory with an impurity and an operator $\mathcal{O}$. The top-down construction is however quite complicated, so they also propose a bottom-up model with the salient properties. We give a brief overview of the top-down construction before moving to the bottom-up model and investigating time-dependent solutions to the Kondo coupling.

7.2 The top-down holographic Kondo model

In [63] the authors consider the following D-brane intersection in type IIB string theory:

	0	1	2	3	4	5	6	7	8	9
N_c D3	×	×	×	×						
N_5 D5	×				×	×	×	×	×	
N_7 D7	×	×			×	×	×	×	×	×

There are different kinds of open strings described by the branes on which they end. These are illustrated in figure 7.3. The worldvolume of each stack of Dq-branes has a $(q+1)$-dimensional maximally supersymmetric super Yang–Mills theory with gauge group $U(N_q)$. This theory comes from the q-q strings. Each worldvolume theory has a Yang–Mills coupling g_q related to the string coupling g_s and α' as $g_q^2 \sim g_s \alpha'^{(q-3)/2}$. We also define a 't Hooft coupling for each theory as $\lambda_q = N_q g_q^2$.

As with the original AdS/CFT correspondence, we are interested in the limit where N_c is large, so there are many D3-branes. We treat the D5-branes and D7-branes as probes. There should not be enough of them to backreact onto the geometry, so $N_5 \ll N_c$ and $N_7 \ll N_c$. As before, in sending $N_c \to \infty$ we keep λ_3 fixed and then send it to infinity as well. When doing this the 't Hooft couplings λ_5 and λ_7 are suppressed by powers of $1/N_c$ so they vanish. As a result, the 5-5 and 7-7 strings decouple from the D3-brane worldvolume theory so their only relevant contribution is the global $U(N_5)$ and $U(N_7)$ symmetry groups.

The worldvolume theory we are interested in is that on the D3-branes. In the Maldacena limit, the 3-3 strings give the usual $\mathcal{N} = 4$ super Yang–Mills theory with gauge group $SU(N_c)$. We also saw that the theories arising from the 5-5 and 7-7 strings decouple. What is more interesting is the contribution from the brane intersections. The 3-7 and 7-3 strings give rise to chiral fermions. They live on the $(1 + 1)$-dimensional intersection between the D3- and D7-branes, so they can be thought of as the conduction band electrons. Also, they transform under an $SU(N_c) \times SU(N_7) \times U(1)$ current algebra, reminiscent of the spin and channel symmetries of the previous section. The 3-5 and 5-3 strings, on the other hand, live in a $(0+1)$-dimensional space that should describe the Kondo impurity. They give rise to the slave fermions. Finally, the 5-7 and 7-5 strings describe the interaction between the impurity and the conduction band.

Let us turn to the gravity side. The near-horizon limit of the D3-branes, as we know, gives $\mathrm{AdS}_5 \times S^5$. The probe D7-branes fill up an $\mathrm{AdS}_3 \times S^5$ subspace of the $\mathrm{AdS}_5 \times S^5$. The duals of the field theory chiral fermions are Chern–Simons fields living on the D7-brane worldvolume. Integrating out the S^5 directions, this is a Chern–Simons field living on AdS_3. The D5-branes span an AdS_2 subspace of the AdS_3. This subspace contains, among other fields, a gauge field which is dual to a charge on the impurity.

The final component on the gravity side comes from the D5/D7 intersection. It represents the Kondo coupling. This intersection contains a tachyonic field that transforms in the bifundamental under $U(N_7) \times U(N_5)$ but is a singlet under the spin symmetry $SU(N_c)$. The operator $\mathcal{O}$ has precisely the correct properties to be identified with the operator defined in equation (7.9). It is dual to a scalar field.

In this section we gave a very rough overview of the top-down Kondo model. The authors of [63] however give a much more detailed treatment.

7.3 The bottom-up holographic Kondo model

The bottom-up model proposed in [63] takes only the essential ingredients from the top-down model. Since the full $(3+1)$-dimensional super Yang–Mills theory is unnecessary, it makes sense to look at only the AdS_3 as the complete spacetime, with a black hole for temperature. In that spacetime the authors place a level-N Chern–Simons field to be dual to the chiral fermions, as well as a brane stretching out in only the radial and time directions. This brane is localised on the boundary; it represents the impurity. It spans an AdS_2 subspace and contains a Yang–Mills gauge field and a complex scalar dual to an operator $\mathcal{O}$.

In this section we review the bottom-up holographic setup in detail, derive the equations of motion and show how they were solved in [63] to give the superconductor solution. This solution then sets the stage for the time-dependent

calculations we present in later sections.

7.3.1 Holographic setup

The gravity background is a fixed (2+1)-dimensional AdS–Schwarzschild (or BTZ) black hole, with metric

$$ds^2 = \frac{1}{z^2}\left(-h(z)dt^2 + \frac{dz^2}{h(z)} + dx^2\right),$$
$$h(z) = 1 - \frac{z^2}{z_H^2}. \tag{7.10}$$

Here z is the holographic coordinate with the AdS boundary at $z = 0$ and the horizon at $z = z_H$. x is a spatial coordinate and t a time coordinate. In these coordinates the AdS radius is set to unity and the Hawking temperature is $T = 1/(2\pi z_H)$.

The geometry has a scaling symmetry. The scale transformation

$$(t, z, z_H, x) \to \lambda(t, z, z_H, x) \tag{7.11}$$

leaves the metric invariant. We will thus use this freedom to choose the geometry size where $z_H = 1$, and work in these "dimensionless" units from now on. Note that this is not a change of coordinates, which is a passive transformation. The coordinate choice was fixed by setting the AdS radius to unity. This is a rescaling of the geometry, which is an active transformation. From now on, any further scale in the setup will not leave the physics invariant when rescaled, because it is implicitly compared to z_H, that is, it takes a value in units of z_H. Factors of z_H can always be restored by dimensional analysis.

The model has a level-N $U(k)$ Chern–Simons gauge field, which is dual to both the charge $U(1)$ and channel $SU(k)_N$ currents. The action for this field is given by

$$S_{CS} = -\frac{N}{4\pi}\int \mathrm{tr}\left(A \wedge dA + \frac{2}{3}A \wedge A \wedge A\right). \tag{7.12}$$

A is the Chern–Simons field and $F = dA + A \wedge A$ its field strength. For our purposes we choose $N = 1$.

Furthermore, the AdS_3 space has an AdS_2 subspace on which additional fields are localised. The AdS_2 is located at $x = 0$; this is meant to model the Kondo impurity in the boundary field theory. It contains a gauge field and a scalar, described by the action

$$S_{AdS_2} = -N\int d^3x\delta(x)\sqrt{-g}\left(\frac{1}{4}\mathrm{tr}f^{mn}f_{mn} + g^{mn}\left(D_m\Phi\right)^\dagger D_n\Phi + M^2\Phi^\dagger\Phi\right). \tag{7.13}$$

$f = da + a \wedge a$ is the field strength for the gauge field a. The indices m, n run over the z and t coordinates only. Φ is a scalar coupling in the bifundamental representation to both gauge fields through the covariant derivative D_m. Each gauge field is the connection for a $U(1)$ gauge group, so the covariant derivative is simply

$$D_m\Phi = \partial_m\Phi + iA_m\Phi - ia_m\Phi, \tag{7.14}$$

where the scalar's $U(1)$ charges are ± 1.

The equations of motion become

$$\varepsilon^{n\mu\nu} F_{\mu\nu} = -4\pi\delta(x) J^n, \tag{7.15}$$

$$\partial_m \left(\sqrt{-g} g^{mp} g^{nq} f_{pq}\right) = -J^n, \tag{7.16}$$

$$\begin{aligned} \frac{1}{\sqrt{-g}} \partial_m \left(\sqrt{-g} g^{mn} \partial_n \Phi\right) &= \Delta^m \Delta_m \Phi - 2i \Delta^m \partial_m \Phi \\ &\quad - \frac{i}{\sqrt{-g}} \partial_m \left(\sqrt{-g} \Delta^m\right) \Phi + M^2 \Phi. \end{aligned} \tag{7.17}$$

The current J^m is defined as

$$J^m \equiv 2\sqrt{-g} g^{mn} \left(\Phi \partial_n \Phi^\dagger - \Phi^\dagger \partial_n \Phi - 2i \Delta_n \Phi \Phi^\dagger\right) \tag{7.18}$$

and we also made use of the definition

$$\Delta_m \equiv A_m - a_m. \tag{7.19}$$

The current is conserved, so $\partial_n J^n = 0$ is another equation of motion, although not independent of the equations (7.15)–(7.17).

Before we can solve these equations, we need to specify a gauge to work in. There are two $U(1)$ gauge fields, and their gauge freedom allows us to set one component of each to zero. We choose to set $a_z = A_z = 0$. It is then straightforward to show that we can also consistently switch off A_t. Doing this, we find that equations (7.16) and (7.17) no longer contain A_x. This means that a_t and Φ can be solved for independently of A_x. They do still source A_x in equation (7.15), however, so after their solution has been found, they can be substituted in to solve for A_x. The main task, then, is to solve for $a_t(t, z)$ and $\Phi(t, z)$.

Near the boundary, equation (7.16) can be solved to show that

$$a_t \asymp \frac{Q}{z} + \mu + \dots. \tag{7.20}$$

Here $\lim_{z\to 0} \sqrt{-g} f^{tz} = -Q$ is the electric flux at the boundary and μ the chemical potential of the dual field theory.

The complex scalar Φ is dual to the operator $\mathcal{O}$. In order to match this operator with the operator in equation (7.9), the complex scalar Φ should have scaling dimension $1/2$. This means the scalar must have an effective mass that coincides with the Breitenlohner-Freedman bound. If Φ has a boundary expansion that goes like $z^{\Delta_\pm}$ as $z \to 0$, equation (7.17) tells us that

$$\Delta_\pm = \frac{1}{2} \pm \frac{1}{2}\sqrt{1 + 4(M^2 - Q^2)}. \tag{7.21}$$

We therefore need that $\Delta_+ = \Delta_- = \frac{1}{2}$, and to achieve this we choose $M = 0$ and $Q = -\frac{1}{2}$. As a result, because the exponents of both of the leading terms are the same, we need to introduce a logarithm so that

$$\Phi \asymp \alpha\sqrt{z} \ln(\Lambda z) + \beta\sqrt{z} + \dots, \tag{7.22}$$

where Λ is an arbitrary energy scale needed to make the argument of the logarithm dimensionless.

7.3.2 The Kondo coupling

The field theory Lagrangian has the "double-trace" deformation proportional to $\kappa\mathcal{O}\mathcal{O}^\dagger$, where κ is the Kondo coupling. The boundary conditions for such a deformation need to be treated with care, as shown in [151,152]. The correct condition to use is

$$\alpha = \kappa\beta. \tag{7.23}$$

This relation is derived as follows. Suppose a perturbation W is added to the field theory action, where $W(x, \mathcal{O}_i, d\mathcal{O}_i)$ is some function of spacetime, operators and derivatives of operators, and that the operators $\mathcal{O}_i$ are dual to fields ϕ_i with boundary expansions

$$\phi_i = \alpha_i(x) z^{\Delta_-} + \beta_i(x) z^{\Delta_+} + \dots. \tag{7.24}$$

If, for example, $W = \int d^d x f(x)\mathcal{O}(x)$, then we know from the standard AdS/CFT dictionary that $\alpha \sim f$ is the source for the vacuum expectation value $\beta \sim \mathcal{O}$. We can write this relationship as

$$\alpha = \frac{\delta W(x,\beta)}{\delta\beta}. \tag{7.25}$$

The idea presented in [151,152] is to use precisely this formula as a generalisation of the standard case. We substitute $\mathcal{O}_i \to \beta_i$ so that $W(x, \mathcal{O}_i, d\mathcal{O}_i) \to W(x, \beta_i, d\beta_i)$, then use the formula.

For the holographic Kondo model, the field theory has the term

$$W \sim \frac{\kappa}{2}\int d^3x \mathcal{O}\mathcal{O}^\dagger \tag{7.26}$$

in the action. This reproduces the relationship (7.23). The first two terms in the expansion (7.22) then become

$$\Phi \asymp \beta\sqrt{z}\left(\kappa \ln(\Lambda z) + 1\right). \tag{7.27}$$

Now, the value of Φ cannot depend on the choice of Λ. On the gravity side, this is because Φ satisfies a second order differential equation and so it only has two degrees of freedom determined by β and κ. On the field theory side, this means that the source and vev must be independent of Λ. Thus Λ is like a renormalisation group energy scale. Demanding the invariance of (7.27) under a change in energy scale Λ means that β and κ must change. Suppose we start with the values β_0, κ_0 and Λ_0, then changing to energy scale Λ means that

$$\kappa = \frac{\kappa_0}{1 - \kappa_0 \ln\left(\frac{\Lambda}{\Lambda_0}\right)} \tag{7.28}$$

and $\beta_0\kappa_0 = \beta\kappa$. So κ and β are renormalised depending on the energy scale Λ.

The renormalisation scale is an additional unphysical scale that needs to be fixed. For every solution for Φ, there is a single parameter's worth of values for κ and β. Earlier we fixed the temperature of the model by choosing $z_H = 1$, so it makes sense to use this choice to fix Λ as well. So when given a solution Φ, we

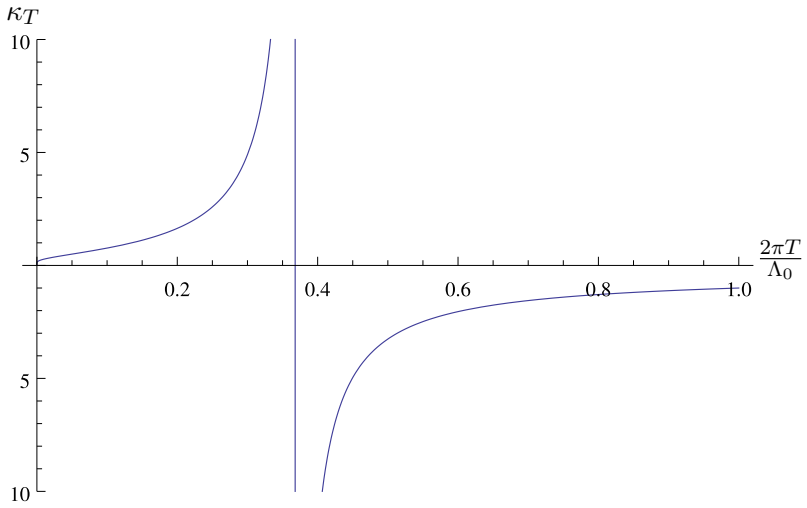

Figure 7.4: The value of κ_T plotted as a function of $\frac{2\pi T}{\Lambda_0}$ for a representative negative value of the coupling $\kappa = -1$. There is a divergence at $\frac{2\pi T}{\Lambda_0} = e^{-1}$ which we identify as the Kondo temperature $T_K = \frac{1}{2\pi}\Lambda_0 e^{-1}$.

use $\Lambda_T = 1/z_H = 2\pi T$ (which simply equals one in our dimensionless units) to determine κ_T and β_T.

Using the renormalisation equation (7.28) we can also work out how κ_T should change with energy scale. Suppose that $\kappa = -1$ at some energy scale Λ_0, where we chose it to be negative because we want an anti-ferromagnetic coupling. We then have

$$\kappa_T = -\frac{1}{1 + \ln\left(\frac{2\pi T}{\Lambda_0}\right)}. \tag{7.29}$$

Figure 7.4 shows κ_T plotted as a function of $\frac{2\pi T}{\Lambda_0}$. It shows that κ_T diverges at a certain temperature, which we call the Kondo temperature $T_K = \frac{1}{2\pi}\Lambda_0 e^{-1}$. Using this definition with equation (7.29), we get that $T/T_K = e^{-1/\kappa_T}$. Note how well this corresponds to the running of the Kondo coupling in (7.4)!

7.3.3 Superconductivity

It was shown in [63] that this model undergoes a superconducting phase transition when the temperature is below a critical value T_c, which is less than T_K for anti-ferromagnetic coupling. The new ground state is found using a shooting method, which we will briefly outline in this section. Since we are only interested in ground states, we search for static solutions. In the next section we turn our attention to solving the time-dependent system.

The static equations of motion in the background (7.10) are

$$0 = \frac{a_t^2 \Phi}{(1-z^2)^2} - \frac{2z\Phi'}{1-z^2} + \Phi'', \tag{7.30}$$

$$0 = \Phi(\Phi^\dagger)' - \Phi^\dagger \Phi', \tag{7.31}$$

$$0 = a_t'' + \frac{2a_t'}{z} + \frac{2a_t \Phi\Phi^\dagger}{z^2(z^2-1)} - \frac{i\Phi^\dagger\Phi'}{z^2} + \frac{i\Phi(\Phi^\dagger)'}{z^2}. \tag{7.32}$$

It is clear that we can choose $\mathrm{Im}(\Phi)$ to be zero. Defining $\phi = \mathrm{Re}(\Phi)$, we have only two remaining equations,

$$0 = \frac{a_t^2 \phi}{(1-z^2)^2} - \frac{2z\phi'}{1-z^2} + \phi'', \tag{7.33}$$

$$0 = a_t'' + \frac{2a_t'}{z} + \frac{2a_t\phi^2}{z^2(z^2-1)}. \tag{7.34}$$

The fields ϕ and a_t each have a second order equation of motion. This means there are four integration constants in total: Q, μ, κ and β. Above we fixed $Q = -\frac{1}{2}$, fixing one of the constants. There are two further constraints coming from regularity at the horizon $z = 1$.

The first regularity constraint is that we need $g^{mn}a_m a_n = g^{tt}(a_t)^2$ to remain finite at the horizon, which of course means we need to set $a_t = 0$ at $z = 1$. As we have already explained in previous chapters, it is not obvious why we need to stop the vector potential from diverging when all that should really matter is that the physical electromagnetic field remains finite. Perhaps the divergence can be gauged away. This cannot be done, however, because we have already made the gauge choice $a_z = 0$. Any further gauge transformations λ can be functions only of t[1]. Thus the z-dependence of a_t cannot be changed with a gauge transformation, and it must be zero at the horizon.

The second regularity constraint can be found by working out the series expansion of equation (7.33) about $z = 1$ and determining the coefficient of the singular term, which must vanish. This gives us a Neumann boundary condition for ϕ: $\partial_z\phi = 0$ at $z = 1$.

Given that three of the four constants are thus fixed, the solution space is parameterised by only the chemical potential μ. As explained earlier, varying μ is equivalent to varying the temperature of the system. The procedure is therefore to choose a temperature, fixing μ, and then find the values of κ and β that give profiles for ϕ and a_t that solve the equations of motion. This procedure is the essence of the shooting method. For given values of Q, μ, κ and β, we can numerically integrate the equations from $z = 0$ to $z = 1$ and determine to what extent they violate the horizon boundary conditions. We vary κ and β until the horizon boundary conditions are satisfied within numerical tolerance.

One thing that we glossed over in the previous paragraph is how to impose the initial boundary conditions at $z = 0$. Since the equations of motion are singular there, this is not possible. We instead have to impose conditions at $z = \varepsilon$ and start the integration there. This means we need to know the values of the fields at $z = \varepsilon$ before we start. These are found by working out the first few terms of the asymptotic expansion of ϕ and a_t at $z = 0$. It turns out that this is not so straightforward because of the presence of powers of $\ln z$ in the expansion. In appendix C we present an algorithm for computing these terms for the full system of time-dependent equations. This allows us to find the boundary expansion for the static fields to tenth order and thus execute the shooting method to find the field profiles.

The main numerical result obtained is that the holographic Kondo model exhibits spontaneous symmetry breaking below a critical temperature, the hallmark of a superconductor. The system is in a superconducting phase when $\mu > \frac{1}{2}$, which

[1] See the end of section 5.1.2 for more details.

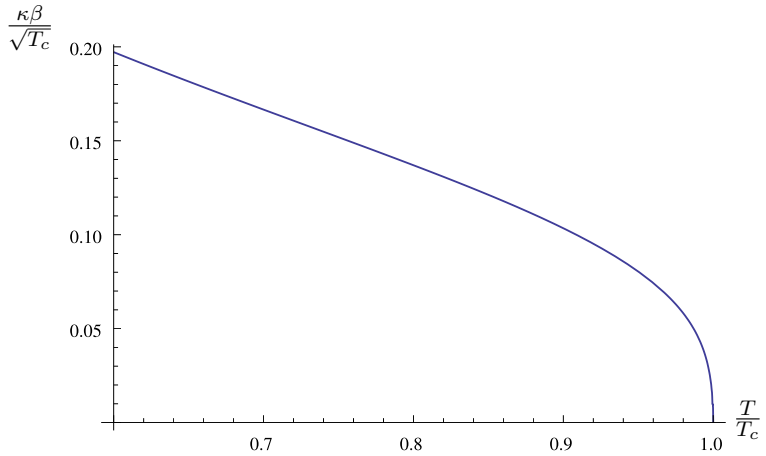

Figure 7.5: $\kappa\beta$ as a function of temperature, showing the condensation of $\mathcal{O}$ below T_c. A fit to the data, done in [63], reveals that the phase transition is mean-field, with $\langle\mathcal{O}\rangle \sim (T - T_c)^{1/2}$.

in dimensionful units means that $\frac{T}{\mu} < \frac{1}{\pi}$. In this phase ϕ has a non-vanishing profile and κ and β are of course non-zero. When $\mu < \frac{1}{2}$, ϕ, κ and β vanish. $\kappa\beta$ as a function of temperature is plotted in figure 7.5. What is not shown in the figure is that $\kappa\beta$ approaches a constant as $T \to 0$. From figure 7.4 we know that this means that $\kappa \to 0$ and $\beta \to \infty$ as $T \to 0$.

7.4 The time-dependent Kondo model in the probe scalar limit

As explained in the introduction, what we would like to do is induce a quench in the Kondo coupling κ. This means that we start from one of the static solutions outlined in the previous section where κ has some fixed value, then add a Gaussian bump $\kappa \sim \kappa_0 + e^{-\sigma^2 t}$ and see how the system evolves.

Unfortunately this is technically hard to do. Let us look at the boundary ($z \to 0$) expansion for the scalar, given by

$$\phi(z) \asymp \alpha\sqrt{z}\ln z + \beta\sqrt{z} - \frac{1}{3}\alpha^3 z^{3/2}(\ln z)^4 + \mathcal{O}(z^{3/2}(\ln z)^3). \tag{7.35}$$

Recall that $\alpha = \kappa\beta$. This means that β is an overall factor of the two largest terms of ϕ near the boundary. A numerical algorithm that attempts to find β given κ is likely to find the solution $\beta = 0$ near the boundary, and not the real solution we are looking for.

As a first approach we therefore work instead with α and β directly. We promote α and β to time-dependent functions. We implement the quench by fixing α to a Gaussian function, $\alpha(t) \sim \alpha_0 + e^{-\sigma^2 t^2}$, and then determine how β responds. Afterwards we can read off $\kappa = \alpha/\beta$ as a result of the quench. We can then try to tune the quench in α so that it gives the form of κ we would like.

At early times α and β take values from the static solution. The quench induces a "bump" in ϕ near the boundary, which travels into the bulk as a result of the wave equation that ϕ satisfies. In the usual AdS–Schwarzschild coordinates, this bump takes an infinite amount of asymptotic time to reach the black hole horizon.

Instead, it makes more sense to move to Eddington–Finkelstein coordinates, where ϕ dies down to an almost-vanishing profile soon after the peak of the Gaussian in the quench.

We approach the problem as follows. In the next section we write down the time-dependent equations in Eddington–Finkelstein coordinates and show how the gauge-fixing from the AdS–Schwarzschild coordinates carries over to the new coordinates. The fields on the brane decouple from the Chern–Simons field, so we have three coupled time-dependent equations for the brane fields left over. These three equations correspond to the three real fields of interest on the brane — one gauge field component and the complex scalar's two components. We then make an assumption: we assume that the gauge field is fixed then solve only for the scalar, treating the scalar as a probe. This allows for a check of the numerical methods. We solve the probe scalar using two different methods. The first is through separation of variables, where we have a high degree of control over the numerics because we only have to solve ordinary differential equations. The second method is by using a time-marching scheme, where we solve the equations at a given spatial slice and then integrate the solutions in time to get a solution for the next spatial slice. The solution using this method agrees with the solution from separation of variables, so we have confidence in the method. The next step is then to generalise it to include backreaction of the scalar onto the gauge field. This is left for future work.

7.4.1 Equations in Eddington–Finkelstein coordinates

We convert to Eddington–Finkelstein coordinates by defining a new time coordinate, v, by

$$dv = dt - \frac{dz}{h(z)}. \tag{7.36}$$

This means that the metric (7.10) becomes

$$ds^2 = -\frac{h(z)}{z^2}dv^2 - 2\frac{dvdz}{z^2} \tag{7.37}$$

Using the explicit expression for h from (7.10), we can integrate to find that

$$v = t - \operatorname{arctanh} z. \tag{7.38}$$

Note that v and t are the same at boundary.

In these new coordinates, the gauge field A becomes

$$A_t \to A_v \qquad A_z \to -\frac{1}{h}A_v + A_z. \tag{7.39}$$

To fix the gauge in AdS–Schwarzschild coordinates, one usually sets the radial component of the gauge field, in this case A_z, to zero. This same gauge in EF coordinates becomes $A_z = \frac{1}{h}A_v$. We also choose $a_z = \frac{1}{h}a_v$. Furthermore we can consistently choose $A_v = 0$.

Using this ansatz, the equations of motion (7.15)–(7.17) become

$$0 = \partial_v A_x + 2\pi i\delta(x)\left(\Phi^\dagger\left(\partial_v\Phi - h\partial_z\Phi\right) + \Phi\left(h\partial_z\Phi^\dagger - \partial_v\Phi^\dagger\right)\right), \tag{7.40}$$

$$0 = \partial_z A_x + 2\pi i\delta(x)\left(\Phi\partial_z\Phi^\dagger - \Phi^\dagger\partial_z\Phi + \frac{2ia_v\Phi\Phi^\dagger}{h}\right), \tag{7.41}$$

$$0 = \frac{z^2\partial_v^2 a_v}{h} - z^2\partial_z\partial_v a_v + ih\Phi^\dagger\partial_z\Phi - i\Phi\left(h\partial_z\Phi^\dagger - \partial_v\Phi^\dagger\right) - i\Phi^\dagger\partial_v\Phi, \tag{7.42}$$

$$\begin{aligned} 0 = {} & +z^2h\partial_z^2 a_v - z^2\partial_z\partial_v a_v + 2zh\partial_z a_v + \left(\frac{z^2h'}{h} - 2z\right)\partial_v a_v \\ & - 2a_v\Phi\Phi^\dagger + ih\left(\Phi\partial_z\Phi^\dagger - \partial_z\Phi\Phi^\dagger\right), \end{aligned} \tag{7.43}$$

$$0 = \partial_z^2\Phi - \frac{2\partial_z\partial_v\Phi}{h} + \frac{h'\partial_z\Phi}{h} + \frac{2ia_v\partial_v\Phi}{h^2} + \frac{\Phi\left(iz^2\partial_v a_v + z^2a_v^2 - M^2h\right)}{z^2h^2}. \tag{7.44}$$

The first two are equations of motion for the Chern–Simons field. These are the only equations in which A_μ appears, so they should be solved after Φ and a_m are known.

7.4.2 Solving for the scalar probe using separation of variables

As a first step we treat the scalar Φ as a probe on top of a fixed solution for the gauge field. Solving for a_v when $\Phi = 0$ gives

$$a_v = \frac{Q}{z} + \mu, \tag{7.45}$$

where we choose $Q = -1/2$. Because a_v must vanish at $z = 1$ for regularity, we have that $\mu = 1/2$.

Using this solution for a_v and choosing $M = 0$, the scalar equation (7.44) becomes

$$0 = \partial_z^2\Phi + \frac{2\partial_z\partial_v\Phi}{z^2-1} + \frac{2z\partial_z\Phi}{z^2-1} + \frac{i\partial_v\Phi}{(z-1)z(z+1)^2} + \frac{\Phi}{4z^2(z+1)^2}. \tag{7.46}$$

We can solve this using the separation of variables ansatz

$$\Phi(z,v) = Z(z)V(v), \tag{7.47}$$

which gives the equations

$$0 = V' + iSV, \tag{7.48}$$

$$0 = Z'' + \frac{2(z-iS)Z'}{z^2-1} + \frac{(4Sz+z-1)Z}{4(z-1)z^2(z+1)^2}. \tag{7.49}$$

for $Z(z)$ and $V(v)$. We chose iS as the separation constant. The equation for V is easy enough to solve analytically. The full solution for Φ is therefore

$$\Phi = \sum_n C_n e^{-iS_n v} Z_n(z, S_n) \tag{7.50}$$

with constants C_n and S_n that we can choose and the functions $Z_n(z, S_n)$ that we have to solve for numerically. Happily equation (7.49) for Z_n is an ordinary differential equation.

How do we choose C_n and S_n? We wish to impose a time-dependent function $\alpha(v)$. The boundary expansion of Z_n is

$$Z_n \asymp \alpha_n \sqrt{z} \log z + \beta_n \sqrt{z} + \mathcal{O}(z^{3/2} \log z). \tag{7.51}$$

From this we can fix C_n and deduce that

$$\alpha(v) = \sum_n \alpha_n e^{-iS_n v}, \quad \beta(v) = \sum_n \beta_n e^{-iS_n v}. \tag{7.52}$$

We can also fix S_n so that these expansions become Fourier series expansions, or indeed take the continuum limit and turn the sums into Fourier transforms. It is easier to work with discrete methods numerically, so we choose to take a Fourier series with $S_n = \frac{2\pi n}{L}$ and make the quench $\alpha(v)$ periodic, so that

$$\alpha(v) = \sum_n \alpha_n e^{-i\frac{2\pi n}{L} v}, \tag{7.53}$$

where L is the period of α.

We thus have a clear strategy. We choose a quench function $\alpha(v)$ and do a Fourier transform to determine the coefficients α_n. Taking a coefficient α_n and $S_n = \frac{2\pi n}{L}$ as input, we solve equation (7.49) using the shooting method described in the previous section. This gives us a coefficient β_n. Using β_n we can reconstruct $\beta(v)$ via the inverse Fourier transform.

Using this strategy we plot the result for a Gaussian quench in figure 7.6. In this figure we choose to quench about a vanishing condensate, so the system starts at T_c. The quench is a "shake" in the boundary conditions of the scalar field, producing a bump that flows into the black hole horizon. If metric backreaction is taken into account, this should result in the black hole growing in size, raising the temperature of the field theory.

The separation of variables method is simple to implement and the numerical results are stable. However, it cannot be generalised to include gauge field backreaction. In this respect the time-marching method described in the following section is superior.

7.4.3 Solving for the scalar probe using a time-marching method

One thing to realise about the probe scalar solution from the previous section is that it is real. It certainly makes sense that we can choose Φ to be real at the boundary using a residual v-dependent gauge transformation, but we cannot choose it to be real for all z. This is because we have already used a z-dependent gauge transformation to fix $A_z = a_z = 0$. In fact, when we include gauge field backreaction we will find that the imaginary part of Φ is in general not zero. For the probe limit, however, we can neglect $\operatorname{Im}\Phi$, and work only with the real part $\phi = \operatorname{Re}\Phi$.

With this choice the equation (7.44) becomes

$$\partial_v \partial_z \phi = -\frac{(1-z)^2 \phi}{8z^2(z^2-1)} + \frac{1}{2}\left(1-z^2\right)\partial_z^2 \phi - z\partial_z \phi \tag{7.54}$$

$$\equiv F(\phi, \partial_z \phi, \partial_z^2 \phi, z), \tag{7.55}$$

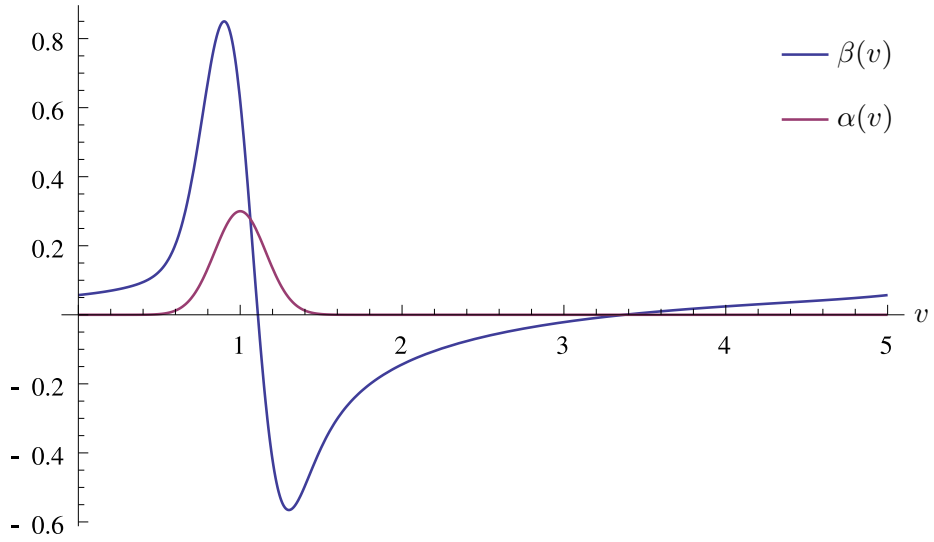

Figure 7.6: The response of $\beta(v)$ to a Gaussian quench in $\alpha(v)$ is plotted. It was calculated using the separation of variables method. Here we choose to quench about a vanishing condensate, so the system is at $T = T_c$. The quench profile for α is $\alpha(v) = 0.3e^{-\frac{(v-1)^2}{0.05}}$.

where we have written it in a form that makes integration in v easier, and defined the function F.

The idea behind a time-marching scheme is simple. We first notice that equation (7.54) has only one term with a v-derivative, which we have written on the left-hand side of the equation. We foliate spacetime in the v-direction and solve for ϕ in discrete steps on these v-slices. Before the quench, on the first v-slice, ϕ takes its initial static value and its spatial derivatives are zero. Then for each consecutive v-slice we can solve for ϕ (and its z-derivatives) based on their values on the previous v-slice using the formula (7.54). To find ϕ on v-slice $n+1$, we discretise the v-derivative so that

$$\partial_z\phi|_{v_{n+1}} = \partial_z\phi|_{v_n} + (v_{n+1} - v_n)\, F|_{v_n}\,. \tag{7.56}$$

We can then find ϕ by numerically integrating $\partial_z\phi$ from $z = 0$ and imposing the boundary condition $\phi|_{z=0} = 0$ to fix the integration constant. Note that this method uses explicit Euler integration for proceeding to the next v-slice, which has a global error of order $\mathcal{O}(v_{n+1} - v_n)$. It is however easy to replace this method with fourth-order Runge–Kutta integration since the equation is already in the correct form. The global error is then of order $\mathcal{O}(v_{n+1} - v_n)^4$. We thus use the Runge–Kutta method for greater running speed and result accuracy.

There are a number of problems with this naive approach, and they are all related to boundary conditions at $z = 0$. First, looking at the boundary expansion (7.35) of ϕ, it is clear that $\partial_z\phi$ is divergent at the boundary. This means that it is not possible to assign a numerical value to $\partial_z\phi$ at $z = 0$. To solve this we decrease the domain of ϕ from $0 \le z \le 1$ to $\varepsilon \le z \le 1 - \varepsilon$, where ε is a small numerical quantity that we can choose. In this domain all the fields and their derivatives are finite, and boundary conditions are imposed at $z = \varepsilon$ by using analytic boundary expansions of the fields. This solution is still not perfect,

however, because even though $\partial_z\phi|_{z=\varepsilon}$ is not singular, it still diverges and thus causes numerical error.

The second problem with the approach above is that it is not clear how to impose $\alpha(v)$. We solve this by defining a new field,

$$\tilde{\phi}(v,z) = \phi(v,z) - \alpha(v)\sqrt{z}\ln z - \beta(v)\sqrt{z}. \tag{7.57}$$

With this new field definition, equation (7.44) for ϕ becomes

$$\begin{aligned} 0 = {} & (z+1)\left(z^2-1\right)\partial_z^2\tilde{\phi} + 2z(z+1)\partial_z\tilde{\phi} + 2(z+1)\partial_z\partial_v\tilde{\phi} + \frac{(z-1)\tilde{\phi}}{4z^2} \\ & + \frac{\left(3z^2+3z+2\right)\beta + 8(z+1)\alpha' + 8z(z+1)\alpha + 4(z+1)\beta'}{4\sqrt{z}} \\ & + \frac{\ln z\left(\left(3z^2+3z+2\right)\alpha + 4(z+1)\alpha'\right)}{4\sqrt{z}}. \end{aligned} \tag{7.58}$$

and equation (7.54) becomes

$$\begin{aligned} \partial_v\partial_z\tilde{\phi} = {} & \frac{1}{2}\left(1-z^2\right)\partial_z^2\tilde{\phi} - z\partial_z\tilde{\phi} - \frac{(1-z)^2\tilde{\phi}}{8z^2\left(z^2-1\right)} \\ & + \frac{\beta\left(2-3z^3+z\right) - 4\left(z^2-1\right)\left(\partial_v\beta + (\ln z+2)\alpha'\right)}{8\sqrt{z}\left(z^2-1\right)} \\ & + \frac{\alpha\left(\left(2-3z^3-z+2z\right)\ln z - 8z\left(z^2-1\right)\right)}{8\sqrt{z}\left(z^2-1\right)} \\ \equiv {} & \tilde{F}(\tilde{\phi}, \partial_z\tilde{\phi}, \partial_z^2\tilde{\phi}, z, \alpha, \beta, \partial_v\beta). \end{aligned} \tag{7.59}$$

Now α and β appear explicitly. We set α directly by performing the quench, but we need to solve for β. A differential equation that is first order in v results from the boundary condition on $\tilde{\phi}$. This allows us to integrate β (in v) while simultaneously integrating $\tilde{\phi}$. We are effectively treating β as a separate field that needs to be solved for. Also notice from the expansion (7.35) that $\partial_z\tilde{\phi}$ is not divergent at the boundary. This should result in increased numerical accuracy at the boundary.

Given the field definition $\tilde{\phi}$ and the cutoff at $z=\varepsilon$, the modified procedure for solving for ϕ on each v-slice works as follows. We start on the first v-slice with $\tilde{\phi}$, α and β all taking their initial, static values. Then for each consecutive v-slice $n+1$, we use

$$\partial_z\tilde{\phi}\Big|_{v_{n+1}} = \partial_z\tilde{\phi}\Big|_{v_n} + (v_{n+1}-v_n)\ \tilde{F}(\tilde{\phi}, \partial_z\tilde{\phi}, \partial_z^2\tilde{\phi}, z, \alpha, \beta, \partial_v\beta)\Big|_{v_n}. \tag{7.60}$$

At v-slice n we know the value of all the fields except for $\partial_v\beta$. To determine $\partial_v\beta$, we use the boundary condition on $\tilde{\phi}$ at the horizon, $z=1$. The horizon expansion for the equation for of motion for $\tilde{\phi}$ is

$$\frac{\partial_z\tilde{\phi}(z=1) + \partial_z\partial_v\tilde{\phi}(z=1) + \partial_v\alpha + \alpha + \frac{\partial_v\beta}{2} + \frac{\beta}{2}}{z-1} + \mathcal{O}(z^0) = 0, \tag{7.61}$$

which implies the constraint

$$\tilde{F}(\tilde{\phi}, \partial_z\tilde{\phi}, \partial_z^2\tilde{\phi}, z, \alpha, \beta, \partial_v\beta) + \partial_z\tilde{\phi} + \partial_v\alpha + \alpha + \frac{\partial_v\beta}{2} + \frac{\beta}{2}\ \Big|_{z=1} = 0. \tag{7.62}$$

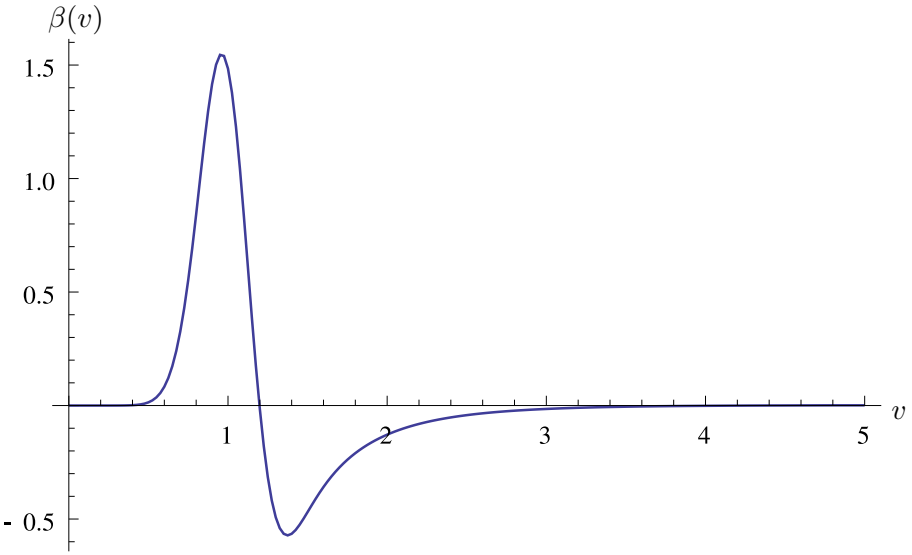

Figure 7.7: β as a function of v, which corresponds to AdS–Schwarzschild time t at the boundary. The quench profile for α is $\alpha(v) = 0.3e^{-\frac{(v-1)^2}{0.05}}$. This solution agrees with that found in figure 7.6, up to an overall scale that is due to a slight dependence of the numerics on the size of the cutoff ε.

In this constraint equation, we know the value of all the fields except for $\partial_v\beta$ at v-slice n, so we can use it to solve for $\partial_v\beta$.

We then use that value of $\partial_v\beta$ to both solve for $\partial_z\tilde{\phi}$ and β at v-slice $n+1$, again using the Runge–Kutta method. At the end of the computation we will have directly solved for both ϕ and β. For a Gaussian quench as described in the previous section, we get the profile for β depicted in figure 7.7. Gratifyingly, this plot is qualitatively similar to the results from the separation of variables approach in figure 7.6. There are two main differences. Firstly, there is a slight difference in the overall scale of the two figures. This can be traced back to the effect of varying the size of the cutoff ε. Some more work is required to make the results stable against changes in ε. Secondly, in figure 7.7, β vanishes at early and late times. It vanishes at early times by the initial conditions. In figure 7.6, β does not vanish at early times because there are no initial conditions set. We leave it for future work to investigate these initial conditions further.

7.5 The time-dependent Kondo model with gauge field backreaction

Now we turn to the question of solving the full set of coupled equations (7.42)–(7.44). So far we have not solved the technical challenges of getting the numerics under control, so in this section we outline the approaches and the difficulties.

The main challenge comes from the boundary expansion of the fields. The expansion is asymptotic, not a Taylor series expansion. The logarithmic terms mean that the singularity at $z = 0$ is essential and so a series expansion about $z = 0$ is impossible. An algorithm for calculating the boundary expansion is

presented in appendix C. The first few terms are

$$\begin{aligned}\phi_1 \asymp\ & \alpha_1(v)\sqrt{z}\log(z) + \sqrt{z}\beta_1(v) \\ & - z^{3/2}\log^4(z)\left(\frac{1}{3}\alpha_1(v)\alpha_2(v)^2 + \frac{1}{3}\alpha_1(v)^3\right) + \mathcal{O}\left(z^{3/2}\log^3(z)\right), \qquad (7.63)\\ \phi_2 \asymp\ & \alpha_2(v)\sqrt{z}\log(z) + \sqrt{z}\frac{\alpha_2(v)\beta_1(v)}{\alpha_1(v)} \\ & - z^{3/2}\log^4(z)\left(\frac{1}{3}\alpha_1(v)^2\alpha_2(v) + \frac{1}{3}\alpha_2(v)^3\right) + \mathcal{O}\left(z^{3/2}\log^3(z)\right), \qquad (7.64)\\ a_v \asymp\ & -\frac{1}{2z} + \mu(v) \\ & - \log(z)\frac{\left(\alpha_1(v)^2+\alpha_2(v)^2\right)\left(-2\alpha_1(v)\beta_1(v)+2\alpha_1(v)^2+\beta_1(v)^2\right)}{\alpha_1(v)^2} \\ & + \log^2(z)\left(-\frac{\alpha_2(v)^2\beta_1(v)}{\alpha_1(v)} - \alpha_1(v)\beta_1(v) + \alpha_1(v)^2 + \alpha_2(v)^2\right) \\ & + \log^3(z)\left(-\frac{1}{3}\alpha_1(v)^2 - \frac{\alpha_2(v)^2}{3}\right) + \mathcal{O}\left(z\log^4 z\right), \qquad (7.65)\end{aligned}$$

where we defined $\Phi = \phi_1 + i\phi_2$. The constraint equation imposes a restriction on the coefficient β_2, which is why β_2 does not appear in the expansion. We can use the residual gauge freedom to set $\alpha_2 = \beta_2 = 0$, and then the first terms in ϕ_2's expansion would appear at $\mathcal{O}\left(z^{3/2}\log z\right)$.

This boundary expansion presents several challenges. Because of the logarithms, the consecutive terms get smaller very slowly. This means that we either need to take many terms in the expansion, or start the numerical integration very close to the boundary. Both approaches have drawbacks. Figure 7.8 shows a typical numerical solution for ϕ_1 in the static case, which was found using the shooting method. We see that the solution is very steep near the boundary, which means that a lot of grid points need to be used, raising the computational cost. Finally, imposing boundary conditions is a challenge. The standard numerical techniques impose Neumann or Dirichlet boundary conditions. In our case this is impossible because of the singularity at $z = 0$. We cannot, for example, impose α_1 as a Dirichlet boundary condition and read off β_1 from the derivative of the solution. Instead we need to use the boundary expansion and work at small ϵ, bringing in an expansion truncation error.

Given the challenges, there are several broad classes of approaches we can take to solve the equations.

Time-marching scheme

We could generalise the time-marching scheme discussed in section 7.4.3. This seems to be the most promising approach. The main difficulty is that the equations can no longer be written in the form $\partial_v\pi = F(\phi_i, a_v, z)$, where $\pi = \phi_i$ or a_v. In other words, we can no longer use an explicit numerical method but have to resort to an implicit method. In an implicit method we have to impose a discretisation

$$\partial_v\pi = \frac{\pi(v_{n+1}) - \pi(v_n)}{v_{n+1} - v_n} \qquad (7.66)$$

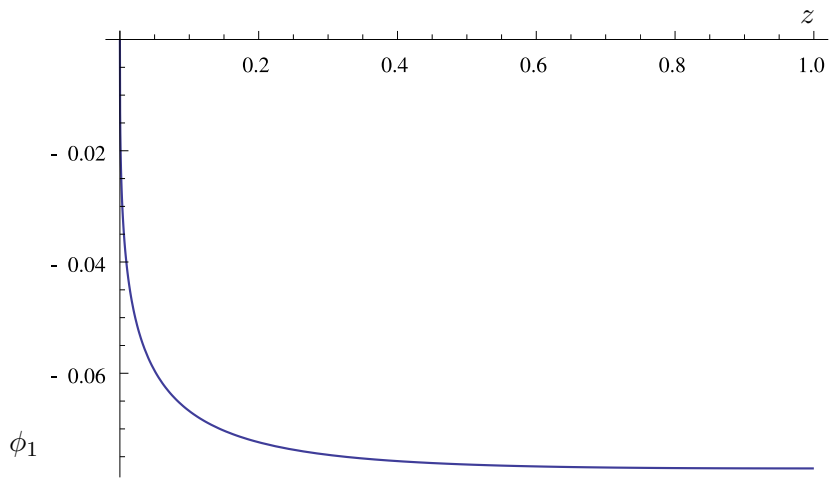

Figure 7.8: ϕ_1 as a function for z for the values $\alpha_1 = 0.10$, $\beta_1 = 0.65$ and $\mu = 0.55$.

to turn the equations of motion into an algebraic equation in v. We then solve the algebraic equations numerically for $\pi(v_{n+1})$. Due to non-linear terms in the equations such a method still introduces both numerical error and the chance that it would find the wrong algebraic solution, but it should work in principle. An example of an implicit method worth trying is the Crank–Nicolson method.

Relaxation method

It is quick and easy to find an initial guess for the field solutions. We could take the quasi-static solution, which is where we use for example the shooting method to solve for a static solution at each time slice n, given the value of $\alpha(v_n)$ at that time slice. Figure 7.9 shows the quasi-static solution for ϕ_1 for a given quench over $\alpha_1(v)$. We could also take the probe limit solution from section 7.4.3.

A *relaxation method* takes this initial guess and uses the equations of motion to refine it. One way of doing this is to choose a grid point, discretise the equations and solve for the value of the grid point given the values of the neighbouring grid points. This is repeated for all grid points and iterated until the desired accuracy is achieved.

Iterative approach

In what we term an *iterative approach*, we solve for each of the fields assuming that the others are fixed. It is similar to a relaxation method. For example, we start with $\Phi = 0$ then solve for a_v. Then we take that solution for a_v, substitute it back into the equations for Φ and solve for Φ. Taking that solution for Φ we can again solve for a_v, getting a more accurate solution this time. We keep iterating this procedure, solving for one field then the other, until we have reached a desired accuracy.

Note that we did not specify how to solve for the fields at each step. We could use one of the other approaches for this, combining the iterative approach with another.

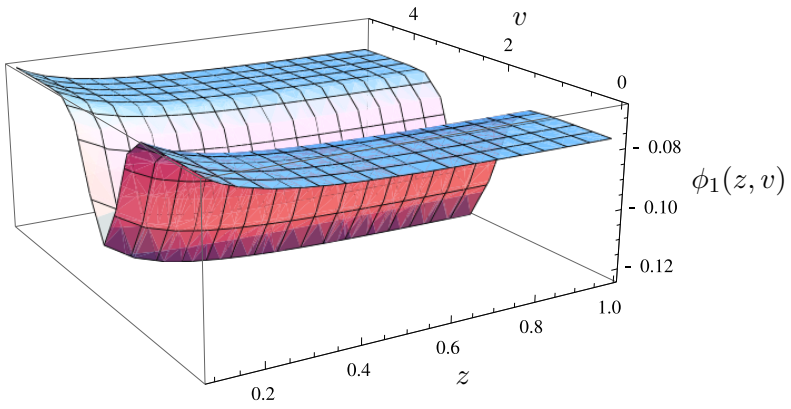

Figure 7.9: The quasi-static solution for ϕ_1 as a function of z and v. The quench is $\alpha_1(v) = 0.1 + 0.1 \exp\left(-\frac{(v-2.5)^2}{0.5^2}\right)$.

Perturbative technique

If all else fails, we could fall back on perturbation theory. The idea is to start with some initial solution, such as the quasi-static solution of figure 7.9, and expand about it in a small corrections parameter. We then solve the equations numerically order by order. The advantage is that the equations at each order are linear, with a source known numerically. With no non-linear terms in the equations, they could be discretised into matrix equations, which are easily inverted.

7.6 Concluding remarks

The Kondo model has been studied ever since Jun Kondo's seminal work in 1964. Even though much is known about it, it still serves as fertile ground for study. It was the first major success of Wilson's numerical renormalisation group method, and it has been fruitfully investigated in the conformal and the large N limits. Recently with the work of [63] it also became a playground for holographic techniques.

In this chapter we investigated the bottom-up holographic model proposed in [63] and made it time-dependent. The goal is to study relaxation times: if we quench the Kondo coupling with a certain profile, how long does it take the system to relax, and does it relax to the same ground state? We addressed this question in a particular probe limit and outlined numerical methods for solving it generally.

There are however other interesting questions to ask about the holographic Kondo model. For example, can we calculate the entanglement entropy of the model, and find quantitatively how the impurity gets bound to the rest of the system as the temperature is lowered? In gauge/gravity duality, the entanglement entropy between two regions in the boundary theory is found using the Ryu–Takayanagi prescription [153]. According to the prescription, the entanglement entropy is equal to the (properly regularised) area of the minimal surface in the bulk AdS spacetime that has its boundary on the border on the AdS boundary between the two regions of interest.

Without taking metric backreaction into account, however, any minimal surface calculation will give the same results as it would if the brane were absent. So we can only find nontrivial entanglement entropy results if we find precisely how the brane at $x = 0$, as well as the matter fields living on it, deform the background. Fortunately gravity in $(2+1)$-dimensions is "trivial", simplifying the problem. What this means is that there are no propagating degrees of freedom in the spacetime curvature tensors. Every small patch with vanishing energy-momentum tensor in the space is locally isometric to AdS_3. And since the Chern–Simons field does not contribute to the energy-momentum tensor, the only source of energy density is the brane.

The visualisation of the model with metric backreaction is depicted in figure 7.10. The brane divides the space in half, with the halves labelled by $\mathcal{M}_\pm$. Each half must be locally AdS_3 (or BTZ if we include a black hole), and they must be glued together at the brane. The brane is described by the embedding functions $x_\pm(z)$ in each half. The goal is then simply to find the embedding functions and identify the points in the separate halves specified by coordinates $x_\pm(z)$ for all z. The embedding functions can be found using the *Israel junction conditions* developed in [154],

$$\left\{K^{ij}\right\} T_{ij} = 0, \tag{7.67}$$

$$[K_{ij} - \gamma_{ij}\ \mathrm{tr}K] = -\kappa T_{ij}, \tag{7.68}$$

where

$$\{A\} \equiv \frac{1}{2}(A_+ + A_-), \tag{7.69}$$

$$[A] \equiv A_+ - A_-, \tag{7.70}$$

for a tensor A defined on both halves, $K_\pm$ are the exterior curvatures of the respective embeddings and T is the energy-momentum tensor on the brane. These junction conditions simply say that the metric is continuous across the brane, that is, $g_+ = g_-$ on the brane, and that $K_\pm$ have well-defined limits from both halves to the brane. They are derived from Einstein's equations and the conservation of the energy-momentum tensor.

Once the embedding functions are found via the Israel junction conditions, which requires knowing the energy-momentum tensor on the brane and therefore having a full numerical solution for the fields Φ and a, the geometry is specified completely. The entanglement entropy can then be calculated. We leave the details for future work, but we can speculate as to what will happen. For $T > T_c$, the scalar condensate vanishes and we should see minimal entanglement entropy between a region including the impurity and the rest of the field theory. When the temperature drops below T_c, the scalar condenses and contributes to the energy-momentum on the brane. This changes the embedding in such a way that the minimal surface changes and the entanglement entropy grows larger. If this is true, it will be a nontrivial test of the validity of the bottom-up holographic Kondo model.

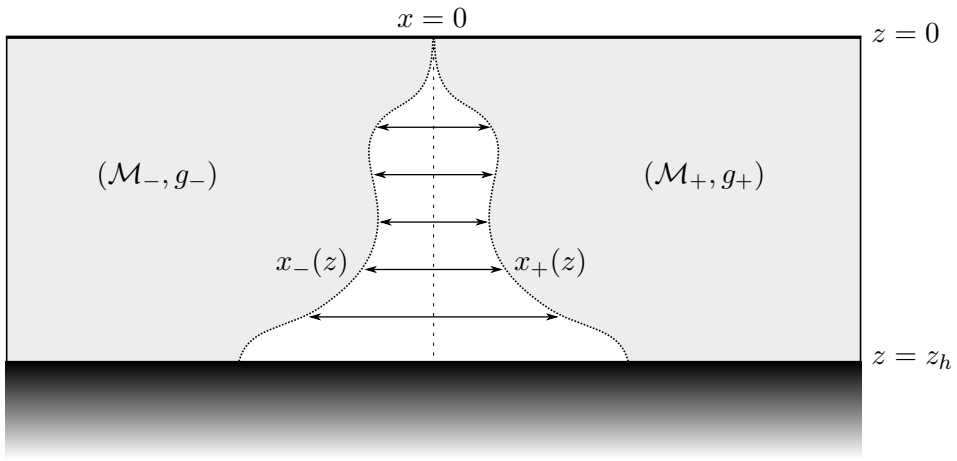

Figure 7.10: The model with metric backreaction. On either side of the brane, the spacetime has to be AdS_3 (or BTZ because if it has a black hole). The spacetime on either side of the brane, $\mathcal{M}_+$ and $\mathcal{M}_-$, need to be "glued" together in some way. This gluing is done using the Israel junction conditions. These provide equations of motion for the embedding functions $x_\pm(z)$ of the brane. This figure was taken from [149] with permission.

Chapter 8

Conclusion

Gauge/gravity duality has its origins in the black hole information paradox, but in spite of this abstract beginning it has turned into a powerful tool with many applications. In this thesis we have used this tool to uncover some of the startling behaviours a strongly coupled system can display.

But a second theme intertwined with our exploration is that of symmetry breaking. Our model of chapter 5 starts with an $SU(2)$ gauge field and then we turn on a magnetic component explicitly. The remaining solution has a $U(1)$ gauge symmetry. Increasing the magnetic field beyond a critical value causes that remaining $U(1)$ symmetry to be broken spontaneously.

A spontaneously broken $U(1)$ symmetry is the defining characteristic of a superconductor. We saw in chapter 3 how the successful Ginzburg–Landau model, an effective description of BCS theory, obtains its essential phenomenology from the Higgs mechanism, which is nothing but $U(1)$ gauge symmetry breaking. In chapter 4 we showed how this simple mechanism can be applied to gauge/gravity duality to construct holographic superconductors. These are holographic models where the focus is on constructing a gravitational background that exhibits symmetry breaking, typically through the condensation of a field. Here the symmetry breaking is typically the result of an interplay between gravity and the charge of the field, where the two forces balance in a certain regime so that stable field modes can form. This is exactly the case for our model from chapter 5 as well: when the magnetic field becomes strong enough compared to the gravitational pull from the black hole, it teases out the other gauge field components through the non-abelian dynamics, causing them to assume a triangular lattice form.

On the field theory side, we learn that the symmetry breaking effects we understand from weak coupling also hold at strong coupling. For example, as we saw in chapter 4 for the holographic s-wave superconductor, a $U(1)$ symmetry is broken by a condensing scalar operator. In this new phase the DC conductivity is infinite, as with superconductors at weak coupling. The difference in strongly coupled models is that there is no quasiparticle description. Whereas BCS theory describes electrons coming together in Cooper pairs triggering the symmetry breaking, in the field theories in holographic models it only makes sense to talk of condensates of operators. This is not because holographic models are in some sense effective in that they hide the microscopic degrees of freedom. On the contrary, gauge/gravity duality tells us that the gravity model is dual to an exact microscopic description of a field theory. The fact that we see only a condensing operator is due to the strong coupling and the large N limit.

But as we discussed in section 4.3, sometimes breaking a $U(1)$ symmetry is not enough. There is a diverse landscape of novel black hole backgrounds that emerge from a phase transition that breaks both the $U(1)$ gauge symmetry and translation symmetry. Our model from chapter 5 shows a small glimpse of this landscape, with the vista slightly extended in chapter 6 by the addition of a chemical potential. But the view is intriguing: a phase diagram depending on chemical potential μ and magnetic field B. The magnetic field enhances superconductivity and induces a triangular vortex lattice ground state. The lattice spacing is adjusted by varying B and, indirectly, μ. On the gravity side, this is a novel black hole solution. In the field theory, this is evidence that the superconducting phase in a strongly coupled system can be triggered by a magnetic field, rather than being inhibited by it, with a ground state similar to an Abrikosov lattice. And these solutions may be novel and interesting, but they are also important for applications. To build a better toy condensed matter model, it is essential to include a lattice.

Even though the Kondo model of chapter 7 is not intended to be a model of superconductivity, it still exhibits spontaneous $U(1)$ symmetry breaking. The Kondo model represents a magnetic impurity in a sea of electrons. In the holographic model, the condensing of a scalar operator below a critical temperature signals the formation of a bound state between the impurity and the electrons. This phase transition is an unintentional artefact of the large N limit because the original Kondo model only has a crossover, but it underscores the ubiquity of spontaneously broken symmetries and the diversity in phenomenology they can lead to.

Vistas

The formation of a triangular vortex lattice in a simple gravity background due to an $SU(2)$ magnetic field is an interesting discovery, but we have not answered any questions about its universality. We saw in chapter 3 that vortex lattices appear in many different contexts. Is it possible to identify a minimal set of ingredients they require? Is it always the triangular lattice that has the minimum energy, or are there circumstances in which it becomes distorted? Investigating these vortex lattices in other gravitational contexts could help answer these questions.

Moreover, we can ask how other matter interacts with the vortex lattice. In section 6.2 we showed how it could be possible to add fermions. It would be interesting to see whether the vortex lines maintain their superconducting properties in a nontrivial gravity background, as well as investigating the effect the vortex line topology has on the fermions' behaviour. We can then ask whether the lattice produces fermion spectral functions in the field theory similar to those observed in analogous condensed matter systems.

Investigations in the holographic Kondo model are just beginning. The results in chapter 7 are obtained in a probe approximation. The obvious next step is to extend the numerical algorithms to deal with backreaction onto both the gauge field and the geometry. This would allow us to answer questions about the entanglement entropy of the system as the temperature is decreased and the Kondo singlet is formed.

The easy holographic condensed matter models have been constructed, so the next question is how realistic they can be made. A lattice is an obvious requirement, so the spontaneously generated lattice presented in this thesis is welcome, as

evidenced by the many researchers investigating spontaneously generated ground states in holography today. But there is more to be done. One notoriously difficult generalisation to be made in holographic models is to go away from the large N limit. This would not only allow us to see a crossover rather than a phase transition in the holographic Kondo model, but would allow for more realistic models of QCD as well.

More broadly, where will the holographic principle lead us next? Is the whole universe a hologram, as Leonard Susskind asks? The question of quantum gravity is certainly not yet settled, but just in asking it we come to touch many different areas of physics. If this is any guide, the one thing we can say for sure is that there is more to be found in the hidden degrees of freedom on a black hole's edge.

Acknowledgements

Producing this thesis was hard. It took three years of my life. But it would have been so much harder without helpful colleagues, supportive friends and a loving family. In particular I would like to thank the following people:

Johanna, thank you for giving me the opportunity to be a part of this excellent group. You were always both approachable and reachable when I ran into trouble. Your support and encouragement helped me come this far.

I'd like to thank Dieter Lüst for the stimulating and productive environment at the Max Planck Institute for Physics, for reading through this thesis as second referee, and for always showing interest when I present at a lunch seminar.

I have also gained much from the IMPRS program, through the workshops they organise and the other PhD students I get to meet. I also appreciate being able to present my work to the other PhD students in the program. For that I thank Frank Steffen and Monika Goldammer.

A number of people helped with proofreading, helpful discussions, explanations of abstruse concepts, working on the papers and the notoriously difficult task of translating the abstract into German. For this and more I thank Ann-Kathrin for being friendly; Charlotte for being dependable; Daniel, for epic and glory! Da-Wei, for the surprises; Hansjörg, for fruitful discussions; Jon, for inspiring me; Mario A. for being reliable; Mario F. for Kafkaesque advice; Max for playfulness; Patrick for showing me how it's done; Steffen for a unique perspective; Stephan for being everything a true officemate should; and Yan-Yan, for meticulous checking. And furthermore, groupmates, you helped make this group awesome!

Ouers, broer en suster, baie dankie vir julle ondersteuning en dat ek weet julle is altyd daar vir my.

Finally, Tamara, I'm sorry I had to go so far away to write a PhD thesis. I hope to come back now.

Thanks guys!

This research was supported by the DFG cluster of excellence 'Origin and Structure of the Universe' (www.universe-cluster.de).

Appendix A

Large N expansion in gauge theories

In all the gauge/gravity models discussed in this thesis, the gauge theory is considered in a particular limit — the *large* N limit. In this section we explain what that means. A pedagogical introduction to this topic can be found in [155].

Consider the toy model discussed in [26], with a scalar transforming in the adjoint of an $SU(N)$ gauge group. The Lagrangian is given by

$$\mathcal{L} \sim \mathrm{tr}\left\{\partial_\mu\phi\partial^\mu\phi\right\} + g\mathrm{tr}\left\{\phi^3\right\} + g^2\mathrm{tr}\left\{\phi^4\right\}, \tag{A.1}$$

where the trace is over the gauge indices and ϕ is written with gauge group generators T^a as $\phi = \phi^a T^a$. With a rescaling $\phi \to g\phi$ this becomes

$$\mathcal{L} \sim \frac{1}{g^2}\left(\mathrm{tr}\left\{\partial_\mu\phi\partial^\mu\phi\right\} + \mathrm{tr}\left\{\phi^3\right\} + \mathrm{tr}\left\{\phi^4\right\}\right). \tag{A.2}$$

The propagator in this theory can be calculated using the $SU(N)$ completeness relation

$$\sum_{a=1}^{N^2-1} (T^a)_i{}^j (T^a)_k{}^l = \frac{1}{2}\left(\delta_i{}^l\delta_k{}^j - \frac{1}{N}\delta_i{}^j\delta_k{}^l\right). \tag{A.3}$$

This yields

$$\begin{aligned}\langle\phi_i{}^j(x)\phi_k{}^l(y)\rangle &= \langle\phi^a(x)\phi^b(y)\rangle (T^a)_i{}^j (T^b)_k{}^l \\ &= \left(\delta_i{}^l\delta_k{}^j - \frac{1}{N}\delta_i{}^j\delta_k{}^l\right)\frac{g^2}{4\pi^2(x-y)^2}.\end{aligned} \tag{A.4}$$

Since we are interested in the limit as $N \to \infty$, the second term above vanishes and we have that the propagator is proportional to g^2. The interaction vertices, as can be seen from A.2 are proportional to $1/g^2$, while loops are proportional to N due to the trace over the colour indices.

As it stands, the perturbative expansion of this theory is senseless; diagrams with higher loops have a higher power of N and thus the terms get larger and larger. To rectify this, Gerard 't Hooft in [69] introduced what is now known as the *'t Hooft coupling*:

$$\lambda = g^2 N. \tag{A.5}$$

The large N limit is then taken while keeping λ fixed. This means that a general diagram, containing propagators, vertices and loops, gives the contribution

$$\left(\frac{\lambda}{N}\right)^E \left(\frac{N}{\lambda}\right)^V N^F. \tag{A.6}$$

Here E is the number of propagators, V is the number of vertices and F is the number of loops. We can make use of Euler's formula for graphs to simplify this expression. The Euler characteristic $\chi = V - E + F$ is related to the genus g of the lowest-dimensional orientable surface on which the diagram can be drawn (with no crossings) as

$$\chi = V - E + F = 2 - 2g. \tag{A.7}$$

This means that a diagram in this theory contributes

$$\lambda^{E-V} N^{V-E+F} = \lambda^{E-V} N^{2-2g}. \tag{A.8}$$

Now we can see that, thanks to the 't Hooft limit, the more complicated non-planar diagrams can be neglected in the perturbative expansion.

Appendix B

Vortex lattice solution to higher orders

B.1 Deriving the equations for $a^3_{x,y}$

We substitute the ansatz (5.15) into the full equations of motion and neglect terms beyond quadratic order in ε. To get rid of all appearances of E_y, we use the relation that $E_y = -iE_x$ from (5.73). Then we find that there are only three equations in which the fluctuations $a^3_{x,y}$ appear. We focus on those three equations.

The simplest equation of the three is the constraint equation, which came from the equation of motion for A^3_u. To quadratic order, this equation is simply

$$\partial_u \partial_x a^3_x + \partial_u \partial_y a^3_y = 0. \tag{B.1}$$

The first thing to do is integrate with respect to u. This gives an integration constant, but by the fact that both a^3_x and a^3_y must vanish at $u = 0$, this integration constant vanishes. So the even simpler constraint is

$$\partial_x a^3_x + \partial_y a^3_y = 0. \tag{B.2}$$

This is all we need to decouple the other two equations in a^3_x and a^3_y. These equations now become

$$\begin{aligned} 0 =& \frac{3}{2} E_x \partial_y \bar{E}_x + \frac{3}{2} \bar{E}_x \partial_y E_x - \frac{1}{2} i E_x \partial_x \bar{E}_x + \frac{1}{2} i \bar{E}_x \partial_x E_x \\ &+ u \partial_u \left(\frac{f}{u} \partial_u a^3_x \right) + \partial_y^2 a^3_x + \partial_x^2 a^3_x, \end{aligned} \tag{B.3}$$

$$\begin{aligned} 0 =& - B_c x \bar{E}_x E_x - \frac{1}{2} i E_x \partial_y \bar{E}_x + \frac{1}{2} i \bar{E}_x \partial_y E_x \\ &- \frac{3}{2} E_x \partial_x \bar{E}_x - \frac{3}{2} \bar{E}_x \partial_x E_x + u \partial_u \left(\frac{f}{u} \partial_u a^3_y \right) + \partial_y^2 a^3_y + \partial_x^2 a^3_y, \end{aligned} \tag{B.4}$$

which are partial differential equations with sources that come from the linear order solutions. These two equations only differ by their source terms, so we will focus on a^3_x. a^3_y should be similar. Using the expression (5.74), we can see that the source term is periodic with $y \sim y + \frac{2\pi}{k}$. a^3_x must have the same periodicity, so we can write it as a Fourier series,

$$a^3_x(x, y, u) = \sum_{n=-\infty}^{\infty} e^{-inky} \tilde{a}^3_x(x, n, u). \tag{B.5}$$

The equation becomes

$$\sum_m -ie^{-\frac{1}{2}B_c\left(-\frac{km}{B_c}+x\right)^2-\frac{1}{2}B_c\left(-\frac{k(n+m)}{B_c}+x\right)^2} kn\bar{C}_m C_{n+m}\mathcal{U}^2$$
$$-k^2n^2\tilde{a}_x^3 + u\partial_u\left(\frac{f}{u}\partial_u\tilde{a}_x^3\right) + \partial_x^2\tilde{a}_x^3 = 0. \tag{B.6}$$

We notice that the source term in this equation is periodic in the x-direction; $x \sim x + \frac{Pk}{B_c}$. This lets us expand $\tilde{a}_x^3$ as a Fourier series in x as well:

$$\tilde{a}_x^3 = \sum_m e^{-i\frac{2\pi mB_c}{Pk}x}\hat{a}_x^3(m,n,u). \tag{B.7}$$

Writing the source term as a series lets us then obtain the equation (5.76) for the coefficients $\hat{a}_x^3(m,n,u)$.

Calling the source term $S(x)$, the naïve way of finding its Fourier coefficients is to use the formula

$$\tilde{S}_n = \frac{B_c}{Pk}\int_0^{\frac{Pk}{B_c}} e^{i\frac{2\pi nB_c}{Pk}x}S(x). \tag{B.8}$$

However, the source terms contains Gaussians, and those are much easier to integrate when the domain of integration is the entire real line. So we do the following trick. Doing a continuous Fourier transform on a periodic function gives a sum of δ-functions,

$$\begin{aligned}\int dx\ e^{ipx}S(x) &= \int dx\ e^{ipx}\sum_m e^{-i\frac{2\pi mB_c}{Pk}x}\tilde{S}_n \\ &= 2\pi\sum_m \tilde{S}_n\delta\left(p-\frac{2\pi mB_c}{Pk}\right).\end{aligned} \tag{B.9}$$

The coefficients in front of the δ-functions are what we are looking for. We get

$$\int dx\ e^{ipx}S(x) = -\sqrt{\frac{\pi}{B_c}}\sum_{m,n} ie^{-\frac{k^2n^2}{4B_c}+\frac{ikmp}{B_c}+\frac{iknp}{2B_c}-\frac{p^2}{4B_c}}kn\bar{C}_m C_{m+n}\mathcal{U}^2. \tag{B.10}$$

Using

$$\sum_{m=-\infty}^{\infty} f(m) = \sum_{m=-\infty}^{\infty}\sum_{l=0}^{P-1} f(Pm+l) \tag{B.11}$$

and then using the symmetry $C_{i+P} = C_i$, the only m-dependence remaining in the sum comes from $e^{\frac{ikPmp}{B_c}}$. Making use of the identity

$$\sum_{m=-\infty}^{\infty} e^{imq} = 2\pi\sum_{m=-\infty}^{\infty}\delta(q-2\pi m) \tag{B.12}$$

and $\delta(\alpha x) = \frac{\delta(x)}{|\alpha|}$ gives us the sum over δ-functions from (B.9). Then we can simply read off the coefficients $\tilde{S}_n$. This gives us the equation (5.76).

B.2 Deriving the equations for $c_{x,n}$, $c_{y,n}$

The third order equations of motion are

$$0 = ia_x^3\partial_u E_x + a_y^3\partial_u E_x - iE_x\partial_u a_x^3 - E_x\partial_u a_y^3 + iB_c x\partial_u e_y + \partial_y\partial_u e_y + \partial_x\partial_u e_x, \tag{B.13}$$

$$\begin{aligned}0 = &-iB_c x a_x^3 E_x - 2B_c x a_y^3 E_x - \bar{E}_x E_x^2 - a_x^3\partial_y E_x + 2ia_y^3\partial_y E_x - a_y^3\partial_x E_x \\ &- 2E_x\partial_y a_x^3 + iE_x\partial_y a_y^3 + E_x\partial_x a_y^3 + iB_c e_y - iB_c x\partial_x e_y - \partial_x\partial_y e_y \\ &- B_c^2 x^2 e_x + 2iB_c x\partial_y e_x + \partial_y^2 e_x + u\partial_u\left(\frac{f}{u}\partial_u e_x\right)\end{aligned} \tag{B.14}$$

$$\begin{aligned}0 = &B_c x a_x^3 E_x + i\bar{E}_x E_x^2 - ia_x^3\partial_y E_x + 2a_x^3\partial_x E_x - ia_y^3\partial_x E_x \\ &+ iE_x\partial_y a_x^3 + E_x\partial_x a_x^3 - 2iE_x\partial_x a_y^3 - iB_c\left(2e_x + x\partial_x e_x\right) \\ &- \partial_x\partial_y e_x + \partial_x^2 e_y + u\partial_u\left(\frac{f}{u}\partial_u e_y\right).\end{aligned} \tag{B.15}$$

The first of these is the constraint equation. We use it to relate e_x and e_y. In order to do this, we first simplify it by noticing that, since

$$e_y = \sum_{n=-\infty}^{\infty} c_{y,n}(u) e^{-inky - \frac{1}{2}B_c\left(x - \frac{nk}{B_c}\right)^2}, \tag{B.16}$$

we have that $iB_c x\partial_u e_y + \partial_y\partial_u e_y = -i\partial_x\partial_u e_y$. We can then integrate the entire equation with respect to u, imposing vanishing boundary conditions at the AdS boundary. The constraint equation then simplifies to

$$0 = -2i\frac{E_x}{\mathcal{U}}J_x - 2\frac{E_x}{\mathcal{U}}J_y + ia_x^3 E_x + a_y^3 E_x + \partial_x e_x - i\partial_x e_y, \tag{B.17}$$

where

$$J_{x,y}(x,y,u) = \int_0^u \mathcal{U}(\tilde{u})\partial_{\tilde{u}} a_{x,y}^3(x,y,\tilde{u})d\tilde{u}. \tag{B.18}$$

This allows us to eliminate e_x in equation (B.15) (after differentiating it by x). We write each function as a Fourier series in y and find an equation for the coefficients $c_{y,n}$. At this point the equation still has an x dependence, which can be eliminated by multiplying the equation by $(nk - B_c x)$ to make it an even function in x and then integrating $\int_{-\infty}^{\infty} dx$. In doing so we use the solution for E_x and the form for e_y given by (B.16), as well as the Fourier series representation of the other functions. Once this is done, we are left with an equation for e_y in the form (5.81).

The resulting equation for $c_{y,n}$ is

$$0 = \sum_{q,r=-\infty}^{\infty}\left\{e^{-\frac{2\pi q\left(ik^2P(n-r)+B_c\pi q\right)}{k^2P^2}}\left[\frac{C_{n-r}\left(-2\left(k^2Pr + 2iB_c\pi q\right)\hat{J}_{x,qr}\right)}{kP}\right.\right. \tag{B.19}$$

$$+\frac{C_{n-r}\left(\left(2ik^2Pr-4B_c\pi q\right)\hat{J}_{y,qr}+\left(2iB_c\pi q\hat{a}^3_x+\left(-ik^2Pr+4B_c\pi q\right)\hat{a}^3_y\right)\mathcal{U}\right)}{kP}\Bigg]$$

$$-\frac{ie^{-\frac{k^2\left(3r^2-3rq+q^2\right)}{3B_c}}\left(3B_c+2k^2q(-2r+q)\right)\bar{C}_{n+q}C_{n+r}C_{n-r+q}\mathcal{U}^3}{3\sqrt{3}B_c}\Bigg\}$$

$$-B_cc_{y,n}+u\partial_u\left(\frac{f}{u}\partial_uc_{y,n}\right), \tag{B.20}$$

where

$$\hat{J}_{i,qr}(u)=\int_0^u\mathcal{U}(\tilde{u})\partial_{\tilde{u}}\hat{a}^3_i(q,r,\tilde{u})d\tilde{u}, \tag{B.21}$$

for $i=x,y$.

A similar procedure gives the constraint equation in terms of the coefficients,

$$\begin{aligned}0=&\,c_{x,n}(u)-ic_{y,n}(u)\\&+\frac{1}{PkB_c}\sum_{q,r=-\infty}^{\infty}\Bigg\{e^{-\frac{2\pi q\left(ik^2P(n-r)+B_c\pi q\right)}{k^2P^2}}\left(-ik^2Pr+2B_c\pi q\right)C_{n-r}\\&\times\left(2\hat{J}_{x,qr}-2i\hat{J}_{y,qr}-(\hat{a}^3_{x,qr}-i\hat{a}^3_{y,qr})\mathcal{U}(u)\right)\Bigg\}.\end{aligned} \tag{B.22}$$

Once the coefficients $c_{y,n}$ are found, we use this to calculate $c_{x,n}$.

B.3 Calculating the energy

The difference between the energy of the superconducting phase and that of the normal phase is

$$\Delta\mathcal{F}=\frac{1}{4\hat{g}^2}\int d^5x\sqrt{-g}\left(F^a_{\mu\nu}F^{a\mu\nu}\big|_{superconducting}-F^a_{\mu\nu}F^{a\mu\nu}\big|_{normal}\right). \tag{B.23}$$

Note that for the AdS Schwarzschild model we implicitly divided by the temperature to make the energy dimensionless. We calculate the energy density by averaging over the domain $0\leq y<\frac{2\pi}{k}$, $0\leq x<\frac{Pk}{B_c}$, $0\leq u\leq 1$ and $t,z\in\mathbb{R}$. Since the integrand is independent of t and z, the averaging amounts to simply dropping the integration over those variables. In the following expression we use

$$\mathcal{E}_{x,y}=\mathcal{A}^1_{x,y}+i\mathcal{A}^2_{x,y}=\sum_n\mathcal{C}_{(x,y),n}(u)e^{-ikny-\frac{1}{2}B_c\left(x-\frac{nk}{B_c}\right)^2}, \tag{B.24}$$

we write $\mathcal{A}^3_x=a^3_x$ and $\mathcal{A}^3_y=xB+a^3_y$, and call the averaged energy $\Delta\Omega$. The result is

$$\begin{aligned}4\hat{g}^2\Delta\Omega=\int du\Bigg\{&\Omega_1(u)+\sum_{m,n=-\infty}^{\infty}\left[\Omega_2(m,n,u)+\Omega_3(m,n,u)+\Omega_4(m,n,u)\right]\\&\sum_{m,n,p,q=-\infty}^{\infty}\Omega_5(m,n,q,r,u)\Bigg\},\end{aligned} \tag{B.25}$$

where

$$\Omega_1 = \frac{\sqrt{\pi B}}{kPu}\sum_{l=0}^{P-1}\frac{B}{2}\left(\sum_{j=x,y}\left(f\partial_u\bar{\mathcal{C}}_{j,l}\partial_u\mathcal{C}_{j,l}+\bar{\mathcal{C}}_{j,l}\mathcal{C}_{j,l}\right)+3(i\bar{\mathcal{C}}_{y,l}\mathcal{C}_{x,l}-i\bar{\mathcal{C}}_{x,l}\mathcal{C}_{y,l})\right), \tag{B.26}$$

$$\Omega_2 = \frac{1}{u}\left\|kn\hat{a}_x^3(m,n,u)-\frac{2Bm\pi}{kP}\hat{a}_y^3(m,n,u)\right\|^2+\frac{f}{u}\sum_{j=x,y}\left\|\partial_u\hat{a}_j^3(m,n,u)\right\|^2, \tag{B.27}$$

$$\begin{aligned}\Omega_3 =& \frac{\sqrt{\pi B}}{2k^2P^2u}\sum_{l=0}^{P-1}e^{-\frac{k^2m^2}{4B}-\frac{i(2l+m)n\pi}{P}-\frac{Bn^2\pi^2}{k^2P^2}}\times\\ &\Big[\left(3k^2mP+2iBn\pi\right)\hat{a}_x^3(n,m,u)\bar{\mathcal{C}}_{x,l+m}\mathcal{C}_{y,l}\\ &+\hat{a}_x^3(n,-m,u)\bar{\mathcal{C}}_{y,l}\left(\left(3k^2mP+2iBn\pi\right)\mathcal{C}_{x,l+m}-2ik^2mP\mathcal{C}_{y,l+m}\right)\\ &+\hat{a}_y^3(n,-m,u)\mathcal{C}_{x,l+m}\left(-4iBn\pi\bar{\mathcal{C}}_{x,l}+\left(ik^2mP+6Bn\pi\right)\bar{\mathcal{C}}_{y,l}\right)\\ &+\hat{a}_y^3(n,m,u)\bar{\mathcal{C}}_{x,l+m}\mathcal{C}_{y,l}\left(-ik^2mP-6Bn\pi\right)\Big],\end{aligned} \tag{B.28}$$

$$\begin{aligned}\Omega_4 =& -\frac{1}{4kPu}\sqrt{\frac{\pi B}{2}}e^{-\frac{k^2\left(m^2+n^2\right)}{2B}}\times\\ &\sum_{l=0}^{P-1}\Big(\bar{\mathcal{C}}_{y,l+m}\bar{\mathcal{C}}_{y,l+n}\mathcal{C}_{x,l}\mathcal{C}_{x,l+m+n}-2\bar{\mathcal{C}}_{x,l+m}\bar{\mathcal{C}}_{y,l+n}\mathcal{C}_{x,l+m+n}\mathcal{C}_{y,l}\\ &+\bar{\mathcal{C}}_{x,l}\bar{\mathcal{C}}_{x,l+m+n}\mathcal{C}_{y,l+m}\mathcal{C}_{y,l+n}\Big),\end{aligned} \tag{B.29}$$

$$\begin{aligned}\Omega_5 =& \frac{\sqrt{\pi B}}{Pku}\sum_{l=0}^{P-1}e^{-\frac{k^2m^2}{4B}-\frac{i(2l+m)n\pi}{P}-\frac{Bn^2\pi^2}{k^2P^2}}\times\\ &\Big[\hat{a}_y^3(n-q,-(m+r),u)\hat{a}_y^3(q,r,u)\bar{\mathcal{C}}_{x,l}\mathcal{C}_{x,l+m}\\ &-\hat{a}_x^3(n-q,r,u)\hat{a}_y^3(q,m-r,u)\bar{\mathcal{C}}_{x,l+m}\mathcal{C}_{y,l}\\ &-\hat{a}_x^3(n-q,r,u)\hat{a}_y^3(q,-(m+r),u)\bar{\mathcal{C}}_{y,l}\mathcal{C}_{x,l+m}\\ &+\hat{a}_x^3(n-q,-(m+r),u)\hat{a}_x^3(q,r,u)\bar{\mathcal{C}}_{y,l}\mathcal{C}_{y,l+m}\Big].\end{aligned} \tag{B.30}$$

In these expressions, $\mathcal{C}_{x,n}$ and $\mathcal{C}_{y,n}$ are functions of u. Their complex conjugates are given by $\bar{\mathcal{C}}_{x,n}$ and $\bar{\mathcal{C}}_{y,n}$, respectively. All the infinite sums in the energy (B.25) can be terminated at a small finite value because of exponential suppression in the $\Omega_{1\ldots5}$ terms.

In deriving this, it helps to make use of the formulae

$$\int_0^L dx\sum_{m=-\infty}^{\infty}e^{-\frac{B_c}{2}(x-mL)^2}=\int_{-\infty}^{\infty}dxe^{-\frac{B_c}{2}x^2}, \tag{B.31}$$

$$\int_0^L dx\sum_{m,n=-\infty}^{\infty}e^{-\frac{B_c}{2}\left(x-\frac{mL}{P}\right)^2-\frac{B_c}{2}\left(x-\frac{nL}{P}\right)^2}h(x,m,n) \tag{B.32}$$

$$=\int_{-\infty}^{\infty}dx\sum_{l=0}^{P-1}\sum_{m=-\infty}^{\infty}e^{-\frac{B_c}{2}\left(x-\frac{mL}{P}\right)^2-\frac{B_c}{2}\left(x-\frac{lL}{P}\right)^2}h(x,m,l), \tag{B.33}$$

where the latter is valid whenever $h(x,m,n)=h(x+L,m+P,n+P)$.

Appendix C

Mathematica code: The holographic Kondo model

The following code was written in Mathematica 9.0. It calculates the boundary asymptotic expansions of the fields $\Phi = \phi_1 + i\phi_2$ and a_v as functions of z and v about $z = 0$. It takes equations (7.42)–(7.44) as input; to run the code, these equations need to have been stored in `eom[Phi1]`, `eom[av, 1]` and `eom[av, 2]`.

```
ExpandAllBnd[order_] := Module[{
          AssignReplacements, i, j, repExpansion, coeff, eqnList,
          equationSeries, solveForList, orderIdx, orderFinished,
          exitCalculation, timeDelta},

  (* Give this function the output of Solve. *)
  repSolutionFunction = {
    HoldPattern[A_[pa__]->B_] :> A -> Function[{pa},B]
  };

  (* Apply func to each term in expr. *)
  TermByTerm[expr_, func_] := (
    If[MatchQ[expr, a_+b_],
      Plus@@(func/@Level[expr,1]),
      func[expr]
    ]
  );

  (* Finds patt in expr and returns its precise form in expr.
     Returns a list of all occurrences. *)
  FindPattern[expr_, patt_] := Part[expr,##]& @@ #& /@ Position[expr, patt];

  AssignReplacements[reps_List]:=(
    Scan[(Evaluate[#[[1]]]=#[[2]])&, reps];
  );

  repExpansion[currentOrder_] := {
    Phi1 -> Function[{z,v},
      Alpha1 Sqrt[z]Log[z] + Beta1 Sqrt[z] +
      Sum[z^((2 ii+1)/2)
        Sum[coeff[Phi1, ii, jj][v]Log[z]^jj,
          {jj,0,4+ ii (ii-1)}
        ],
        {ii,1, currentOrder+1}
      ]
    ],

    Phi2 -> Function[{z,v}, 0],

    av->Function[{z,v}, 1/z (-1/2) + Mu +
      Sum[z^ ii
```

```
      Sum[coeff[av,ii+1,jj][v]Log[z]^jj,
        {jj,0,3+1/2 ii(3ii-1)}
      ],
      {ii,0,currentOrder+1}
    ]
  ]
};
coeff[av,1,0]=Function[{v}, 0];
eqnList={eom[Phi1], eom[av, 2], eom[av, 1]};

For[i=1,i<=Length[equationSeries],i++,
  equationSeries[[i]]=Select[equationSeries[[i]],(#=!=0)&];
];

exitCalculation=False;

For[orderIdx=1,orderIdx<=order,orderIdx++,
  Module[{orderEquations},

    orderEquations=Expand[#[[(orderIdx)]]]& /@ equationSeries;

    (* Split these up into equations for coefficients of Log terms. *)
    orderEquations=(CoefficientList[#, Log[z]])& /@ orderEquations;

    orderFinished=False;
    While[!orderFinished,
      Module[{coefficientEquations, shortestEquationIndex,
          shortestEquationLength, shortestEquation,equationLength},

        (* Get the largest coefficient equation for each eom. *)
        coefficientEquations = ConstantArray[0, Length[orderEquations]];
        For[i = 1,i <= Length[coefficientEquations], i++,
          j = Length[orderEquations[[i]]];
          While[(j>0) && (Expand[orderEquations[[i,j]]]===0),
            j--;
            orderEquations[[i]] = orderEquations[[i]][[1;;j]];
          ];
          If[j>0, coefficientEquations[[i]] = orderEquations[[i,j]]];
        ];
        coefficientEquations = Select[coefficientEquations,#=!=0&];

        shortestEquationLength = Infinity;
        For[j=1, j <= Length[coefficientEquations], j++,
          With[{coeffPattern =
                  FindPattern[coefficientEquations[[j]],coeff[__]]},
            If[FindPattern[coeffPattern, coeff[_,orderIdx+1,_]]=!={},
              Continue[];
            ];
            equationLength=Length[coeffPattern];
          ];
          If[equationLength < shortestEquationLength,
            shortestEquationLength = equationLength;
            shortestEquationIndex = j;
          ];
        ];

        If[shortestEquationLength == Infinity,
          Print["No equations left at this order."];
          orderFinished = True;
          Break[];
        ];

        (* Simplify shortestEquation so that the resulting
           coefficient has a smaller analytic expression. *)
        shortestEquation = TermByTerm[
          Expand[coefficientEquations[[shortestEquationIndex]]],
          Simplify
        ];

        With[{coeffSolution = Flatten[
```

```
                Solve[shortestEquation==0, FindPattern[
                    shortestEquation, coeff[__][v]
                  ]
                ]
              ]
            },
            AssignReplacements[
              Simplify[coeffSolution,TimeConstraint->1] /.
                repSolutionFunction
            ];
          ];
        ];

        Put[(#->Function[{z,v}, Evaluate[
              #[z,v] /. repExpansion[order]/.coeff[__][_]->0
            ]
          ])& /@ {Phi1,Phi2,av},
          FileNameJoin[{NotebookDirectory[],
              "data","BoundaryExpansionIntermediate.m"}]];
        If[exitCalculation,Break[]];
      ];
    ];
    (* Return expansion. *)
    (#->Function[{z,v},Evaluate[
        Collect[(#[z,v]/.repExpansion[order]/.coeff[__][_]->0),{z,Log[z]}]
    ]])& /@ {Phi1,Phi2,av}
];
```

Bibliography

[1] M. Ammon, J. Erdmenger, P. Kerner, and M. Strydom, "Black Hole Instability Induced by a Magnetic Field," *Phys.Lett.* **B706** (2011) 94–99, arXiv:1106.4551 [hep-th].

[2] Y.-Y. Bu, J. Erdmenger, J. P. Shock, and M. Strydom, "Magnetic field induced lattice ground states from holography," *JHEP* **1303** (2013) 165, arXiv:1210.6669 [hep-th].

[3] J. Erdmenger, P. Kerner, and M. Strydom, "Holographic superconductors at finite isospin density or in an external magnetic field," *PoS* **FACESQCD** (2010) 004.

[4] Y.-Y. Bu, J. Erdmenger, M. Strydom, and J. Shock, "Holographic Superfluidity from a Magnetic Field," *PoS* **ConfinementX** (2012) 268.

[5] J. D. Bekenstein, "Black holes and entropy," *Phys.Rev.* **D7** (1973) 2333–2346.

[6] S. Hawking, "Particle Creation by Black Holes," *Commun.Math.Phys.* **43** (1975) 199–220.

[7] G. 't Hooft, "Dimensional reduction in quantum gravity," arXiv:gr-qc/9310026 [gr-qc].

[8] L. Susskind, "The World as a hologram," *J.Math.Phys.* **36** (1995) 6377–6396, arXiv:hep-th/9409089 [hep-th].

[9] S. Weinberg, "The Quantum theory of fields. Vol. 1: Foundations,".

[10] **ATLAS** Collaboration, G. Aad *et al.*, "Observation of a new particle in the search for the Standard Model Higgs boson with the ATLAS detector at the LHC," *Phys.Lett.* **B716** (2012) 1–29, arXiv:1207.7214 [hep-ex].

[11] **CMS** Collaboration, S. Chatrchyan *et al.*, "Observation of a new boson at a mass of 125 GeV with the CMS experiment at the LHC," *Phys.Lett.* **B716** (2012) 30–61, arXiv:1207.7235 [hep-ex].

[12] P. W. Higgs, "Broken Symmetries and the Masses of Gauge Bosons," *Phys.Rev.Lett.* **13** (1964) 508–509.

[13] F. Englert and R. Brout, "Broken Symmetry and the Mass of Gauge Vector Mesons," *Phys.Rev.Lett.* **13** (1964) 321–323.

[14] G. Guralnik, C. Hagen, and T. Kibble, "Global Conservation Laws and Massless Particles," *Phys.Rev.Lett.* **13** (1964) 585–587.

[15] A. Einstein, "The Foundation of the General Theory of Relativity," *Annalen Phys.* **49** (1916) 769–822.

[16] **BICEP2** Collaboration, P. Ade *et al.*, "BICEP2 I: Detection Of B-mode Polarization at Degree Angular Scales," `arXiv:1403.3985 [astro-ph.CO]`.

[17] **BICEP2** Collaboration, P. A. R. Ade *et al.*, "BICEP2 II: Experiment and Three-Year Data Set," `arXiv:1403.4302 [astro-ph.CO]`.

[18] H. Georgi and S. Glashow, "Unity of All Elementary Particle Forces," *Phys.Rev.Lett.* **32** (1974) 438–441.

[19] R. Blumenhagen, D. Lüst, and S. Theisen, *Basic Concepts of String Theory*. Theoretical and Mathematical Physics. Springer, 2012. `http://books.google.de/books?id=-3PNFQn6AzcC`.

[20] J. Polchinski, *String Theory: Volume 1, An Introduction to the Bosonic String*. Cambridge Monographs on Mathematical Physics. Cambridge University Press, 1998. `http://books.google.de/books?id=jbM3t_usmX0C`.

[21] J. Polchinski, *String Theory: Volume 2, Superstring Theory and Beyond*. Cambridge Monographs on Mathematical Physics. Cambridge University Press, 2005. `http://books.google.de/books?id=tJtOMAEACAAJ`.

[22] J. Dai, R. Leigh, and J. Polchinski, "New Connections Between String Theories," *Mod.Phys.Lett.* **A4** (1989) 2073–2083.

[23] P. Horava, "Background Duality of Open String Models," *Phys.Lett.* **B231** (1989) 251.

[24] J. M. Maldacena, "The Large N limit of superconformal field theories and supergravity," *Adv.Theor.Math.Phys.* **2** (1998) 231–252, `arXiv:hep-th/9711200 [hep-th]`.

[25] E. Witten, "Anti-de Sitter space and holography," *Adv.Theor.Math.Phys.* **2** (1998) 253–291, `arXiv:hep-th/9802150 [hep-th]`.

[26] J. Erdmenger, "Introduction to gauge/gravity duality," *Lect.Notes Phys.* **851** (2012) 99–145.

[27] J. Erdmenger, N. Evans, I. Kirsch, and E. Threlfall, "Mesons in Gauge/Gravity Duals - A Review," *Eur.Phys.J.* **A35** (2008) 81–133, `arXiv:0711.4467 [hep-th]`.

[28] D. J. Gross and F. Wilczek, "Ultraviolet Behavior of Nonabelian Gauge Theories," *Phys.Rev.Lett.* **30** (1973) 1343–1346.

[29] H. D. Politzer, "Reliable Perturbative Results for Strong Interactions?," *Phys.Rev.Lett.* **30** (1973) 1346–1349.

[30] S. Durr, Z. Fodor, J. Frison, C. Hoelbling, R. Hoffmann, *et al.*, "Ab-Initio Determination of Light Hadron Masses," *Science* **322** (2008) 1224–1227, arXiv:0906.3599 [hep-lat].

[31] H. J. Schulz, "Fermi liquids and non–Fermi liquids," *eprint arXiv:cond-mat/9503150* (Mar., 1995) , cond-mat/9503150.

[32] J. Bednorz and K. Muller, "Possible high Tc superconductivity in the Ba-La-Cu-O system," *Z.Phys.* **B64** (1986) 189–193.

[33] P. Kovtun, D. T. Son, and A. O. Starinets, "Viscosity in strongly interacting quantum field theories from black hole physics," *Phys.Rev.Lett.* **94** (2005) 111601, arXiv:hep-th/0405231 [hep-th].

[34] U. Heinz, C. Shen, and H. Song, "The viscosity of quark-gluon plasma at RHIC and the LHC," *AIP Conf.Proc.* **1441** (2012) 766–770, arXiv:1108.5323 [nucl-th].

[35] M. Rangamani, "Gravity and Hydrodynamics: Lectures on the fluid-gravity correspondence," *Class.Quant.Grav.* **26** (2009) 224003, arXiv:0905.4352 [hep-th].

[36] S. S. Gubser, "Breaking an Abelian gauge symmetry near a black hole horizon," *Phys.Rev.* **D78** (2008) 065034, arXiv:0801.2977 [hep-th].

[37] S. A. Hartnoll, C. P. Herzog, and G. T. Horowitz, "Building a Holographic Superconductor," *Phys.Rev.Lett.* **101** (2008) 031601, arXiv:0803.3295 [hep-th].

[38] S. Weinberg, "Superconductivity for Particular Theorists," *Prog.Theor.Phys.Suppl.* **86** (1986) 43.

[39] W. Meissner and R. Ochsenfeld, "Ein neuer Effekt bei Eintritt der Supraleitfähigkeit," *Naturwissenschaften* **21** (Nov., 1933) 787–788.

[40] J. Erdmenger, M. Kaminski, P. Kerner, and F. Rust, "Finite baryon and isospin chemical potential in AdS/CFT with flavor," *JHEP* **0811** (2008) 031, arXiv:0807.2663 [hep-th].

[41] C.-N. Yang and R. L. Mills, "Conservation of Isotopic Spin and Isotopic Gauge Invariance," *Phys.Rev.* **96** (1954) 191–195.

[42] A. Abrikosov, "On the Magnetic properties of superconductors of the second group," *Sov.Phys.JETP* **5** (1957) 1174–1182.

[43] A. Abrikosov, *Fundamentals of the Theory of Metals*. North-Holland, Amsterdam, 1988.

[44] J. Bardeen, L. N. Cooper, and J. R. Schrieffer, "Microscopic Theory of Superconductivity," *Physical Review* **106** (Apr., 1957) 162–164.

[45] J. Bardeen, L. N. Cooper, and J. R. Schrieffer, "Theory of Superconductivity," *Physical Review* **108** (Dec., 1957) 1175–1204.

[46] V. L. Ginzburg and L. D. Landau, "On the Theory of superconductivity," *Zh.Eksp.Teor.Fiz.* **20** (1950) 1064–1082.

[47] N. Nielsen and P. Olesen, "An Unstable Yang-Mills Field Mode," *Nucl.Phys.* **B144** (1978) 376.

[48] N. Nielsen and P. Olesen, "Electric Vortex Lines From the Yang-Mills Theory," *Phys.Lett.* **B79** (1978) 304.

[49] H. B. Nielsen and P. Olesen, "A Quantum Liquid Model for the QCD Vacuum: Gauge and Rotational Invariance of Domained and Quantized Homogeneous Color Fields," *Nucl.Phys.* **B160** (1979) 380.

[50] J. Ambjørn and P. Olesen, "On the Formation of a Random Color Magnetic Quantum Liquid in QCD," *Nucl.Phys.* **B170** (1980) 60.

[51] J. Ambjørn and P. Olesen, "A Color Magnetic Vortex Condensate in QCD," *Nucl.Phys.* **B170** (1980) 265.

[52] M. Chernodub, "Superconductivity of QCD vacuum in strong magnetic field," *Phys.Rev.* **D82** (2010) 085011, `arXiv:1008.1055 [hep-ph]`.

[53] M. Chernodub, "Electromagnetically superconducting phase of QCD vacuum induced by strong magnetic field," *AIP Conf.Proc.* **1343** (2011) 149–151, `arXiv:1011.2658 [hep-ph]`.

[54] M. Chernodub, J. Van Doorsselaere, and H. Verschelde, "Electromagnetically superconducting phase of vacuum in strong magnetic field: structure of superconductor and superfluid vortex lattices in the ground state," `arXiv:1111.4401 [hep-ph]`.

[55] M. Chernodub, "Spontaneous electromagnetic superconductivity of vacuum in strong magnetic field: evidence from the Nambu–Jona-Lasinio model," *Phys.Rev.Lett.* **106** (2011) 142003, `arXiv:1101.0117 [hep-ph]`.

[56] V. Braguta, P. Buividovich, M. Chernodub, A. Y. Kotov, and M. Polikarpov, "Electromagnetic superconductivity of vacuum induced by strong magnetic field: numerical evidence in lattice gauge theory," *Phys.Lett.* **B718** (2012) 667–671, `arXiv:1104.3767 [hep-lat]`.

[57] M. Chernodub, J. Van Doorsselaere, and H. Verschelde, "Magnetic-field-induced superconductivity and superfluidity of W and Z bosons: in tandem transport and kaleidoscopic vortex states," *Phys.Rev.* **D88** (2013) 065006, `arXiv:1203.5963 [hep-ph]`.

[58] J. Ambjørn and P. Olesen, "On Electroweak Magnetism," *Nucl.Phys.* **B315** (1989) 606.

[59] J. Ambjørn and P. Olesen, "A Condensate Solution Of The Electroweak Theory Which Interpolates Between The Broken And The Symmetric Phase," *Nucl.Phys.* **B330** (1990) 193.

[60] J. Ambjørn and P. Olesen, "Electroweak Magnetism: Theory And Application," *Int.J.Mod.Phys.* **A5** (1990) 4525–4558.

[61] J. Ambjørn and P. Olesen, "Electroweak magnetism, W condensation and antiscreening," arXiv:hep-ph/9304220 [hep-ph].

[62] J. Kondo, "Resistance Minimum in Dilute Magnetic Alloys," *Progress of Theoretical Physics* **32** no. 1, (1964) 37–49, http://ptp.oxfordjournals.org/content/32/1/37.full.pdf+html. http://ptp.oxfordjournals.org/content/32/1/37.abstract.

[63] J. Erdmenger, C. Hoyos, A. O'Bannon, and J. Wu, "A Holographic Model of the Kondo Effect," *JHEP* **1312** (2013) 086, arXiv:1310.3271 [hep-th].

[64] K. G. Wilson, "The renormalization group: Critical phenomena and the Kondo problem," *Rev. Mod. Phys.* **47** (Oct, 1975) 773–840. http://link.aps.org/doi/10.1103/RevModPhys.47.773.

[65] J. Polchinski, "Introduction to Gauge/Gravity Duality," arXiv:1010.6134 [hep-th].

[66] S. Weinberg and E. Witten, "Limits on Massless Particles," *Phys.Lett.* **B96** (1980) 59.

[67] E. D'Hoker and D. Z. Freedman, "Supersymmetric gauge theories and the AdS / CFT correspondence," arXiv:hep-th/0201253 [hep-th].

[68] O. Aharony, S. S. Gubser, J. M. Maldacena, H. Ooguri, and Y. Oz, "Large N field theories, string theory and gravity," *Phys.Rept.* **323** (2000) 183–386, arXiv:hep-th/9905111 [hep-th].

[69] G. 't Hooft, "A planar diagram theory for strong interactions," *Nuclear Physics B* **72** (Apr., 1974) 461–473.

[70] J. D. Bekenstein, "Entropy bounds and black hole remnants," *Phys.Rev.* **D49** (1994) 1912–1921, arXiv:gr-qc/9307035 [gr-qc].

[71] K. Skenderis, "Lecture notes on holographic renormalization," *Class.Quant.Grav.* **19** (2002) 5849–5876, arXiv:hep-th/0209067 [hep-th].

[72] A. Karch and E. Katz, "Adding flavor to AdS / CFT," *JHEP* **0206** (2002) 043, arXiv:hep-th/0205236 [hep-th].

[73] T. Sakai and S. Sugimoto, "Low energy hadron physics in holographic QCD," *Prog.Theor.Phys.* **113** (2005) 843–882, arXiv:hep-th/0412141 [hep-th].

[74] T. Sakai and S. Sugimoto, "More on a holographic dual of QCD," *Prog.Theor.Phys.* **114** (2005) 1083–1118, arXiv:hep-th/0507073 [hep-th].

[75] N. Callebaut, D. Dudal, and H. Verschelde, "Holographic rho mesons in an external magnetic field," arXiv:1105.2217 [hep-th].

[76] O. Aharony, O. Bergman, D. L. Jafferis, and J. Maldacena, "N=6 superconformal Chern-Simons-matter theories, M2-branes and their gravity duals," *JHEP* **0810** (2008) 091, arXiv:0806.1218 [hep-th].

[77] A. Hamilton, J. Murugan, A. Prinsloo, and M. Strydom, "A Note on dual giant gravitons in AdS(4) x CP**3," *JHEP* **0904** (2009) 132, arXiv:0901.0009 [hep-th].

[78] J. Erdmenger, P. Kerner, and H. Zeller, "Non-universal shear viscosity from Einstein gravity," *Phys.Lett.* **B699** (2011) 301–304, arXiv:1011.5912 [hep-th].

[79] J. Erdmenger and S. Steinfurt, "A universal fermionic analogue of the shear viscosity," *JHEP* **1307** (2013) 018, arXiv:1302.1869 [hep-th].

[80] J. L. L. Susskind, *An Introduction to Black Holes, Information and the String Theory Revolution.* World Scientific Publishing Co. Pte. Ltd. Singapore, 2005.

[81] J. I. Kapusta and C. Gale, *Finite-temperature field theory. Principle and applications. 2nd ed.* Cambridge Monographs on Mathematical Physics. Cambridge: Cambridge University Press., 2006.

[82] J. W. York, "Role of Conformal Three-Geometry in the Dynamics of Gravitation," *Phys. Rev. Lett.* **28** (Apr, 1972) 1082–1085. http://link.aps.org/doi/10.1103/PhysRevLett.28.1082.

[83] G. W. Gibbons and S. W. Hawking, "Action integrals and partition functions in quantum gravity," *Phys. Rev. D* **15** (May, 1977) 2752–2756. http://link.aps.org/doi/10.1103/PhysRevD.15.2752.

[84] L. P. Gor'kov, "Microscopic derivation of the ginzburg-landau equations in the theory of superconductivity," *Sov. Phys. JETP* **9** (1959) 1364–1367.

[85] F. London and H. London, "The Electromagnetic Equations of the Supraconductor," *Proceedings of the Royal Society of London. Series A - Mathematical and Physical Sciences* **149** no. 866, (1935) 71–88. http://rspa.royalsocietypublishing.org/content/149/866/71.short.

[86] H. B. Nielsen and P. Olesen, "Vortex Line Models for Dual Strings," *Nucl.Phys.* **B61** (1973) 45–61.

[87] G. Veneziano, "Construction of a crossing - symmetric, Regge behaved amplitude for linearly rising trajectories," *Nuovo Cim.* **A57** (1968) 190–197.

[88] D. Djukanovic, M. R. Schindler, J. Gegelia, and S. Scherer, "Quantum electrodynamics for vector mesons," *Phys.Rev.Lett.* **95** (2005) 012001, arXiv:hep-ph/0505180 [hep-ph].

[89] M. Chernodub, "Can Nothing be A Superconductor and A Superfluid?," *PoS* **FACESQCD** (2010) 021, arXiv:1104.4404 [hep-ph].

[90] S. S. Gubser, "Colorful horizons with charge in anti-de Sitter space," *Phys.Rev.Lett.* **101** (2008) 191601, arXiv:0803.3483 [hep-th].

[91] S. S. Gubser and S. S. Pufu, "The Gravity dual of a p-wave superconductor," *JHEP* **0811** (2008) 033, arXiv:0805.2960 [hep-th].

[92] J.-W. Chen, Y.-J. Kao, D. Maity, W.-Y. Wen, and C.-P. Yeh, "Towards A Holographic Model of D-Wave Superconductors," *Phys.Rev.* **D81** (2010) 106008, arXiv:1003.2991 [hep-th].

[93] K.-Y. Kim and M. Taylor, "Holographic d-wave superconductors," *JHEP* **1308** (2013) 112, arXiv:1304.6729 [hep-th].

[94] S. A. Hartnoll, C. P. Herzog, and G. T. Horowitz, "Holographic Superconductors," *JHEP* **0812** (2008) 015, arXiv:0810.1563 [hep-th].

[95] G. T. Horowitz, "Introduction to Holographic Superconductors," *Lect.Notes Phys.* **828** (2011) 313–347, arXiv:1002.1722 [hep-th].

[96] P. Breitenlohner and D. Z. Freedman, "Stability in Gauged Extended Supergravity," *Annals Phys.* **144** (1982) 249.

[97] D. T. Son and A. O. Starinets, "Minkowski space correlators in AdS / CFT correspondence: Recipe and applications," *JHEP* **0209** (2002) 042, arXiv:hep-th/0205051 [hep-th].

[98] M. Tinkham, *Introduction to Superconductivity*. Robert E. Krieger Publishing Company, Malabar, Florida, 1980.

[99] J. S. Toll, "Causality and the Dispersion Relation: Logical Foundations," *Phys. Rev.* **104** (Dec, 1956) 1760–1770. http://link.aps.org/doi/10.1103/PhysRev.104.1760.

[100] M. Ammon, J. Erdmenger, M. Kaminski, and P. Kerner, "Flavor Superconductivity from Gauge/Gravity Duality," *JHEP* **0910** (2009) 067, arXiv:0903.1864 [hep-th].

[101] G. T. Horowitz, J. E. Santos, and D. Tong, "Optical Conductivity with Holographic Lattices," *JHEP* **1207** (2012) 168, arXiv:1204.0519 [hep-th].

[102] R. Flauger, E. Pajer, and S. Papanikolaou, "A Striped Holographic Superconductor," *Phys.Rev.* **D83** (2011) 064009, arXiv:1010.1775 [hep-th].

[103] K. Maeda, T. Okamura, and J.-i. Koga, "Inhomogeneous charged black hole solutions in asymptotically anti-de Sitter spacetime," *Phys.Rev.* **D85** (2012) 066003, arXiv:1107.3677 [gr-qc].

[104] D. v. d. Marel, H. J. A. Molegraaf, J. Zaanen, Z. Nussinov, F. Carbone, A. Damascelli, H. Eisaki, M. Greven, P. H. Kes, and M. Li, "Quantum critical behaviour in a high-T_c superconductor," *Nature* **425** (Sept., 2003) 271–274, cond-mat/0309172.

[105] G. T. Horowitz, J. E. Santos, and D. Tong, "Further Evidence for Lattice-Induced Scaling," *JHEP* **1211** (2012) 102, arXiv:1209.1098 [hep-th].

[106] G. T. Horowitz and J. E. Santos, "General Relativity and the Cuprates," arXiv:1302.6586 [hep-th].

[107] S. K. Domokos and J. A. Harvey, "Baryon number-induced Chern-Simons couplings of vector and axial-vector mesons in holographic QCD," *Phys.Rev.Lett.* **99** (2007) 141602, arXiv:0704.1604 [hep-ph].

[108] W.-y. Chuang, S.-H. Dai, S. Kawamoto, F.-L. Lin, and C.-P. Yeh, "Dynamical Instability of Holographic QCD at Finite Density," *Phys.Rev.* **D83** (2011) 106003, arXiv:1004.0162 [hep-th].

[109] O. Bergman, N. Jokela, G. Lifschytz, and M. Lippert, "Striped instability of a holographic Fermi-like liquid," *JHEP* **1110** (2011) 034, arXiv:1106.3883 [hep-th].

[110] C. B. Bayona, K. Peeters, and M. Zamaklar, "A Non-homogeneous ground state of the low-temperature Sakai-Sugimoto model," *JHEP* **1106** (2011) 092, arXiv:1104.2291 [hep-th].

[111] S. Takeuchi, "Modulated Instability in Five-Dimensional U(1) Charged AdS Black Hole with R**2-term," *JHEP* **1201** (2012) 160, arXiv:1108.2064 [hep-th].

[112] S. Nakamura, H. Ooguri, and C.-S. Park, "Gravity Dual of Spatially Modulated Phase," *Phys.Rev.* **D81** (2010) 044018, arXiv:0911.0679 [hep-th].

[113] H. Ooguri and C.-S. Park, "Holographic End-Point of Spatially Modulated Phase Transition," *Phys.Rev.* **D82** (2010) 126001, arXiv:1007.3737 [hep-th].

[114] A. Donos and J. P. Gauntlett, "Helical superconducting black holes," *Phys.Rev.Lett.* **108** (2012) 211601, arXiv:1203.0533 [hep-th].

[115] A. Donos and J. P. Gauntlett, "Black holes dual to helical current phases," *Phys.Rev.* **D86** (2012) 064010, arXiv:1204.1734 [hep-th].

[116] T. Albash and C. V. Johnson, "A Holographic Superconductor in an External Magnetic Field," *JHEP* **0809** (2008) 121, arXiv:0804.3466 [hep-th].

[117] E. Nakano and W.-Y. Wen, "Critical magnetic field in a holographic superconductor," *Phys.Rev.* **D78** (2008) 046004, arXiv:0804.3180 [hep-th].

[118] T. Albash and C. V. Johnson, "Phases of Holographic Superconductors in an External Magnetic Field," arXiv:0906.0519 [hep-th].

[119] T. Albash and C. V. Johnson, "Vortex and Droplet Engineering in Holographic Superconductors," *Phys.Rev.* **D80** (2009) 126009, arXiv:0906.1795 [hep-th].

[120] K. Maeda, M. Natsuume, and T. Okamura, "Vortex lattice for a holographic superconductor," *Phys.Rev.* **D81** (2010) 026002, arXiv:0910.4475 [hep-th].

[121] A. Donos, J. P. Gauntlett, and C. Pantelidou, "Spatially modulated instabilities of magnetic black branes," *JHEP* **1201** (2012) 061, arXiv:1109.0471 [hep-th].

[122] A. Donos and J. P. Gauntlett, "Holographic striped phases," *JHEP* **1108** (2011) 140, arXiv:1106.2004 [hep-th].

[123] S. Bolognesi and D. Tong, "Monopoles and Holography," *JHEP* **1101** (2011) 153, arXiv:1010.4178 [hep-th].

[124] P. Sutcliffe, "Monopoles in AdS," *JHEP* **1108** (2011) 032, arXiv:1104.1888 [hep-th].

[125] J. Erlich, E. Katz, D. T. Son, and M. A. Stephanov, "QCD and a holographic model of hadrons," *Phys.Rev.Lett.* **95** (2005) 261602, arXiv:hep-ph/0501128 [hep-ph].

[126] L. Da Rold and A. Pomarol, "Chiral symmetry breaking from five dimensional spaces," *Nucl.Phys.* **B721** (2005) 79–97, arXiv:hep-ph/0501218 [hep-ph].

[127] A. Nunez and A. O. Starinets, "AdS / CFT correspondence, quasinormal modes, and thermal correlators in N=4 SYM," *Phys.Rev.* **D67** (2003) 124013, arXiv:hep-th/0302026 [hep-th].

[128] M. Kaminski, K. Landsteiner, F. Pena-Benitez, J. Erdmenger, C. Greubel, *et al.*, "Quasinormal modes of massive charged flavor branes," *JHEP* **1003** (2010) 117, arXiv:0911.3544 [hep-th].

[129] B. Rosenstein and D. Li, "Ginzburg-Landau theory of type II superconductors in magnetic field," *Rev. Mod. Phys.* **82** (Jan, 2010) 109–168. http://link.aps.org/doi/10.1103/RevModPhys.82.109.

[130] W. H. Kleiner, L. M. Roth, and S. H. Autler, "Bulk Solution of Ginzburg-Landau Equations for Type II Superconductors: Upper Critical Field Region," *Phys. Rev.* **133** (Mar, 1964) A1226–A1227. http://link.aps.org/doi/10.1103/PhysRev.133.A1226.

[131] K. Wong, "A Non-Abelian Vortex Lattice in Strongly Coupled Systems," *JHEP* **1310** (2013) 148, arXiv:1307.7839 [hep-th].

[132] R. Jackiw and P. Rossi, "Zero Modes of the Vortex - Fermion System," *Nucl.Phys.* **B190** (1981) 681.

[133] E. Witten, "Superconducting Strings," *Nucl.Phys.* **B249** (1985) 557–592.

[134] B. Béri, D. Tong, and K. Wong, "Gauge Dynamics and Topological Insulators," *JHEP* **1309** (2013) 025, arXiv:1305.2414 [hep-th].

[135] M. Chernodub, T. Kalaydzhyan, J. Van Doorsselaere, and H. Verschelde, "Fermion zero modes in a chromomagnetic vortex lattice," *Phys.Rev.* **D89** (2014) 065021, arXiv:1401.5974 [hep-th].

[136] M. Henningson and K. Sfetsos, "Spinors and the AdS / CFT correspondence," *Phys.Lett.* **B431** (1998) 63–68, arXiv:hep-th/9803251 [hep-th].

[137] R. Contino and A. Pomarol, "Holography for fermions," *JHEP* **0411** (2004) 058, arXiv:hep-th/0406257 [hep-th].

[138] N. Iqbal and H. Liu, "Real-time response in AdS/CFT with application to spinors," *Fortsch.Phys.* **57** (2009) 367–384, arXiv:0903.2596 [hep-th].

[139] P. Basu, J. He, A. Mukherjee, and H.-H. Shieh, "Holographic Non-Fermi Liquid in a Background Magnetic Field," *Phys.Rev.* **D82** (2010) 044036, arXiv:0908.1436 [hep-th].

[140] W. de Haas, J. de Boer, and G. van dën Berg, "The electrical resistance of gold, copper and lead at low temperatures," *Physica* **1** no. 7–12, (1934) 1115 – 1124. http://www.sciencedirect.com/science/article/pii/S0031891434803102.

[141] I. Affleck and A. W. Ludwig, "The Kondo effect, conformal field theory and fusion rules," *Nucl.Phys.* **B352** (1991) 849–862.

[142] I. Affleck, "Conformal field theory approach to the Kondo effect," *Acta Phys.Polon.* **B26** (1995) 1869–1932, arXiv:cond-mat/9512099 [cond-mat].

[143] I. Affleck and A. W. Ludwig, "Critical theory of overscreened Kondo fixed points," *Nucl.Phys.* **B360** (1991) 641–696.

[144] I. Affleck and A. W. Ludwig, "Universal noninteger 'ground state degeneracy' in critical quantum systems," *Phys.Rev.Lett.* **67** (1991) 161–164.

[145] I. Affleck, "A Current Algebra Approach to the Kondo Effect," *Nucl.Phys.* **B336** (1990) 517.

[146] I. Affleck and A. W. W. Ludwig, "Exact conformal-field-theory results on the multichannel Kondo effect: Single-fermion Green's function, self-energy, and resistivity," *Phys. Rev. B* **48** (Sep, 1993) 7297–7321. http://link.aps.org/doi/10.1103/PhysRevB.48.7297.

[147] F. Haupt, S. Smolka, M. Hanl, W. Wüster, J. Miguel-Sanchez, A. Weichselbaum, J. von Delft, and A. Imamoglu, "Nonequilibrium dynamics in an optical transition from a neutral quantum dot to a correlated many-body state," *Phys. Rev. B* **88** (Oct, 2013) 161304. http://link.aps.org/doi/10.1103/PhysRevB.88.161304.

[148] S. M. Cronenwett, T. H. Oosterkamp, and L. P. Kouwenhoven, "A Tunable Kondo Effect in Quantum Dots," *Science* **281** no. 5376, (1998) 540–544, http://www.sciencemag.org/content/281/5376/540.full.pdf. http://www.sciencemag.org/content/281/5376/540.abstract.

[149] M.-N. Newrzella, "Calculation of time-dependent phenomena in the AdS/CFT correspondence," *Abschlussarbeit im Masterstudiengang Kern-, Teilchen- und Astrophysik* (2014) .

[150] N. D. Mermin and H. Wagner, "Absence of Ferromagnetism or Antiferromagnetism in One- or Two-Dimensional Isotropic Heisenberg Models," *Phys. Rev. Lett.* **17** (Nov, 1966) 1133–1136. http://link.aps.org/doi/10.1103/PhysRevLett.17.1133.

[151] E. Witten, "Multitrace operators, boundary conditions, and AdS / CFT correspondence," arXiv:hep-th/0112258 [hep-th].

[152] M. Berkooz, A. Sever, and A. Shomer, "'Double trace' deformations, boundary conditions and space-time singularities," *JHEP* **0205** (2002) 034, arXiv:hep-th/0112264 [hep-th].

[153] S. Ryu and T. Takayanagi, "Holographic derivation of entanglement entropy from AdS/CFT," *Phys.Rev.Lett.* **96** (2006) 181602, arXiv:hep-th/0603001 [hep-th].

[154] W. Israel, "Singular hypersurfaces and thin shells in general relativity," *Nuovo Cim.* **B44S10** (1966) 1.

[155] S. Coleman, *Aspects of Symmetry: Selected Erice Lectures*. Cambridge University Press, 1988. http://books.google.de/books?id=PX2Al8LE9FkC.